The Early Paleogene Succession at Tora, New Zealand; Stratigraphy and Paleoclimate

A critical North Island Eocene temperature record and a crucial linkage between the depositional settings of the central and southern East Coast Basin

MSc Thesis Presented by

Benjamin R. Hines

October
2012

TE WHARE WĀNANGA O TE ŪPOKO O TE IKA A MĀUI
VICTORIA
UNIVERSITY OF WELLINGTON

Submitted in partial fulfilment for the degree of Master of Science (MSc)
School of Geography, Environmental and Earth Sciences
Victoria University of Wellington

"If I see anything vital around me, it is precisely that spirit of adventure, which seems indestructible and is akin to curiosity" – Marie Curie

ABSTRACT

This study has utilised the Mg/Ca paleothermometry method to provide a new, North Island reference of sea temperatures in the Southwest Pacific during a period of extreme global warming, referred to as the Early Eocene Climatic Optimum (EECO; ~53-50 Ma). This period of Earth's history is of great interest as it represents the warmest climates of the Cenozoic. Importantly the climate dynamics of this period as simulated by computer models do not appear to match paleo-proxy data, specifically with regard to the latitudinal distribution of heat.

Development of this paleoceanographic record involved detailed mapping of three sections in the Wairarapa region (41.506199 S, 175.517663 E) of New Zealand's North Island. Three primary stratigraphic sections (Pukemuri, Awheaiti and Te Oroi Streams) were described and dated using foraminiferal and calcareous nannofossil biostratigraphy, with supplementary observations and measurements included from sections at Manurewa and Te Kaukau Points. These sediments are primarily siliciclastic sandstones and mudstones in composition, and sedimentary structures within these sections include turbidite sequences, channelisation and syn-sedimentary slumping, suggesting the EECO interval here is represented by sedimentation within a mid-bathyal submarine channel and fan environment. In contrast, the Early Paleocene Manurewa and Awhea Formations have previously been interpreted as a shallow, marginal marine environment which is at odds with benthic foraminiferal paleodepth indicators and trace fossil assemblages identified in this study.

Selected genera of planktic foraminifera were extracted from the EECO interval and paleo-water temperatures determined from Mg/Ca values measured by Laser Ablation Inductively Coupled Plasma Mass Spectrometry (LA ICPMS). This method was selected as it allows specific targeting of analysis sites, enabling avoidance of contaminated and altered parts of the test. This method also provides simultaneous measurements of other trace elements (Al, Si, Ti, Mn, Zn, Sr, Ba) that can be used as a guide to preservation state of the test (for example, Al, Ti and Si are considered indicators of detrital contamination levels). Four foraminifera genera were selected as suitable paleotemperature indicators of separate components of the water column. *Morozovella* spp. and *Acarinina* spp. were selected for surface mixed layer paleotemperature estimates, *Subbotina* spp. for thermocline temperature values, and *Cibicides* spp. for bottom water temperature determinations.

SEM images, combined with trace element data were used to parse the resulting Mg/Ca data and only those that met strict quality criterion, including low detrital contamination and lack of visual evidence for recrystalisation were used for temperature reconstruction. Planktic Mg/Ca data were converted to temperature using the relationship $(Mg/Ca = [Mg/Ca_{sw-t}]/[Mg/Ca_{sw-0}] \times 0.38^{\,0.09 \times T})$ and benthic Mg/Ca temperatures calculated using $(Mg/Ca = [Mg/Ca_{sw-t}]/[Mg/Ca_{sw-0}] \times 0.87^{\,0.109 \times T})$, each assuming an early Eocene seawater Mg/Ca value of 4.1 mol/mol. Calibrated Mg/Ca results show peak sea surface temperatures of 29°C for *Morozovella* and *Acarinina* in the East Coast Basin during the Early Eocene, with bottom water temperatures of 17°C obtained from *Cibicides*. These data are consistent with the high sea surface temperatures reconstructed by previous workers in the nearby Canterbury Basin. The data from this new reference point support the idea that the EECO was characterised by a lower, possibly absent latitudinal temperature gradient in the mid-latitude Southwest Pacific, than numerical models suggest, indicating a fundamental gap in the knowledge of climate dynamics in conditions much warmer than today.

TABLE of CONTENTS

LIST of FIGURES

LIST of TABLES

LIST of ACRONYMS

ACC	Antarctic Circumpolar Current
AR	Analytical Reagent
BFEE	Benthic Foraminiferal Extinction Event
BSI	Back Scatter Electron Image
BWT	Bottom Water Temperature
CCD	Carbonate Compensation Depth
CCP	Cretaceous Cenozoic Programme
DSDP	Deep Sea Drilling Project
EAC	East Australian Current
ECB	East Coast Basin
ECDB	East Coast Deformed Belt
EECO	Early Eocene Climatic Optimum
EPMA	Electron Probe Micro-Analysis
GCMs	Global Circulation Models
GDGT	Glycerol Dialkyl Glycerol Tetraethers
FAD	First Appearance Datum
FRF	Fossil Record File
HO	Highest Occurrence
HSM	Hikurangi Subduction Margin
K/Pg	Cretaceous-Paleogene boundary
LAD	Last Appearance Datum
LA-ICP-MS	Laser Ablation Inductively Coupled Plasma Mass Spectrometry
LINZ	Land Information New Zealand
LO	Lowest Occurrence
MD	Maximum Dimension
MECO	Middle Eocene Climatic Optimum
NIST 610	National Institute of Standards and Technology 610
NZMS	New Zealand Map Sheet
ODP	Ocean Drilling Project
PETM	Paleocene-Eocene Thermal Maximum
RO	Reduced Oxygen
SEI	Scanning Electron Image
SEM	Scanning Electron Microscope
SST	Sea Surface Temperature
STF	Subtropical Front
TC	Tasman Current
TEX_{86}	Tetra-Ether indeX of the 86 carbon chain

PUBLICATIONS AND ADDITIONAL OUTPUTS

During the course of this research, additional analyses of associated early Paleogene successions were conducted in parallel with this study. While this is not formally presented here, pertinent results are referred to for the purposes of comparison. The additional analyses include Mg/Ca paleothermometry of the Early Eocene Kurinui Formation at Hampden Beach, Mg/Ca analysis of latest Paleocene to Early Eocene foraminifera from DSDP Site 277, and a quantitative and qualitative assessment of Early Eocene foraminiferal test preservation using laser ablation trace element analysis, electron probe microanalysis and scanning electron microscopy. The Hampden Mg/Ca paleothermometry record has already been published in Hollis *et al.* (2012), with the additional work currently in preparation for publication.

Published Manuscripts

Hollis, C. J., Taylor, K. W. R.., Handley, L., Pancost, R. D., Huber, M., Creech, J. B., **Hines, B. R.**, Crouch, E. M., Morgans, H. E. G., Crampton, J. S., Gibbs, S., Pearson, P. N. & Zachos, J. C. (2012). Early Paleogene temperature history of the Southwest Pacific Ocean: Reconciling proxies and models. *Earth and Planetary Science Letters.* Vol. 349-350, pp. 53-66. Doi:10.1016/j.epsl.2012.06.024

Manuscripts in Preparation

Hines, B. R., Kulhanek, D. D., Hollis, C. J., Atkins, C. B. & Morgans, H. E. G. The Paleogene stratigraphy and paleoenvironment of the Tora area, southeast Wairarapa, New Zealand. *Manuscript submitted to New Zealand Journal of Geology and Geophysics.*

Hines, B. R., Hollis, C. J., Baker, J. A., Atkins, C. B., Kulhanek, D. D. & Morgans, H. E. G. The Early Eocene Paleothermometry of the central East Coast Basin, North Island, New Zealand. *Manuscript in Preparation for Earth and Planetary Science Letters.*

Hines, B. R., Marr, J. P., Strong, C. P., Hollis, C. J., Baker, J. A. Preservation potential of some Early Paleogene foraminifera: Implications for Mg/Ca paleothermometry. *Manuscript in Preparation for Paleoceanography.*

Kulhanek, D. K., Strong, C. P., Hollis, C. J., **Hines, B. R**., Littler, K., Zachos, J. C. Tropical conditions in the southern Pacific Ocean (DSDP Site 277, 65°S) during the Paleocene-Eocene thermal maximum. *Manuscript in Preparation for Nature Geoscience/Geology.*

Conference Presentations

Hines, B. R., Atkins, C., Hollis, C. J., Morgans, H. E. G., Kulhanek, D. & Baker, J. (2011). The Early Eocene Succession at Tora, Wairarapa: Stratigraphy and Paleoclimate. New Zealand Geosciences Conference, Nelson, New Zealand. 27th November - 1st December [Poster].

Hines, B. R., Hollis, C. J., Atkins, C. B., Baker, J., Morgans, H. E. G. & Kulhanek, D. K. (2012). Early Eocene Mg/Ca Paleothermometry of the Central East Coast Basin. New Zealand Geosciences Conference, Nelson, New Zealand. 25th-28th November 2012 [Presentation].

Hollis, C. J., Taylor, K. W. T., Pancost, R. D., **Hines, B. R**., Littler, K., Zachos, J. C., Kulhanek, D. K. & Strong, C. P. (2012). Early Paleogene temperature history of the Southwest Pacific Ocean. New Zealand Geosciences Conference, Nelson, New Zealand. 25th-28th November 2012 [Presentation].

INTRODUCTION

1.1   General Introduction

Concerns about present global warming have promoted study of Earth's past climates in order to better understand the effects and implications that anthropogenically-driven increases of atmospheric carbon dioxide (CO_2) concentrations may have on future climate systems. The early Eocene (55.8–49 Ma) was the most recent period in Earth's history to have experienced atmospheric CO_2 levels as high as those forecast for the peak in CO_2 emissions by the year 2400 (Zachos *et al.*, 2008). Paleoclimate models suggest that the Pacific Ocean played a significant role in early Paleogene climate dynamics, and is estimated to have been responsible for up to 80% of global heat transport during this time (Huber & Sloan, 2001).

This study uses the Mg/Ca ratios of carbonate tests of fossil foraminifera to reconstruct sea temperatures within the East Coast Basin of New Zealand during the early to middle Eocene. The primary aim was to constrain temperature estimates for the Early Eocene Climatic Optimum (EECO) and the post-EECO decline in the middle Eocene. Previous temperature estimates derived from foraminiferal Mg/Ca ratios and other geochemical temperature proxies (Bijl *et al.,* 2009; Hollis *et al.*, 2009; Creech *et al.*, 2010; Sluijs *et al.*, 2011) indicate that southwest Pacific sea surface temperatures (SSTs) at high latitudes (55–65°S) were as high as 30°C during the Paleocene Thermal Maximum (PETM) and EECO. These tropical-like temperatures are difficult to reconcile with known climate dynamics and paleoclimate models (e.g. Huber & Caballero, 2011), as they imply that almost no latitudinal temperature gradient existed between the tropics and polar regions.

The southern Hawke's Bay and Wairarapa area currently lies at 40°S on the East Coast of the North Island, New Zealand. However, during the Eocene the New Zealand subcontinent occupied a position 10–15° further south (*Figure 1.1*). The Chatham Rise was a major barrier to ocean circulation during the early Paleogene, and location of the East Coast Basin northwards of the Chatham Rise, and north of previously studied sites in the Canterbury Basin, means that Eocene rocks from this region are ideally suited for the study of high latitude, southwest Pacific Ocean temperature dynamics in the Paleogene. This region is especially important in the critical period that preceded the development of the modern, global deep-water circulation driver (i.e., the Antarctic Circumpolar Current (ACC)). Therefore, this study examines the possibility of a

thermal gradient between sites to the south (Burgess *et al.*, 2008; Creech *et al.*, 2010; Hollis *et al.*, 2012) and in the tropics (Tripati *et al.*, 2003) during the early Eocene.

The primary study area examined in this thesis is a Paleocene to middle Eocene succession located on the southeast Wairarapa coast. Complex vertical and lateral facies changes in this succession necessitated the establishment of a robust age and stratigraphic framework, which involved extensive field mapping and detailed measurement of stratigraphic sections along with microfossil sampling. A secondary comparative sample suite was selected from the sections at Tawanui and Aropito in southern Hawke's Bay to provide an additional sample set for geochemical analysis. Outcrop studies generated the stratigraphic, microfossil and geochemical information, providing a new East Coast Basin record of climatic and oceanographic conditions during this past period of extreme global warmth in the "greenhouse" world. This information can be used to test modelled scenarios for climate and ocean conditions.
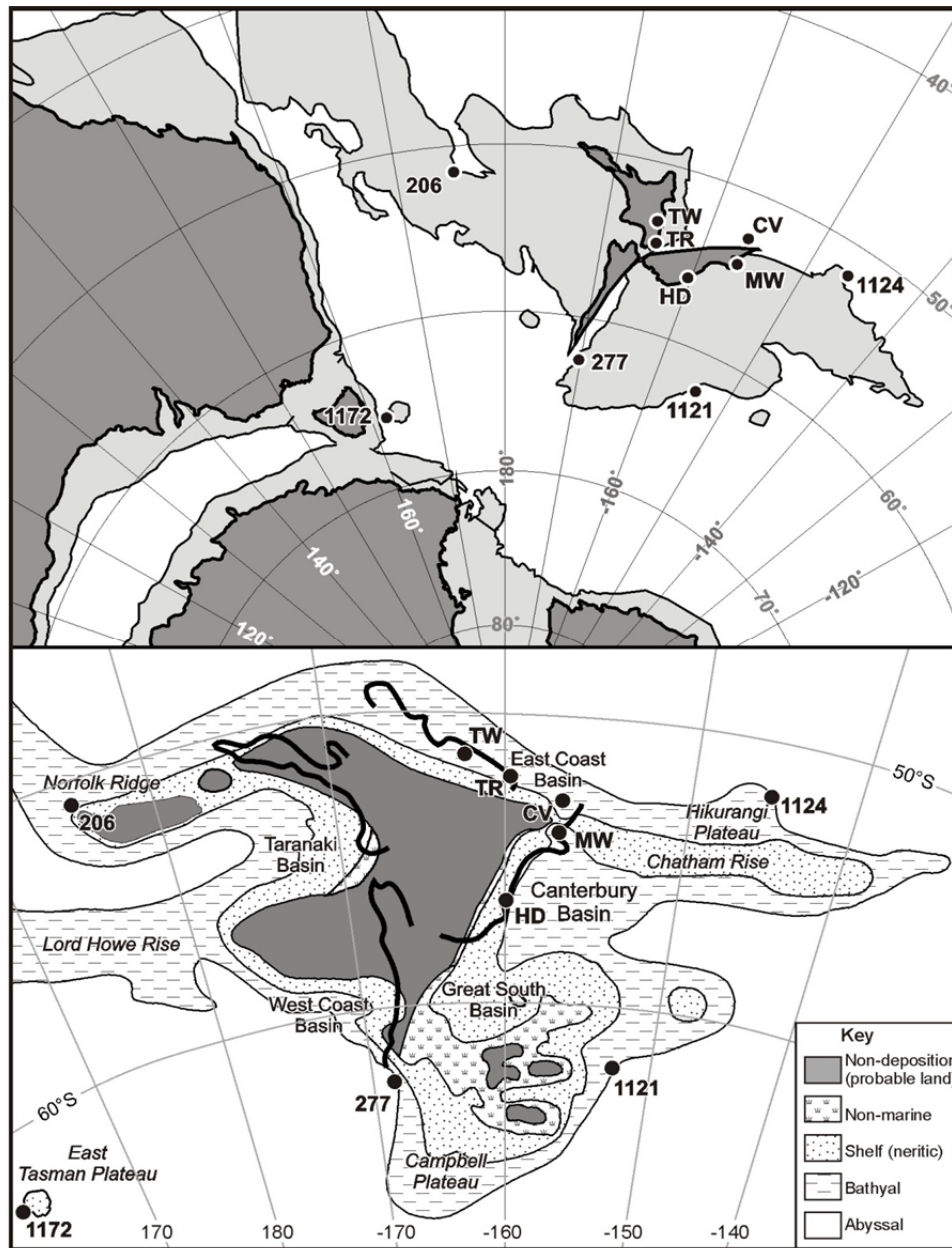
Figure 1.1: Paleoenvironmental reconstruction of the southwest Pacific during the early Eocene (54 Ma), displaying the locations of key localities utilised in this study (adapted from Hollis *et al.*, 2012). Sections studied were: TW = Tawanui, TR = Tora, MW = Mid-Waipara River, HD = Hampden Beach, CV = Clarence Valley. Core sites are: DSDP 206 and DSDP 277. Also plotted are ODP cores 1121, 1124 and 1172, which sampled Paleogene records for the southwest Pacific (e.g. ODP 1172: Bijl *et al.*, 2009; Sluijs *et al.*, 2011).

1.2   Location and Site Setting

The location of the New Zealand subcontinent occupied a position approximately 10-15° further south during the Eocene than the present (*Figure 1.1*). Consequently, passive margin sedimentary sequences deposited in the East Coast Basin during the early Paleogene record aspects of southwest Pacific Ocean climate during this time. For the purposes of this study, two different successions from the central East Coast Basin were selected. The Tora area in southeast Wairarapa was selected as the primary field area, along with comparative sections and sample suites from the Aropito and Tawanui sections in the southern Hawke's Bay.

The Paleogene strata of the Tora area provide a sequence of sedimentary rocks deposited between the clastic-rich sequence of the rest of the North Island and the pelagic-hemipelagic succession of Marlborough (Field, Uruski *et al.*, 1997). The stratigraphy at Tora has long been recognised as distinctly different from the successions in these other regions but has received remarkably little attention since the original descriptions by Waterhouse & Bradley (1957). There is increasing interest in the Cretaceous-Paleogene sequence at Tora because it provides an onshore analogue for prospective petroleum basins offshore eastern New Zealand, particularly the Pegasus Basin (Uruski & Bland, 2011). The sequence also has potential to contribute to studies of past greenhouse climates as it includes expanded intervals of the Paleocene and Eocene that can be compared with coeval intervals to the north in Hawke's Bay (Crouch *et al.* 2001, 2003) and to the south in Canterbury Basin (e.g. Burgess *et al.* 2008; Hollis *et al.* 2005a; 2009; 2012).

Tora

The Tora area is located on the southeastern Wairarapa coast, located 40 km south of Martinborough township (*Figure 1.2*). The 50 km^2 field area is bounded by the coast to the east, and by large faults and the older rocks of the Aorangi Mountains to the west. Outcrop is generally restricted to the shore platform and stream cuttings in several small catchments that drain the coastal ranges. Land use is primarily privately held farmland used for grazing livestock, and permission is required for access to some stream and coastal sections. Topography surrounding the area is rugged, rising to 400 m above sea level less than 1 km from the coast, and stream access is occasionally hindered by narrow gorges and waterfalls. Although outcrops are predominantly confined to stream beds, they are generally well-exposed with only a moderate degree of weathering.

A moderately coherent package of early Eocene strata is exposed in Awheaiti and Pukemuri Streams at Tora. Stratigraphic relationships are complicated by faulting, folding and occasional poor exposure in places, but comprehensive mapping and detailed measurement of stratigraphic sections has documented a complete succession containing Early to Middle Eocene strata. Samples collected during this fieldwork provided foraminifera and calcareous nannofossil assemblages for age, paleotemperature and paleoenvironmental reconstructions.

Tawanui and Aropito Composite Section

A composite section was produced from two sparsely sampled sections in southern Hawke's Bay to produce a comparative record from elsewhere in the central East Coast Basin, in order to eliminate uncertainty arising from local climate variability during the Eocene and post-depositional diagenetic effects which may have affected the Tora specimens.

The Tawanui section is located in a tributary of the upper reaches of the Akito River and the Aropito section is located *ca.* 10 km north of Tawanui in Aropito Stream, a tributary of the Mangaorapa River (*Figure 1.2*). The Paleocene–Eocene sedimentary succession at Aropito and Tawanui is represented by smectitic mudstones of the Wanstead Formation (Moore & Morgans, 1987).
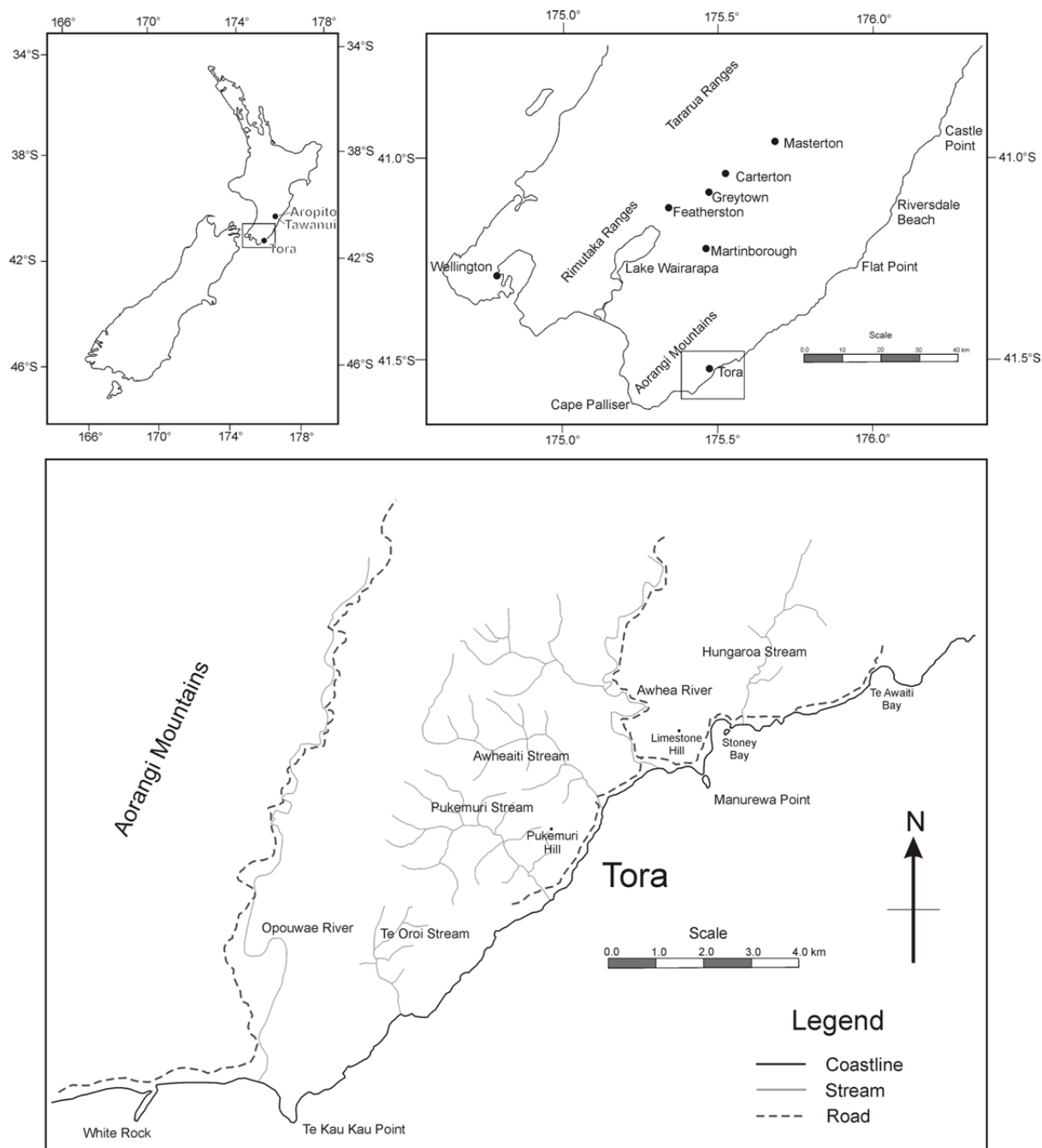
Figure 1.2: Location of the Tora field area and the position of the Aropito and Tawanui sections in the southern Hawke's Bay.

1.3 Paleogene Climate

The climate of the late Cretaceous and early Paleogene is characterised by temperatures that were significantly warmer than the present day, reaching a peak during the early Eocene (*Figure 1.3*). These warm temperatures characterise the 'greenhouse' world of the late Cretaceous to the early Paleogene before the onset of cooling which began in the latest Eocene – early Oligocene, leading to the icehouse conditions of the Miocene to the present.

Eocene climate was characterised by some of the warmest temperatures during the Cenozoic (Zachos *et al.*, 2001; Tripati *et al.*, 2003). Gradual widespread warming was initiated in the late Paleocene (~58 Ma) and culminated in the EECO (53–50 Ma), and was punctuated by an abrupt, 150 kyr duration, hyperthermal event (PETM) at the Paleocene-Eocene boundary (56 Ma) (Zachos *et al.*, 2001; Bijl *et al.*, 2009; McInerney & Wing, 2011; Sluijs *et al.*, 2011). Stable oxygen isotope and Mg/Ca trace element studies on fossil planktic foraminifera from deep sea sediments indicate a 5–8°C warming during the PETM (Thomas *et al.*, 2002; Zachos *et al.*, 2003). The PETM was also associated with a massive release of ^{13}C-depleted carbon, which appears in the sedimentary record as a negative carbon isotope excursion, and implies a large, transient increase in atmospheric CO_2 concentrations at this time (Zachos *et al.*, 2008; Zeebe *et al.*, 2009; Sluijs *et al.*, 2011). A similar negative carbon isotope excursion is associated with the EECO, suggesting a similar triggering mechanism (Zachos *et al.*, 2001).

TEX_{86} sea temperature reconstructions from the southwest Pacific Ocean suggest that SSTs reached 34°C during the PETM and EECO, and gradually decreased to 21°C by the late Eocene (36 Ma) (Bijl *et al.*, 2009; Hollis *et al.*, 2009; Sluijs *et al.*, 2011). Even though recent reviews of these datasets suggest that SSTs may have been overestimated by 5–8°C (Hollis *et al.*, 2010, 2011, 2012), cool subtropical temperatures (*ca.* 25–27°C) for southern mid- to high latitudes are only marginally cooler than equatorial regions (e.g. Tripati *et al.*, 2003), implying that meridional temperature gradients were unusually low in the early Eocene.

A 17 Myr cooling trend began at the termination of the EECO, and by the end of the Eocene (~34 Ma) the first major Antarctic ice sheets had appeared, suggesting that significant cooling had occurred and signalling the onset of the 'Icehouse' world (*Figure 1.3*; Zachos *et al.*, 2001; Bijl *et al.*, 2009). A decline in deep sea $\delta^{18}O$ is inferred to represent the combined effects of declining temperature (from *ca.* 12°C to 4.5°C at 34 Ma; *Figure 1.3*) and growth of Antarctic ice volume (Zachos *et al.*, 2001). During the latest Eocene to earliest Oligocene, the Tasman Gateway had opened sufficiently to allow the development of a circumpolar current, consequently resulting in

the thermal isolation of the Antarctic continent (Carter *et al.*, 1996). This was followed by a period of unstable ice sheet fluctuations with permanent ice sheets and complete icehouse conditions developing during the middle Miocene (*Figure 1.3*; Zachos *et al.*, 2001; Miller *et al.*, 2005).
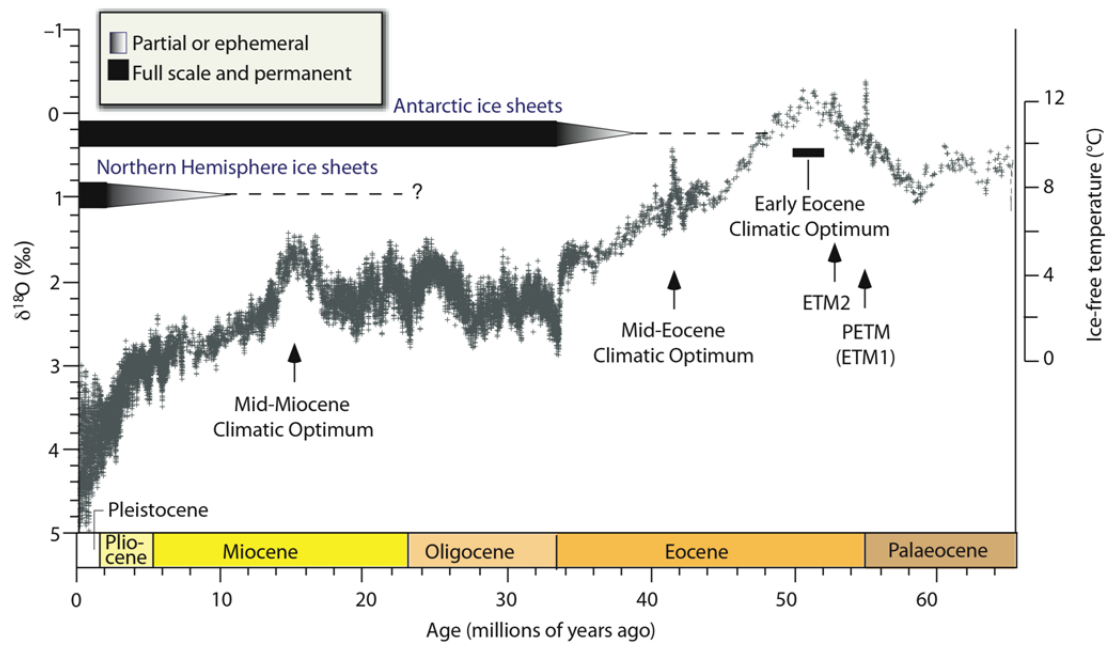
Figure 1.3: Global climate record from stacked deep-sea benthic foraminiferal oxygen isotope data based on Deep Sea Drilling Project (DSDP) and Ocean Drilling Program (ODP) cores. Also shown is the presence of permanent or partial ice sheets. The temperature scale was calculated assuming ice-free conditions, and therefore does not apply following the glaciation of Antarctica (*ca.* 35 Ma). Figure modified from Zachos *et al.* (2008).

1.4   Unresolved Questions about Paleogene Climate

Several outstanding questions remain regarding the climate of the early Paleogene. Independent proxy records have proven notoriously difficult to verify unequivocally due to inherent uncertainties that are unique to each proxy method. Furthermore, modelled early Paleogene climate reconstructions are difficult to reconcile with existing geochemical proxy evidence, which indicate significantly lower temperature gradients between the equator and the poles than that predicted by global circulation models (GCMs). During times of peak warmth in the Early Eocene, geochemical proxies indicate sea surface temperatures in excess of 30°C in the high latitude southwest Pacific, comparable to low latitude estimates, implying a systematic breakdown of the equator-to-pole thermal gradient which cannot be reconciled with the known climate dynamics that control climate and circulation models (Hollis *et al.*, 2012).

The presence or absence of Antarctic ice sheets during the Early to Middle Eocene has long been a controversial point. This is significant given the influence Antarctic ice exerts on global ocean circulation, latitudinal temperature gradients, and the oxygen isotope ratio of seawater. Given that global deep ocean waters are primarily derived from cooling and sinking of dense saline water in polar regions (largely during the winter), the deep sea benthic foraminifera record may also provide a record of high-latitude winter sea surface temperatures (Zachos *et al.*, 2001). However, high-latitude SSTs (>25°C) are difficult to reconcile with early Eocene bottom water temperatures (BWT) of 10–13°C suggested by deep sea benthic foraminiferal Mg/Ca and $\delta^{18}O$ (*Figure 1.3*; Zachos *et al.*, 2001, 2008; Cramer *et al.*, 2011).

Early to middle Eocene temperature estimates made using the $\delta^{18}O$ temperature proxy rely on an inherent assumption of global ice volume. Small ephemeral ice sheets may have been present on the Antarctic continent since the middle Eocene (Ehrmann & Mackensen, 1992; Burgess *et al.*, 2008). By applying the Mg/Ca paleotemperature proxy, which is independent of ice volume effects, these uncertainties can be eliminated. However, the Mg/Ca proxy is not without its own complications. The Mg/Ca ratio of seawater has varied significantly over time (Coggon *et al.*, 2010), and as foraminifera precipitate calcite in equilibrium with the seawater in which they lived, the Mg/Ca content of seawater exerts a significant control over Mg/Ca paleo-ocean temperature reconstructions. Unfortunately, there are no direct and unequivocal records for Eocene seawater cation concentrations, with only modelled values (e.g. Wilkinson & Algeo, 1989; Stanley & Hardie, 1998) and indirect evidence from mid-ocean ridge calcite veins (Coggon *et al.*, 2010), biogenic calcite (Lear *et al.*, 2002; Dickson, 2004) and halite fluid inclusions (Zimmermann, 2000; Lowenstien *et al.*, 2001; Horita *et al.*, 2002).

1.5   Aims and Objectives of this Thesis

The global transition from the 'greenhouse' world of the early Eocene into an 'icehouse' climate remains poorly constrained, with relatively few temperature records from southern high latitude regions. This study aims to generate a new southern high latitude record from the East Coast Basin of New Zealand documenting the greenhouse climate of the Early Eocene prior to the decline to icehouse conditions. These results can then be compared with other intra-basinal records, thereby contributing to a robust regional understanding of Eocene conditions throughout the New Zealand region. In order to achieve this, the stratigraphy, age and paleoenvironment of the sedimentary succession at Tora first had to be reliably determined. This required a review and revision the Paleogene stratigraphy at Tora, development of a depositional model and demonstration of how Paleogene units and facies may be correlated to the rest of the East Coast Basin and included the following approaches:

I) *Field Mapping and Establishing a Lithostratigraphic Framework*

Geological field mapping was an essential prerequisite in this study in order to establish the extent and coherency of the stratigraphic succession at Tora. This addressed structural complications and exposure. Detailed measured sections were recorded providing a lithostratigraphic framework for moderately high resolution microfossil sampling and correlation and sedimentological interpretation of paleoenvironments.

II) *Biostratigraphic Analysis*

Bulk rock samples yielded foraminifera and calcareous nannofossil assemblages that were used to interpret the paleoenvironmental and oceanic conditions at the time of deposition, as well as providing age constraints.

III) *Geochemical Analysis*

A subset of foraminifera species were selected, prepared and subsequently analysed using laser ablation inductively coupled plasma mass spectrometry (LA-ICP-MS). Mg/Ca ratios derived from LA-ICP-MS analysis of foraminiferal calcite were used to construct a paleo-sea temperature record for the selected interval. Subsets of bulk samples were analysed by the National Isotope Centre (Institute of Geological and Nuclear Sciences) for bulk carbonate δ^{13}C and δ^{18}O values.

The results of this study provide a southwest Pacific marine paleotemperature record from the Tora, Aropito and Tawanui sections, which can be compared with existing records and used to enhance and refine regional paleoclimate reconstructions. Particular focus is given to comparing the results obtained with existing studies at Hampden Beach (Burgess *et al.*, 2008) and mid-Waipara River (Hollis *et al.*, 2009; Creech *et al.*, 2010) in the Canterbury Basin (*Figure 1.1*).

1.6   Thesis Structure and Outline

Chapter One briefly describes the motivation for this research, and relevant background material. Chapter Two outlines the general stratigraphic relationships of the East Coast Basin, describes previous work conducted in the Tora field area, introduces the climatic conditions of the Paleogene, and the analytical framework of this study. Chapter Three presents in detail the field and analytical methods employed in this study, as well as describing key concepts surrounding the development of the paleotemperature record and analytical methodology. Measured section results and revised formation descriptions, as well as age and environmental interpretations, are presented in Chapter Four. Chapter Five outlines the results of geochemical sampling and analysis at Tora and the Aropito–Tawanui composite section as well as discussion, integration and interpretation of the results along with an inter-basinal comparison of early to middle Eocene proxy records. Chapter Six provides a summary of the key findings of this study, their implications, and suggestions for future work. All field and analytical data are tabulated and listed in Appendices 1 and 2.

Two manuscripts are currently in preparation as a direct consequence of the material reported in this thesis; a revised stratigraphy of the early Paleogene succession of the Tora area (Hines *et al.*, in prep [1]) as well as the first quantitative paleotemperature history of the early Eocene reported in the North Island of New Zealand (Hines *et al.*, in prep. [2]). Additional related work which is beyond the scope of this thesis include Mg/Ca analysis of additional records from the Hampden Beach section (Canterbury Basin), published in Hollis *et al.* (2012), a Mg/Ca paleotemperature record from DSDP Site 277 spanning the late Paleocene to early Eocene with particular emphasis on the PETM interval (Kulhanek *et al.*, in prep.), and a study on quantifying the effect of diagenetic alteration on Early Eocene foraminifera via coupled laser ablation, electron microprobe analysis SEM and optical imaging (Hines *et al.*, in prep. [3]).

STRATIGRAPHIC AND PALEOCLIMATIC FRAMEWORK

2.1   Regional Stratigraphy

Passive margin thermal subsidence following the Late Cretaceous Rangitata Orogeny resulted in the formation of several marine sedimentary basins around New Zealand (King *et al.*, 1999; Furlong & Kamp, 2009). During the Late Cretaceous and Paleogene, thick sequences of marine sediment were deposited in these gradually subsiding basins offshore of New Zealand at a paleo-latitude of between 48–65° south (Lawver *et al.*, 1992; King *et al.*, 1999). Thus, the sediments of the East Coast Basin comprise an overall fining-upwards succession from Cretaceous sandstone to Paleocene–Eocene mudstone and muddy limestone (Field, Uruski *et al.*, 1997).

Moore *et al.* (1986) divided the Cretaceous-Paleogene stratigraphy of the East Coast Basin into three broad lithological divisions. These were subsequently adopted by Field, Uruski *et al.* (1997) in a review of the stratigraphy of the East Coast Basin. The subdivisions are:

I.   A clastic sandstone, mudstone and conglomerate sequence (Early to Late Cretaceous).

II. A fine-grained clastic sequence that becomes increasingly calcareous upwards. This is a transitional sequence between divisions I and III (Late Cretaceous to Paleocene).

III. A calcareous, fine-grained sequence comprising smectitic mudstone, micritic limestone and glauconitic sandstone (Eocene to Oligocene).

These divisions are readily recognisable within the general sedimentary succession of the East Coast Basin. Correlation of these sedimentary units has allowed the development of a structural and stratigraphic framework that enables the relationships between various lithostratigraphic components of the East Coast Basin to be determined. Distinct contrasts in the stratigraphy and structure were recognised and utilised by Moore *et al.* (1986) and Moore (1988a) to propose the division of the East Coast Basin into structural blocks. These blocks are grouped into the Western Sub-belt and the Eastern Sub-belt, and have provided a basis for future studies of the complex tectonic processes that have affected the basin following the onset of convergent margin tectonism in the late Oligocene to early Miocene (*Figure 2.1*).

In the southern North Island, the Western Sub-belt consists of the Aorangi, Woodville and Pongaroa Blocks (*Figure 2.1*). The Eastern Sub-belt is subdivided into the Coastal and Tora Blocks, which are approximately analogous to the narrow (≤10 km wide) onshore expression of an accretionary wedge (*Figure 2.1*). Post-Oligocene east–west orientated compression associated with the Kaikoura Orogeny, in conjunction with westward-dipping thrust faulting, has resulted in complex folding and faulting relationships in the Tora and Coastal Blocks (Moore, 1988a; Berryman *et al.*, 2011). The onshore exposure of the Tora Block is separated from the Pongaroa and Coastal Blocks by the Ewe, Hungaroa, Tutu and Adams-Tinui Fault systems (*Figure 2.1*). The eastern and southern extent of the Tora Block is undetermined, but seismic mapping and modelling (Barnes *et al.*, 2010; Berryman *et al.*, 2011) suggest that a significant thrust system lies close to the Tora-Glenburn coast. The upper Cretaceous strata of the Tora Block are considered laterally continuous with the Coastal Block to the north (Crampton, 1997; after Moore *et al.*, 1986), with the Tora Block distinguished primarily by poorly-defined facies differences in the Paleogene sediments.
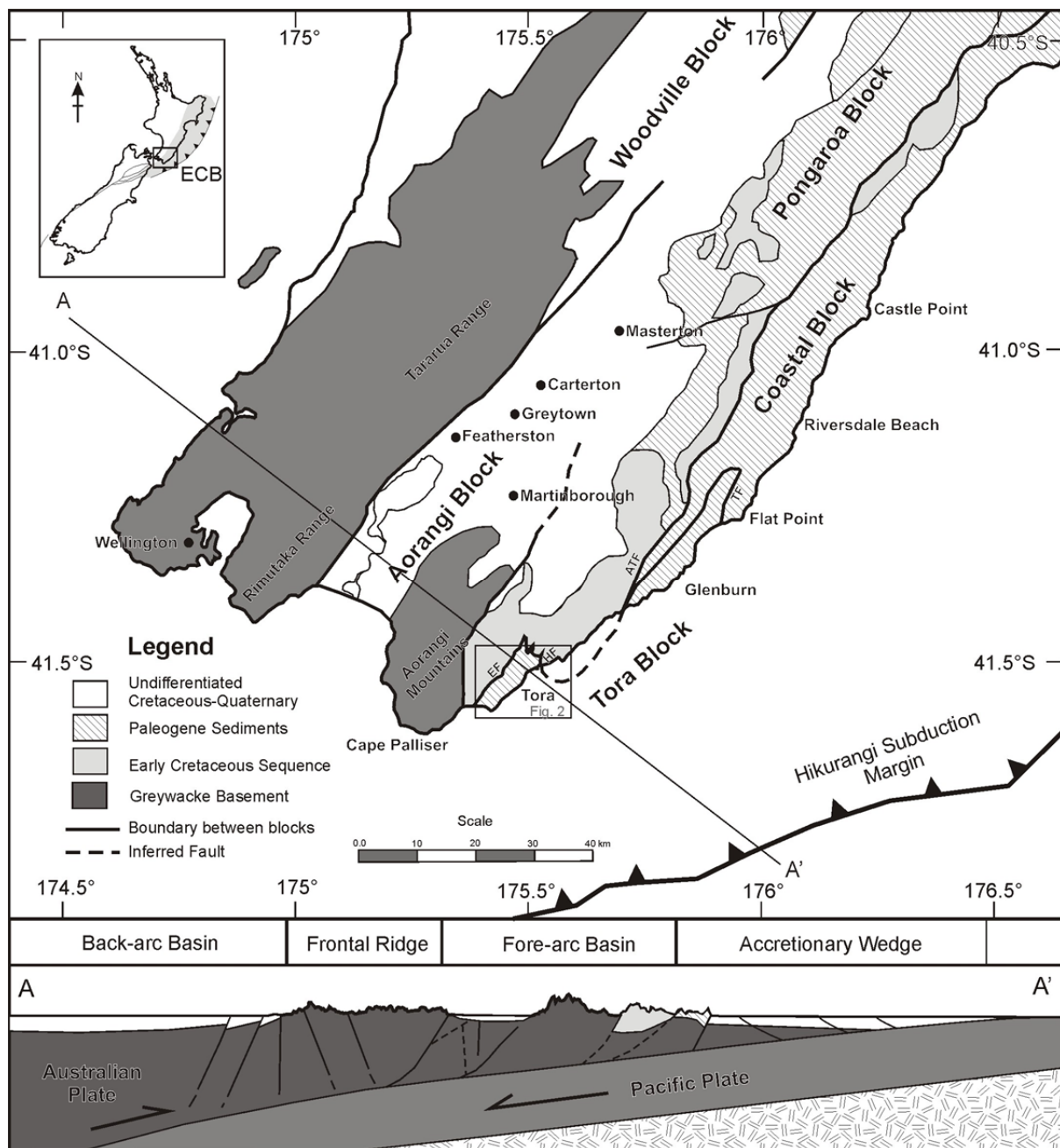
Figure 2.1: Simplified geological map and structural setting of the southern North Island, New Zealand, and schematic cross-section (*after* Moore, 1988a; Little *et al.*, 2009). Key to acronyms: ECB = East Coast Basin, EF = Ewe Fault, HF = Hungaroa Fault, ATF = Adams-Tinui Fault, TF = Tutu Fault.

2.2   Tora Stratigraphy

Previous Work

Crawford (1868) noted possible Mesozoic limestones and sandstones on the East Coast, describing the rocks as "traversed by reefs of diallage"; a probable reference to the greensand dykes that are pervasive through the Whangai, Manurewa and Mungaroa Formations. McKay (1878) visited White Rock, describing the limestone as "beyond all doubt Amuri Limestone", suggesting a connection between this locale and northern Marlborough. King (1930) also visited the White Rock area, but added little more than stating that the limestone is "certainly Notocene" in age (Upper Cretaceous to Recent; Carter *et al.*, 1974). McLean (1953) completed mapping of the area, although his study predominantly focused on the Early Cretaceous sedimentary sequence in the Aorangi Ranges, but did not map the Paleogene succession at Tora.

The Paleogene stratigraphy at Tora was originally mapped by Waterhouse (1955). Waterhouse & Bradley (1957) published a comprehensive description of the stratigraphy and deformation of the Tora succession, as well as formally identifying the formations, assigning ages to the strata and discussing the depositional and deformation history. Kirk (1966) completed a BSc Honours study on the origin and emplacement of greensand dykes in the Manurewa Formation and the Mungaroa Limestone. Moore & Speden (1984) mapped and described the Lower Cretaceous succession bounding the Tora Block, but did not refine the Upper Cretaceous–Paleogene stratigraphy. Subsequently, Pukemuri Stream was later utilised as a reference section for the Upper Cretaceous Whangai Formation (Moore, 1988b). In addition to this, Moore & Morgans (1990) measured sections of the Late Cretaceous–Paleogene succession in Awheaiti, Pukemuri and Te Oroi Streams for the East Coast Cretaceous–Cenozoic Programme (Field, Uruski *et al.*, 1997). This was followed by Alexander (1990), who completed a structural field study of the northern Tora area for his BSc Honours thesis. North of the Tora field area, Lee (1995) conducted a structural study of deformed sediments at Huatokitoki Stream, Glenburn, utilising Pukemuri Stream at Tora as a reference section for the Late Cretaceous–Early Paleocene stratigraphy.

Several studies have recognised the Cretaceous–Paleogene (K/Pg) Boundary section at Tora in investigations of Late Cretaceous–Early Paleocene sediments (Wasmuth, 1996; Laird *et al.*, 2003; Vellekoop, 2010). However, the younger Paleogene sediments remained largely unstudied, perhaps due to the difficulties posed by intraformational slumping, variable exposure, tectonic deformation and poor access.

2.3   Stratigraphy of the Tora Area

Previous studies have divided the late Cretaceous–Paleogene stratigraphy into eight lithostratigraphic units overlying early to mid-Cretaceous Torlesse Supergroup basement (*Figure 2.2*).

Pahaoa Group (Early–Middle Cretaceous)

The Pahaoa Group sediments are generally considered the basement rocks of southern Wairarapa. In the Tora area, this is largely represented by the Mangapokia Formation. The mid-Cretaceous (Motuan) Mangapokia Formation represents the youngest part of the Torlesse accretionary wedge and predominantly consists of sandstone, argillite and conglomerate along with minor pebbly-mudstone, scattered spilitic igneous rocks and associated volcanogenic sediments (Moore & Speden, 1984; Barnes & Korsch, 1991). The accreted submarine fan turbidite sequence is weakly metamorphosed and complexly deformed (Barnes, 1988; Barnes & Korsch, 1991).

Glenburn Formation (Late Cretaceous)

The Glenburn Formation comprises an alternating sequence of fine to very-fine sandstone that is exposed on a narrow coastal strip at Tora. It has a minimum thickness of 62 m (Laird *et al.*, 2003), and is inferred to unconformably overlie Mangapokia Formation. A Santonian (late Piripauan) age is inferred from inoceramids and dinoflagellates (Crampton, 1996; Laird *et al.*, 2003). Much of the Glenburn Formation was deposited in a submarine fan environment at bathyal depths (Crampton, 1997). However, only the uppermost part of the unit is exposed at Tora and sedimentary structures suggest a shallow marine setting (Laird *et al.*, 2003).

Whangai Formation (Late Cretaceous)

The Rakauroa Member of the Whangai Formation occurs throughout the East Coast Basin, and is the only member of the Whangai Formation formally identified at Tora (Moore, 1988b). The formation consists of hard, non-calcareous, micaceous siltstone with sparse beds of calcareous, glauconitic sandstone. The formation has an estimated minimum thickness of *ca.* 350 m. The

basal contact with the Glenburn Formation is faulted at Tora (Moore, 1988b; Wasmuth, 1996; Laird *et al.*, 2003).

Foraminifera from lower in the formation indicate deposition at shelf depths, possibly with reduced oxygen levels (Moore, 1988b). Dinoflagellate assemblages give an early Campanian (early Haumurian) age for the base of the section at Pukemuri Stream and a late Campanian–Maastrichtian (late Haumurian) age for the uppermost Whangai Formation at Manurewa Point (Laird *et al.*, 2003).

Manurewa Formation (Late Cretaceous–Paleocene)

The Manurewa Formation overlies the Whangai Formation with a sharp, channelised lower contact (Moore, 1988b; Laird *et al.*, 2003) and exhibits significant variability along strike (Waterhouse & Bradley, 1957; Wasmuth, 1996). The formation comprises two informal members; a lower limestone member and an upper greensand member. The 4 m-thick lower member consists of thin, interbedded glauconitic mud and calcareous beds which grade upwards from coarse pebbly sandstones and glauconitic mudstone into pure limestone (Waterhouse & Bradley, 1957). The upper member is a *ca.* 15 m-thick laminated greensand that contains abundant pyrite nodules. The basal contact of the upper member is channelised into underlying strata and in some sections the lower member is absent (Waterhouse & Bradley, 1957).

Dinoflagellate and foraminiferal assemblages indicate a Maastrichtian to Paleocene (late Haumurian to Teurian) age, with an environment of deposition at middle to lower bathyal depths (Wasmuth, 1996; Wilson, 1998; Begg & Johnston, 2000). Several studies have identified the Cretaceous–Paleogene boundary at the base of the upper member (Wasmuth, 1996; Laird *et al.*, 2003; Vellekoop, 2010). Dinoflagellate assemblages from the lower member of the Manurewa Formation are assigned to the latest Cretaceous *Manumiella druggii* Zone, whereas the upper member contains an assemblage that is correlated to the early Paleocene *Trithyrodinium evitii* Zone (Laird *et al.*, 2003).

Epoch	Sub-Epoch	NZ Series	New Zealand Stage	Waterhouse (1955)	Waterhouse & Bradley (1957)	Moore & Morgans (unpublished)	Wasmuth (1996)	Laird et al. (2003)	Vellekoop (2010)	This Study
Oligocene	Early	Landon	Whaingaroan	Kandahar Formation	(X)	(X)	Not Studied	Not Studied	Not Studied	(X)
Eocene	Late	Arnold	Runangan	Pukemuri Zst.						
			Kaiatan	Oroan Formation						Wanstead Formation
			Bortonian		Kandahar Formation	Wanstead Formation				
	Middle		Porangan	(X)	(X)	(X)				(X)
		Dannevirke	Heretaungan	Awhea Formation	Pukemuri Siltstone					Pukemuri Siltstone
	Early		Mangaorapan	(X)	Awheaiti Formation	Pukemuri Siltstone				
			Waipawan		Mungaroa Limestone					(X)
Paleocene	Late		Teurian	Manurewa Fm.	Awhea Formation	Mungaroa Limestone				Awheaiti Fm.
	Mid			Hunter Formation		Awhea Formation	Awhea Formation	Awhea Formation	Awhea Formation	Mungaroa Limestone
	Early				Manurewa Formation					Awhea Formation
					Manurewa Fm.	Manurewa Fm.	Manurewa Formation	Manurewa Fm.	Manurewa Fm.	
Cretaceous	Late	Mata	Haumurian	(X)	Whangai Formation	Whangai Formation (Rakuaroa Mbr.)	Whangai Formation (Rakuaroa Mbr.)	Whangai Formation (Rakuaroa Mbr.)	Whangai Formation (Rakuaroa Mbr.)	Not Studied
							Not Studied			
			Piripauan	Tyan Formation	Piripauan Sst.	Glenburn Fm.		Glenburn Fm. (X)	Not Studied	

Figure 2.2: Summary of Late Cretaceous–Paleogene stratigraphic units and nomenclature of the Tora area based on previous studies (Waterhouse, 1955; Waterhouse & Bradley, 1957; Moore & Morgans, 1990; Wasmuth, 1996; Laird *et al.*, 2003; Vellekoop, 2010), compared to the findings of this study.

The majority of the lower Paleogene formations at Tora were placed into the 'Awhea' Group by Moore *et al.* (1986) and consists of the Manurewa Formation, Awhea Formation, Mungaroa Limestone and Awheaiti Formation. The Manurewa Formation is conformably overlain by the Awhea Formation, consisting of 270 m of well-bedded glauconitic sandstone (Waterhouse & Bradley, 1957; Field, Uruski *et al.*, 1997; Begg & Johnston, 2000). The Mungaroa Limestone conformably overlies the Awhea Formation, and is divided into three recognisable members; a white calcareous siltstone (base), an alternating sequence of sandstones and siltstones (middle) and a porcellaneous micritic limestone (upper) (Waterhouse & Bradley, 1957; Browne, 1987). The limestone member is either considerably thinner or entirely absent in several stream sections at Tora. However, excellent exposures of the limestone member are observed at Te Kaukau and Manurewa Points (Waterhouse & Bradley, 1957; Browne, 1987). The Mungaroa Limestone is overlain by cm- to dm-bedded sandstone and siltstone of the Awheaiti Formation (Waterhouse & Bradley, 1957). Overlying the Awhea Group are an additional two formations; the Pukemuri Siltstone and the Wanstead Formation. An angular unconformity of *ca.* 15° separates the Awheaiti Formation and Pukemuri Siltstone (Waterhouse, 1955). The Pukemuri Siltstone is unconformably overlain by the basal conglomerate of the Wanstead Formation (previously the Kandahar Formation of Waterhouse (1955) and Waterhouse & Bradley (1957)). The Wanstead Formation comprises an estimated thickness of *ca.* 200 m of largely undifferentiated smectitic, calcareous mudstone that is extensively slumped and deformed, displaying poor outcrop expression. With the exception of the Wanstead Formation, these Paleogene units are restricted to the Tora Block. The Paleogene formations of the Tora area are described in detail in Chapter Four.

2.4   Paleoceanographic Setting during the Paleogene

The Antarctic continent is currently thermally isolated by the Antarctic Circumpolar Current (ACC), which plays a significant role in the global thermohaline circulation (Kennett & Exon, 2004; Lyle *et al.*, 2007). The Antarctic region also played a major oceanographic role in the early Paleogene, with Global Circulation Models (GCMs) suggesting that the Pacific Ocean alone was responsible for 80% of the global heat distribution (Huber & Sloan, 2001). The geometry of the Southern Hemisphere ocean basins differed significantly during the early Paleogene. Most notably, the modern Southern Ocean did not exist, there was no deep water flow through the Tasman Gateway between Australia and Antarctica, and the Drake Passage between South America and Antarctica had yet to open, preventing the development of a circumpolar current (Carter *et al.*, 1996; Exon *et al.*, 2004). Consequently, no significant oceanic fronts existed in the Southwest Pacific Ocean sector during the early Eocene until the initiation of a proto-subtropical front (STF) during the late Eocene and the development of the ACC in the Oligocene (Kennett *et al.*, 1975; Nelson & Cooke, 2001).

Model outputs and examination of proxy evidence produce conflicting evidence of ocean circulation patterns in the Southwest Pacific Ocean during the Eocene, resulting in two opposing models (*Figure 2.3*). Reconstructions based on proxy evidence (e.g. Murphy & Kennett, 1986; Nelson & Cooke, 2001) imply a warm, saline East Australian Current (EAC) which transported warm water masses polewards during the Eocene, potentially providing a mechanism for Antarctic warmth during this period (*Figure 2.3a*). Model outputs (e.g. Huber *et al.*, 2004) suggest that a northward flowing Tasman Current (TC) prevented the EAC from extending into the high southern latitudes (*Figure 2.3b*), which would imply that southward heat transport by the EAC is less significant than suggested by proxy evidence.

Paleotemperature studies through the Paleocene-Eocene transition (Bijl *et al.*, 2009; Hollis *et al.*, 2009, 2012) suggest that both scenarios may have operated at different times in the Paleogene, and help to explain the pronounced temperature contrast of *ca.* 10°C between the late Paleocene and the early Eocene: the TC and cool cyclonic gyre being predominant in the Paleocene; and the EAC and warm anticyclonic gyre predominant in the early Eocene. Given that the transition zone between these gyral systems currently straddles the Chatham Rise (i.e. the Subtropical Front), it is particularly useful to compare and contrast temperature records obtained from the East Coast and Canterbury Basins.
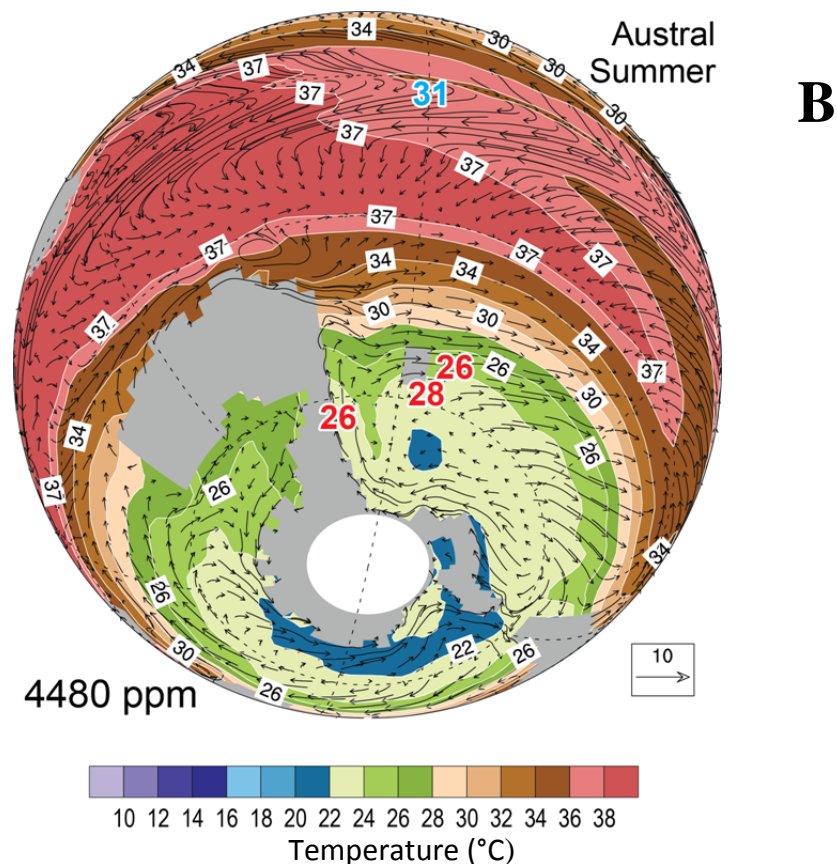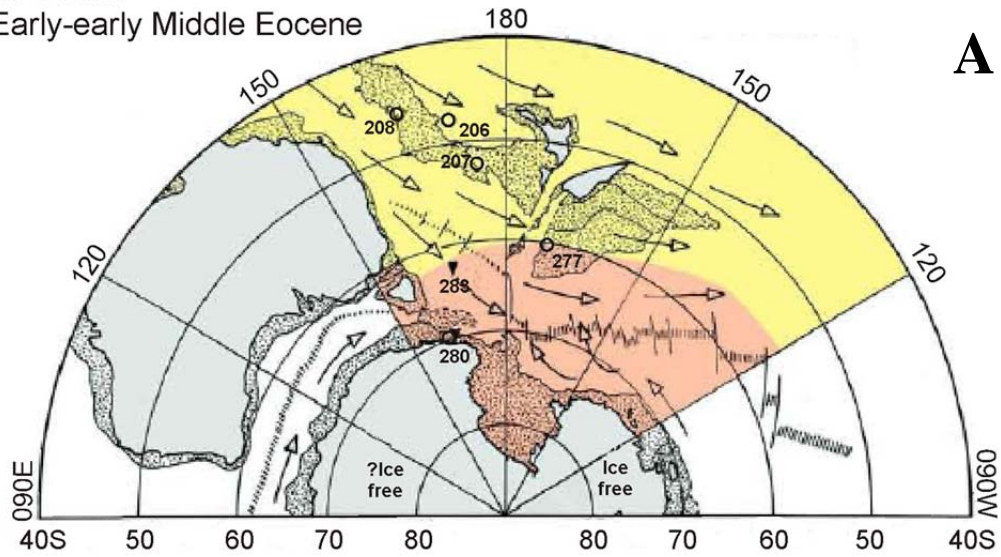
Figure 2.3: Alternative oceanographic scenarios for the Southwest Pacific Ocean during the Early to Middle Eocene. **A**) Reconstruction based on proxy-derived evidence modified from Nelson & Cooke (2001). DSDP drill sites labelled. **B**) Temperature and circulation patterns from a climate model output with an atmospheric CO_2 concentration of 4480 ppm. Arrow depicts vector magnitude. Modified from Hollis *et al*. (2012).

2.5 Sea Temperature Evolution of the Southwest Pacific

Stable isotope analysis of DSDP cores 277, 279 and 281 (Shackleton & Kennett, 1975) provided the founding basis for the development of a Paleogene marine temperature history in the Southwest Pacific region. Warm temperatures of the early Eocene were followed by a rapid cooling to the Eocene-Oligocene boundary, marking the onset of deep-water circulation in the Pacific. The New Zealand fossil record during the early Eocene is characterised by a warm subtropical or marginally tropical climate, as suggested by marine biota (e.g. the tropical planktic foraminifera genus *Morozovella*), coastal mangroves and *Cocos* trees (Hornibrook, 1992).

Multiple studies using a variety of proxies have been used to reconstruct sea temperatures during the early Paleogene in the Southwest Pacific (*Figure 2.4*). While the proxies show general agreement in the overall temperature trends, there are differences in the actual temperature variations. Recent sea temperature studies in the Southwest Pacific (Bijl *et al.*, 2009; Hollis *et al.*, 2009; Sluijs *et al.*, 2011) indicate that sea surface temperatures (SSTs) rose from *ca.* 26°C during the late Paleocene to *ca.* 33°C during the PETM (*Figure 2.4*). However, early Eocene TEX$_{86}$ SST values for the mid-latitude Southwest Pacific are >10°C warmer than predicted by climate model simulations for this latitude during the early Eocene (Sluijs *et al.*, 2011). A review of these data by Hollis *et al.* (2012) suggests that a combination of factors have resulted in anomalously warm temperature estimates derived from the TEX$_{86}$ proxy: choice of calibrations (use of the low temperature calibration reduces maximum temperatures by *ca.* 5°C); the role of the EAC delivering warm subtropical to tropical water into the SW Pacific; and a likely summer bias that applies to all proxy SST data (including Mg/Ca-based SSTs).

An equatorial Pacific Mg/Ca sea temperature record (ODP Site 865) displays a long-term warming trend from 27°C in the late Paleocene to 30°C in the early Eocene between 51.2–48.5 Ma (EECO), with a rapid cooling to *ca.* 28°C at 48 Ma (assuming 4.1 mol/mol Eocene Mg/Ca seawater concentration) (Tripati *et al.*, 2003; Hollis *et al.*, 2012). Kozdon *et al.* (2011) obtain similar temperatures (*ca.* 33°C) during the PETM from ion microprobe $\delta^{18}O$ analysis of foraminifera from ODP 865. This temperature record is several degrees warmer than previous $\delta^{18}O$ temperature estimates for the same site (Bralower *et al.*, 1995), with the likely cause of the discrepancy attributed to secondary calcite overgrowths on foraminiferal tests (Tripati *et al.*, 2003; Kozdon *et al.*, 2011). These low-latitude Pacific studies provide ocean temperature estimates comparable to those obtained from the mid- to high-latitude Southwest Pacific suggesting that minimal or no meridional temperature gradient characterised the early Eocene Pacific Ocean.
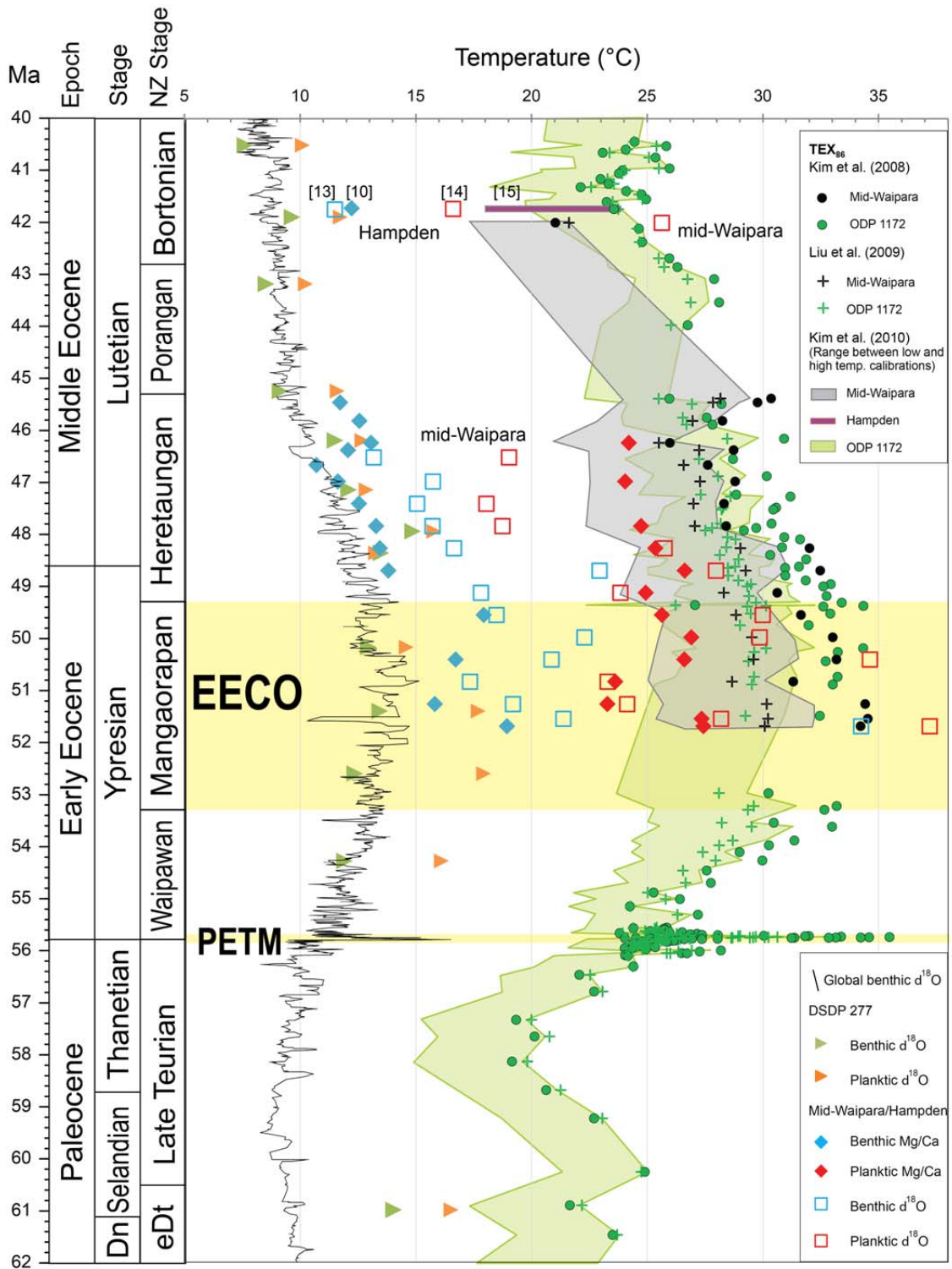
Figure 2.4: A compilation of Paleogene ocean temperatures from different proxies (TEX$_{86}$, δ^{18}O and Mg/Ca) for the Late Paleocene to Early Eocene of the Southwest Pacific plotted alongside the global benthic δ^{18}O record. Significantly elevated benthic (bottom water, BWT) and planktic (sea surface, SST) temperatures are evident for the Paleocene–Eocene Thermal Maximum (PETM) and the Early Eocene Climatic Optimum (EECO). Four alternative calibrations are shown for TEX$_{86}$-derived SSTs, with current studies (Hollis *et al.*, 2012) indicating that the low temperature calibration of Kim *et al.* (2010) is the best estimate of Paleocene–Eocene SST in the Southwest Pacific. Figure supplied by C. Hollis.

2.6   Trace Element Chemistry of Foraminifera

Calcium in biogenic calcite skeletal structures can be substituted by a variety of divalent cations such as Cd, Fe, Mg, Ni, Sr, Co, Zn and Mn (Nurnberg *et al.*, 1996). Ratios of these elements in seawater reflect their addition and removal from the oceans and exert a control over many geochemical processes, such as the precipitation of aragonite (high seawater Mg/Ca concentrations) as opposed to calcite (low seawater Mg/Ca concentrations), as well as affecting precipitation of biogenic carbonates and the distribution of carbonate sediments (Coggon *et al.*, 2010).

Fluxes in the major ion chemistry of seawater (Na^+, K^+, Ca^{2+}, Cl^-, SO_4^{2-} and HCO_3^-) are largely driven by geochemical processes, particularly changes in the rate of carbonate deposition, continental weathering, and the production and hydrothermal alteration of oceanic crust (Elderfield & Schultz, 1996; Lowenstein *et al.*, 2001). Trace element concentrations in seawater (e.g. Ti, Mn, Zn, Ba) are more readily affected by biological processes, terrigenous and hydrothermal inputs, precipitation of insoluble particulate phases (e.g. barite), and 'scavenging' (adsorption into solid surfaces) by particulate matter of dissolved cations from solution as they progress through the water column (Balistrieri *et al.*, 1981). Particular elements serve different roles in the ocean system and can provide proxies for environmental information (Boyle, 1981; Marchitto *et al.*, 2000, Anand *et al.*, 2003; Morel & Price, 2003). A primary consideration in the extraction of environmental proxy records from foraminiferal calcite is the ocean residency time of the elements in seawater, which vary on differing timescales (*Table 2.1*). Elements incorporated in foraminiferal calcite and analysed in this study are discussed below.

Table 2.1: Oceanic residency times of elements used in this study.

Element	Ocean residency Time (*ca.* Ma)	Source
Mg	13×10^0	Broeker & Peng (1982)
Al	6.2×10^{-4}	Brand *et al.* (1983); Morel *et al.* (1991)
Si	1.7×10^{-4}	Savenko (2008)
Ca	1.0×10^0	Broeker & Peng (1982)
Ti	8.6×10^{-3}	Savenko (2008)
Mn	76×10^{-5}	Savenko (2008)
Zn	5.1×10^{-4}	Brand *et al.* (1983); Morel *et al.* (1991)
Sr	5.0×10^0	Broeker & Peng (1982)
Ba	10×10^{-3}	Paytan *et al.* (2007)

Magnesium

The primary source of Mg in the ocean is the weathering of continental rocks, and its removal from the ocean system is due to deposition of dolomite and hydrothermal alteration in mid-ocean ridge settings. The application of Mg incorporation into carbonates as a paleo-ocean thermometer has long been recognised. Clark & Wheeler (1922) proposed the potential of Mg substitution in carbonates as a paleo-ocean temperature proxy. Emiliani (1955) recognised the implications of detrital contaminants artificially increasing the trace element concentrations (particularly Mg, Al, Zn and Ba) of foraminiferal calcite, and the potential impact on Mg/Ca paleo-ocean thermometry. Subsequent experimental studies demonstrated that the substitution of Mg into inorganic calcite was temperature dependent (e.g. Mucci & Morse, 1983; Oomori *et al.*, 1987).

Culturing experiments have shown that the concentration of Mg into foraminiferal calcite is dependent on the endothermic substitution of Mg for Ca within the calcite matrix (e.g. Nurnberg *et al.*, 1996; Lea *et al.*, 1999), forming the basis of the Mg/Ca paleo-ocean thermometer. Mg/Ca values exhibit an exponential relationship with temperature, indicating that temperature is the primary control on the incorporation of Mg into foraminiferal calcite (Lear *et al.*, 2002). This process is favoured at high temperatures, resulting in an exponential increase in the Mg/Ca ratio of *ca.* 3–9%/°C in foraminiferal calcite (Anand *et al.*, 2003). The consequence of this is that as a paleo-ocean thermometer, the Mg/Ca proxy increases in sensitivity at higher temperatures.

Temperature dependency of Mg incorporation into foraminifera varies between species, requiring species-specific calibrations. Sea temperatures are calculated using an exponential relationship between Mg/Ca and temperature expressed in *Equation 2.1*, where *A* and *B* are species-dependent pre-exponential and exponential constants, respectively, Mg/Ca_{sw-t} is the paleo-Mg/Ca seawater ratio, Mg/Ca_{sw-0} is the modern Mg/Ca seawater ratio, and *T* is temperature (Lear *et al.*, 2002; Anand *et al.*, 2003).

$$Mg/Ca = \frac{Mg/Ca_{sw-t}}{Mg/Ca_{sw-0}} \times A \times \exp^{B \times T} \qquad \qquad Equation\ 2.1$$

The temperature sensitivity of foraminiferal calcite to Mg incorporation means that secondary environmental factors (e.g. salinity and carbonate ion saturation) have a less significant control on the incorporation of Mg in foraminiferal calcite.

There are two possible mechanisms suggested for the incorporation of trace metals into foraminiferal calcite. The first mechanism involves substitution of the trace element directly into foraminiferal calcite via solid solution (Lea, 1999). The second mechanism involves 'trapping', where the metal ion becomes imbedded within the calcite lattice during the precipitation of the calcite (Lea, 1999; Erez, 2003). However, the actual mechanism of incorporation is not known at present, and potentially varies between both species and trace elements. In addition to Mg, several of the transition metals form solid solutions in the carbonate phase and may be utilised as proxies for environmental conditions other than temperature and as indicators for post-depositional chemical alteration of primary foraminiferal calcite. Additional trace elements analysed in this study include Al, Si, Ti, Mn, Zn, Sr and Ba.

Aluminium, Titanium & Silicon

Aluminium, Ti and Si do not directly substitute into calcite, but indicate the presence of detrital sediments which have high concentrations of Al, Ti and Si relative to calcite, and are utilised in this study to monitor potential silicate contamination from clay minerals. Silicate minerals are high in Mg, and thus silicate contamination of foraminiferal samples can cause temperature estimates derived from the Mg/Ca paleo-ocean thermometer to be erroneously high. Al/Ca, Si/Ca and Ti/Ca ratios are commonly applied to screen for the effects of silicate contamination in foraminiferal Mg/Ca (e.g. Barker *et al.*, 2003; Greaves *et al.*, 2005).

Conventionally, Al has been used to quantitatively determine the amount of terrigenous material in marine sediments (Murray & Leinen, 1996). However, scavenging of Al by particulate matter as it descends down through the water column can create Al enrichment. Consequently, the sole use of Al as an indicator of terrigenous sediment may overestimate the true terrigenous load by a factor of two, particularly in biogenic sediments (Murray & Leinen, 1996). Titanium, which is mineralogically bound to the terrigenous fraction (with >95% of Ti contained in silicate phases, as compared with Al of which *ca.* 50% is associated with biogenic components), can provide a better indication of terrigenous input (Murray & Leinen, 1996). Titanium is a common minor constituent element in clay minerals, pyroxenes and amphiboles (Skrabal & Terry, 2002). The most commonly occurring Ti-bearing phases are ilmenite ($FeTiO_3$), sphene ($CaSiTiO_5$), titaniferous magnetite (Fe_3O_4) and hematite (Fe_2O_3), as well as the TiO_2 polymorphs (rutile, anatase and brookite). The high resistance of titaniferous minerals to chemical weathering has resulted in the use of Ti as an index element against which the mobility of other elements is

measured (Correns, 1978). Acid dissolution can make Ti soluble, allowing its mobilisation in rocks and minerals (Skrabal & Terry, 2002). As such, Ti may indicate both dissolution and silicate contamination in foraminiferal calcite. The major processes controlling the concentration of dissolved Ti in seawater is scavenging in particulate matter in low salinity zones of the surface ocean and regeneration in the deep ocean (Orians *et al.*, 1990; Skrabal & Terry, 2002).

Sediment derived from terrigenous sources is particularly high in Si, especially in the case of quartz- and feldspar-dominated mineral assemblages. However, in marine settings, silica in sediments can also have a biogenic origin.

Manganese

Variations in the Mn/Ca values of foraminiferal calcite can add to the understanding of factors that influence test composition that are unrelated to primary elemental changes in seawater chemistry (Lea & Martin, 1996). The Mn content of foraminiferal calcite typically reflects post-depositional diagenetic processes and the precipitation of Mn carbonate and oxyhydroxide phases (Boyle, 1983; Lea, 1999). These phases are an important product of redox reactions in suboxic sediments and are often associated with significantly elevated Mg/Ca ratios (Boyle, 1983; Pena *et al.*, 2005).

Zinc

Zinc is concentrated in the deep ocean due to its role as an ocean micronutrient and subsequent biogenic export from surface waters to the deep ocean (Morel & Price, 2003). Zinc is remobilised by dissolution, and Zn/Ca ratios of benthic foraminifera track dissolved bottom water Zn concentrations and the calcite saturation state of bottom water (Marchitto *et al.*, 2000). Dissolved Zn concentrations of bottom water are controlled by the circulation of deep-water masses. Therefore, Zn/Ca ratios may provide a record of the distribution and circulation of deep water masses as well as carbonate ion concentrations (Marchitto *et al.*, 2000). The utilisation of fossil foraminiferal Zn as a nutrient proxy is restricted due to its high susceptibility to contamination by secondary diagenetic effects (Boyle, 1981; Lea, 1999).

Strontium

In addition to Ca and Mg, Sr forms one of the most important solid solution substitutions in the carbonate series. The larger ionic radius of Sr^{2+} compared with Ca^{2+} causes it to typically form a solid solution with the aragonite structure (Speer, 1983). Strontium content has been shown to increase with the increasing Mg content of carbonates, although no temperature control has been demonstrated for the incorporation of Sr into foraminiferal calcite (Lea *et al.*, 1999).

Despite this, Sr is a useful element to monitor because both the Sr/Ca ratio and isotopic concentration of pore fluids are sensitive to carbonate recrystallisation (Schrag *et al.*, 1995). Due to biological effects, carbonate precipitated from pore-waters in sea floor sediments is enriched in Sr relative to biogenic calcite precipitated in equilibrium with seawater (Schrag *et al.*, 1995). Dissolution of carbonate on the sea floor increases the Sr concentration of pore fluids and, therefore, secondary calcite precipitated from solution is enriched in Sr relative to primary biogenic calcite (Schrag *et al.*, 1995). Variations in Sr/Ca values of foraminiferal calcite can thus identify diagenetic or growth factors that may in turn have influenced the concentrations of other trace elements (Lea & Martin, 1996).

Barium

Barium tends to be depleted in surface waters and enriched at depth which is primarily a function of the precipitation of barite at the surface, which is formed in conjunction with particulates, and subsequently sinks and re-dissolves at depth or becomes incorporated into sediments (Bishop, 1988; Lea, 1999). Barium may represent an oceanic productivity indicator, as elevated Ba concentrations are found beneath the most productive areas of the oceans (Shimmield *et al.*, 1988; Dymond *et al.*, 1992). The Ba/Ca ratio of benthic and planktic foraminifera can be used to reconstruct the Ba composition of ocean floor and surface waters, respectively (Lea & Boyle, 1989; 1991). Therefore, Ba/Ca ratios may be a proxy for biological productivity and changes in deep ocean circulation (Lea, 1999), although Ba/Ca ratios of foraminifera are readily biased by the presence of barite in sediments and diagenetic overprints.

2.7 Key Parameters and Assumptions in Mg/Ca Paleo-Ocean Thermometry

In order to reliably reconstruct a sea temperature history from fossil foraminiferal calcite using *Equation 2.1*, a number of variables and factors must be taken into account apart from just the measured Mg/Ca ratio. The most notable of these are the Mg/Ca ratio of seawater at the time the species was extant, foraminiferal vital effects that are corrected by the application of species-specific calibration constants, and assessment of whether the primary foraminiferal calcite Mg/Ca value has indeed been preserved.

2.7.1 Eocene Seawater Mg/Ca ratio

The Mg/Ca ratio of seawater has changed over time as a function of variations in the flux of Mg into the ocean (hydrothermal and continental weathering) and Mg drawdown into marine sediments. Due to the oceanic residence time of Mg (10–13 Myr) and Ca (1–2 Myr), changes in seawater Mg/Ca ratios are insignificant on glacial-interglacial time scales, but become relevant on timescales of tens of millions of years (Lear *et al.*, 2002). The Mg/Ca ratio of Eocene seawater (Mg/Ca$_{sw}$) has been the subject of much debate. Low values (<3 mol/mol; *Table 2.2*) suggested by long-term modelling and inorganic geochemistry result in unreasonably high sea temperatures (Tripati *et al.*, 2003; Sexton *et al.*, 2006a; Hollis *et al.*, 2012). *Figure 2.5* shows how the assumed seawater Mg/Ca ratios affects sea temperature determinations from foraminiferal calcite.

Table 2.2: Estimates of values for Eocene seawater Mg/Ca ratios.

Study	Method	Eocene Mg/Ca$_{sw}$ (mol/mol)
Wilkinson & Algeo (1989)	Modelled	4.07
Stanley & Hardie (1998)	Modelled	1.6
Zimmermann (2000); Lowenstein *et al.* (2001)	Fluid inclusions	2.5–3.7
Lear *et al.* (2002)	Foraminifera Mg/Ca	3.3–4.6
Dickson (2004)	Echinoderms	1.7
Horita *et al.* 2002	Halite inclusions	2.4
Coggon *et al.* (2010)	CaCO$_3$ veins	1.5–2.5

The relationship between benthic foraminiferal Mg/Ca ratios and bottom water temperatures was revised by Lear *et al.* (2002), and application of the revised calibration to Cenozoic foraminifera used to infer that Eocene Mg/Ca_{sw} was no more than 35% lower than the modern value of 5.16 mol/mol, and most likely within the range of 3.3–4.6 mol/mol. Tripati *et al.* (2003) utilised bracketed Mg/Ca_{sw} values of 3.0–3.5 and 5.1 mol/mol for tropical Mg/Ca paleo-ocean temperature reconstructions. Sexton *et al.* (2006a) combined paired Mg/Ca and $\delta^{18}O$ records from well-preserved Eocene foraminifera, and showed that for Eocene Mg/Ca_{sw} values of 3.1–5.1 mol/mol, the higher values resulted in the best fit with $\delta^{18}O$-based temperatures (assuming ice-free conditions). Middle Eocene paleo-ocean temperatures derived by Burgess *et al.* (2008) utilised a Mg/Ca_{sw} value of 4.07 mol/mol (after Wilkinson & Algeo, 1989), which yielded a good agreement between Mg/Ca, $\delta^{18}O$ and TEX_{86} proxies. A Mg/Ca_{sw} ratio of 3.35 mol/mol was adopted for paleo-ocean temperature reconstructions in the Canterbury Basin, based on the Lear *et al.* (2002) findings (Hollis *et al.*, 2009; Creech *et al.*, 2010; Creech, 2010). However, Hollis *et al.* (2012) adopted a higher value of 4.0 mol/mol, which is consistent with Cenozoic Mg/Ca_{sw} ratios modelled by Wilkinson & Algeo (1989) and in line with the observations of other studies (Lear *et al.*, 2002; Tripati *et al.*, 2003, Sexton *et al.*, 2006a). Reconciling the discrepancies between estimates for Eocene Mg/Ca_{SW} derived from foraminifera and other methods will require more thorough consideration of the effects of carbonate ion saturation state and in Mg partitioning during calcification (Lear *et al.*, 2010; Hasiuk & Lohmann, 2010; Cramer *et al.*, 2011). In this study, a Mg/Ca_{SW} value of 4.1 mol/mol has been adopted to provide conservative temperature estimates for the Early Eocene that are in line with multiproxy paleotemperature determinations (after Hollis *et al.*, 2012).
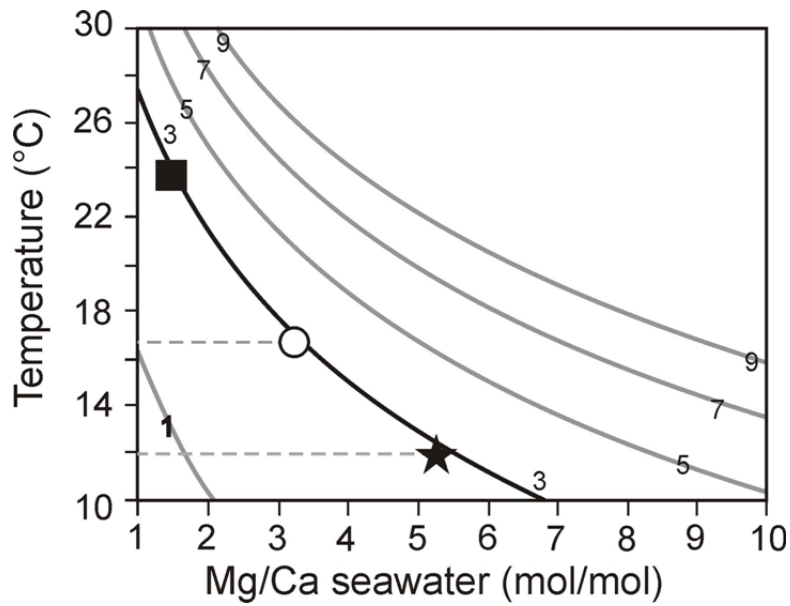
Figure 2.5: Demonstration of the sensitivity of temperature reconstructions to seawater Mg/Ca ratios at 48–49 Ma (adapted from Billups & Schrag, 2003). Contours represent benthic foraminiferal Mg/Ca ratios (in mmol/mol) derived using the Lear *et al.* (2002) calibration. The square denotes the intersection between foraminiferal Mg/Ca ratios and seawater Mg/Ca ratios from Stanley & Hardie (1998). The open circle marks the intersection between foraminiferal Mg/Ca ratios and the seawater Mg/Ca ratios of Wilkinson & Algeo (1989) and the star shows the relationship between observed foraminiferal calcite Mg/Ca and modern Mg/Ca ratio of seawater (Elderfield & Schultz, 1996).

2.7.2   Mg/Ca–Temperature Calibration

Only a few genera of Eocene foraminifera are still extant, necessitating the use of calibrations developed from modern species (e.g. Lear *et al.*, 2000, 2002) and multi-species calibrations (e.g. Anand *et al.*, 2003) in this study. A calibration is required to translate the exponential relationship between foraminiferal calcite Mg/Ca values to a sea temperature record (*Figure 2.6*). A number of Mg/Ca sea temperature calibrations exist for modern planktic foraminifera (*Table 2.3*), but there are limited calibrations available for benthic foraminifera (Billups & Schrag, 2003). Biological or vital effects on the incorporation of Mg into foraminiferal calcite appear to be exaggerated in benthic foraminifera, making genus-specific calibrations essential for the reliable determination of past bottom water temperatures.
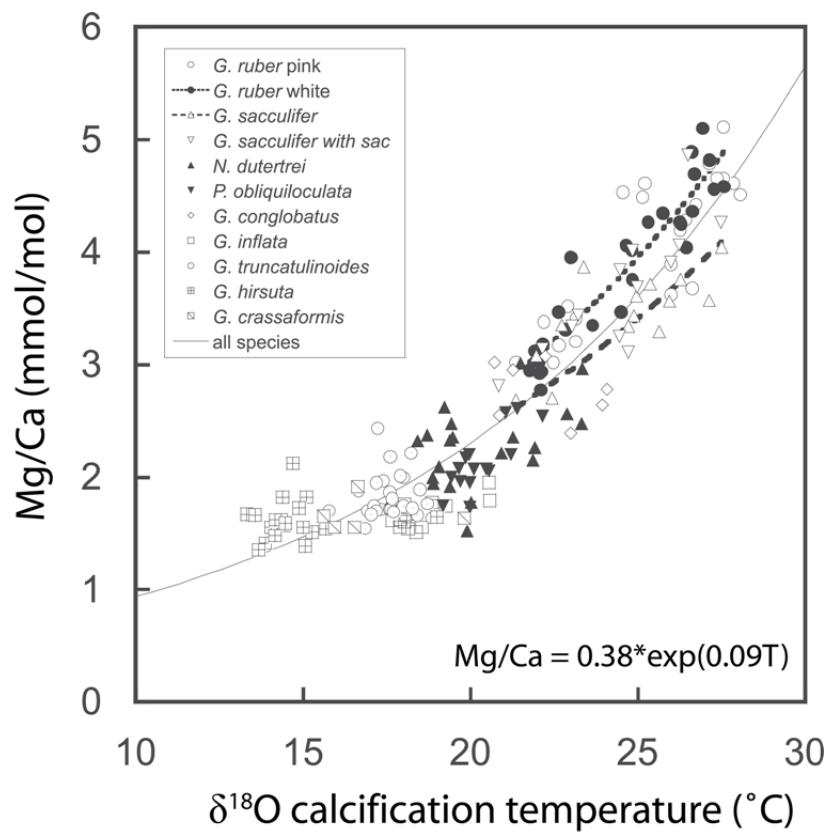
Figure 2.6: Mg/Ca–temperature calibration from ten planktic foraminifera species selected from coretop samples, with a fitted calibration curve displaying the exponential relationship between the Mg/Ca ratio of foraminiferal calcite and the calcification temperature (determined by oxygen isotope data). Modified after Anand *et al.* (2003).

Table 2.3: Examples of species-specific calibration constants for various foraminifera.

Species	Source	*A*	*B*	Reference
Neogloboquadrina pachyderma	Coretop samples	0.46	0.088	Nurnberg *et al.* (1995)
Globigerina sacculifer	Culture	0.39	0.089	Nurnberg *et al.* (1996)
Globigerina bulloides	Culture	0.53	0.102	Lea *et al.* (1999)
Globigerinoides ruber	Coretop samples	0.30	0.089	Lea *et al.* (2000)
Mixed	Coretop samples	0.52	0.100	Elderfield & Ganssen (2000)
Mixed	Sediment trap	0.38	0.09	Anand *et al.* (2003)
Cibicidoides spp.	Coretop samples	0.87	0.109	Lear *et al.* (2002)
Hoeglundina elegans	Coretop samples	0.96	0.034	Rosenthal *et al.* (2006)

2.7.3   Preservation of Foraminiferal Calcite

In order to reliably reconstruct past ocean temperatures from the chemistry of foraminifera tests, it is important to ascertain the extent to which diagenesis has affected test chemistry, particularly the stable isotope and trace element chemistry. Ocean thermometers dependent on biogenic calcite ($\delta^{18}O$ and Mg/Ca) are influenced by the presence and composition of secondary calcite, with recrystallisation generally biasing temperature estimates towards cooler values (Tripati *et al.*, 2003). Subsequently, ambiguities associated with interpreting the $\delta^{18}O$ record have yielded a discrepancy between proxy records, termed the 'cool tropics paradox' (Tripati *et al.*, 2003; Sexton *et al.*, 2006a), which is now inferred to be a function of diagenetic overprinting, whereby the oxygen isotope ratios of decalcified outgrowths bias recovered sea temperatures to erroneously low values (Kozdon *et al.*, 2011). Temperatures may be biased towards higher values by the addition of secondary calcite from diagenetic fluids post-burial, and contamination from Mg-rich silicate minerals.

A range of diagenetic processes may affect a foraminiferal test after death during its descent through the water column and subsequent incorporation and burial in sea floor sediment. These processes may be divided into three distinct categories; overgrowths, dissolution, and recrystallisation (Pearson & Burgess, 2008).

Overgrowth occurs when inorganic calcite is precipitated on the exterior or interior surfaces of the test. In calcareous sediments, it is common for tests to be completely infilled with diagenetic calcite. This inorganic calcite can often be visually distinguished because it consists of large equant and euhedral crystals. Dissolution has been shown to preferentially remove Mg^{2+} during early stages of dissolution, resulting in lower Mg/Ca ratios (Pearson *et al.*, 2006). Recrystallisation is a less obvious process in which the original microgranular structure of the test is replaced by larger, more equant crystals, with the end state of this process typically consisting of loosely packed, blocky calcite crystals (Pearson & Burgess, 2008). One of the most obvious indicators of recrystallisation is the replacement of the translucent ('glassy') appearance of well-preserved specimens with an opaque 'frosty' texture (*Figure 2.7*; Pearson *et al.*, 2001; 2006; Pearson & Burgess, 2008). These two conditions, 'glassy' and 'frosty' represent end-member states, with a continuum of potential appearances in between these. Frequently, frosty material has only undergone comparatively minor diagenetic alteration, and material that has processed further through the process may be described as 'chalky'. Foraminifera may be entirely recrystallised without displaying any significant overgrowths or infilling, whilst in other cases they may be

completely infilled whilst retaining the original microgranular structure (Pearson & Burgess, 2008).

The mode of diagenetic alteration depends on a combination of several factors, including time, burial history, sediment composition, pore water chemistry and burial temperature (Pearson & Burgess, 2008). Fossil tests sourced from relatively impermeable clay-rich sediments tend to exhibit near-pristine microgranular structures, whereas tests from carbonate oozes in deeper oceanic settings are almost always recrystallised to some degree (*Figure 2.7*; Pearson *et al.*, 2001; Pearson & Burgess, 2008).
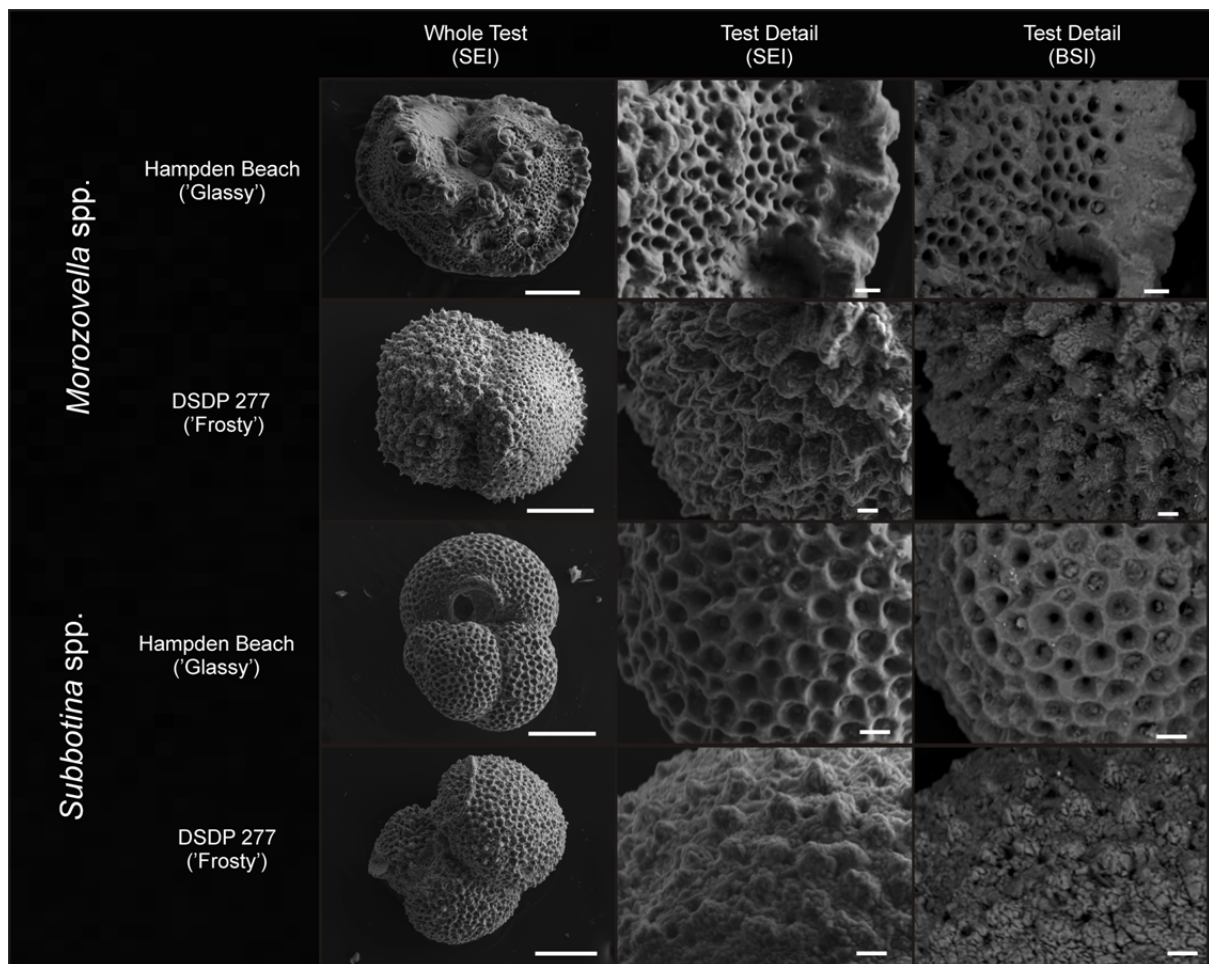
Figure 2.7: Comparison of examples of 'glassy' and 'frosty' *Morozovella* spp. and *Subbotina* spp. foraminifera in early Eocene sediments from Hampden Beach and DSDP Site 277 showing how 'frosty' foraminifera may appear to be well preserved, yet display signs of recrystallisation of micron-scale features on the test surface. Scale bars on whole test images images are 100 μm in length, whilst scale bars on test surface images are 10 μm long. SEI = scanning electron image, BSI = back-scatter electron image. Hines, *unpublished data.*

2.7.4 *Laser Ablation Analysis*

The application of the laser ablation method allows distinct chamber and chamber wall layer compositions to be resolved within tests and individual chambers (Eggins *et al.,* 2003). Surface veneers enriched in Mg, Mn, Zn and Ba are found on all fossil specimens and live-sampled (plankton-tow) tests of *Globerginoides ruber*, potentially suggesting a biological, rather than diagenetic origin for the enriched mantle (Eggins *et al.*, 2003). These veneers would induce a warm temperature bias in bulk test composition analyses that is not reflective of the true environmental conditions (Eggins *et al.*, 2003). The application of the laser ablation inductively coupled plasma mass spectrometry (LA-ICP-MS) method avoids this issue. A further major advantage of using the laser ablation method is that the foraminifera test is preserved for any subsequent work, such as stable isotope analysis or electron microscopy, which allows sources of potential error or contaminant(s) to be identified. This is particularly important for the application to Eocene foraminifera in this study, where there are limited numbers of foraminifera, and considerable potential for detrital and diagenetic contamination.

An additional benefit of applying the laser ablation technique is that less exhaustive cleaning measures are required prior to the analysis of individual foraminifer tests. Oxidative and reductive cleaning methods can significantly reduce the measured Mg/Ca values of fossil foraminifera (Martin & Lea, 2002). Mg-bearing contaminants originating from remnant foraminiferal organic matter can be removed through thorough rinsing of the test in distilled water and methanol (Martin & Lea, 2002). Although this method does not remove exterior Fe-Mn oxy(hydroxides) and mixed Mn-Ca-Mg authigenic coatings, which form a fine film on the exterior of the fossil tests, the effects of these contaminants can be avoided by the application of the laser ablation method and the screening of individual ablation depth profiles (refer to Chapter Three).

2.8 Other Relevant Paleoclimate Proxies Utilised in this Study

2.8.1 Bulk Carbonate Stable Carbon and Oxygen Isotopes

Changes in the ratio of carbon stable isotopes (^{12}C, ^{13}C) in carbonates provide information regarding perturbations of the carbon cycle. Typically, stable carbon isotopes represent the modulation of a global signal by local effects. Changes in the marine $\delta^{13}C$ record generally reflect changes in the size of the terrestrial biosphere and/or a disruption of the carbon cycle due to alteration of a geological source or sink, release of gas hydrates, volcanic degassing or organic matter accumulation (Zachos et al., 2008; Zeebe et al., 2009). The onset of the PETM and EECO were both accompanied by a large negative shift in $\delta^{13}C$ recorded in marine sediments (Zachos et al., 2001), making carbon isotope analysis a useful correlation tool in calcareous sediments of this age (e.g. Hollis et al., 2005b). Carbon isotopes are less prone to diagenetic alteration than oxygen isotopes as the $\delta^{13}C$ ratio of pore waters is buffered by the seafloor carbonate reservoir (Sexton et al., 2006a).

The ratio of the stable isotopes of oxygen (^{16}O, ^{18}O) is perhaps the most established geochemical paleo-ocean thermometer, which provided the first quantitative Cenozoic paleo-ocean temperature records (Shackleton & Kennett, 1975). The use of oxygen stable isotopes of oxygen as a paleo-ocean thermometer was first suggested by Urey (1947), and further developed by Epstein et al. (1951), who determined a calibration for the temperature-dependent fractionation of oxygen isotopes between molluscan carbonate and water. Emiliani (1955) then applied this method to planktic foraminifera from deep sea cores, showing that foraminifera precipitate their tests in isotopic equilibrium with seawater, enabling their application in paleoclimatic studies, provided the isotopic composition of seawater ($\delta^{18}O_{sw}$) is known.

The ratio of ^{18}O to ^{16}O ($\delta^{18}O$) of foraminiferal calcite is primarily dependent on two factors; temperature and global ice volume. $\delta^{18}O_{sw}$ is dependent on ice volume because the lighter isotope (^{16}O) is preferentially removed from the oceans by evaporation, and when this is precipitated as snow and locked in continental ice sheets, the ocean becomes enriched in the heavier ^{18}O isotope. The precipitation and accumulation of "lighter" water in continental ice sheets removes a substantial proportion of ^{16}O from the system. Therefore, changes in global ice volume can have a significant effect on the $\delta^{18}O$ value of seawater. This can lead to some uncertainty in paleo-ocean temperature determinations, particularly during the Eocene, where the presence or absence of Antarctic ice sheets is a matter of controversy (Dawber & Tripati, 2011).

Therefore, certain assumptions must be made with respect to ice volume and the isotopic composition of ice sheets when applying the stable oxygen isotope paleo-ocean thermometer. When applying an ice volume correction for paleo-ocean temperature calculations, values used for $\delta^{18}O_{sw}$ assuming an ice-free world are usually either –1.0‰ or –1.2‰ PDB (e.g. Shackleton & Boersma, 1981; Zachos *et al.*, 1994).

The bulk carbonate $\delta^{18}O$ signal represents an amalgamation of values sourced from planktic and benthic foraminifera, calcareous nannofossils, as well as any inorganic calcite present. Typically, the bulk carbonate $\delta^{18}O$ record has an intermediate value between planktic and benthic foraminiferal $\delta^{18}O$ values, with diagenetic calcite creating more negative values. The $\delta^{18}O$ signal can be affected by diagenesis and interaction with pore waters (Hollis *et al.*, 2003). Nelson & Smith (1996) showed that Late Cretaceous to early Paleogene micritic limestones in New Zealand yield more depleted $\delta^{18}O$ values than many other Cenozoic limestones. Several potential explanations are possible, including increased burial pressures and tectonic stresses, diagenetic alteration, and/or warmer (and more $\delta^{18}O$ depleted) oceans during the Late Cretaceous to early Paleogene.

Both the isotopic ratios of carbon and oxygen in carbonates are usually expressed in delta notation in per mil (‰) units difference, relative to a standard (typically the Pee Dee Belemnite (PDB) for carbonates). Calculation of the delta notation for oxygen isotopes is shown in *Equation 2.2*.

$$\delta^{18}O\ (\text{‰}) = \left(\frac{\left[\frac{^{18}O}{^{16}O}\right]_{sample} - \left[\frac{^{18}O}{^{16}O}\right]_{standard}}{\left[\frac{^{18}O}{^{16}O}\right]_{standard}} \right) \times 1000 \qquad \textit{Equation 2.2}$$

2.8.2 *GDGT-based SST proxies*

The development of thaumarchaeol lipid-derived SSTs, such as TEX_{86}, which are based on the relative abundance of glycerol dialkyl glycerol tetraethers (GDGTs), provides an alternative quantitative temperature proxy that is independent of foraminiferal calcite. The TEX_{86} index (TetraEther indeX of the tetraethers consisting of 86 carbon atoms) is based on the distribution of cyclopentane rings in sedimentary membrane lipids derived from marine thaumarchaeota, which has a linear correlation with mean annual SST. Using this correlation, Schouten *et al.*

(2002) developed a calibration relating the TEX_{86} index to SST. As laboratory studies and core-top sampling has progressed, several new calibrations have been developed (e.g. Liu *et al.*, 2009; Kim *et al.*, 2010). Most recently, Hollis *et al.* (2012) developed a paleo-calibration by relating TEX_{86} values to independently-derived SST estimates in several Eocene records. They showed that for the middle- to high-latitude Southwest Pacific, the best match between the paleo-calibration and modern calibrations was with the low temperature calibration of Kim *et al.* (2010).

2.8.3   *Faunal assemblages*

In addition to providing chronologic constraints, marine microfossil assemblages can provide qualitative assessments of paleoenvironmental and paleoclimatic conditions through comparison with modern assemblages and their known environmental preferences. Marine microfossils have been extensively used to both qualitatively and quantitatively reconstruct paleoenvironmental conditions, including ocean temperatures, salinity, oxygenation, nutrient availability and productivity. Various microfossils preserved in sediments can be utilised, such as radiolarians, dinoflagellates, foraminifera and nannofossils (Crouch & Brinkhuis, 2005; Hollis, 2006). These organisms are particularly useful for age and paleoenvironmental identification as they tend to be widespread, and at least one group is preserved in most types of marine sediment (Brasier, 1980).

Benthic foraminifera are particularly useful to provide paleodepth constraints in addition to bottom water oxidation, temperature and salinity (Kaiho, 1994; Hayward *et al.*, 2010) as well as the redox state of the seafloor sediments. However, benthic foraminifera can tolerate a wide range of conditions, so it is often beneficial to consider the entire benthic assemblage.

The proportion of cold and temperate species present in planktic foraminiferal assemblages can indicate the temperature of the overlying water column. However, the temperature preferences of early Paleogene foraminifera are not known with certainty as there are no extant representatives of this fauna. Despite this, the restricted latitudinal extent of particular species can make them reasonable indicators of relative SSTs. In addition, stable isotope analysis of individual foraminifera species within an assemblage can provide constraints on their depth preference within the water column (*Figures 2.8 & 2.9*).

2.9   Foraminiferal Ecology

An important factor that should be taken into consideration for Mg/Ca paleo-ocean temperature estimates is species-specific habitats and life cycles. Foraminifera are a diverse group of marine, single-celled protists that shield their protoplasm with a secreted calcareous ($CaCO_3$) skeletal structure, called a test, and inhabit all aspects of the marine environment from shallow marginal marine environments to abyssal settings below the carbonate compensation depth (CCD) (Wade *et al.*, 2008; Hayward *et al.*, 2010). The preservation and accumulation of foraminifera tests in the sedimentary fossil record can be interpreted to determine the relationships between climatic and paleoceanographic controls (Wade *et al.*, 2008).

The environment inhabited by particular foraminifera species has significant implications for paleo-ocean temperature interpretations. The foraminifera species used in this study are extinct, and information pertaining to the ecology of these species is somewhat limited. Test morphology is not a particularly strong indicator of the ecology of planktic foraminifera. For example, *Acarinina* and *Morozovella* species have both been shown to be strongly photosymbiotic with non-spinose tests, which strongly contrasts with all modern foraminifera known to bear photosymbionts that are muricate and non-keeled (D'Hondt *et al.*, 1994). In the late Paleocene to middle Eocene, spinose and keeled *Morozovella* and *Acarinina* species dominated near-surface planktic foraminiferal faunas, whereas spinose and non-keeled taxa (e.g. *Subbotina* spp.) inhabited deeper and cooler water masses. This is the opposite of the relationship between test morphology and habitat occupation exhibited by planktic foraminifera in the modern oceans (D'Hondt *et al.*, 1994).

Carbon and oxygen stable isotope analysis of individual species within an assemblage provide some of the most robust insights into the ontogeny (life cycle) of extinct Paleogene planktic foraminifera. Foraminifera that contained photosymbionts exhibit higher values of $\delta^{13}C$, whilst asymbiotic taxa demonstrate lower values with considerable variability (*Figure 2.8*). Details of species utilised in this study are listed in *Table 2.4*.
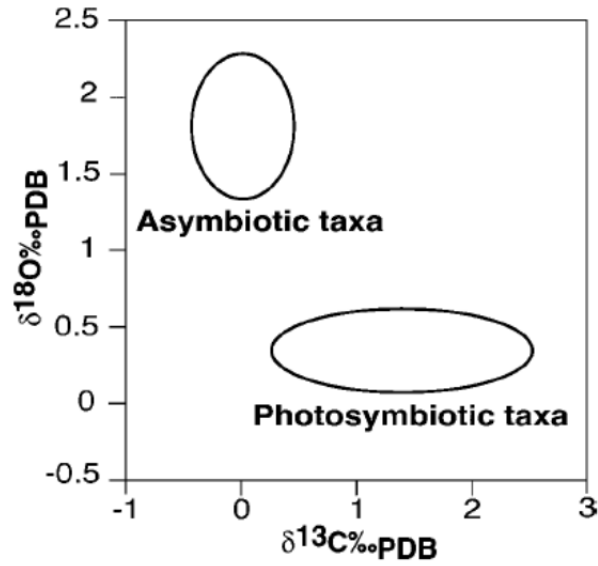
Figure 2.8: Model for the identification of symbiotic relationships in planktic foraminiferal calcite from carbon and oxygen stable isotope variations. Figure taken from Quillévéré *et al.* (2001).
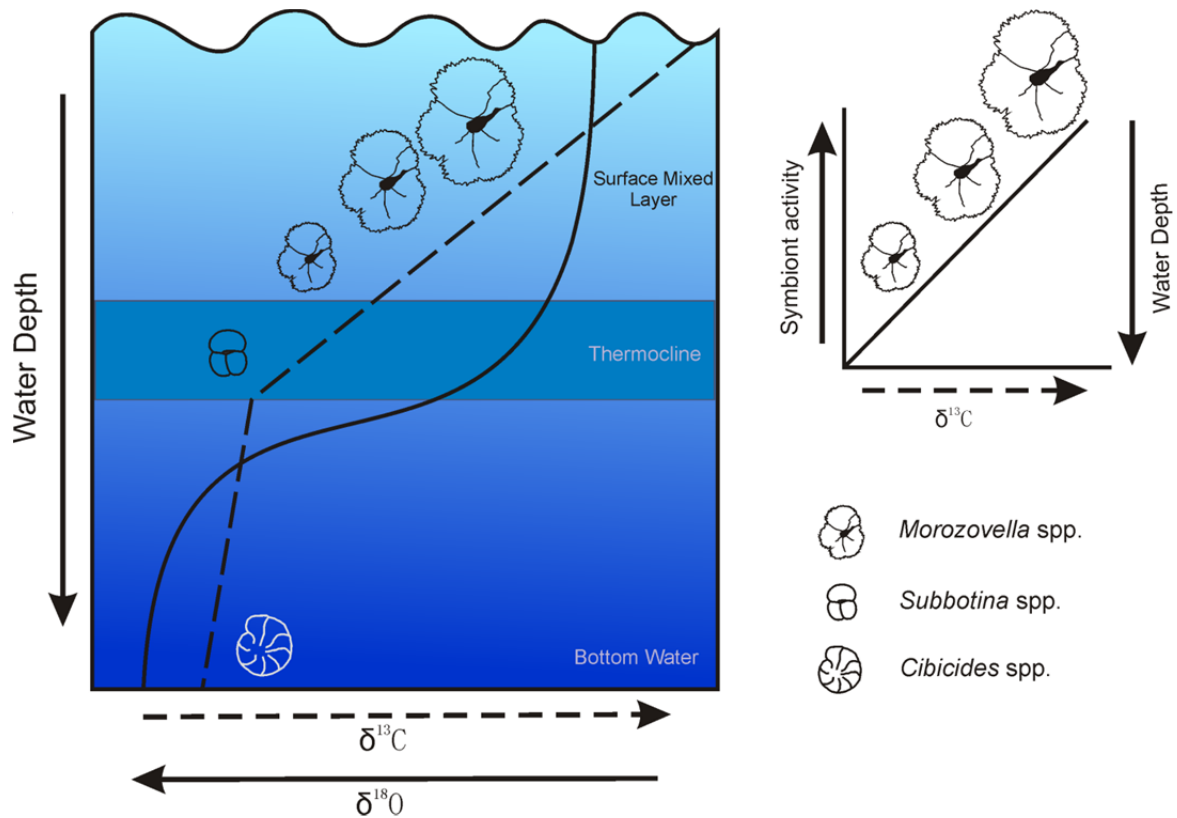
Figure 2.9: A) Changes in stable isotopes (δ^{13}C, δ^{18}O) relative to depth in the water column. **B**) Inverse relationship between test size and stable isotopes (δ^{13}C, δ^{18}O) with respect to decreasing water depth. Image modified from Wade *et al.* (2008), after Birch *et al.* (2012).

Genera of Foraminifera used in this Study

The muricate planktic foraminifera genus *Morozovella* was an abundant and diverse taxon during the late Paleocene to middle Eocene, dominating tropical to subtropical assemblages before a significant biotic turnover in the late Middle Eocene resulted in the extinction of the *Morozovella* lineage (Wade, 2004). Oxygen and carbon stable isotopes indicate that *Morozovella* species likely occupied the warmest and shallowest levels of the surface mixed layer (Birch *et al.*, 2012), and the presence of dinoflagellate symbionts suggests this genus occupied an environment within the photic zone of the ocean (upper *ca.* 200 m). An inverse relationship between test size and $\delta^{18}O$ is present in *Morozovella* suggesting larger morozovellids occupied higher levels in the water column (Birch *et al.*, 2012). Due to the strongly symbiotic relationship of morozovellids, individuals living deeper in the water column, where light intensity and temperatures are lower would have reduced photosymbiont activity and therefore resulted in smaller tests (*Figure 2.9*; Birch *et al.*, 2012). Two species, *Morozovella crater* and *Morozovella lensiformis* (*Figure 2.10; Table 2.4*) were utilised for Mg/Ca paleo-ocean thermometry in this study.

The genus *Acarinina* generally had a cosmopolitan distribution and, unlike *Morozovella*, some species were adapted to cool, high-latitude conditions (Pearson *et al.*, 2006). Most *Acarinina* species occupied a mixed layer habitat (Pearson *et al.*, 2006). Two species, *A. primitiva* and *A. collactea* were preferentially picked from the *Acarinina* genus for Mg/Ca paleo-ocean thermometry in this study (*Figure 2.10; Table 2.4*).

Subbotina was a cosmopolitan genus common at high latitudes (Pearson *et al.*, 2006). The absence of a $\delta^{13}C$ symbiosis 'fingerprint' indicates that the taxa was asymbiotic and maintained a relatively constant depth habitat within or below the thermocline, representing temperatures from around *ca.* 400 m water depth (D'Hondt *et al.*, 1994; Pearson *et al.*, 2006; Birch *et al.,* 2012). The test wall structure of *Subbotina* is very similar to the modern planktic foraminifera *Globigerinoides sacculifer*, with a coarsely cancellate wall produced from a well-developed pore-ridge system (Sexton *et al.*, 2006b). Some Eocene specimens display extensive, heavy gametogenic calcification (Pearson *et al.*, 2006). *Subbotina* generally were not subdivided at species level for this study.

The rotaline benthic genus *Cibicides* may have had an attaching epifaunal habitat either above or on the sediment–water interface, and is indicative of oxic water conditions (Kaiho, 1994). Two species, *C. eocaenus* and *C. truncatus* were preferentially picked from assemblages (*Figure 2.11; Table 2.4*).
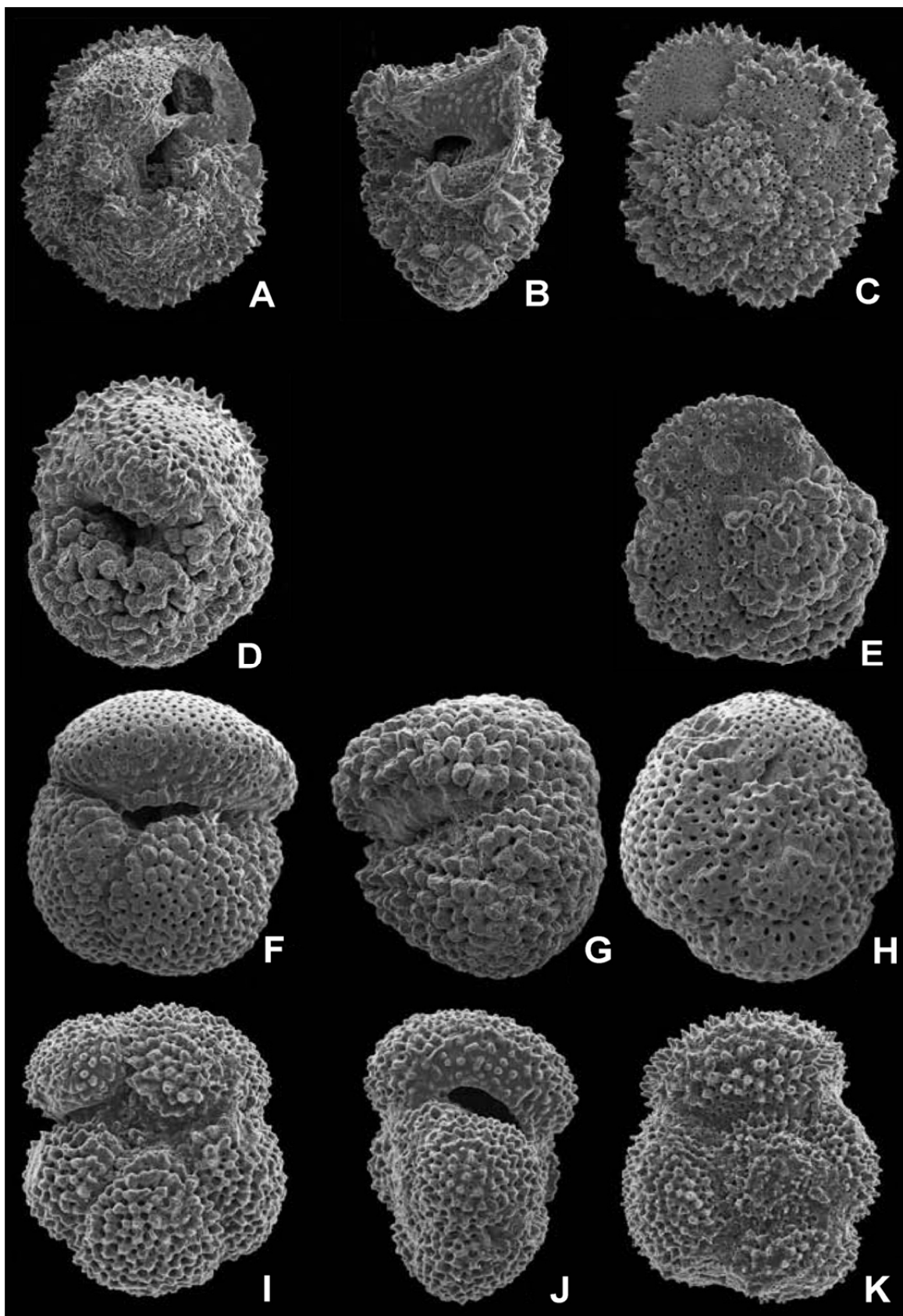
Figure 2.10: Examples of well-preserved *Morozovella* and *Acarinina* species from the Hampden Beach section. **A–C**) *Morozovella crater* (md = 0.41 mm); **D** & **E**) *Morozovella lensiformis* (maximum dimension (md) = 0.31 mm); **F–H**) *Acarinina primitiva* (md = 0.23 mm); **I–K**) *Acarinina collactea* (md = 0.31 mm). Images adapted from Morgans (2009).
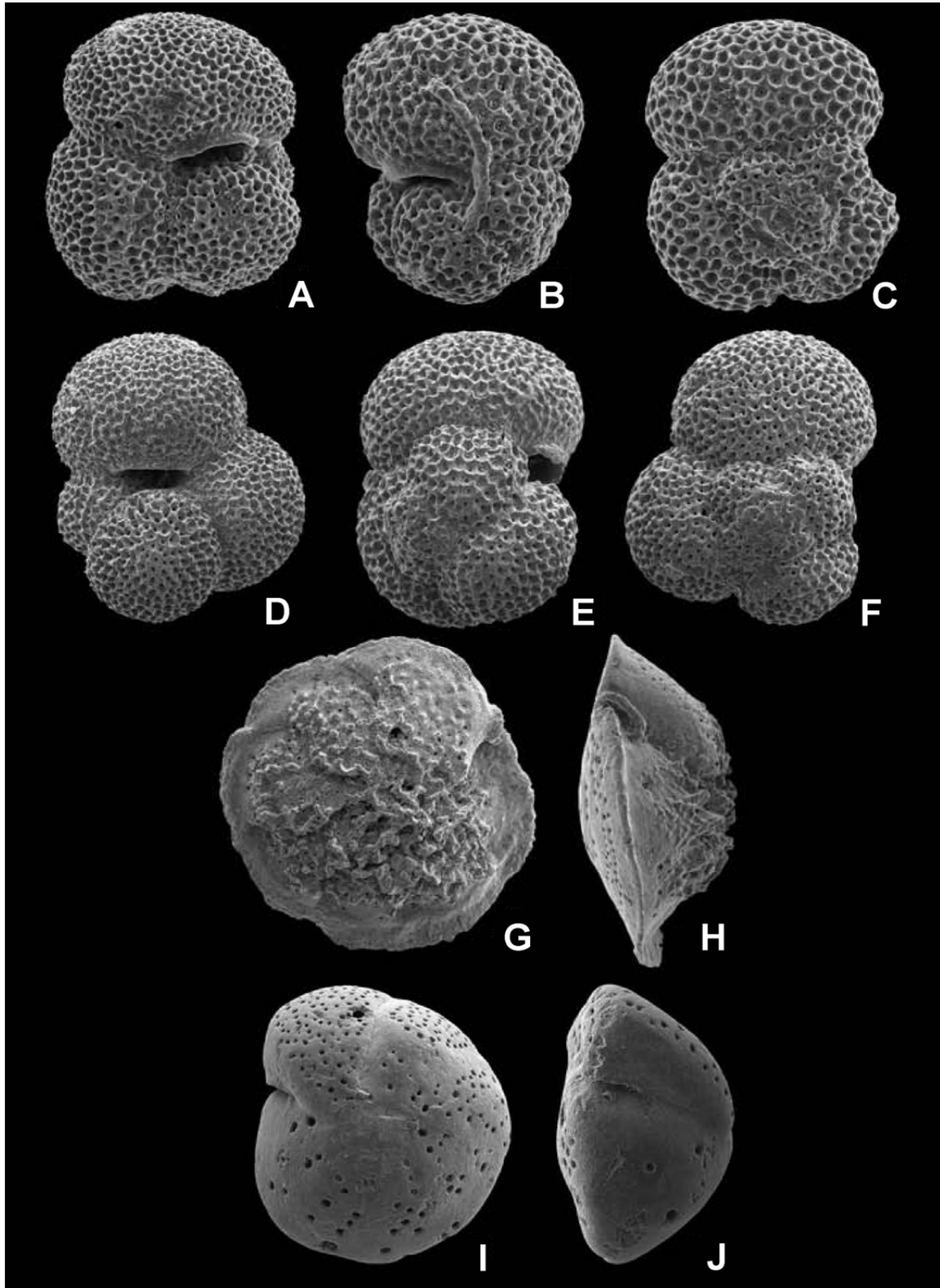
Figure 2.11: Examples of well-preserved *Subbotina* and *Cibicides* species from the Hampden Beach section. **A–C**) *Subbotina linaperta* (md = 0.31 mm) **A**) View of final whorl, **B**) Apertural view, **C**) Umbilicus view; **D–F**) *Subbotina eocenica* (md = 0.34 mm); **D**) View of final whorl, **E**) Apertural/side view, **F**) Umblicus view; **G & H**) *Cibicides truncatus* (md = 0.85 mm); **I & J**) *Cibicides eoceanus* (md = 0.56 mm). Images adapted from Morgans (2009).

Table 2.4: Summary of important statistical information for the foraminiferal species utilised for trace element analysis in this stud

Species	*Morozovella crater*	*Morozovella lensiformis*	*Acarinina primitiva*	*Acarinina collactea*	*Subbotina* spp.	*Cibicides eocaenus*	*Cibicides truncatus*
Morphotype	Planktic	Planktic	Planktic	Planktic	Planktic	Benthic	Benthic
Age Range (Ma)	53.3–49.3	54.52–53.06	55.8–38.5	53.3–37.43	Dt–lLwh	53.3–27.3	53.3–30.4
Latitudinal Range	Mid- to high latitudes	Mid- to high latitudes	High latitudes, less common at low latitudes	Mid- to high latitudes	High latitudes	-	-
Environment	Surface mixed layer (<200 m)	Surface mixed layer (<200 m)	Surface mixed layer (<200 m)	Surface mixed layer (<200 m)	Thermocline (*ca.* 400 m)	Epifaunal (>200 m)	Epifaunal
Test Structure	Muricate, keeled	Muricate, keeled	Muricate	Muricate	Coarsely cancellate	Porcellaneous	Porcellaneous
Description	Plano-conical form with five chambers in the final whorl, spinose keel, wide umbilicus surrounded by strongly muricate distal ends of chambers, dextrally coiled	Four chambers in the final whorl, keel present only on final chamber, sinstrally coiled except at top of range	Angular form with flattened inner chamber faces, deeply incised sutures and strongly muricate test	Small inflate hispid form with five chambers in the final whorl and low, arched aperture	Typically $3–3^{1/2}$ chambers in the final whorl, spinose	Rounded, strongly planoconvex form with coarsely punctuate surface on uncoiled side	Dorsally evolute, smooth, gently convex, ventrally strongly reticulate and flat or gently convex with strongly carinate periphery
Symbionts	Yes	Yes	Yes	Yes	No	No	No

Chapter Three

FIELDWORK AND LABORATORY TECHNIQUES

Fieldwork at Tora initially focused on geological mapping to delineate structural complications and ensure the establishment of a coherent stratigraphy. Once this was completed, locations of sections to be investigated in detail were selected and subsequently measured, and bulk rock samples collected. Samples were split for various analyses and then processed for microfossil and bulk rock analysis.

3.1   Stratigraphy & Field Measurements

3.1.1   *Geological Mapping & Section Measuring*

Field mapping was conducted with the aid of enlarged copies of the Topo50 BR34 map sheet (NZMS 260 sheet S28 map grid replacement; *Figure 3.1*). Sample localities are referenced in the New Zealand Fossil Record File (FRF) with respect to the old NZMS 260 map series. Given that Land Information New Zealand (LINZ) has recently converted the NZMS 260 map sheets to the Topo250 and Topo50 map sheets, which utilise a different co-ordinate system, a conversion table between the two co-ordinate systems is provided in *Appendix 1*.

Geological mapping included traverses along the main streams and tracing faults in outcrop, in addition to examining aerial photographs and satellite images. Outcrop descriptions of the gross lithology and sedimentology were described in the field, in addition to identification of trace fossil assemblages.

The tape and compass method was utilised to produce measured sections. Strikes and dips were recorded several times along each section, and the true stratigraphic thickness calculated utilising the 'Sections' programme developed by Dr James Crampton (GNS Science) to calculate the true stratigraphic thickness of the section. Bulk rock samples of approximately 1000 g were collected during the measurement of sections. A handheld GPS unit with an accuracy of ±3.0 m provided supplementary data for field mapping and was used to record the location of sections and samples.
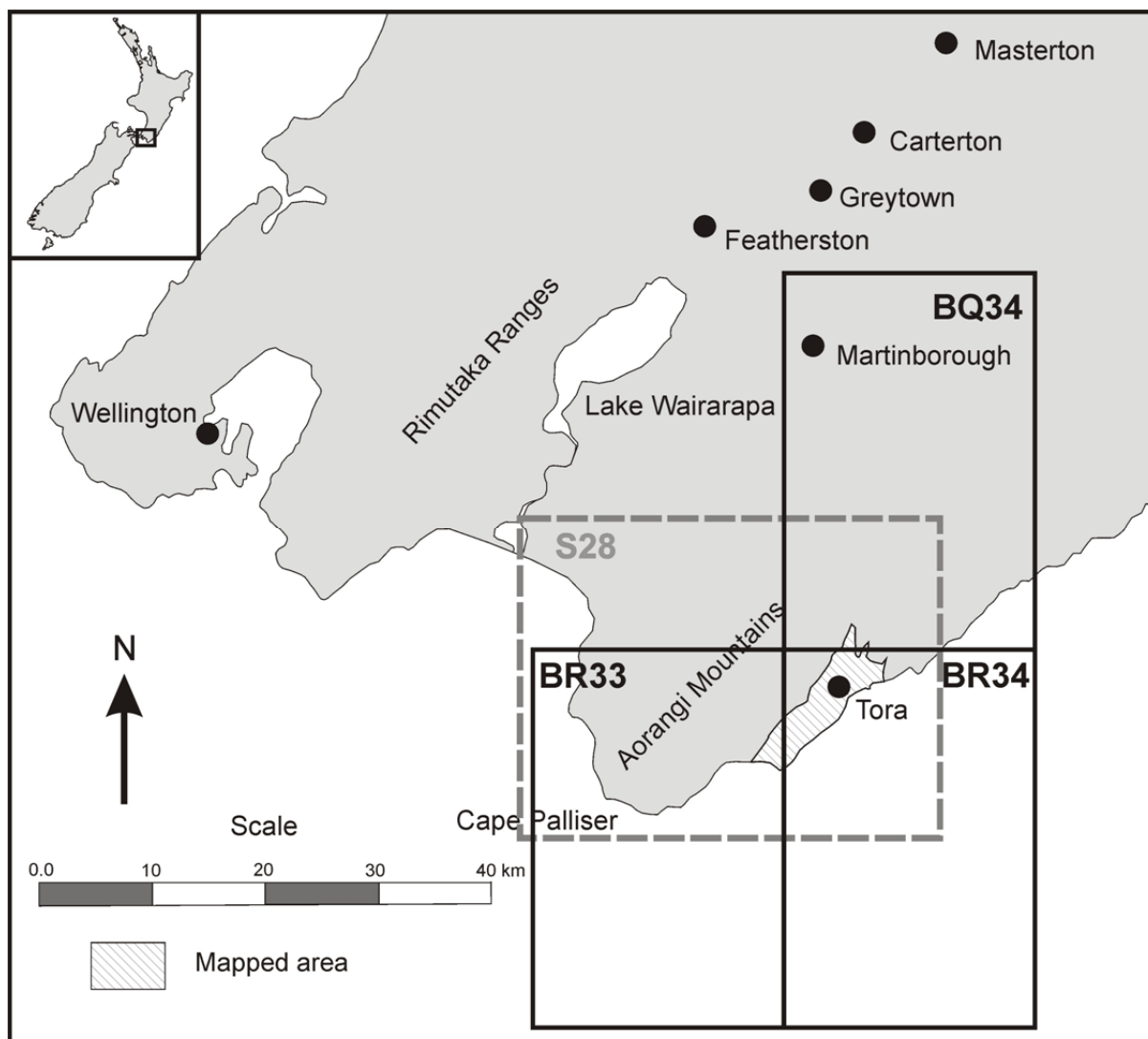
Figure 3.1: Location of NZMS 260 S28 map sheet and the superseding Topo50 map sheets BQ34, BR33 and BR34 covering the field area mapped in this thesis.

3.1.2   Paleo-Current Directions

Paleo-current directions were calculated from the orientation of long-axis of large elongate foraminifera (*Bathysiphon*) which are common in the Awheaiti Formation in Pukemuri Stream. The specimens observed in outcrop at Tora range from 6-50 mm in length and display a preferred orientation, from which ninety individual lineation measurements were recorded (*Appendix 1*). The measurements were then subdivided into 10° increments and plotted against frequency as a rose diagram.

3.1.3   Paleo-Slope Directions

Paleo-slope directions were determined from the orientation of the axial plane of syn-depositional slump folds formed by the plastic deformation of soft sediment (*Figure 3.2*). The axis of the slump fold reflects the direction of downslope slumping during deposition. Slump folds were measured in Te Oroi and Pukemuri streams and data plotted on a stereo-net to correlate and evaluate relationships between folds.
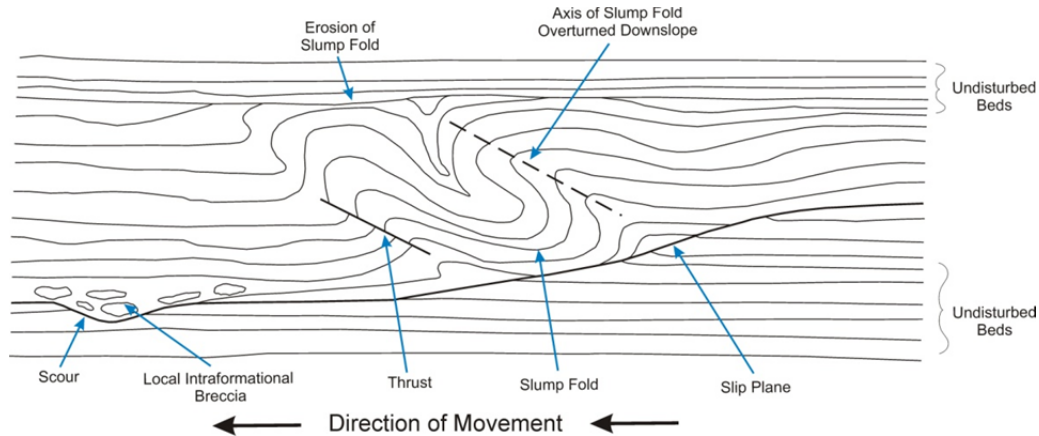
Figure 3.2: Schematic diagram displaying slump orientation relative to movement. Image adapted from Tucker (2011). The slope direction corresponds with the direction of movement.

Regional tilting of strata in the Tora necessitated removal of tectonic influences. A regional correction of 30° was applied to correct for tilting. In addition, resulting data was rotated 40° anticlockwise to correct for a regional rotation of the East Coast Basin since the Eocene (King *et al.*, 1999). Strikes and dips of bedding surrounding slump structures and paleocurrent lineations were measured and used to remove structural deformation influences on the directionality of these features by manually plotting measurements on stereonets. In stereonet rotations, it is assumed that there has been no rotation around the vertical axis during deformation.

3.2   Sample Processing

Each bulk rock sample was split into four fractions, with a quarter each used for nannofossil and stable isotope analysis, foraminifera extraction, bulk rock analysis, and the remaining fraction stored for later use. Archived Cretaceous–Cenozoic Programme (CCP) samples were also processed to produce foraminiferal residues for this study (*Appendix 1*).

Collections

Samples utilised for paleontological study include 20 archived samples from the Te Oroi, Pukemuri and Awheaiti Stream sections stored in the National Paleontology Collection (GNS Science, Lower Hutt) and new collections made in the Pukemuri Stream (39 samples) and Awheaiti Stream (26 samples) sections in 2010-2011 (*Appendix 1*). Sampling intervals for the archive samples are sparse, often with only 1–2 samples per formation. New collections of the Pukemuri Stream section have sample intervals that rarely exceed 5–8 m. Collections in Awheaiti Stream are more varied, with sample intervals ranging from 1–20 m, due to structural complications and limited outcrop in some locations. All samples were assigned Fossil Record File (FRF) numbers (*Appendix 1*) and sample numbers were recorded in the FRF administered by GNS Science and the Geological Society of New Zealand (www.fred.org.nz). Samples referred to in text are preceded by the prefix S28/f... in standard FRF format.

3.3   Paleontology and Age Assignment

Biostratigraphic data used for age and environmental control in this study are from micropaleotological analyses that were carried out by Hugh Morgans (foraminifera) and Denise Kulhanek (calcareous nannofossils) of GNS Science. Foraminifera and calcareous nannofossil assemblage data is compiled in *Appendix 1*.

3.3.1.   *Foraminifera*

A total of 20 samples were processed for foraminifera (*Appendix 1*). Sample splits were crushed to 5 mm diameter pieces then dried at 40°C. Each sample was then weighed, soaked for 24 h in a solution of Calgon and water, then thoroughly washed over a 63 µm screen until the sample had suitably disaggregated. The residue was then dried at 40°C for 24 h, before being dry sieved and divided into >500 µm, 500–300 µm, 300–150 µm and <150 µm sediment fractions. Foraminifera were picked from the >150 µm fraction under a binocular microscope. Given the low abundance of foraminifera in the Tora samples, all specimens were picked and adhered to a faunal slide pre-coated with a solution of gum tragacanth. International and local stage assignments and cited ages are based on the 2010 New Zealand Geological Timescale (*Figure 3.3*; Hollis *et al.*, 2010).

3.3.2   Calcareous Nannofossils

The following calcareous nannofossil methodology was provided by D. Kulhanek of GNS Science. A total of 48 calcareous nannofossil samples (37 from Pukemuri Stream and 11 from Awheaiti Stream) were prepared following standard smear-slide techniques (e.g. Bown & Young, 1998). A small amount of sediment was scraped onto a coverslip from a fresh surface on each sample using a razor blade. The sediment was mixed with a drop of distilled water and spread evenly over a coverslip, dried on a hot plate, affixed to a glass microscope slide using Norland Optical Adhesive 61 and cured under ultraviolet light. Slides were examined at 1000 and 630 times magnification using a Leitz Ortholux II POL-BK microscope or an Olympus BX53 microscope under cross-polarised and plain-transmitted light. A minimum of four coverslip traverses (approximately 800 fields of view at 1000 times magnification) were observed for each slide and the following qualitative scale used to estimate the abundance of each species:

A (abundant) =	>10 specimens/field of view
C (common) =	1–10 specimens/field of view
Fr (frequent) =	1 specimen/2–10 fields of view
F (few) =	1 specimen/11–100 fields of view
R (rare) =	1 specimen/>100 fields of view
B (barren) =	no nannofossils observed within ~800 fields of view
? (questionable) =	questionable identification of a specimen
* =	reworked specimen

Results are correlated to the biostratigraphic zonation scheme of Martini (1971). Taxonomic concepts for species are those given in Perch-Nielsen (1985) and Bown (1998). Calcareous nannofossil results are presented in *Appendix 1*.

Era	Period	Epoch	Series	Stage	Symbol	Age of base, Ma	Dura-tion, Ma	Lower boundary defining event (and currently used proxy)	Boundary stratotype (or reference section)
CENOZOIC	Quaternary	Holo-cene	Wanganui	Haweran	Wq	0.34	0.34	Base of Rangitawa Tephra	Rangitawa Stream, Rangitikei Valley
		Pleistocene		Castlecliffian	Wc	1.63	1.29	Base of Ototoka Tephra	Wanganui coast, Ototoka Stream
				Nukumaruan	Wn	2.4	0.77	LO *Zygochlamys delicatula*	Base Hautawa Shellbed, Old Hautawa Road, Rangitiki Valley (recommended SSP)
				Mangapanian	Wm	3	0.6	LO *Phialopecten thompsoni*	Base Mangapani Shellbed, Mangapunipuni Stm, Waitotara
		Pliocene		Waipipian	Wp	3.6	0.6	HO *Reticulofenestra pseudoumbilica* (provisional)	To be determined
				Opoitian	Wo	5.33	1.73	LO *Globoconella puncticulata* (provisional)	To be determined
	Neogene	Miocene	Taranaki	Kapitean	Tk	7.2	1.87	LO *Sectipecten wollastoni* (LO *Globoconella conomiozea*)	To be determined
				Tongaporutuan	Tt	11.01	3.81	Base *Globoconella miotumida* Kaiti Coiling Zone	To be determined
			Southland	Waiauan	Sw	12.98	1.97	HO *Fohsella peripheroronda* (HO *Globoconella conica*)	To be determined
				Lillburnian	Sl	15.1	2.12	LO *Orbulina suturalis*	Clifden, Waiau River, Southland
				Clifdenian	Sc	15.9	0.8	LO *Praeorbulina curva*	Clifden, Waiau River, Southland
			Pareora	Altonian	Pl	18.7	2.8	LO *Globoconella praescitula*	To be determined
				Otaian	Po	21.7	3	LO *Ehrenbergina marwicki* group	(Bluecliffs, Otaio River, south Canterbury)
		Oligo-cene	Landon	Waitakian	Lw	25.2	3.5	LO *Globoquadrina dehiscens*	Trig Z, Otiake, Waitaki Valley
				Duntroonian	Ld	27.3	2.1	LO *Notorotalia spinosa*	(Landon Creek, Oamaru)
				Whaingaroan	Lwh	34.5	7.2	HO *Globigerapsis index*	Point Elizabeth, Westland
	Paleogene	Eocene	Arnold	Runangan	Ar	36	1.5	LO *Bolivina pontis* (LO *Ismolithus recurvus* and HO *Recticulofenestra reticulata*)	Point Elizabeth, Westland
				Kaiatan	Ak	38.4	2.4	HO *Acarinina primitiva* (new)	(Hampden coastal section, north Otago)
				Bortonian	Ab	42.77	4.37	LO *Globigerapsis index*	Hampden coastal section, north Otago
			Dannevirke	Porangan	Dp	45.3	2.53	LO *Elphidium saginatum* (HO *Morozovella crater*)	(Te Uri Stream, southern Hawkes Bay)
				Heretaungan	Dh	49.3	4	LO *Elphidium hampdenensis* (LO *Discoaster sublodensis*)	(Te Uri Stream, southern Hawkes Bay)
				Mangaorapan	Dm	53.3	4	LO *Morozovella crater* (LO *Discoaster lodensis*)	(Te Uri Stream, southern Hawkes Bay)
				Waipawan	Dw	55.8	2.5	Onset of PETM carbon isotope excursion	Tawanui Stream, southern Hawkes Bay
		Paleo-cene		Teurian	Dt	65.5	9.7	Base of Boundary clay and iridium anomaly	Flaxbourne River, eastern Marlborough
MESOZOIC	Cretaceous	Late	Mata	Haumurian	Mh	83.5	18	LO *Nelsoniella aceras*	Ben More Stream, eastern Marlborough
				Piripauan	Mp	86.5	3	LO *Inoceramus pacificus*	Ben More Stream, eastern Marlborough
			Raukumara	Teratan	Rt	88.6	2.1	LO *Inoceramus opetius*	Mangaotane Stream, Raukumara Peninsula
				Mangaotanean	Rm	93.0	4.4	LO *Cremnoceramus bicorrugatus matamuus*	Mangaotane Stream, Raukumara Peninsula
				Arowhanan	Ra	95.2	2.2	LO *Magadiceramus rangatira haroldi*	Mangaotane Stream, Raukumara Peninsula
			Clarence	Ngaterian	Cn	100.2	5	LO *"Inoceramus" tawhanus*	"Te Waka Stream", Raukumara Peninsula
		Early		Motuan	Cm	103.3	3.1	LO *Aucellina euglypha*	Motu Falls, Raukumara Peninsula
				Urutawan	Cu	108.4	5.1	LO *Mytiloides ipuanus*	Motu Falls, Raukumara Peninsula
			Taitai	Korangan	Uk	117.5	9	*Aucellina* cf. *radiatostriata* assemblage	(Koranga, Raukumara Peninsula)
				no stages designated	U	145.5	27.2	LO *Ruffordiaspora australiensis*	
	Jurassic		Oteke	Puaroan	Op	148.5	3.0	LO *Hibolithes arkelli grantmackiei*	Moewaka Stream, Port Waikato
			Kawhia	Ohauan	Ko	153.5	5	LO *Retroceramus haasti*	Whakapirau Road, Kawhia Harbour
				Heterian	Kh	157.5	4	LO *Retroceramus (R.) galoi*	Hetere Point, south coast, Kawhia Harbour
				Temaikan	Kt	178.0	20.5	LO *Belemnopsis deborahae*	Opuatia Stream, Port Waikato
			Herangi	Ururoan	Hu	190.0	12	LO *Pseudaucella marshalli*	Otamaehu Point, near Ururoa Point, Kawhia
				Aratauran	Ha	200.0	10	LO psiloceratid ammonites	Taylors Stm, Hokonui Hills, Southland

Figure 3.3: The 2010 New Zealand Geological Timescale (NZGTS 2010) displaying ages for stage boundaries, duration of stages, defining events and boundary stratotypes (Hollis *et al.*, 2010).

3.4   Bulk Rock Components

3.4.1   Percent Mud Content

At least 200 g of bulk rock was crushed and then dried at 40°C for 24 h to remove any residual moisture before the sample was weighed. The sample was then disaggregated, dispersed in calgon and washed over a 63 μm screen. The remaining residue was then dried at 40°C for 24 h and weighed. Due to the degree of induration of the samples, several samples did not disaggregate completely so a modified equation (*equation 3.1*) was used to determine the percentage of mud within the bulk sample.

$$\frac{(\text{Initial Weight} - \text{Final Weight})}{(\text{Initial Weight} - \text{Unprocessed Fraction})} \times 100 = \% \text{ Mud} \qquad \textit{Equation 3.1}$$

3.4.2   Percent Bulk Carbonate Content

The gravimetric method (by loss of carbon dioxide) was used to determine the carbonate component of bulk rock material. When carbonates are dissolved with acid, CO_2 gas is released (*Equation 3.2*), with the decrease in sample mass resulting from CO_2 loss providing an index for the carbonate content (Demars & Chaney, 1982). The mass of CO_2 lost is determined by the difference in the initial and final weights of the flask, sample and acid combined.

$$CaCO_{3(s)} + 2\ HCl_{(aq)} \rightarrow CaCl_{2(aq)} + CO_{2(g)} + H_2O_{(l)} \qquad \textit{Equation 3.2}$$

Approximately 50 g of bulk rock was crushed then dried for 24 h. The sample was then reweighed to ascertain the exact weight, and 50 mL of 10% hydrochloric acid (HCl) solution was added to the sample, ensuring the sample was completely saturated. The sample was then left to digest for 24 h. Once effervescence had stopped, the flask and all its contents were weighed, and *Equation 3.3* used to determine the percentage of bulk carbonate within the rock sample. The difference in mass is multiplied by the molecular weight of $CaCO_3$ divided by the molecular weight of CO_2 (= 2.274) following Loeppert & Suarez (1996).

$$\frac{\text{Final Weight}}{\text{Initial Weight}} \times 2.274 \times 100 = \%\text{wt } CaCO_3 \qquad \textit{Equation 3.3}$$

3.4.3   Bulk Carbonate Stable Isotopes

Bulk rock samples from the Pukemuri Stream section were processed at the National Isotope Centre (GNS Science), Gracefield, to determine the carbon and oxygen stable isotope ratios ($\delta^{13}C$ and $\delta^{18}O$) of the bulk carbonate fraction.

Carbonate samples were processed using a GV Instruments Isoprime Carbonate Preparation System at a reaction temperature of 25°C and analysed on an Isoprime Isotope Ratio Mass Spectrometer (IRMS) via a dual inlet. All results are reported relative to VPDB (Vienna Pee Dee Belemnite) and normalised to the GNS Marble internal standard with reported values of 2.04‰ for $\delta^{13}C$ and -6.40‰ $\delta^{18}O$. Five samples were run in duplicate to provide an estimate of the reproducibility of the analyses (0.05‰ for $\delta^{13}C$ and 0.12‰ for $\delta^{18}O$).

3.5   Paleoenvironmental Classification

Paleodepth estimates are based on selected benthic foraminifera species with calibrated minimum upper depth ranges (*Table 3.1*; *Figure 3.4*). The percent abundance of planktic foraminifera can also be used to characterise the overlying water mass (*Figure 3.4*). These calibrations are derived from several sources, including the depth distribution of New Zealand recent benthic foraminifera (Hayward *et al.*, 2010), calibrated depth limits from New Zealand petroleum exploration wells (Hayward, 1986), and Deep Sea Drilling Project (DSDP) and Ocean Drilling Program (ODP) sites (Morkhoven *et al.*, 1986).

Benthic foraminifera typically occupy a variety of depths, although the upper depth limit of a species can be a particularly useful paleoenvironmental and paleobathymetric tool (Morkhoven *et al.*, 1986). Key paleodepth indicative taxa are listed in *Table 3.1*. Benthic foraminifera can also provide an indication of bottom water oxygenation (epifaunal species) and the oxygenation state of seafloor sediments (infaunal species) (Kaiho, 1994).

Table 3.1: Upper paleodepth limits applied to key benthic taxa used for paleoenvironment interpretation.

Taxa	Paleodepth (m)	Source
Anomalina aotea	200	Hayward (1986)
Anomalina aotea	600	Morkhoven *et al.* (1986)
Anomalina aotea	1000	Tjalma & Lohmann (1983)
Nuttallides carinotruempyi	400	Hayward (1986)
Vulvulina zespinosa	400	Hayward (1986)
Vulvulina spp.	1000	Tjalma & Lohmann (1983)
Cassidulina subglobosa	500	Hayward *et al.* (2010)
Karreriella bradyi	500	Hayward *et al.* (2010)
Oridorsalis umbonatus	600	Hayward *et al.* (2010)
Osangularia sp.	600	Hayward *et al.* (2010)
Pleurostomella spp.	600	Hayward *et al.* (2010)
Nuttallides florealis	1000	Morkhoven *et al.* (1986)
Pleurostomella spp.	1000	Hayward & Buzas (1979)
Cibicides eocaenus	1000	Tjalma & Lohmann (1983)
Stilostomella spp.	1000	Tjalma & Lohmann (1983)
Tritaxilina zealandica	1500	Hayward (1986)
Glomospira gordialis	2000	Hayward *et al.* (2010)
Abyssamina poagi	3500	Morkhoven *et al.* (1986)
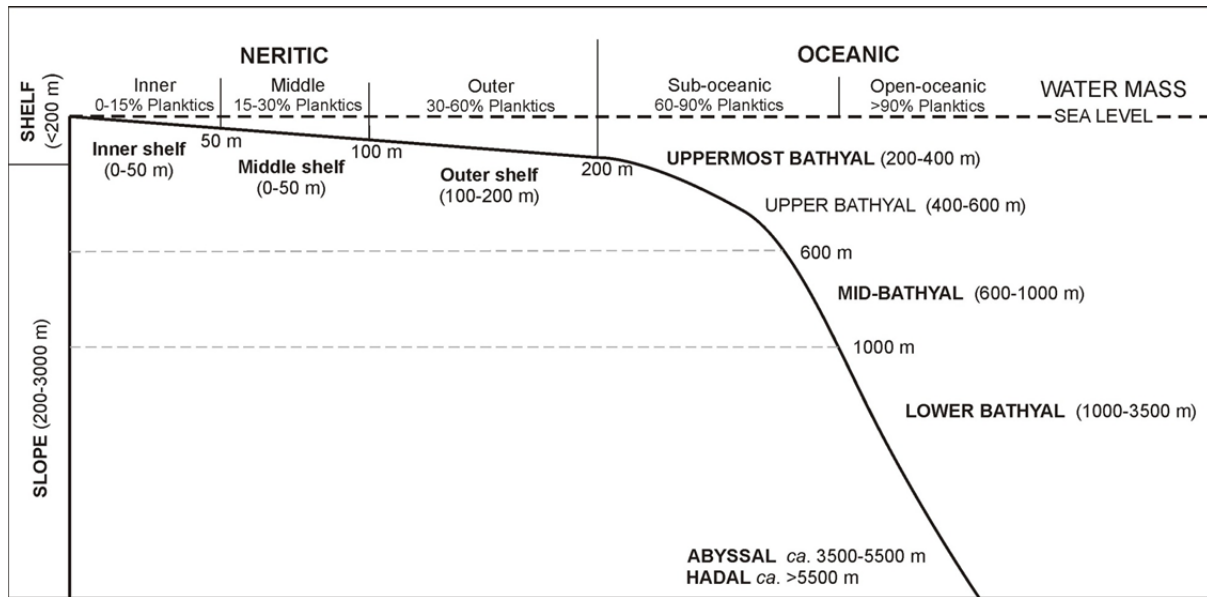
Figure 3.4: Paleodepth classification scheme adopted for this study. Figure taken and modified from Hayward *et al.* (2010), after Morgans (2009).

3.6   Trace Element Geochemistry

3.6.1   Sample Preparation

Bulk rock samples were crushed and then dried before being washed over a 75 μm screen to disaggregate the material and remove the unwanted fine fraction. The remaining sediment fraction (>75 μm) was subsequently dried, and selected species of foraminifera were handpicked and mounted on slides. The foraminifera were washed in ultra-clean water, then methanol, and the process was repeated a further three times to remove any loosely adhering detritus, followed by a final wash in ultra-clean water. The foraminifera were then mounted on adhesive paper which was attached to a National Institute of Standards and Technology (NIST) glass standard NIST-SRM610 using double-sided cellotape (*Figure 3.5*) at which point they are ready for analysis using the laser ablation inductively coupled plasma mass spectrometry (LA-ICP-MS) method.
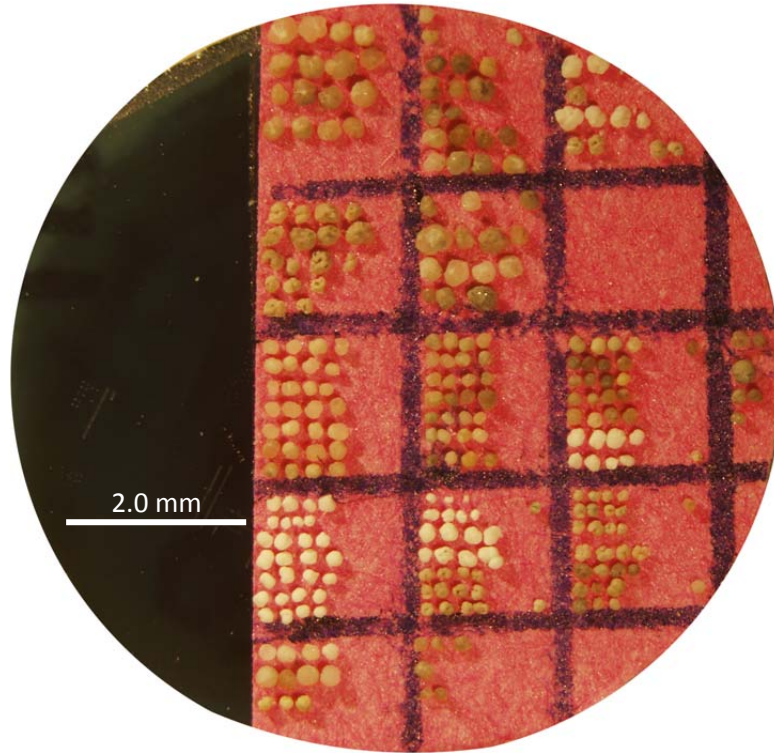
Figure 3.5: Prepared NIST610 silicate glass standard, with selected planktic foraminifera adhered to adhesive paper.

3.6.2   Selecting Foraminifera for LA-ICP-MS analysis

Foraminifera inhabit various levels within the water column, which has a direct bearing on sea temperature determinations. Four genera were selected for Mg/Ca analysis in this study: *Morozovella*, *Acarinina*, *Subbotina* and *Cibicides*. The species *Morozovella crater*, *Acarinina primitiva* and *Cibicides eocaenus* (*Figures 2.10 and 2.11*) were preferentially picked throughout the record to retain consistency in sample analysis. Where these particular species were not available, *M. lensiformis*, *A. collactea*, and *C. truncatus* were picked and analysed (*Figures 2.10 and 2.11*). *Subbotina* specimens were not identified to species level.

These genera were selected for the environment and position within the oceanic water column in which they lived. *Morozovella* and *Acarinina* (*Figure 2.10*) were surface–mixed layer dwelling planktic forms (Pearson *et al.*, 2006; Sexton *et al.*, 2006b) and, therefore, temperatures derived from these foraminifera are indicative of sea surface temperatures. *Subbotina* spp. (*Figure 2.11*) were generally thermocline dwellers (Pearson *et al.*, 2006), and thus derived temperature estimates are cooler than those of sea surface dwelling planktic species. The benthic genus *Cibicides* (*Figure 2.11*) provides a record of sea floor temperatures.

3.6.3   LA-ICP-MS Analytical Technique

The LA-ICP-MS technique was used to measure elemental ratios of the tests (shells) of planktic and benthic foraminifera species selected from the Eocene samples. *In situ* elemental ratios of key isotopes (^{24}Mg, ^{27}Al, ^{29}Si, ^{47}Ti, ^{55}Mn, ^{66}Zn, ^{88}Sr, ^{138}Ba) relative to ^{43}Ca were measured to determine paleo-sea temperatures and potentially, changes in productivity, nutrient availability, environmental conditions and also to screen analyses for post-depositional contamination and diagenesis of the samples.

A New Wave deep ultraviolet (193 nm) laser ablation system operated at a spot size of 35 μm, with a laser repetition rate of 5 Hz, was used to ablate foraminifera tests. Operating under these conditions, the laser progressively ablates a pit into the surface of the foraminifera test at an estimated rate of 0.2–0.3 μm/s. Analytical running conditions are presented in *Table 3.2*. Each pit was ablated to a depth not less than 25 μm, allowing the construction of trace element/Ca profiles through the test (*Figure 3.6*). The ablation process was conducted in a helium atmosphere, which is subsequently introduced into an Agilent 7500cs ICP-MS using a helium-argon mixture as a carrier gas. Instrumental trace element fractionation during the course of analyses is corrected using bracketing analyses of the NIST-SRM610 glass standard between clusters of nine to twelve analyses (*Figure 3.7*). The NIST standard is doped with 61 elements of known concentration (Pearce *et al.*, 1997). Each foraminifer was ablated at least three times in order to produce a mean value attributable to each individual, and in order to avoid and reduce the influence of anomalous values from contamination and diagenetic alteration. The resulting trace element depth profiles enable the identification and avoidance of zones of external and internal contamination in the sample, as well as exclusion of digenetic coatings and mineralisation that may have formed in the post-depositional environment (*Figure 3.6*).

Table 3.2: LA-ICP-MS analytical conditions during tuning, NIST analysis and ablation of foraminiferal calcite.

Laser Ablation

Laser ablation system	New Wave 193 nm (deep UV) solid state
Ablation mode	Static spot analyses
Spot size	35 μm
Depth ablated/pulse	0.05 μm

ICP-MS

ICP-MS system	Agilent 7500cs
Acquisition mode	Peak hopping
Detection mode	Pulse counting

Tuning

Tuning standard	NIST-SRM610
Ablation mode	Rastering (2 μm/s) beneath a 35 μm spot
Monitored isotopes	^{24}Mg, ^{27}Al, ^{29}Si, ^{43}Ca, ^{47}Ti, ^{55}Mn, ^{66}Zn, ^{88}Sr, ^{138}Ba (% RSD for each isotope typically 4–8%)
Carrier gas (Ar)	0.83–0.90 L/min
Optional gas (He)	77–86%
RF power	1500 W
RF matching	1.72 V
Repetition rate	5 Hz
Laser power	80%

Standards and Calibration

Calibration standard	NIST-SRM610
Repetition rate	5 Hz
Laser power	80%
Background acquisition	60 s
Sample data acquisition	60 s
Washout time	30 s
Measured isotopes	^{24}Mg, ^{27}Al, ^{29}Si, ^{43}Ca, ^{47}Ti, ^{55}Mn, ^{66}Zn, ^{88}Sr, ^{138}Ba
Dwell time	60 s

Foraminifera Method

Repetition rate	5 Hz
Laser power	55 or 60%
Background acquisition	60 s
Sample data acquisition	60 s
Washout time	30 s
Measured isotopes	^{24}Mg, ^{27}Al, ^{29}Si, ^{43}Ca, ^{47}Ti, ^{55}Mn, ^{66}Zn, ^{88}Sr, ^{138}Ba
Dwell time	60–90 s

Figure 3.6: Examples of trace element depth profiles produced by laser ablation analysis displaying a variety of profiles. **A**) An example of a 'good' profile showing an trace element enriched veneer on the exterior of the test and a large proportion of primary calcite. **B**) A profile displaying enrichment of Ti on the exterior and interior surfaces of the test, indicating detrital sediment contamination, with a significant proportion of primary biogenic calcite preserved between these zones. **C**) A profile displaying only a short section of primary calcite. **D**) A profile that is too short to be integrated for sea temperature analysis. **E**) A complex profile displaying elevated trace element values produced by the laser ablating the test surface obliquely and/or continuous contamination from surface ornamentation. **F**) Extensively altered profile where the primary calcite signal has been completely overprinted by diagenetic processes.

3.6.4 Data Reduction

During the course of LA-ICP-MS analysis, there is an observed increase in ion transmission with the increasing isotope mass causing a deviation in the measured elemental ratio from the true elemental ratio (Rosenthal *et al.*, 1999). As there is no existing homogenous carbonate standard that is comparable to the calcite matrix of foraminifera, the silicate glass standard (NIST-SRM610) is used to correct for the effects of instrumental fractionation. Elemental fractionation is corrected by external normalisation to NIST-SRM610. Raw data files were processed with a script in Matlab which formats the raw data (counts per second [cps] for each element) into Microsoft Excel spreadsheets, and corrects for the effects of background counts and instrumental drift during the course of the analysis as well as normalising fractionation effects to the NIST-SRM610 standard (Reference values used: Mg/Ca = 9.38, Al/Ca = 195.9, Si/Ca = 5.73, Ti/Ca = 4.40, Mn/Ca = 3.86, Zn/Ca = 3.42, Sr/Ca = 2.78, Ba/Ca = 1.51 mmol/mol; Pearce *et al.*, 1997). Resultant spreadsheets were processed with a Microsoft Excel macro modified from one created by Victoria University of Wellington staff and previous postgraduate students. The macro converts cps data into trace element/Ca ratios that were plotted against ablation time, producing a depth profile of the foraminiferal test chemistry from the exterior to interior (*Figure 3.6*), allowing the data to be screened for the effects of diagenetic alteration and contamination.
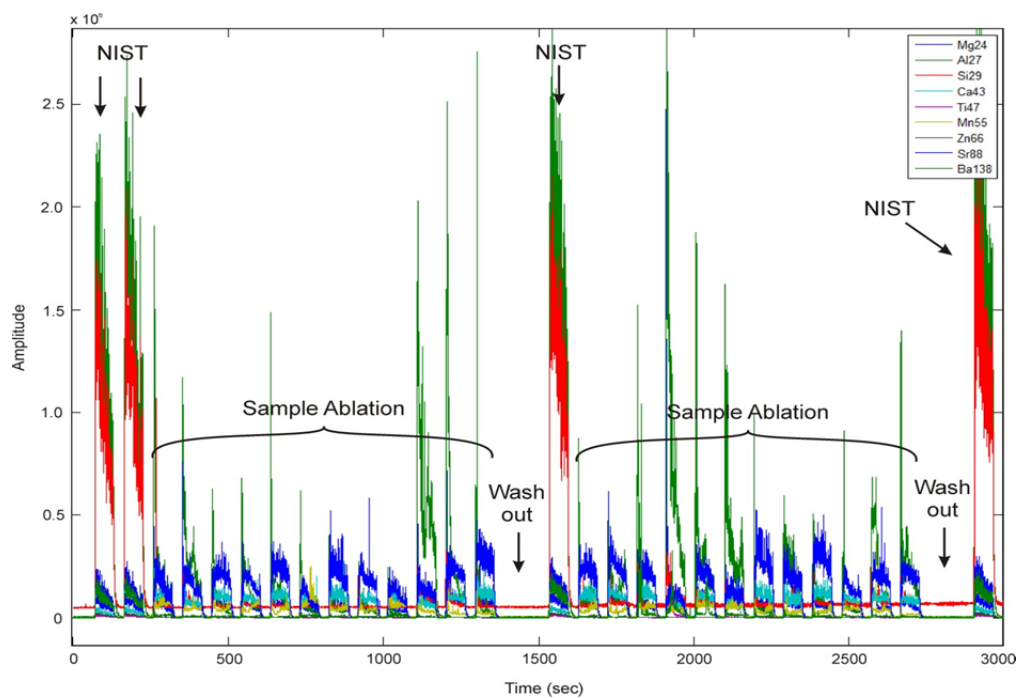
Figure 3.7: Raw cps data in the Matlab processing step displaying how foraminiferal calcite analyses are bracketed by ablation of the NIST610 standard to correct for instrumental trace element fractionation during the course of data collection.

Almost all trace element depth profiles display a zone of significantly elevated element/Ca ratios at the beginning of each analysis followed by a relatively constant zone of lower Mg/Ca values and other trace element/Ca ratios (*Figure 3.6*). These zones in the profile correspond to the test wall and primary foraminiferal calcite, respectively, and are consistent with previous LA-ICP-MS foraminifera studies (e.g., Eggins *et al.*, 2003; Creech *et al.*, 2010; Marr *et al.*, 2011). Changes in the trace element chemistry of the test are distinguishable in the profiles allowing only data from the zone of primary calcite to be selected and utilised in Mg/Ca sea temperature calculations.

3.6.5   Data Screening Limits

Following the preliminary screening of trace element/depth profiles, summary data exhibiting high Mg/Ca, Sr/Ca and Ba/Ca values were discarded. Mg/Ca values >7.0 mmol/mol were discarded as these generate unrealistic temperature values when combined with the Eocene seawater Mg/Ca value of 4.1 mol/mol, which should provide conservative paleotemperature estimates. Previous laser ablation studies have shown that strontium typically occurs at uniform levels throughout the foraminifera test, making it a useful indicator of severe alteration or secondary calcification (Eggins *et al.*, 2003). On this principle, samples with Sr/Ca values outside the range of 1.0-1.6 mmol/mol were also removed from the dataset.

Screening limits for silicate contamination were determined following the method of Creech (2010) after Barker *et al.* (2003). Unscreened, whole test Mg/Ca data was plotted against Al/Ca, Si/Ca and Ti/Ca values, resulting in quasi-linear correlations, indicating silicate contamination arising from sediment infilling pores and adhering to the exterior and interior surfaces of the test (*Figure 3.8*). Adapting the method of Barker *et al.* (2003) and Creech (2010), the Si, Al and Ti composition of the contaminant phase can be identified by plotting Mg/Ca against Al/Ca, Si/Ca and Ti/Ca. Subsequently, the inverse of the slope of the linear regression determines the Al/Mg, Si/Mg and Ti/Mg ratios of the sediment (*Table 3.3*).

Table 3.3: Calculated silicate contaminant values for each species used in sea temperature determinations.

Species	Contaminant		
	Al/Mg	Si/Mg	Ti/Mg
Morozovella spp.	7.58	22.22	0.19
Acarinina spp.	7.48	29.50	0.17
Subbotina spp.	4.90	17.86	0.26
Cibicides spp.	7.99	22.12	0.19

Al/Mg, Si/Mg and Ti/Mg ratios were then used to calculate the screening limits for each species used in this study. Given that sedimentary contamination has the effect of increasing the Mg/Ca value, resulting in overestimates of sea temperatures, calculation of the screening limit depends on the calibration used and the typical Mg/Ca ratio for each species. When the typical Mg/Ca value and the calibration are substituted into *Equation 3.4*, and assuming a maximum sensitivity of Mg/Ca to 1°C of temperature of 9% (after Anand *et al.*, 2003), the increase in Mg/Ca required to increase temperature estimates by 1°C can be calculated. For example, the genus *Morozovella* yields a typical Mg/Ca value of 3.8 mmol/mol in this study. Using the planktic calibration of Anand *et al.* (2003), an increase of 9% (0.34 mmol/mol) would be required to increase sea temperature estimates by 1°C.

The screening limit is then determined by multiplying the Mg/Ca excess by the sediment composition. Following the example above, the screening limit for Al/Ca is calculated by 0.34 × 7.58 = 2.57 mmol/mol. Screening limits for Al/Ca, Si/Ca and Ti/Ca are given in *Table 3.4*. The application of these screening limits to summary trace element data means that no Mg/Ca sea temperatures in this study should be overestimated by more than 1°C (as a result of post-mortem diagenetic effects). Values obtained in this study for the sediment Al/Mg ratio, and the Al/Ca screening limits, are comparable to those calculated by Creech (2010).

Table 3.4: Silicate mineral contamination screening limits (Al/Mg, Si/Mg and Ti/Mg) calculated for all species used for sea temperature estimates.

Species	Average Mg/Ca (mmol/mol)	Mg/Ca Sensitivity + 1°C (mmol/mol)	Screening Limit (mmol/mol)		
			Al/Ca	Si/Ca	Ti/Ca
Morozovella spp.	3.8	0.34	2.57	7.55	0.07
Acarinina spp.	3.3	0.29	2.20	8.66	0.05
Subbotina spp.	3.2	0.29	1.41	5.13	0.08
Cibicides spp.	3.3	0.30	2.37	6.56	0.06
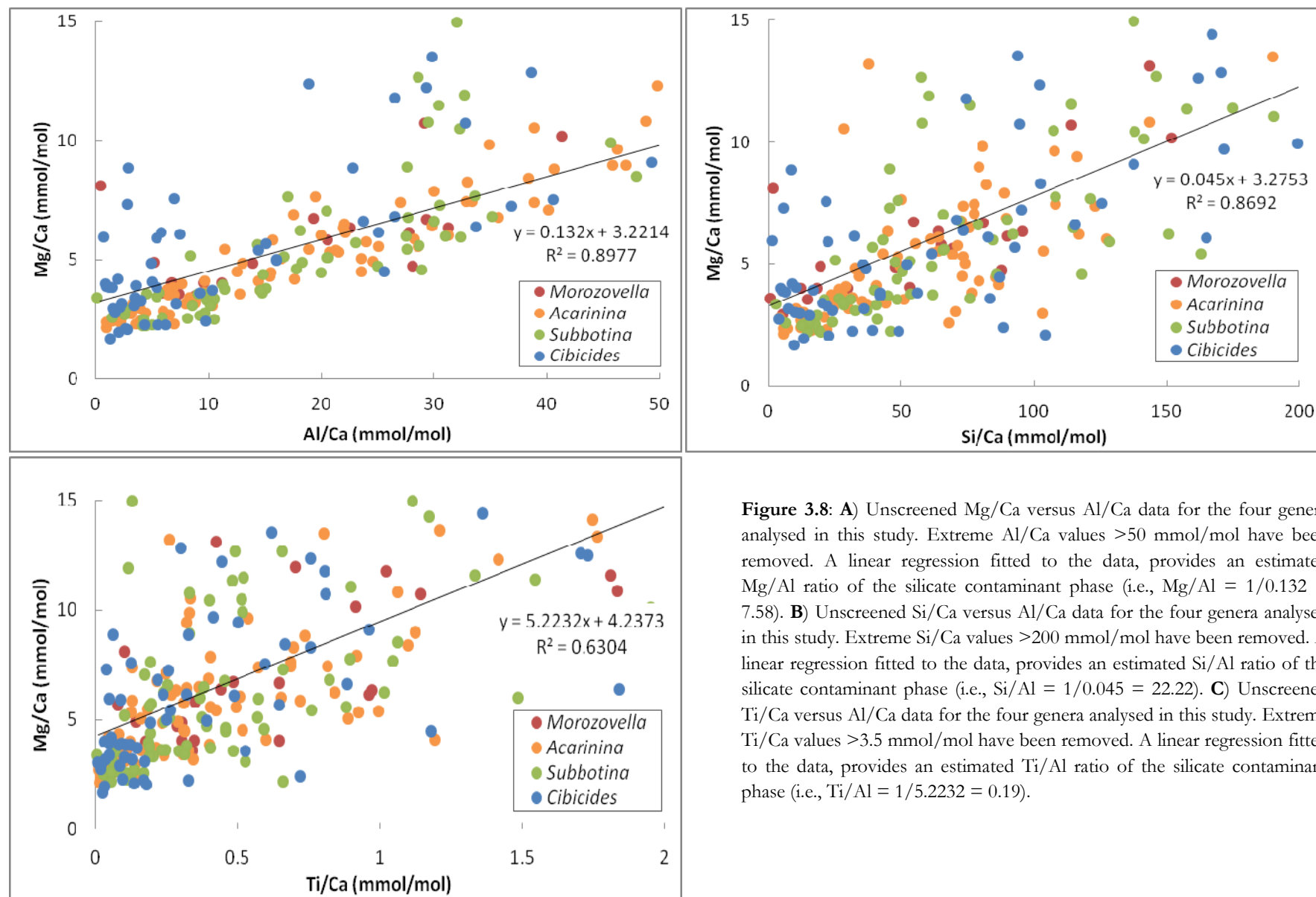
Figure 3.8: **A**) Unscreened Mg/Ca versus Al/Ca data for the four genera analysed in this study. Extreme Al/Ca values >50 mmol/mol have been removed. A linear regression fitted to the data, provides an estimated Mg/Al ratio of the silicate contaminant phase (i.e., Mg/Al = 1/0.132 = 7.58). **B**) Unscreened Si/Ca versus Al/Ca data for the four genera analysed in this study. Extreme Si/Ca values >200 mmol/mol have been removed. A linear regression fitted to the data, provides an estimated Si/Al ratio of the silicate contaminant phase (i.e., Si/Al = 1/0.045 = 22.22). **C**) Unscreened Ti/Ca versus Al/Ca data for the four genera analysed in this study. Extreme Ti/Ca values >3.5 mmol/mol have been removed. A linear regression fitted to the data, provides an estimated Ti/Al ratio of the silicate contaminant phase (i.e., Ti/Al = 1/5.2232 = 0.19).

3.6.6 *Scanning Electron Microprobe Imaging*

Upon completion of LA-ICP-MS analysis, selected foraminifera were removed from the double-sided tape adhering them to the NIST standard, transferred to an aluminium Scanning Electron Microprobe (SEM) stub pre-coated with carbon tape, and then subsequently coated with a 14–24 μm thick carbon film. Imaging was conducted using a JEOL JXA-8230 'Superprobe' electron probe microanalyser, utilising a probe current of 4.3 nA and an accelerating voltage of 15 kV.

Scanning electron images (SEI) were produced for whole foraminifer tests and, where available, SEI and backscattered electron images (BSI) were also produced for ablation pits, allowing direct comparison between the ablation site and the LA-ICP-MS analysis results in order to highlight potential sources of error caused by sedimentary contamination and/or diagenetic alteration of the specimen (*Figure 3.9*). After initial imaging, the stubs were removed from the SEM and individual foraminifer chambers levered apart with a pick, or crushed beneath a glass slide, then re-coated with carbon, enabling SEI and backscattered imaging of the microcrystalline test structure. This step allows fine details of microcrystalline structures and the test surface to be examined for effects of diagenetic alteration and assessment of the preservation of the foraminiferal test (*Figure 3.9*).
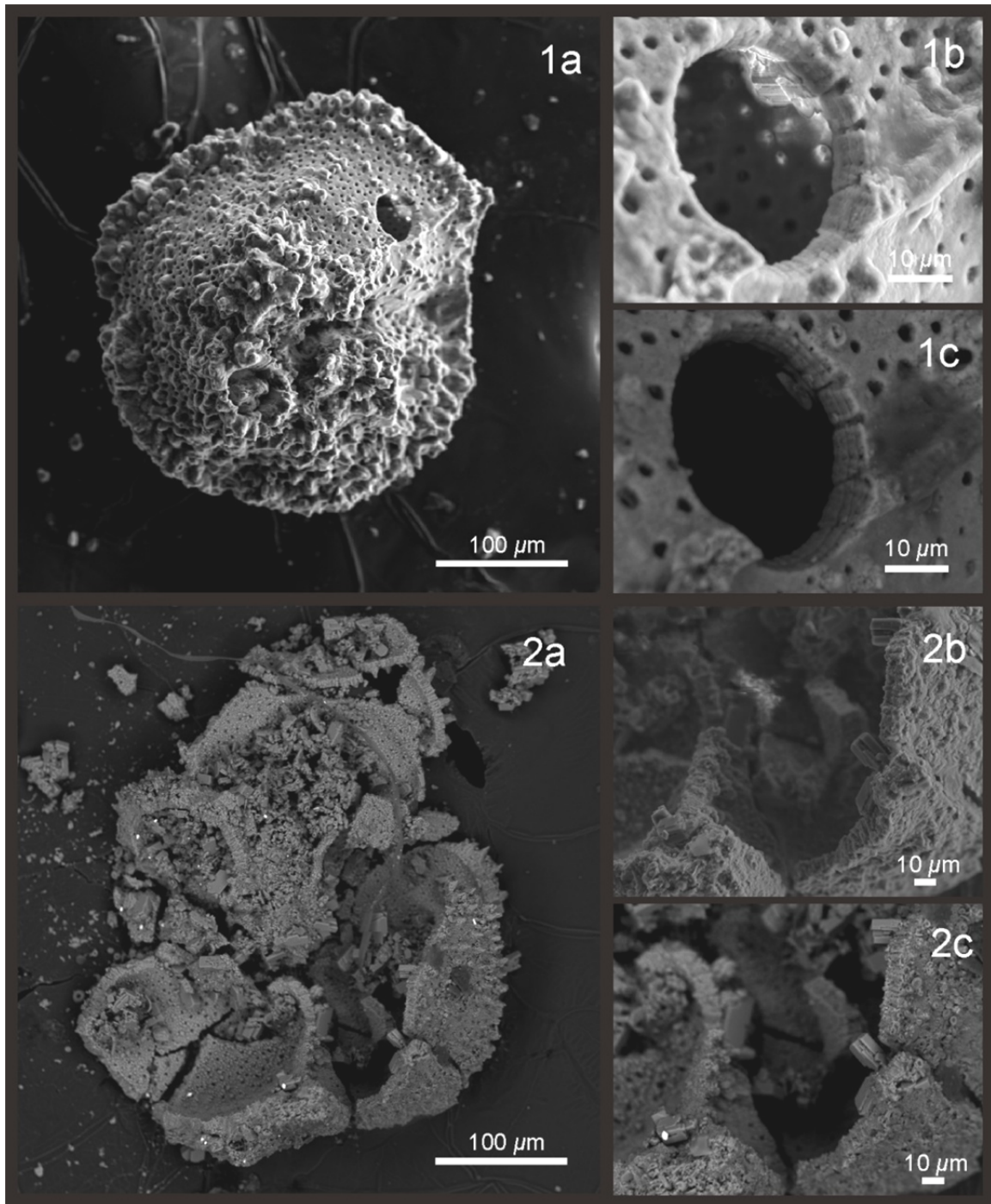
Figure 3.9: A suite of SEM images from a single Morozovella crater specimen. **1a**) Whole test SEM image to assess the general condition of the test. **1b** and **1c**) Selected images of laser ablation pits, and SEM images (**1b**) and back-scattered electron images to determine the condition of the test surface and the presence or absence of potential contamination and/or diagenetic calcite at the ablation site. The test was then crushed (**2a**) and scanning electron (**2b**) and back-scattered (**2c**) images produced of the test wall structure to assess subtle changes to the test's crystalline structure.

3.6.7   EPMA Element Distribution Mapping

The whole tests of selected foraminifera were imaged to produce SEI and BSI images, then removed from the aluminium stub and inserted into a pre-drilled, 25 mm diameter epoxy disc and back-filled with epoxy. The prepared blank was left to cure in a vacuum chamber for 30 minutes then removed and cured at 50°C overnight. The mount was then progressively polished using 10 μm grit, and progress regularly checked under a transmitted light microscope, until a satisfactory cross-section of each foraminifera was achieved. The mount was then finished using 1 μm grit, and checked to ensure all scratches were removed. A *ca.* 14 nm thick carbon film was applied and the epoxy mount inserted into a LH9 holder for imaging on a JEOL JXA-8230 'Superprobe' electron probe microanalyser, fitted with five energy dispersive (EDS) and wavelength dispersive (WDS) spectrometers. The cross-sectioned foraminifera were initially imaged using both scanning electron imaging and backscatter electron imaging modes to identify zones for mapping. Element mapping was conducted at 15.0 kV and a probe current of 20.0 nA, with a dwell time of 1000 ms and a spot size of 1 μm. The five EDS channels were used to map the distribution of calcium, magnesium, aluminium, iron and manganese, whilst WDS was used to record the distribution of silicon and calcium in addition to other irrelevant, but abundant elements present in the epoxy and carbon coating (notably; carbon, oxygen and chlorine).

The basic principle is that the intensity and wavelengths of characteristic x-rays emitted from a point on the sample where the stationary electron beam is focused are measured. The wavelength of the x-ray identifies the element, and the concentration is related to the x-ray intensity by a procedure called a ZAF calculation. Counts are processed through a ZAF calculation in an internal computer control program, which accounts for inelastic electron scattering and energy loss related to atomic number (Z), absorption of x-rays by the sample (A), and an x-ray fluorescence correction (F). The beam effectively scans a predetermined area in a grid-like pattern, producing element distribution maps for the selected elements, with a resolution of 1 μm.

3.7   Paleo-Sea Temperature Calculations

Sea temperatures were calculated using *Equation 3.4*, inherent to which are four key assumptions that need to be addressed when considering the reliability of these calculations.

$$\text{Mg/Ca} = \frac{\text{Mg/Ca}_{sw\text{-}t}}{\text{Mg/Ca}_{sw\text{-}0}} \times A \times \exp^{\,B \times T}$$

Equation 3.4

3.7.1   Inter-specific Ecological Differences

Inter-specific offsets are common and widely recognised in the composition of $\delta^{18}O$ records (Shackleton & Kennett, 1975). The same is also true for Mg/Ca ratios of foraminifera and relates to the mechanisms employed by individual species in the precipitation of calcite, and has been shown to vary significantly between spinose and non-spinose as well as symbiotic and asymbiotic species (Lea, 1999). The simplest means to curtail this issue is to select a single representative species and normalise the offset observed in the other species to the representative.

Morozovella and *Acarinina* are both used to derive sea surface temperatures, however raw Mg/Ca ratios of *Morozovella* are consistently offset to lower values than *Acarinina* ratios. The consistency of this means it is likely to be a manifestation of an inter-species difference in Mg incorporation into the test and can be remedied with a simple correction. A significant offset is observed between *Subbotina* and the other planktic species, mainly as a function of the deeper, cooler environment in which *Subbotina* calcified. No correction has been applied to *Subbotina* data as it provides a useful indicator of thermocline temperatures. Given that *Cibicides* is the only benthic genus analysed in this study it is not necessary to account for any inter-specific offsets in benthic genera. Creech *et al.* (2010) showed that the multispecies calibration of Anand *et al.* (2003) yielded consistent temperature values for the planktic genera *Morozovella* and *Acarinina*, noting that *Acarinina primitiva* yielded marginally cooler temperature that *Morozovella crater*, and *Acarinina collactea* produced temperature values slightly warmer than *M. crater* suggesting subtle differences in the Mg/Ca – temperature calibration between morozovellids and acarininds.

3.7.2 Preservation of Primary Calcite

A quantitative and unambiguous assessment of the degree of preservation of primary foraminiferal calcite is difficult. However, diagenetic factors typically affect the test surface and are largely surmounted by the laser ablation method employed in this study and the rigorous screening of trace element depth profiles. The preservation of primary calcite was further ascertained by qualitative visual inspection via reflected light microscopy and SEM imaging.

3.7.3 Eocene Seawater Mg/Ca values

Eocene seawater is considered to have had a lower Mg/Ca value than the modern seawater value of 5.16 mol/mol (Lear *et al.,* 2002). Sea temperatures for this study have been calculated using an estimated seawater value of 4.1 mol/mol, which yields conservative temperature estimates (i.e., low) that are consistent with multi-proxy comparisons (e.g. Hollis *et al.,* 2012).

3.7.4 Mg/Ca–Temperature Calibrations

As there are no extant species of the planktic genera utilised in this study, temperature calculations for planktic taxa were made using a multi-species Mg/Ca–temperature calibration from modern tropical–subtropical planktic foraminifera (*Table 3.5*; Anand *et al.,* 2003). Benthic temperatures were calculated using a calibration obtained from core-top calibration of three modern *Cibicidoides* species; *C. wuellerstorfi, C. pachyderma* and *C. compressus.* (*Table 3.5*; Lear *et al.,* 2002).

Table 3.5: Calibration constants used in Mg/Ca sea temperature determinations (Equation 3.4).

Calibration	*A*	*B*	Source
Planktic	0.380	0.090	Anand *et al.* (2003)
Benthic	0.867	0.109	Lear *et al.* (2002)

3.7.5   Calculation of Errors

Three types of errors were considered for the sea temperatures derived from Mg/Ca ratios. These include the analytical error, a standard calibration error, and the sample error. The analytical error is accounted for in the data processing step and typically produces very small uncertainties ($\pm$ 1–3%; 2 se) associated with counting statistics during ablation and data acquistion. The calibration error is the residual error of ±1.5°C on the regression of the multi-species calibrations established by Lear *et al.* (2002) and Anand *et al.* (2003). The sample error pertains to the 95% confidence interval calculated for the mean temperature value obtained from multiple analyses within a single sample. The confidence interval is calculated by:

$$\bar{x} \pm t \times \frac{\sigma}{\sqrt{n}}$$ *Equation 3.5*

where $\bar{x}$ is the sample mean, t is is the inverse of the student's t-distribution, σ represents the standard deviation and *n* is the number of analyses. The cumulative error calculated from the sum of all three errors is applied to each temperature value, providing upper and lower uncertainties. However, these calculations greatly underestimate the true uncertainty of Mg/Ca-derived sea temperatures when the number of individuals analysed (*n*) is small, as previous studies (Sadekov *et al.*, 2008; Bolton *et al.*, 2011; Marr *et al.*, 2011) of plankton tow, core-top and Quaternary foraminifera have shown that in single samples the inter-individual variability in foraminiferal Mg/Ca ratios is large (*ca.* $\pm$ 60% about the mean). This presumably reflects some, as yet unknown, foraminiferal vital effects during the precipitation of calcite. Within a single sample, different individual planktic foraminifera show a range of values that can be up to 50–70% higher or lower than the cumulative mean of individuals in that sample. When a large number of foraminifera are analysed then this effect is largely diminished, but in this study, where *n* is small, this uncertainty becomes the greatest source of errors on calculated sea temperatures.

A Monte Carlo method of modelling these errors (Baker, pers. comm.) has been used to determine how the temperature uncertainties of planktic species changes with *n*, and to robustly estimate the percent standard error (% 2 se) of Mg/Ca ratios as a function of the number of individuals analysed (*Figure 3.10*). This method utilises samples for which a large number of foraminifera have been analysed and then randomly samples n analyses (*n* = 1 to 15) multiple times. The multiply sampled analyses for each *n* are then averaged and a % 2 sd and % 2 se calculated, with the % 2 se considered to provide the best estimate of how the uncertainty on Mg/Ca ratios varies as a function of *n*. For example, *Figure 3.10* shows that for *Globigerina bulloides* the % 2 se on Mg/Ca ratios decreases as a power law function from *ca.* $\pm60\%$, $\pm25\%$, $\pm18\%$ and

±14% for n = 1, 2, 3 and 4, respectively. Benthic foraminiferal data from Creech (2010) also clearly display the same inter-individual variability as planktic species, despite a maximum number of six individuals being analysed per sample, so the same % 2 se estimates were used for both benthic and planktic species.

The chart shows data points with a fitted curve. The equation and correlation coefficient displayed are:

$$y = 53.905x^{-0.992}$$
$$R^2 = 0.9907$$

The y-axis is labelled "% 2 se on Mg/Ca" ranging from 0 to 70. The x-axis is labelled "Number of Individuals (n)" ranging from 0 to 16.
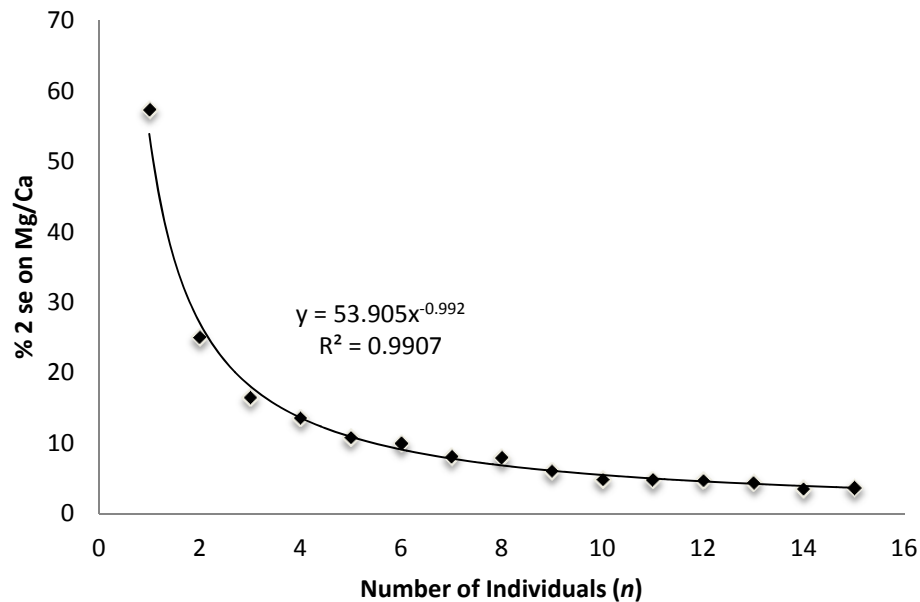
Figure 3.10: Modelled effect of the number of individuals analysed on the % 2 se on Mg/Ca ratios for planktic species (*G. bulloides*) from four Quaternary samples showing a decrease in the error applied to Mg/Ca ratios as n increases. Figure supplied by J. Baker.

PALEOGENE STRATIGRAPHY OF TORA

4.1   Introduction

The Paleogene stratigraphy of the East Coast Basin in the Tora area of the southern Wairarapa region contains important records of paleoenvironmental changes that occurred within the New Zealand region during the Paleogene, including Eocene climatic events, and represents an important locality for potential hydrocarbon source and reservoir units, as the area may contain the only onshore expression of key units derived from the Pegasus Sub-basin.

Initial field mapping for this study identified a coast parallel-striking stratigraphic succession bisected by several small streams perpendicular to the coast (*Figure 4.1*). Field mapping identified good exposure of all formations and minimal structural complications in Pukemuri Stream, which is designated as the reference section for the Tora area. Small-scale deformational structures are prevalent in Awheaiti and Te Oroi Streams, but good outcrop in Awheaiti Stream makes it suitable as a secondary section in support of the Pukemuri reference section. Te Oroi Stream was measured and described as a further accessory section. In addition, key units from Manurewa and Te Kaukau Points are described, as some units are not preserved in the stream sections (*Figure 4.1*). Measured section results from three sections (Pukemuri, Awheaiti and Te Oroi Streams) are reported here with supplementary details from Manurewa and Te Kaukau Points. Extensive sampling was carried out in the Pukemuri and Awheaiti Stream sections. Foraminiferal and calcareous nannofossil assemblage data referred to in this chapter is presented in *Appendix 1*.

Original lithological divisions identified by Waterhouse (1955) and Waterhouse & Bradley (1957) have largely been confirmed and adopted by this study. Notable exceptions include the identification of Glenburn Formation by Laird *et al.* (2003), replacing the Piripauan Sandstone of Waterhouse & Bradley (1957), and identification of Wanstead Formation in lieu of the Kandahar Formation (after Moore *et al.*, 1986; 1988a; Field, Uruski *et al.*, 1997). It should be noted that field mapping for this study identified three members in the Mungaroa Limestone (as identified by Waterhouse & Bradley, 1957; Browne, 1987), but not all members are present in all sections. A revised stratigraphy of the Tora area is presented in this chapter.
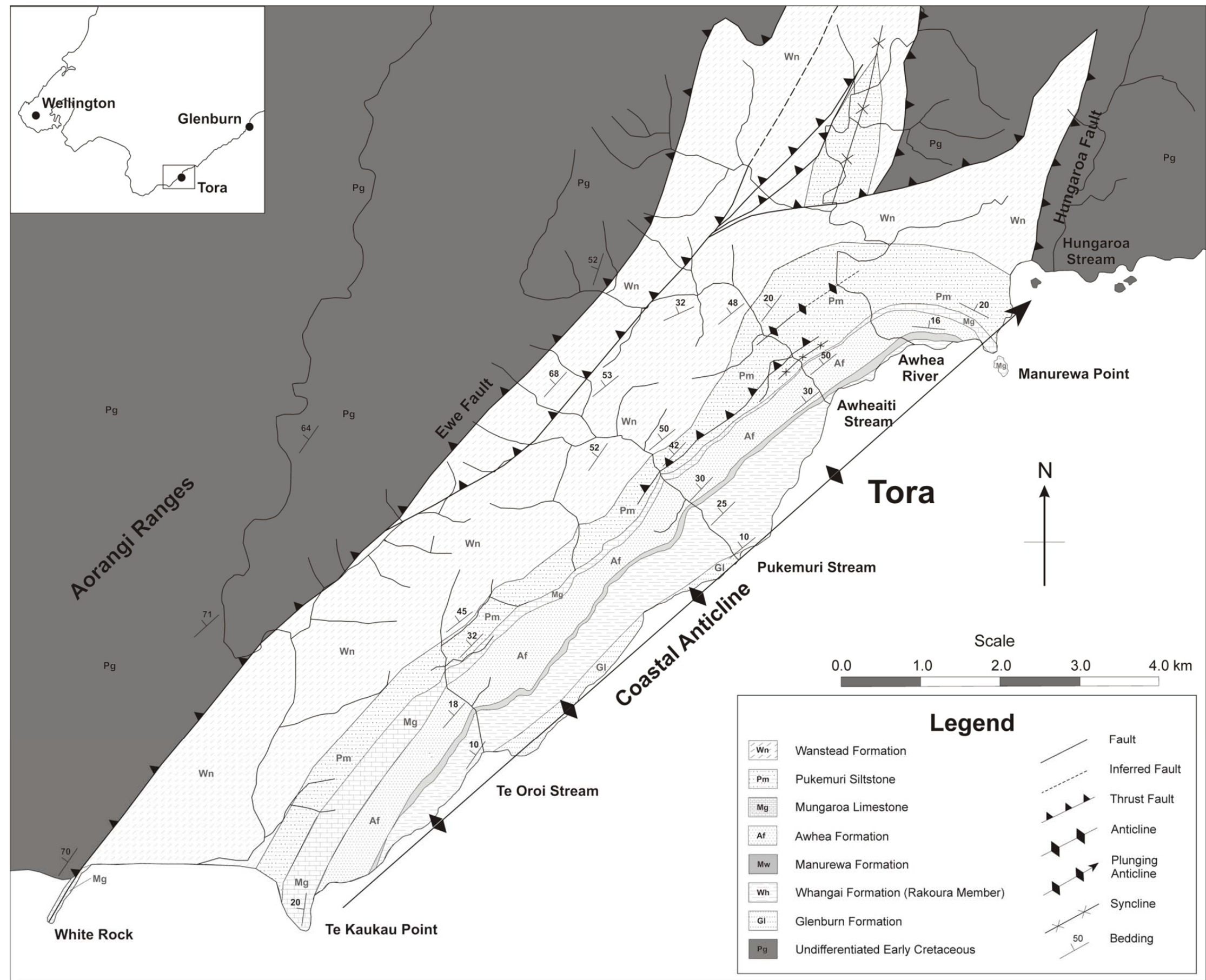
Figure 4.1: Geological map of the late Cretaceous to early Paleogene sequence exposed at Tora, on the southeast Wairarapa coast, North Island, New Zealand.

Legend

Wn	Wanstead Formation	
Pm	Pukemuri Siltstone	
Mg	Mungaroa Limestone	
Af	Awhea Formation	
Mw	Manurewa Formation	
Wh	Whangai Formation (Rakoura Member)	
Gl	Glenburn Formation	
Pg	Undifferentiated Early Cretaceous	

Fault
Inferred Fault
Thrust Fault
Anticline
Plunging Anticline
Syncline
Bedding

4.2   Structural Geology of the Tora Area

The dominant structures in the Tora area are the Ewe and Hungaroa Faults and the Coastal Anticline (Waterhouse 1955; Waterhouse & Bradley, 1957; Laird *et al.,* 2003). The Ewe Fault separates the Paleogene sequence of the Tora area from Early Cretaceous rocks of the Aorangi Ranges, and is readily traced in outcrop and in aerial and satellite imagery from White Rock in the south, northwards to the Awhea River (*Figure 4.1*). The Ewe Fault consists of at least two fault splays separated by *ca.* 70 m, demonstrating a reverse sense of displacement, striking 040° and dipping at 62° northwest. Based on conservative thickness estimates from field mapping, the fault zone represents a minimum vertical displacement of 1000 m between the Upper Cretaceous-Lower Paleogene succession exposed on the eastern footwall block and the Lower Cretaceous strata of the western hanging wall block. Micritic limestone is observed thrust up along the fault trace at several locations, with one such example forming the reef at White Rock (*Figure 4.2a*).

The axis of the Coastal Anticline trends 040° dipping at 20° to the northeast and roughly follows the Tora coastline, and is well-exposed on the shore platform between Te Oroi and Pukemuri Streams and at Manurewa Point (*Figure 4.1*). Normal faulting occurs near the crest of the anticline in the Mungaroa and Awhea Formations (*Figure 4.2b*), likely associated with folding of the anticline. The parallel trends of the Coastal Anticline and the Ewe Fault suggest that they are probably associated with the same tectonic regime. At least two deformational episodes are associated with the formation of the Coastal Anticline; the first folding the strata, and the second tilting the anticline by 20°. This second event may be associated with the development of the Hungaroa Fault, which obliquely truncates the Coastal Anticline in the north of the Tora area (*Figure 4.1*). The shear zone associated with the Hungaroa Fault is 20 m-wide, with a well-developed shear fabric exposed on a wave cut section near the mouth of Hungaroa Stream (*Figure 4.2c, d*).

An unnamed, small-scale reverse fault can be traced in outcrop between Pukemuri and Awheaiti Streams, representing a displacement of approximately 60 m. In Pukemuri Stream this causes repetition of the middle Mungaroa Limestone member - Awheaiti Formation - lower Pukemuri Siltstone sequence (*Figure 4.2e*), whereas in Awheaiti Stream it simply repeats the lower section of the Pukemuri Siltstone. Extensive small-scale folding, shearing and fault repetition of the Pukemuri and Wanstead Formations has resulted in an over-thickening of the formations in the Awheaiti Stream section (*Figure 4.2f*), with the apparent repeated thickness decreasing southwards towards Te Kaukau Point.

Figure 4.2: Aspects of structural geology observed in the Tora area. **A**) Mungaroa Limestone thrust up along the Ewe Fault at White Rock forming a reef. (Highest point is 15 m) **B**) Small-offset normal faulting in Awhea Formation near the crest of the Coastal Anticline, Manurewa Point. **C**) Hungaroa Fault zone outcropping on the shore platform, with lower Cretaceous Mangapokia Formation thrust over middle to late Eocene Wanstead Formation. **D**) Well-developed shear fabric of the Hungaroa Fault zone exposed on the shore platform at Stoney Bay. Hammer is 33 cm long. **E**) Unnamed reverse fault exposed in Pukemuri Stream causing repetition of the Mungaroa Limestone-lower Pukemuri Siltstone sequence. **F**) Small-scale folding of Wanstead Formation, Pukemuri Stream.

4.3   Measured Section Results

Initial geological mapping identified several areas where suitable outcrop and reasonably coherent stratigraphy occurred. Tape and compass maps and stratigraphic sections were measured for the Paleogene strata in Pukemuri, Awheaiti and Te Oroi Streams. These sections are several kilometres apart (*Figure 4.1*), providing a basis for correlating changes in the stratigraphic succession.

The tape and compass maps, cross-sections, micro-fossil sample locations and measured sections are presented for the Pukemuri and Awheaiti Stream sections. Foraminiferal assemblages were collected from each measured section, and calcareous nannofossil assemblages collected from the Pukemuri and Awheaiti Stream sections for age and environmental determinations (this chapter). Foraminiferal and calcareous nannofossil assemblages are presented in *Appendix 1*. Foraminiferal assemblages from Cretaceous-Cenozoic Programme (CCP) samples collected in each of the stream sections were also used in this study (*Appendix 1*). Bulk rock samples and foraminiferal collections from these measured sections were used for geochemical analyses presented in Chapter Five.

4.3.1   Pukemuri Stream

The Pukemuri Stream section extends from the base of the Paleocene Awhea Formation (grid reference: S28 175 618) to the middle Eocene Wanstead Formation (grid reference: S28 168 626) (*Figures 4.3* and *4.4*). The base of the Manurewa Formation outcrops 500 m upstream of the mouth of Pukemuri Stream. This formation has been studied in detail by Wasmuth (1996) and Laird *et al.* (2003), so the measured section began at the upper contact with the Awhea Formation, represented by a 3 m-thick glauconitic sandstone bed.

The reference sections selected by Waterhouse (1955) and Waterhouse & Bradley (1957) were unable to be identified due to poor documentation and obscured sections. However, Pukemuri Stream has excellent exposure of all nine formations present in the Tora area, and a minimum of structural complications. Consequently, Pukemuri Stream has been designated the reference section in this study for the stratigraphic succession at Tora.
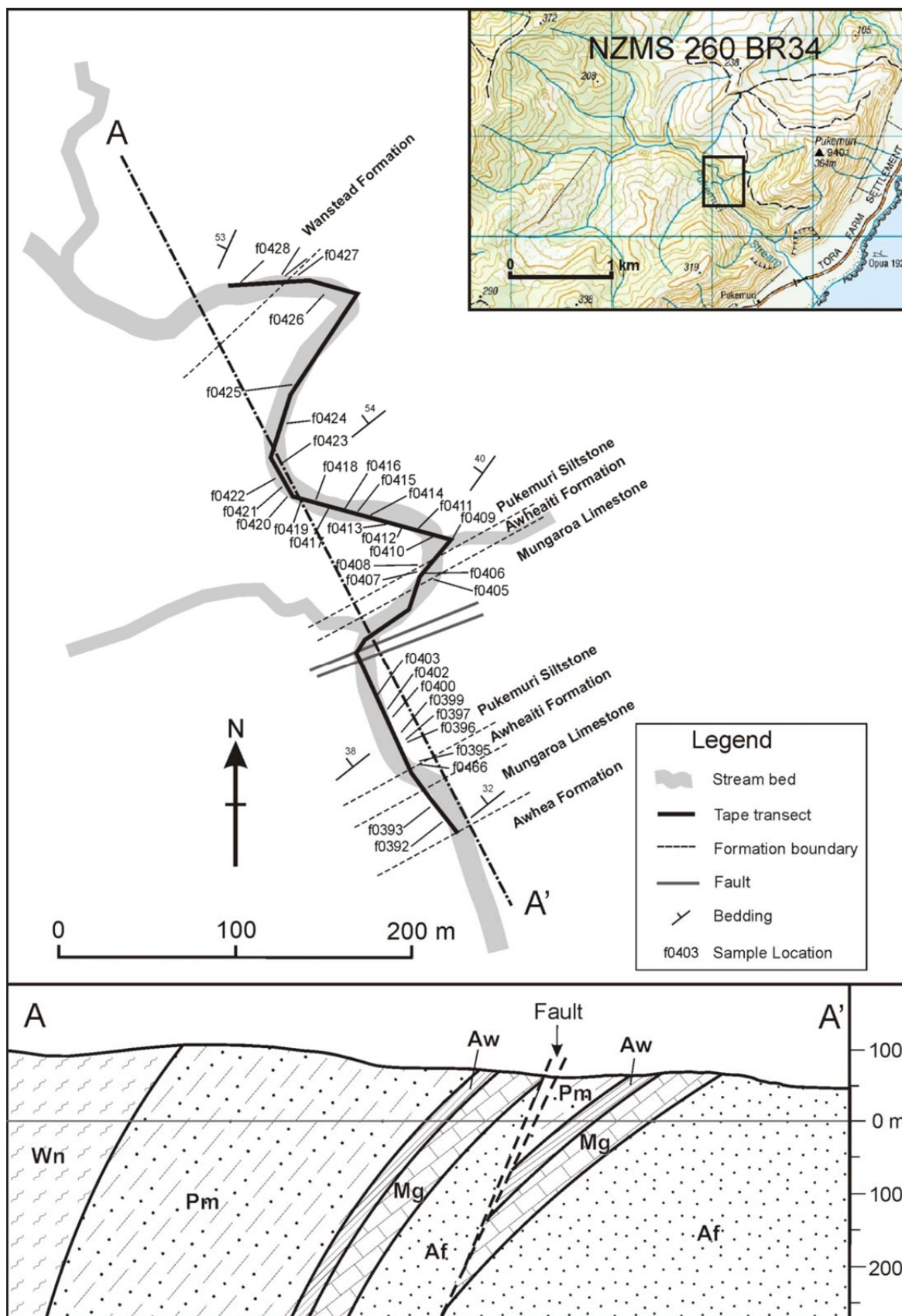
Figure 4.3: Pukemuri Stream tape and compass map and schematic cross-section. Key to abbreviations: Af = Awhea Formation, Mg = Mungaroa Limestone, Aw = Awheaiti Formation, Pm = Pukemuri Siltstone, Wn = Wanstead Formation.
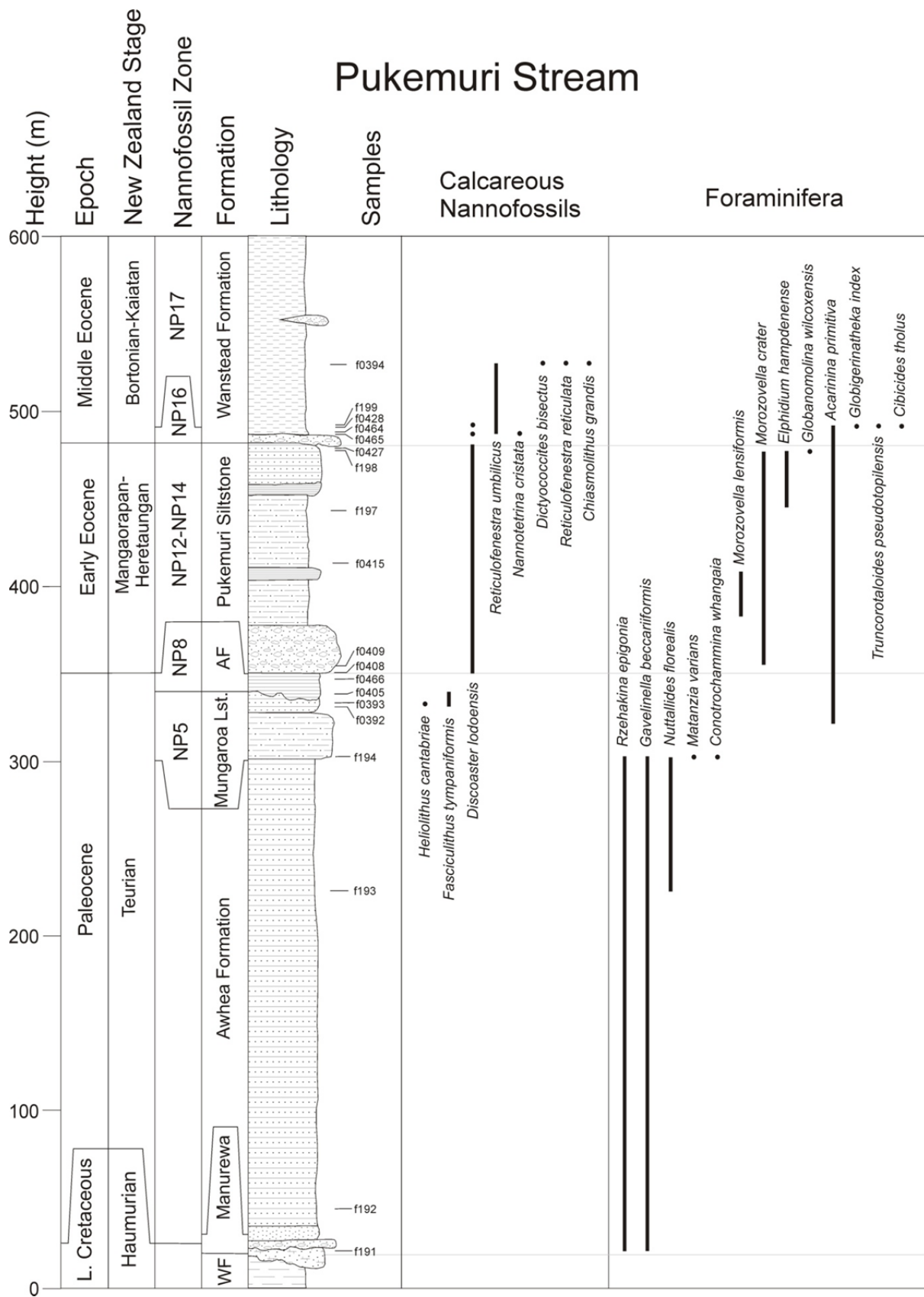
Figure 4.4: Stratigraphic column for Pukemuri Stream showing key lithostratigraphy and biostratigraphic datums.

Awhea Formation

Lithostratigraphy

The base of the Awhea Formation is marked by a 3 m-thick glauconitic sandstone bed, exposed 1 km upstream from the mouth of Pukemuri Stream. The Awhea Formation conformably overlies Manurewa Formation with 275 m of hard, cm- to dm-bedded, glauconitic sandstone beds with sharp basal contacts, separated by thin, calcareous, micaceous mudstone. The lower Awhea Formation outcrops as prominent, steeply inclined dip slopes (*Figure 4.5a*), and shows extensively bioturbated bedding surfaces. Vertical and horizontally oriented burrows are commonly infilled with pyrite (*Figure 4.5b*). Occasional fragments of carbonaceous material occur near the base of the formation (*Figure 4.5c*). The formation becomes progressively thinner bedded, finer grained and less glauconitic towards the top of the formation and bioturbation becomes less extensive (*Figure 4.5d, e*).

Paleontology and Age

A sample (S28/f192) from the lower Awhea Formation contains a long-ranging agglutinated foraminiferal assemblage that extends from the Campanian to Paleocene (Haumurian to Teurian). Identification of the Cretaceous/Paleogene (K/Pg) boundary in the underlying Manurewa Formation (Wasmuth, 1996; Laird *et al.*, 2003) and a sample (S28/f1093) from the middle of the Awhea Formation contains the Teurian marker species *Nuttalides florealis*, constraining the age of the Awhea Formation to the Paleocene (*Figure 4.4*). Agglutinated taxa (>90%) dominate assemblages from samples S28/f0192 and S28/f0193, which also contain the benthic foraminifera *Bathysiphon* sp., *Ammodiscus cretaceous*, *Gavelinella beccariiformis* and *N. florealis* (*Appendix 1*). Extensive trace fossil assemblages exposed on bedding planes in lower Awhea Formation include *Planolites*, *Ophiomorpha*, *Paleodictyon*, *Nereites, Scolicia* and occasional *Zoophyco*s.
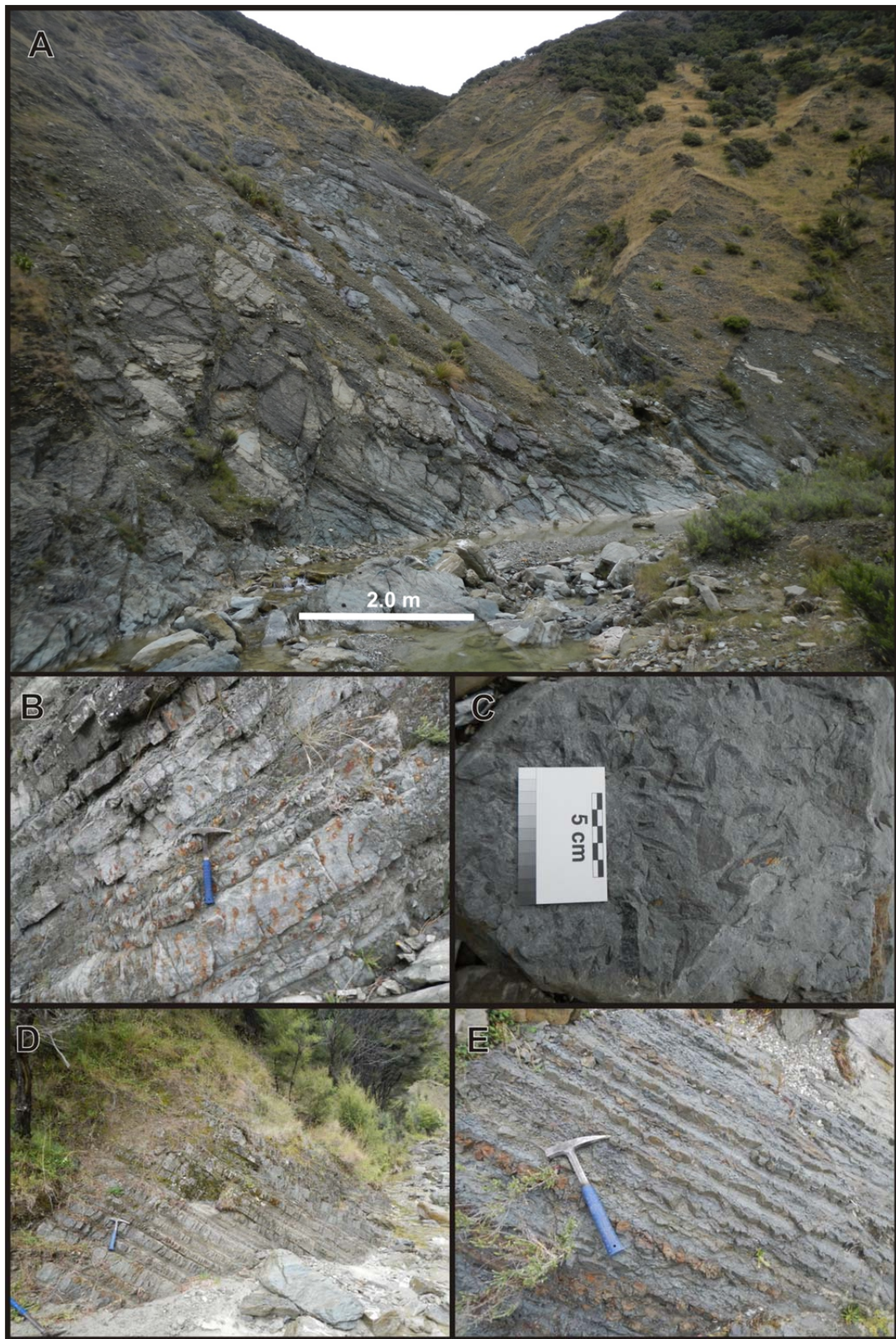
Figure 4.5: Features of the Awhea Formation exposed in Pukemuri Stream. **A**) Steeply inclined dip-slopes of the Awhea Formation. **B**) Lower Awhea Formation displaying sandstone beds separated by thin mudstone layers and an abundance of weathered, pyrite filled burrows. **C**) Carbonaceous material from the lower Awhea Formation. **D**) Well-bedded middle Awhea Formation displaying consistent bedding thickness and classic turbidite characteristics. Hammer for scale. **E**) Uppermost extent of the Awhea Formation, exhibiting significant thinning of beds.

Mungaroa Limestone

Lithostratigraphy

Much of the Mungaroa Limestone outcrops in a 20 m-high waterfall (*Figure 4.6a*) 1500 m from the mouth of Pukemuri Stream, where it conformably overlies the Awhea Formation. The lower 20 m of Mungaroa Limestone is pale grey, calcareous, glauconitic, interbedded fine sandstone with minor mudstone displaying dm-scale bedding. This unit represents the lower member of the Mungaroa Limestone. Conformably overlying this interval is a 10 m-thick unit of green-grey, cm- to dm-bedded glauconitic sandstone and mudstone (*Figure 4.6b*), with sharp lower contacts on moderately sorted sandstone beds, grading up into mudstone with dark laminae, which occasionally outline small-scale cross-bedding (Bouma sequences A, B, C; *Figure 4.6c, d, e*). This unit is identified as the middle member of the Mungaroa Limestone, and the upper micritic limestone member is absent in the Pukemuri Stream section. The middle member is extensively bioturbated on some bedding planes, including traces of *Scolicia* and *Zoophycos*.

Paleontology and Age

A sample from the base of the Mungaroa Limestone (S28/f0194) contains a Paleocene (Teurian) foraminiferal assemblage that includes *Conotrochammina whangaia*, *Matanzia varians*, *Gavelinella beccariiformis* and *Nuttalides florealis* (*Figure 4.4*). In addition, the benthic foraminiferal assemblage also contains *Osangularia* sp., *Rzehakina epigona*, *Glomospira charoides* and *Lituotuba* sp.

Calcareous nannofossil assemblages from two samples (S28/f0392 and S28/f0393) from the upper unit of the Mungaroa Limestone in Pukemuri Stream are correlated with Nannofossil Zone NP5 (middle Paleocene, late Teurian). The relatively sparse assemblages are characterised by *Coccolithus pelagicus*, *Chiasmolithus* spp., *Prinsius* spp., *Toweius* spp. and *Fasciculithus* spp. The samples are assigned to Zone NP5 based on the presence of zonal marker *Fasciculithus tympaniformis* and the absence of *Heliolithus kleinpellii*, which marks the base of Zone NP6. Sample S28/f0393 contains *Heliolithus cantabriae*, which first occurs within Zone NP5 (*Figure 4.4*).

Figure 4.6: Features of the Mungaroa Limestone outcropping in Pukemuri Stream. **A**) 20 m-high waterfall, with the contact between the lower and middle members (white dashed line). Figure for scale. **B**) Outcrop of dm-bedded glauconitic sandstone of the middle member above the waterfall. **C**) Example of well-bedded, normal graded sandstones fining into mudstone **D**) Fining upwards, cross-laminated mudstone and sharp contact with overlying sandstone. **E**) Detail of small cross-lamination outlined by carbonaceous material in mudstone.

<u>Awheaiti Formation</u>

Lithostratigraphy

In Pukemuri Stream, the Awheaiti Formation is best exposed in a fault-repeated section, above a small waterfall (S28 171 622). The Awheaiti Formation is channelised into the underlying Mungaroa Limestone, and the lower portion of the formation is composed of *ca.* 60 cm-thick cross-bedded sandstone layers, with channelised contacts between beds (*Figure 4.7a, b*). The remainder of the 11 m-thick unit is well-bedded, laminated, micaceous mudstone and glauconitic fine sandstone (*Figure 4.7c, d*). Bedding surfaces 2 m below the upper contact contain abundant *Bathysiphon* sp., up to 5 cm-long, displaying a northwest-southeast current lineation (*Figure 4.7e*). In addition, the trace fossils *Ophiomorpha* sp. and *Planolites* occur on bedding planes.

Paleontology and Age

Four samples from the Awheaiti Formation at Pukemuri Stream were examined for calcareous nannofossils (S28/f0466, f0406 and f0407), although the latter two were barren (*Appendix 1*). The lowest sample (S28/f0466) contains the best assemblage, with frequent, moderately well-preserved nannofossils. The assemblages are correlated with Nannofossil Zone NP7 or lower NP8 (late Paleocene, late Teurian) based on the presence of *Discoaster mohleri* and absence of *Discoaster nobilis* (*Figure 4.4*). A foraminiferal residue examined from Awheaiti Formation (S28/f0196) provided a very poor fauna with no age or environmentally diagnostic taxa.
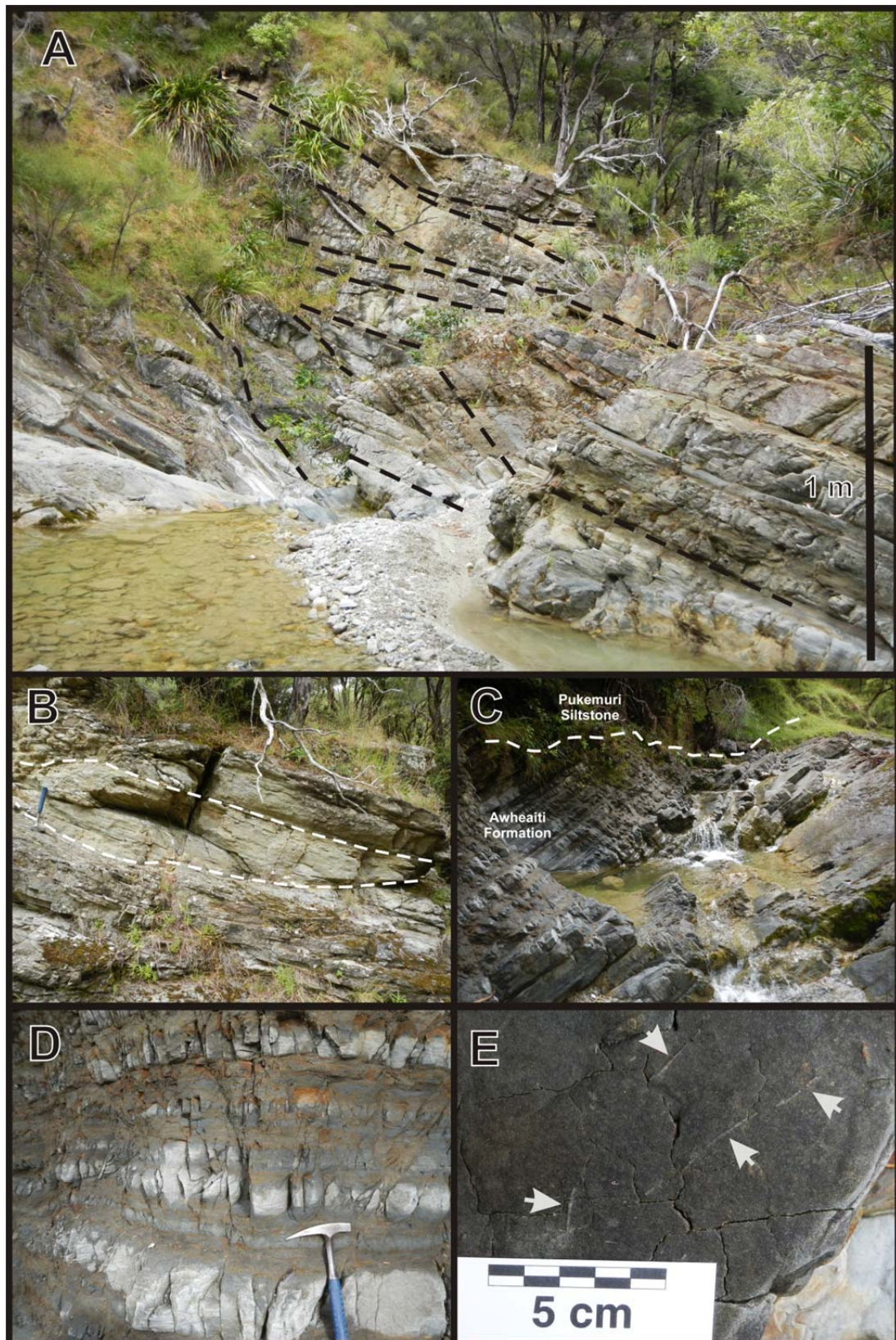
Figure 4.7: Features of the Awheaiti Formation exposed in Pukemuri Stream. **A**) Channelisation of the Awheaiti Formation in the Pukemuri Stream outcrop. **B**) Example of channelised sandstones of the Awheaiti Formation. Hammer for scale. **C**) Exposure of Awheaiti Formation in Pukemuri Stream and the unconformable upper contact with the Pukemuri Siltstone. **D**) Detail of laminated and dm-bedded fine sandstone and mudstone of the Awheaiti Formation **E**) ≤5 cm long *Bathysiphon* foraminifera (arrowed).

Pukemuri Siltstone

Lithostratigraphy

The Pukemuri Siltstone unconformably overlies the Awheaiti Formation with an angular discordance of *ca.* 20°. The basal contact at Pukemuri Stream is represented by a 1 m-thick massive, pebbly-sandstone, with poorly-sorted, well-rounded clasts and a glauconitic sandy matrix (*Figure 4.8a*). Above this is a 30 m-thick pebbly-mudstone unit with well-rounded pebbles of mixed lithologies, mostly indurated sandstone and occasional chert (*Figure 4.8b*). These pebbles rarely exceed 10 cm in size and are supported within a glauconitic, grey sandy-mudstone matrix. Pebbles become less frequent and scattered towards the top of the unit, which grades into blue-grey, faintly cm-bedded mudstone that displays some convolute bedding and intraformational slumping interspersed amongst undisturbed layers (*Figure 4.8c*). A 1 m-thick layer of light brown mudstone occurs in the middle of this succession and contains a 25 cm-thick glauconitic sandstone layer. The glauconitic sandstone appears faintly cross-bedded and includes small, 5 cm-long sideritic concretions and well-rounded, brown mudstone clasts (*Figure 4.8d*).

Immediately above the glauconitic sandstone layer is a large boulder (2 × 6 m) of cemented, clast-supported conglomerate and several well-rounded boulders of hard, cemented sandstone up to 1.5 m in diameter (*Figure 4.8e*). The upper part of the formation consists of 50 m of grey, thin-bedded sandstone and mudstone and 5 m of cm-laminated, purple-brown micaceous mudstone with glauconitic laminae between layers. This is overlain by 30 m of grey, well-bedded, laminated mudstone at the top of the formation (*Figure 4.8f*), with 20 cm of soft, grey, calcareous mudstone immediately beneath the unconformable contact with the overlying Wanstead Formation.

Paleontology and Age

Two samples from the Pukemuri Siltstone (S28/f0197 and S28/f0198) produced extensive foraminiferal assemblages; with zonal markers (e.g. *Acarinina primitiva, Elphidium hampdenense, Morozovella crater)* from an additional 27 samples providing supplementary information. Sample S28/f0198 in the upper Pukemuri Siltstone contains the key index species *Morozovella crater* and *Elphidium hampdenense*, indicating a Heretaungan age (latest Early Eocene to early Middle Eocene). Sample S28/f0197 from slightly lower in the section contains a less definitive fauna, giving a Waipawan to Porangan (Early to Middle Eocene) age.

Sample S28/f0197 has a benthic assemblage that includes; *Lenticulina* spp., *Bulimina pupula*, *Cibicides truncatus*, *Anomalinoides* sp., *Bathysiphon* sp., *Bolivinopsis* cf. *spectabilis*, and *Gyroidinoides* cf. *neosoldanii*, while the benthic foraminiferal assemblage from sample S28/f0198 is characterised by *Tritaxilina zealandica*, *Gyroidinoides neosoldanii, Kalamopsis grzybowskii, Chilostomella* sp., *Pleurostomella* sp., *Nuttallides carinotruempyi* and *Anomalina aotea.*

Twenty-seven calcareous nannofossil samples from the Pukemuri Siltstone contain Early to Middle Eocene assemblages. The presence of *Discoaster lodoensis* throughout the formation, indicates correlation with Nannofossil Zones NP12-14 (late Early to early Middle Eocene), consistent with foraminiferal biostratigraphy (*Figure 4.4*). Despite the high sampling resolution, no further zonal subdivision is possible.
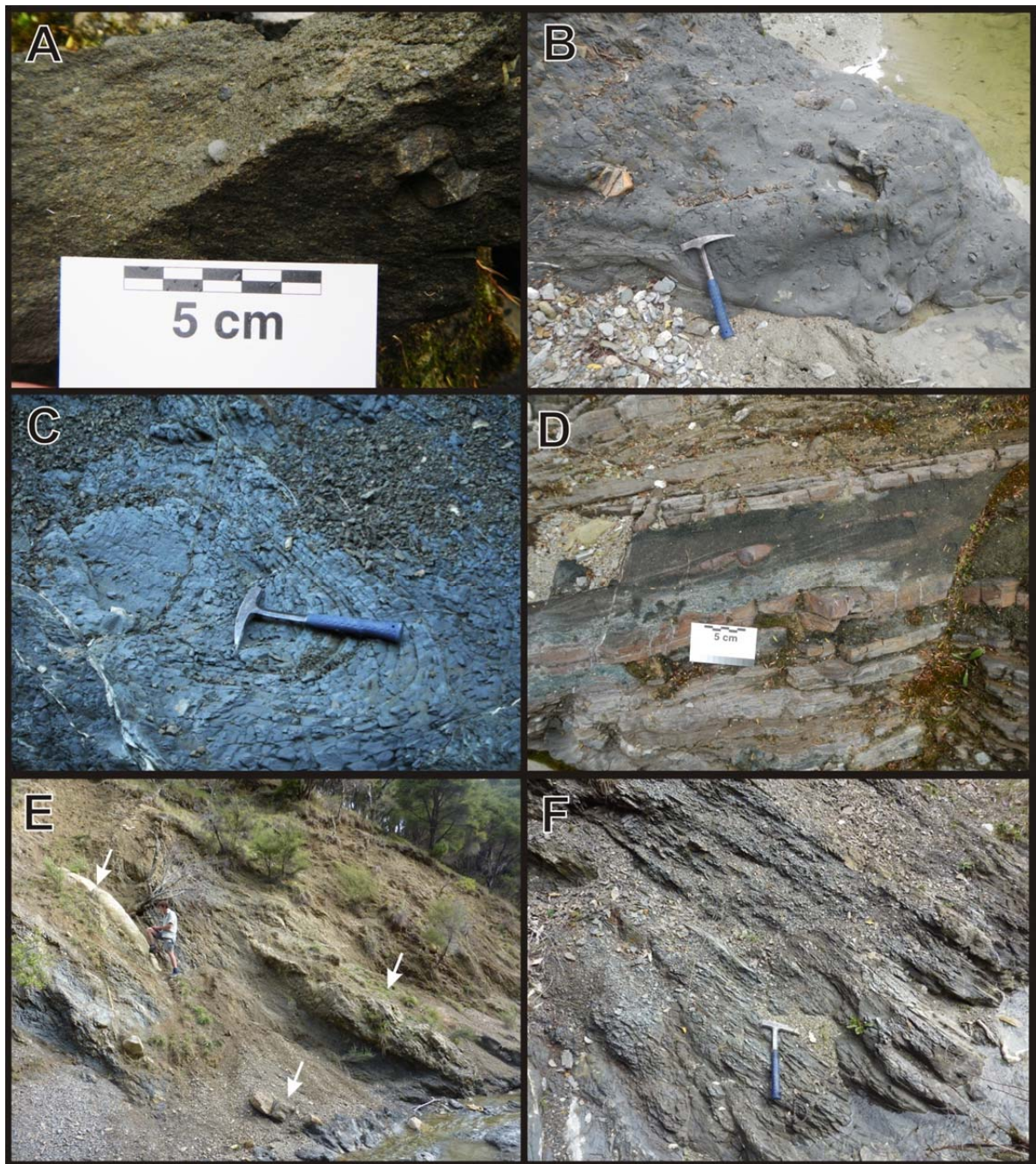
Figure 4.8: Details of the Pukemuri Siltstone in Pukemuri Stream. **A**) Pebbly-sandstone immediately above the basal contact of the Pukemuri Siltstone. **B**) Pebbly mudstone unit of the lower Pukemuri Siltstone. **C**) Soft sediment slump structure in the Pukemuri Siltstone. **D**) Glauconitic sandstone incorporating well-rounded brown mudstone clasts. **E**) Indurated conglomerate and sandstone boulders (arrowed) included within the lower Pukemuri Siltstone. Person for scale. **F**) Thin-bedded, grey, flaggy mudstone typical of much of the Pukemuri Siltstone.

<u>Wanstead Formation</u>

Lithostratigraphy

Outcrops of the Wanstead Formation in Pukemuri Stream are typically slumped and poorly exposed (*Figure 4.9a*). The Wanstead Formation unconformably overlies the Pukemuri Siltstone, with a basal 1 m-thick poorly-sorted, clast-supported conglomerate (*Figure 4.9b*) separating the grey mudstone of the Pukemuri Siltstone from the typical green mudstones of the Wanstead Formation. The remainder of the formation is *ca.* 200 m-thick, intensely sheared and deformed green-grey calcareous mudstone (*Figure 4.9c*), with occasional thin glauconitic sandstone beds and thin (<0.5 m), laterally-restricted, lenses of grey, well-cemented sedimentary breccia (*Figure 4.9d, e*). Undeformed mudstones display a mottled texture and little or no primary sedimentary structures. The top of the section is not exposed.

Paleontology and Age

A late Middle Eocene (Bortonian) age applied to the basal portion of the formation immediately above the conglomerate is based on the presence of the planktic foraminifera index species *Globigerinatheka index* and *Acarinina primitiva* in sample S28/f0199 (*Figure 4.4*). Conversely, the presence of *Elphidium hampdenense* and *Morozovella crater* some 200 m higher in the section (S28/f200) gives an older Heretaungan (late Early to early Middle Eocene) age. The Wanstead Formation foraminiferal faunas (S28/f199 and S28/f200) contain similar benthic assemblages including the benthic foraminifera *Abyssamina poagi*.

Ages derived from calcareous nannofossil assemblages from the lower Wanstead Formation are consistent with foraminiferal results. Four samples from lowermost Wanstead Formation were examined for calcareous nannofossils. Two samples (S28/f0465 and S28/f0428) are identified as reworked clasts from Pukemuri Siltstone based on the continued presence of *Discoaster lodoensis* and other similarities with the underlying assemblages (*Appendix 1*). Sample S28/f0464 contains an assemblage characterised by *Reticulofenestra* spp. (including *R. umbilicus*), *Coccolithus formosus*, *Chiasmolithus* spp., *Sphenolithus radians*, *Zygrhablithus bijugatus* and *Nannotetrina* spp. The presence of *R. umbilicus* and *Nannotetrina* spp., as well as the absence of *Reticulofenestra reticulata*, indicates a correlation with lower Zone NP16 (late Middle Eocene; *Figure 4.4*). The overlying sample S28/f0394 contains a somewhat younger assemblage that includes *Reticulofenestra reticulata*, *Dictyococcites bisectus* and *Chiasmolithus grandis*. The co-occurrence of *D. bisectus* and *C. grandis* indicates a correlation with upper Zone NP17 (latest Middle to earliest Late Eocene) age.
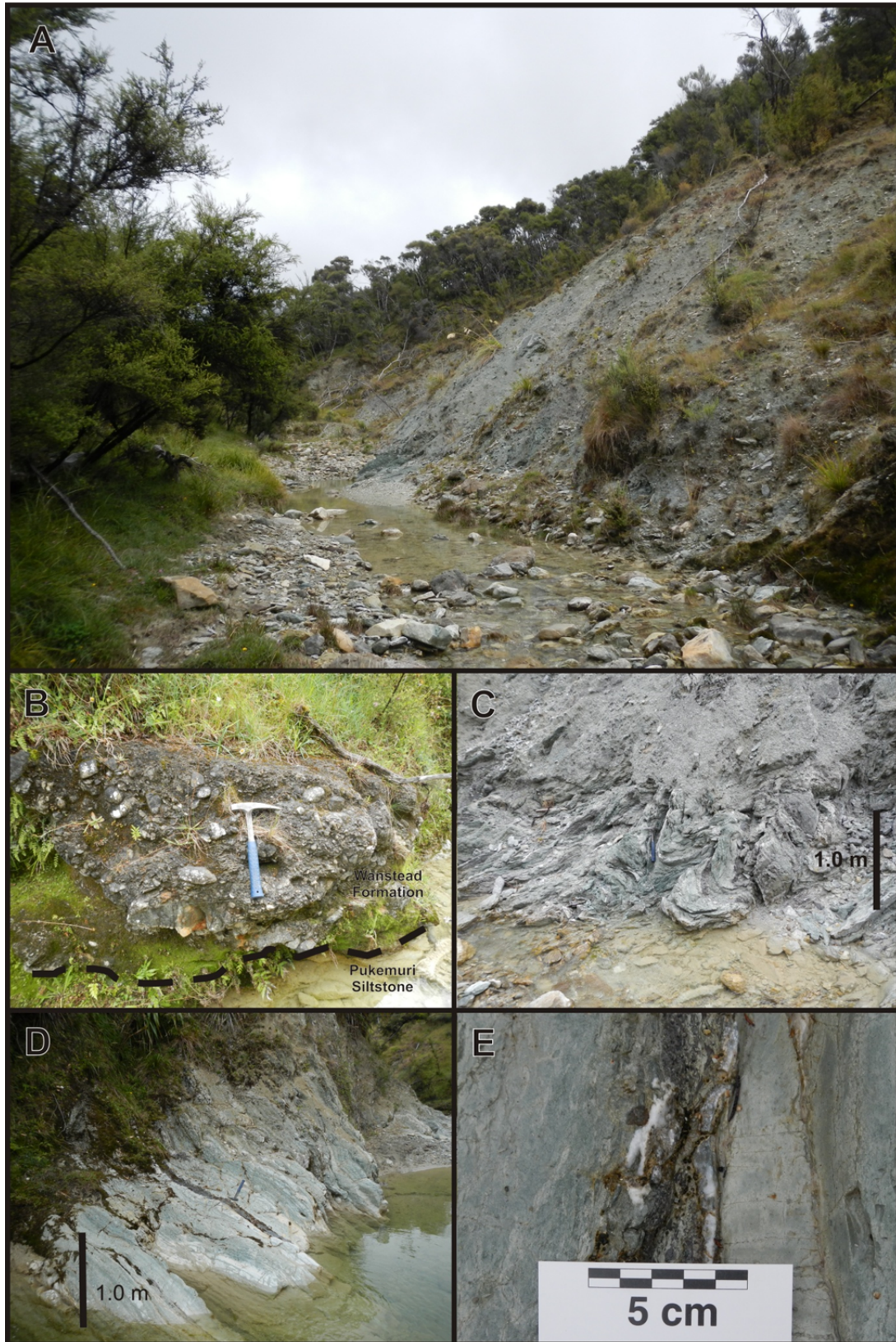
Figure 4.9: Features of the Wanstead Formation exposed in Pukemuri Stream. **A**) Typical slumped outcrop of the Wanstead Formation. Slip is 10 m high. **B**) Clast-supported basal conglomerate, marking the contact between Pukemuri Siltstone and Wanstead Formation. **C**) Intensely deformed section, common in the Wanstead Formation. **D**) Outcrop of coherent green mudstone. Note dark grey 10 cm-thick breccia lens **E**) Detail of breccia lens showing 3-4 mm subangular clasts and calcite cement.

4.3.2 Awheaiti Stream

The Awheaiti Stream section provides a secondary section for comparison to the primary reference section in Pukemuri Stream. The Awheaiti section is a composite section (*Figures 4.10, 4.11 & 4.12*) measured and described from the base of the Awhea Formation (grid reference: S28 191 632) through to the Wanstead Formation (grid reference: S28 183 642) (*Figures 4.10 & 4.11*). The stratigraphy of the upper Pukemuri and Wanstead Formations is difficult to trace in this section due to the high degree of slumping, shearing and folding of exposures, along with fault repetition of units, which creates an over-thickening of the Pukemuri and Wanstead Formations.
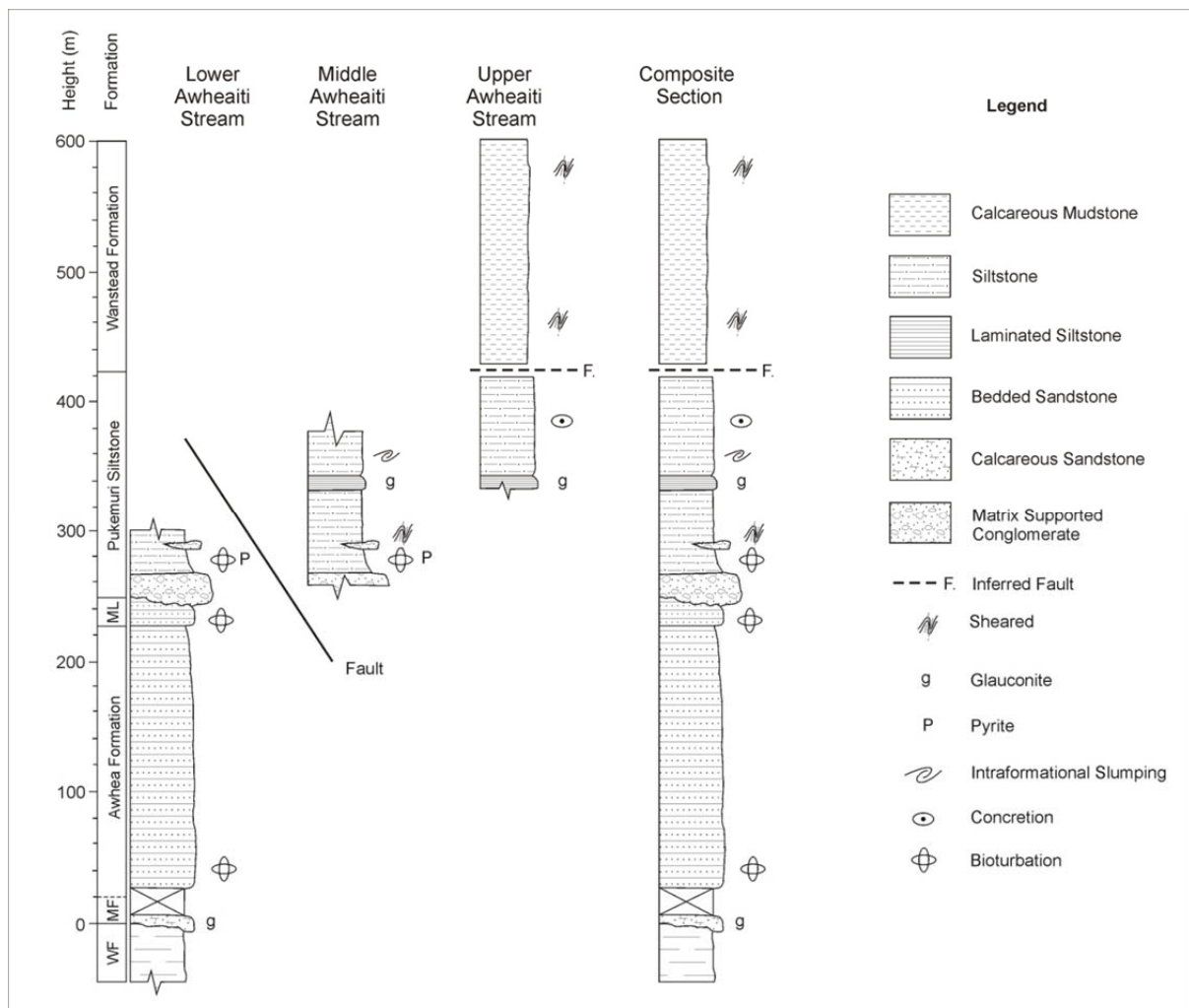
Figure 4.10: Construction of composite sections from three sections outcropping in Awheaiti Stream. Key to abbreviations: WF = Whangai Formation, MF = Manurewa Formation, ML = Mungaroa Limestone.
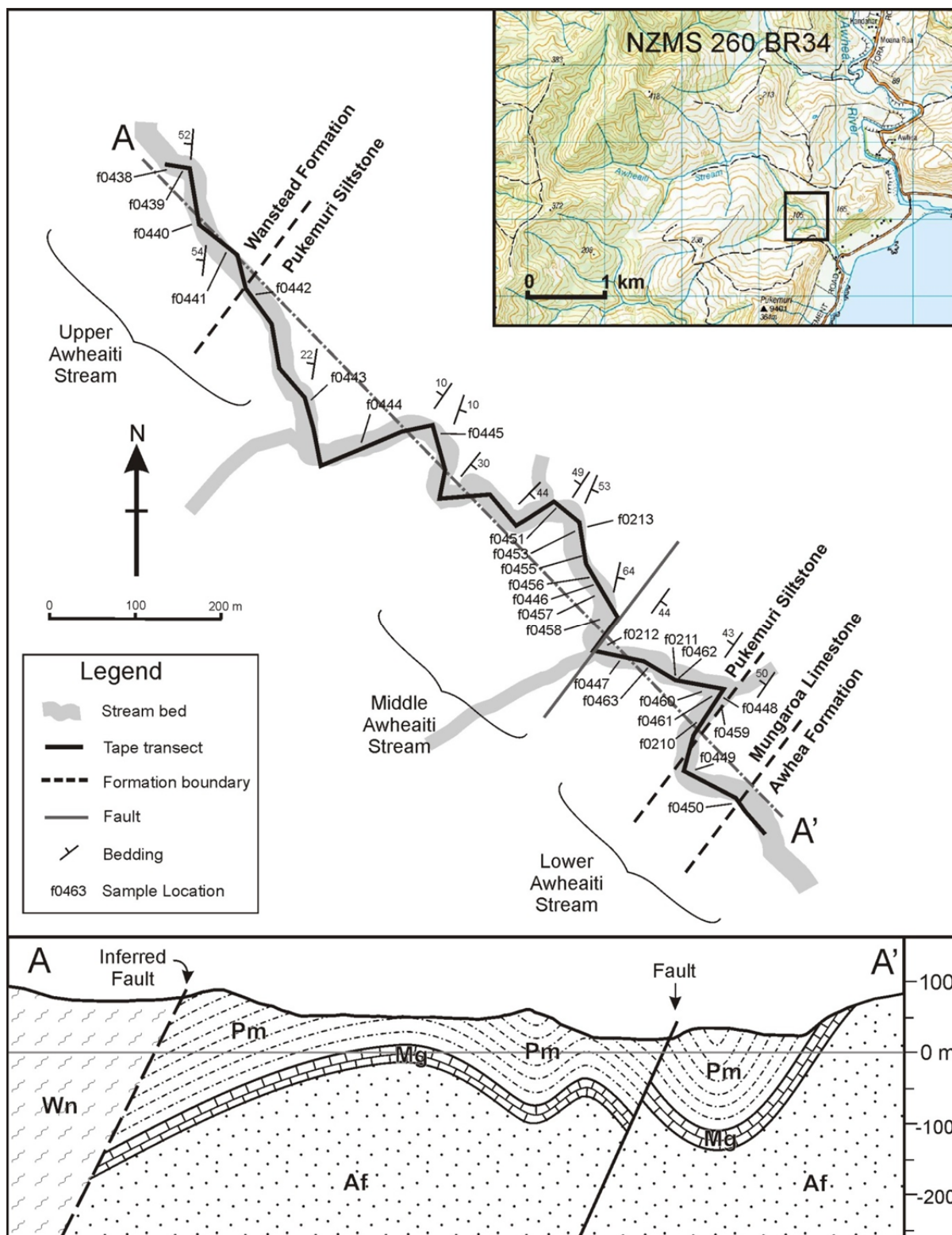
Figure 4.11: Awheaiti Stream tape and compass map and schematic cross-section. Af = Awhea Formation, Mg = Mungaroa Limestone, Aw = Awheaiti Formation, Pm = Pukemuri Siltstone, Wn = Wanstead Formation.
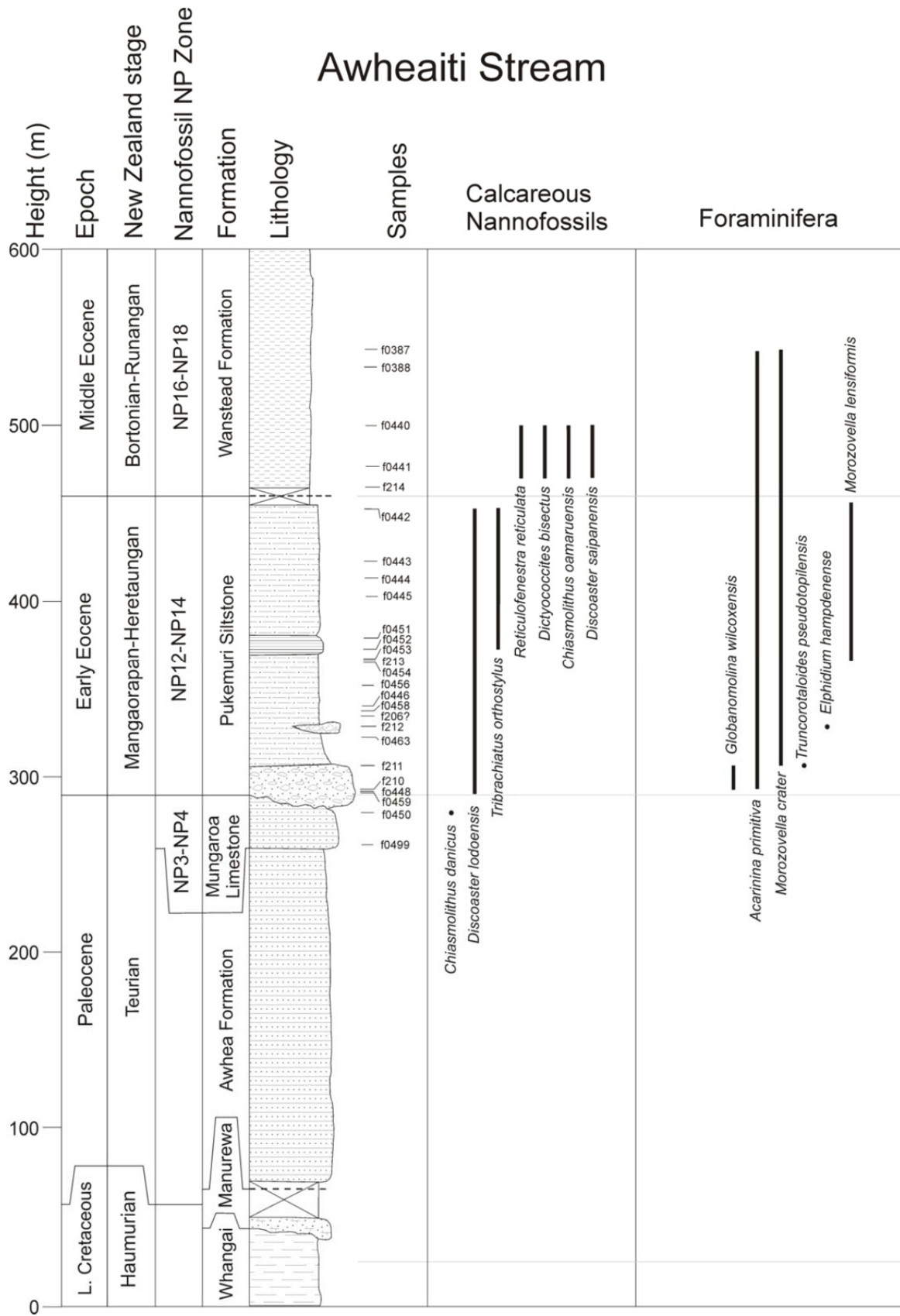
Awheaiti Stream

Figure 4.12: Stratigraphic column for Awheaiti Stream showing lithostratigraphy and key calcareous nannofossil and foraminiferal biostratigraphic datums.

Awhea Formation

Lithostratigraphy

The Awhea Formation is poorly exposed in Awheaiti Stream. The basal contact with the Manurewa Formation lies *ca.* 80 m from the mouth of the stream but has poor outcrop exposure and is obscured by vegetation. The formation consists of 200 m of hard, grey, cm- to dm-bedded, glauconitic sandstone with sharp basal contacts and minor mudstone layers separating beds. No samples were collected for paleontology, age or environmental interpretation.

Mungaroa Limestone

Lithostratigraphy

The Mungaroa Limestone is exposed in a small gorge 350 m upstream from the mouth of Awheaiti Stream (*Figure 4.13a*). The formation has a gradational lower contact with the underlying Awhea Formation, and is distinguished by increases in the carbonate content, cementation and bedding thickness (*Figure 4.13b*). The basal Mungaroa Limestone comprises 20 m of grey, dm-bedded, glauconitic, medium to coarse calcareous sandstone with minor mudstone separating layers, progressively grading into alternating sandstone and mudstone further up section (*Figure 4.13c, d*). Repeated alternation of sandstone, fining upwards into laminated mudstone is clearly displayed within bedding sequences in the upper part of the section. Bioturbation is absent at the base of the formation but scattered trace fossils become evident, including *Zoophycos* and c.f. *Planolites*, increasing in frequency on occasional bedding surfaces towards the top of the formation (*Figure 4.13e*).

Paleontology and Age

Sample S28/f0450, collected from the base of the Mungaroa Limestone (*Figures 4.11* and *4.12*) contains a calcareous nannofossil assemblage that is assigned to Nannofossil Zones NP3-4 (early Paleocene) based on the presence of *Chiasmolithus bidens* and absence of *Fasciculithus tympaniformus*.
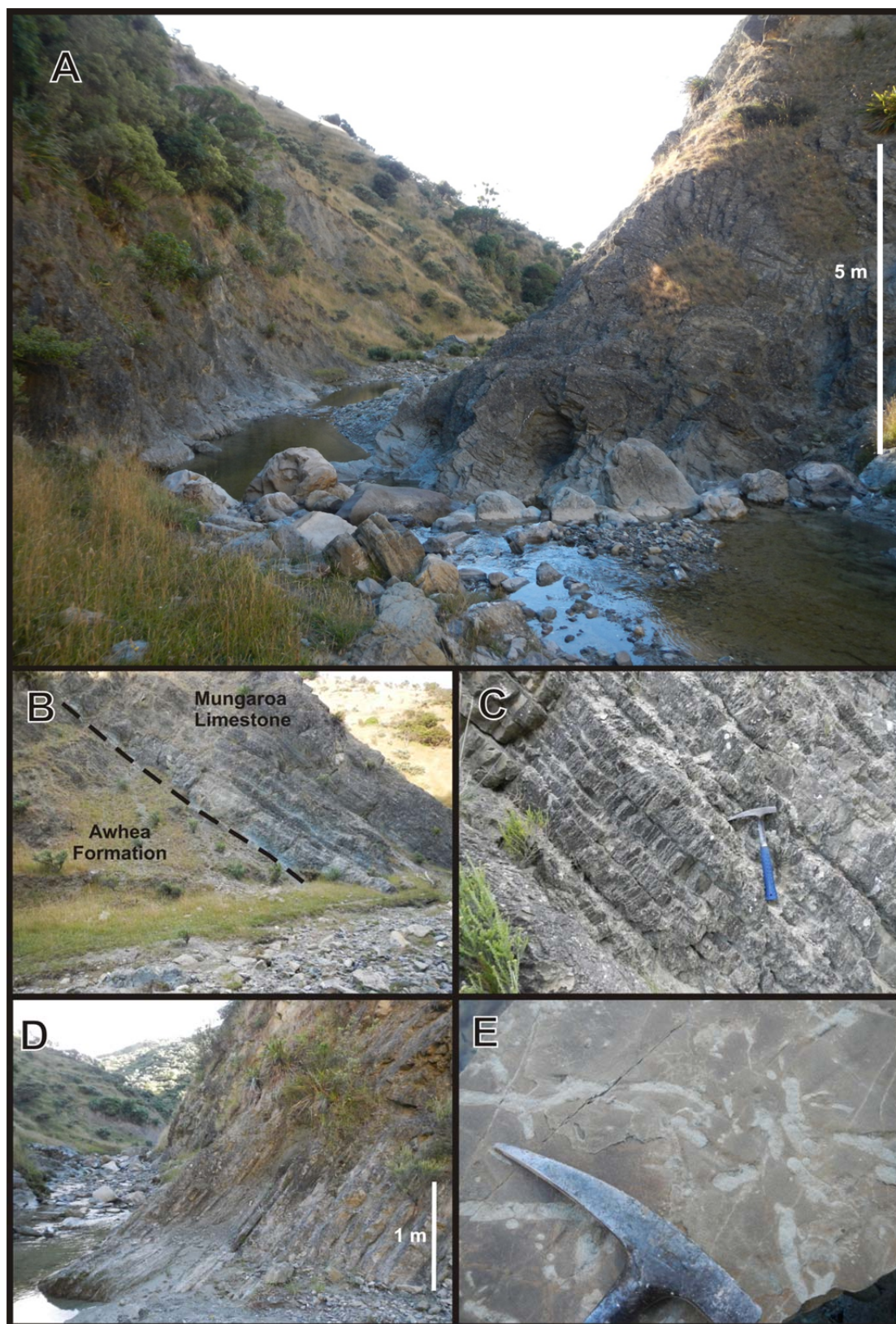
Figure 4.13: Details of Mungaroa Limestone in Awheaiti Stream. **A**) Small gorge with outcropping lower Mungaroa Limestone. **B**) Conformable contact between the Awhea Formation and overlying Mungaroa Limestone. Bluff in the centre of the image is 5 m high. **C**) Well-bedded, dm-scale bedding of the lower Mungaroa Limestone, with thin mudstone layers separating calcareous sandstone beds. **D**) Alternating sandstone/mudstone near the top of the formation. **E**) c.f. *Planolites* exposed on bedding plane near the top of the section.

Lithostratigraphy

The Pukemuri Siltstone unconformably overlies the Mungaroa Limestone and has an estimated thickness of 170 m. True stratigraphic thickness is difficult to determine due to structural complexities, and estimated thickness is based on the correlation of three logged subsections in Awheaiti Stream (*Figure 4.10*) The base of the formation crops out above a small gorge, where the Awheaiti Stream flows along the strike of a dip-slope formed by the top of the Mungaroa Limestone. The basal unit of the Pukemuri Siltstone comprises 30 m of pebbly-mudstone, containing clasts of indurated sandstone, limestone and chert, with occasional greywacke pebbles within a matrix of sandy, blue-grey mudstone (*Figure 4.14a, b*). This is overlain by 60 m of hard, blue-grey, laminated, glauconitic, calcareous, micaceous mudstone displaying rare horizontal burrows and abundant pyrite. Above this is an 8 m-thick interval of brown glauconitic mudstone with a 50 cm-thick layer of glauconite, bearing sedimentary breccia and sideritic concretions (*Figure 4.14c*), which probably correlates with a similar interval in Pukemuri Stream. The layer is offset by cm-scale normal faults. A grey, well-bedded, laminated, poorly calcareous mudstone unit lies above the brown mudstone (*Figure 4.14d*), displaying rare slump folds (*Figure 4.14e*). This is overlain by *ca*. 20 m of weakly calcareous to non-calcareous, massive, grey mudstone with frequent 3-12 mm-thick calcite veins. Above this lies approximately 50 m of massive to faintly laminated blue-grey mudstone containing occasional concretions up to 4 m in diameter (*Figure 4.14f*).

Paleontology and Age

Foraminifera and calcareous nannofossils provide good age control for this unit in Awheati Stream. The planktic foraminifera *Morozovella crater* occurs in all but the lowermost sample, indicating a Mangaorapan-Heretaungan (late Early to early Middle Eocene) age range. An isolated occurrence of *Elphidium hampdenense* in sample S28/f212 suggests that the upper part of the unit is Heretaungan. This correlation is consistent with calcareous nannofossil assemblages, with the base of Nannofossil Zone NP12 (lower Mangaorapan) identified by the first occurrence of *Discoaster lodoensis* at the base of the formation (*Figure 4.12*).

Samples S28/f0210 and S28/f0211 from basal Pukemuri Siltstone produce a foraminiferal assemblage containing the planktics *Globanomalina wilcoxensis*, *Acarinina primitiva, Planorotalites*

laevigata, *Morozovella* cf. *aquea rex*, and *M. crater*. These species, along with the benthic species *Buliminella browni*, indicate a late Waipawan to Heretaungan (late Early to early Middle Eocene) age range (*Appendix 1*). The absence of the benthic *E. hampdenense*, which is a Heretaungan index species, may restrict the age of these samples to the early Eocene (upper Waipawan to Mangaorapan). Samples higher in the section (S28/f0206, S28/f0213 and S28/f0214) contain *M. crater* and *M. lensiformis* indicating a late Early to early Middle Eocene (Mangaorapan to Heretaungan) age, which is constrained to the latest Early to early Middle Eocene (Heretaungan) by the presence of *E. hampdenense* in sample S28/f0212. Benthic foraminiferal assemblages include; *Vulvulina zesprinosa*, *Ellipsoglanulina* sp. (S28/f0210), *Chilostomella* sp. and *Anomalina visenda* (S28/f0211), *E. hampdenense* and *Stilostomella* sp. (S28/f0212), *Allomorphina conica*, *Kalamopsis grzybowskii*, *Chilostomella* sp., *Pleurostomella* sp. and *Nuttallides carinotruempyi* (S28/f0206).

Five calcareous nannofossil samples from the Pukemuri Siltstone at Awheaiti Stream contain late Early to earliest Middle Eocene (Mangaorapan to early Heretaungan) assemblages characterised by *Reticulofenestra* spp., *Toweius callosus*, *D. lodoensis*, *Discoaster kuepperi*, *Coccolithus formosus*, *Zygrhablithus bijugatus*, *Neococcolithes* spp. and *Sphenolithus radians* (*Appendix 1*). The presence of *D. lodoensis* indicates a zonal assignment of NP12-14 (*Figure 4.12*). The sporadic and rare occurrence of *Tribrachiatus orthostylus* (NP12 restricted) in several samples is likely due to reworking if the occurrence of *E. hampdenense* is reliable.
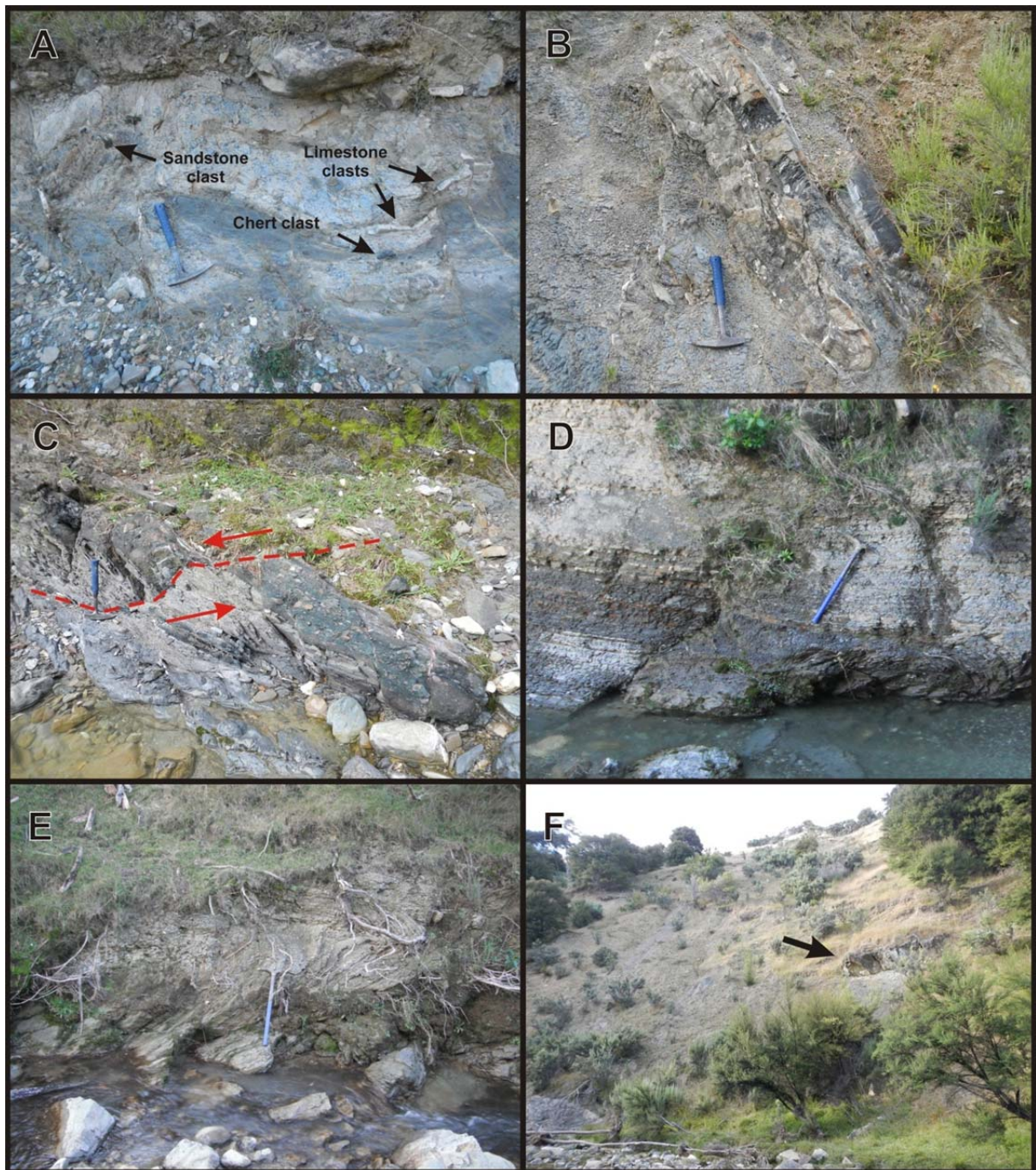
Figure 4.14: Features of the Pukemuri Siltstone exposed in Awheaiti Stream. **A**) Pebbly mudstone of lowermost Pukemuri Siltstone containing limestone, chert and indurated sandstone clasts (arrowed). **B**) Large chert clast in lower Pukemuri Siltstone. **C**) Glauconitic sandstone containing breccia and sideritic concretions offset by small-scale normal faulting. Hammer for scale. **D**) cm-bedded mudstones of the Pukemuri Siltstone. Rock pick (80 cm long) for scale. **E**) Soft sediment deformation structure. Rock pick for scale. **F**) Large concretion (arrowed) in Pukemuri Siltstone, 1 × 4 m in size.

Wanstead Formation

Lithostratigraphy

Overlying the Pukemuri Siltstone is a highly deformed and strongly sheared interval of Wanstead Formation mudstone. The lower contact is obscured but inferred to be faulted based on a reversal in younging direction indicated by the biostratigraphy. The formation varies from pale grey to green to red-brown mudstone, although it is predominantly composed of extensively sheared, highly-calcareous, green mudstone (*Figure 4.15*). It contains frequent calcite veins up to 20 mm-thick with crystals forming in voids. Infrequent dm- to m-thick beds of glauconitic sandstone and white calcareous mudstone also outcrop in the formation.

Paleontology and Age

Two samples from the base of the Wanstead Formation at Awheaiti Stream (S28/f0441 and S28/f0440) contain an early Late Eocene (upper Kaiatan to lowermost Runangan) calcareous nannofossil assemblage distinctly different from assemblages in the underlying Pukemuri Siltstone (*Appendix 1*). The assemblage includes *Reticulofenestra* spp. (including *R. umbilicus* and *R. reticulata*), *Dictyococcites bisectus*, *Coccolithus formosus*, *Discoaster saipanensis*, *Zygrhablithus bijugatus* and *Chiasmolithus oamaruensis*. The co-occurrence of *C. oamaruensis* with *R. reticulata* and *D. saipanensis* indicate a correlation with Nannofossil Zone NP18 (*Figure 4.12*). Two samples from approximately 30 m higher in the section (S28/f0387 and fS28/0388) contain an older nannofossil assemblage assigned a Middle Eocene (late Heretaungan to early Bortonian) age, indicating faulting or an overturned section not readily obvious within the exposed outcrop due to shearing and poor exposure. The assemblage is characterised by *Reticulofenestra* spp., *C. formosus*, *Neococcolithes* spp., *S. radians* and *Z. bijugatus*. The nannofossil zonal assignment of upper NP14 to lower NP16 is based on the absence of *Discoaster lodoensis* (LAD within Zone NP14) and absence of *R. umbilicus* (FAD in Zone NP16), as well as the questionable occurrence of *Nannotetrina cristata* in one sample.

An Early to early Middle Eocene (Mangaorapan to Heretaungan) age is favoured for a single foraminiferal sample (S28/f0214), which contained the index fossil *Morozovella crater*, although the absence of *Elphidium hampdenense* may indicate a Mangaorapan restricted age. The benthic foraminiferal assemblage in sample S28/f0214 contains; *Pleurostomella* sp., *Karreriella bradyi*, *Anomalina visenda*, *Trochamminoides* sp., *Aragonia zealandica* and *Quadrimorphina allomorphinoides*.

Figure 4.15: Features of the Wanstead Formation in Awheaiti Stream. **A**) Typical, sheared, green-grey mudstone of the Wanstead Formation. Rock pick for scale (80 cm long). **B**) Outcrop of light grey and red-brown mudstone. **C**) Extensively sheared outcrop of the Wanstead Formation in Awheaiti Stream.

4.3.3   Te Oroi Stream

The Te Oroi Stream section is utilised as an accessory section in this study, and was measured and described from the base of the Awhea Formation (grid reference: S28 148 592) to lower Wanstead Formation (grid reference: S28 144 600). Outcrop, sampling and paleontological data for the section is limited, and neither a map or stratigraphic section are presented. However, brief descriptions are included in this study to establish changes in stratigraphic thickness of formations and confirm age and paleoenvironmental assessments. No calcareous nannofossil assemblages were examined from Te Oroi Stream, and foraminiferal data is only available from sparse CCP samples from the Awhea, Pukemuri and Wanstead Formations.

Awhea Formation

Lithostratigraphy

The Awhea Formation consists of 290 m of cm- to dm-scale, well-bedded, glauconitic, slightly calcareous, fine to very fine sandstones and grey micaceous mudstones. Occasional thicker beds (0.5-1.0 m) occur towards the middle of the formation, becoming less well-bedded and softer near the top of the formation.

Paleontology and Age

The age of the lower Awhea Formation (sample S28/f0202) is poorly constrained, with a sparse, entirely agglutinated foraminifera fauna indicating an age range of Campanian to Paleocene (Haumurian to Teurian) based on the presence of *Rzehakina epigona* (*Appendix 1*). Sample S28/f0202 also contained *Bathysiphon* sp. and *Kalamopsis gryzbowskii*. A somewhat richer fauna from the middle of the Awhea Formation (sample S28/f0203) from the upper Awhea Formation contains a Paleocene (Teurian) assemblage that includes *Gavelinella beccariiformis*, *Nuttalides florealis*, *Acarinina* sp. and *Globigerina* sp., in addition to *Gyroidinoides* cf. *globosus*, *Dorothia* cf. *bullata*, *Bolivinopsis spectabilis* and *Ammodiscus cretaceus*.

Mungaroa Limestone

Lithostratigraphy

The Mungaroa Limestone outcrops as a largely inaccessible bluff exposed by a 70 m-high waterfall in Te Oroi Stream (*Figure 4.16a*). The basal Mungaroa Limestone consists of 25 m of hard, poorly-bedded, green-grey calcareous mudstone with *Zoophycos* traces (= the lower member), overlain by 20 m of hard, cm-bedded, light green to white-grey, slightly glauconitic sandstone (= the middle member). The top of the formation consists of 40 m of hard, well-bedded, white, micritic limestone with abundant *Zoophycos*, *Scolicia* and *Planolites* traces (= the upper limestone member). The Mungaroa Limestone in Te Oroi Stream was not sampled for foraminifera, and no age diagnostic data is available.

Awheaiti Formation

Lithostratigraphy

The Awheaiti Formation unconformably overlies Mungaroa Limestone with an angular discordance of 15-20° (*Figure 4.16b*). The formation is composed of several metres of cm-bedded, laminated, grey-brown, micaceous, slightly glauconitic mudstone and fine sandstones (*Figure 16c*). The contact between Mungaroa Limestone and Awheaiti Formation in the Te Oroi Stream section is unconformable, but does not display any evidence of channelisation as observed at Pukemuri Stream. No paleontological data is available.
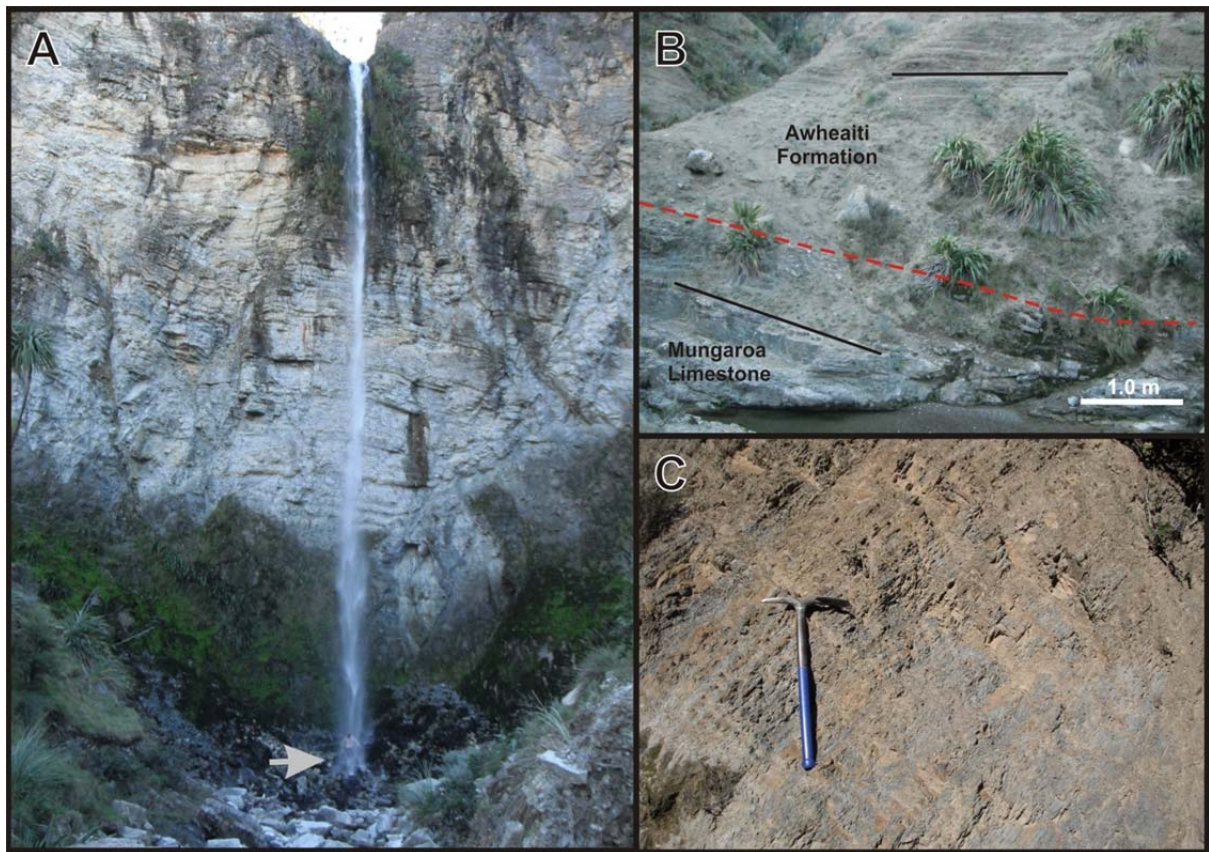
Figure 4.16: Features of the Mungaroa and Awheaiti Formations in Te Oroi Stream. **A**) Mungaroa Limestone outcropping in 70 m-high waterfall. Person for scale (arrowed). **B**) Contact and angular discordance between bedding in the Mungaroa Limestone and the Awheaiti Formation **C**) Typical, thin-bedded Awheaiti Formation in Te Oroi Stream.

Pukemuri Siltstone

Lithostratigraphy

The Pukemuri Siltstone unconformably overlies the Awheaiti Formation. The lower part of the formation is a 20 m-thick, grey mudstone containing abundant, ≤10 cm, well-rounded pebbles at the base, which decrease in frequency and size up-section. This grades into a massive, grey, glauconitic, fine-grained calcareous sandstone and mudstone up to 20 m-thick. This is overlain by 6 m of calcareous, brown, laminated mudstone. Overlying the mudstone is 30 m of poorly calcareous, massive or cm-bedded grey mudstone, displaying evidence of syn-depositional slumping, rare clasts up to 20 cm in size and scattered pebbles. This is overlain by 15 m of laminated, cm- to dm-bedded, grey, fine sandstone and mudstone. The upper 20 m of the formation consists of massive, grey, calcareous mudstone.

Paleontology and Age

A single sample from the base of the Pukemuri Siltstone (sample S28/f0204) contains a sparse foraminiferal fauna, including the key planktic species *M. crater*, indicating a late Early Eocene to earliest Middle Eocene (Mangaorapan to Heretaungan) age. The absence of benthic index species *E. hampdenense* could restrict the age to late Early Eocene (Mangaorapan); however, its absence may be due to the sparse nature of the assemblage rather than an indication of an older age. The benthic foraminiferal assemblage includes common *Cibicides wahoensis*, *Oridorsalis umbonatus*, *Hyperammina* sp., *Bathysiphon* sp. *Bolivinopsis compta* and elongate nodosariids.

Wanstead Formation

Lithostratigraphy

Exposure of the Wanstead Formation is limited to several tens of metres of poorly-exposed, cm-bedded, green-grey, bioturbated, highly calcareous mudstone and thin, glauconitic fine sandstones. The base of the formation is largely obscured, but appears to be unconformable and consists of a cemented, clast-supported, poorly-sorted basal conglomerate, containing well-rounded clasts of mixed lithologies including chert and indurated sandstone within a grey, sandy matrix.

Paleontology and Age

The base of the Wanstead Formation (sample S28/f0205) is assigned a late Middle Eocene (Bortonian) age based on the co-occurrence of the planktic foraminifera *Globigerinatheka index, Truncorotaloides pseudotopilensis* and *Acarinina primitiva*. The assemblage also contains the benthic taxa; *Cassidulina subglobosa*, *Karreriella bradyi*, *Pleurostomella* sp., *Osangularia* sp., *Glomospira gordialis, Nuttallides subtruempyi, Kalamopsis grzybowskii, Arenobulimina* sp. and *Abyssamina poagi*.

4.4   Additional Stratigraphic Data

Additional features that are useful for the environmental and age interpretation of the Mungaroa Limestone occur in coastal outcrops north and south of the main sections. The upper micritic limestone member of the Mungaroa Limestone, which is absent or inaccessible in stream sections has good outcrop exposure at Te Kaukau Point (*Figure 4.17a*), and the base of the member is well exposed at Manurewa Point. The upper member consists of well-bedded, muddy limestone, micritic limestone and glauconitic sandstone, with sharp contacts between beds. Complex folding of the Mungaroa Limestone occurs at the base of the Manurewa Point section (*Figure 4.17b*). Stylolitic surfaces are observed within the micritic limestone member at Te Kaukau Point, which indicate pressure solution during burial. Several east to southeast directed slump folds and plastic deformation of bedding is observed in the upper limestone member at Manurewa and Te Kaukau Points (*Figure 4.17c*). Intrusive sedimentary dykes composed of greensand penetrate perpendicular to strata in the middle member in Pukemuri Stream and the upper member at Manurewa and Te Kaukau Points. At Manurewa and Te Kaukau Points, bedding in the micritic limestone is observed to be displaced upwards by the injection of greensand dykes (*Figure 4.17d & e*). The dykes also contain angular to sub-angular limestone clasts, suggesting that the limestone was semi-lithified at the time of intrusion.

Sampling of the upper micritic member of the Mungaroa Limestone at Te Kaukau Point indicates deposition within Radiolarian Zone RP5 (Late Paleocene), marked by the presence of primary index species *Buryella tetradica* (C. Hollis; pers. comm.).

At Te Kaukau and Manurewa Points the upper micritic limestone member hosts two dark, fine-grained layers separated by 1.5 m of cm- to dm- bedded alternating layers of white micritic limestone and grey sandstone (*Figure 4.18a*). At Te Kaukau Point this is identified as 'Waipawa facies' and comprises two 50 cm-thick, dark-grey siliceous, organic-rich mudstone layers (*Figure 4.18b & c*). Ripple cross-bedding up to 5 cm high is observed within both mudstone layers and occasional intervening sandstone beds (*Figure 4.18c & d*).
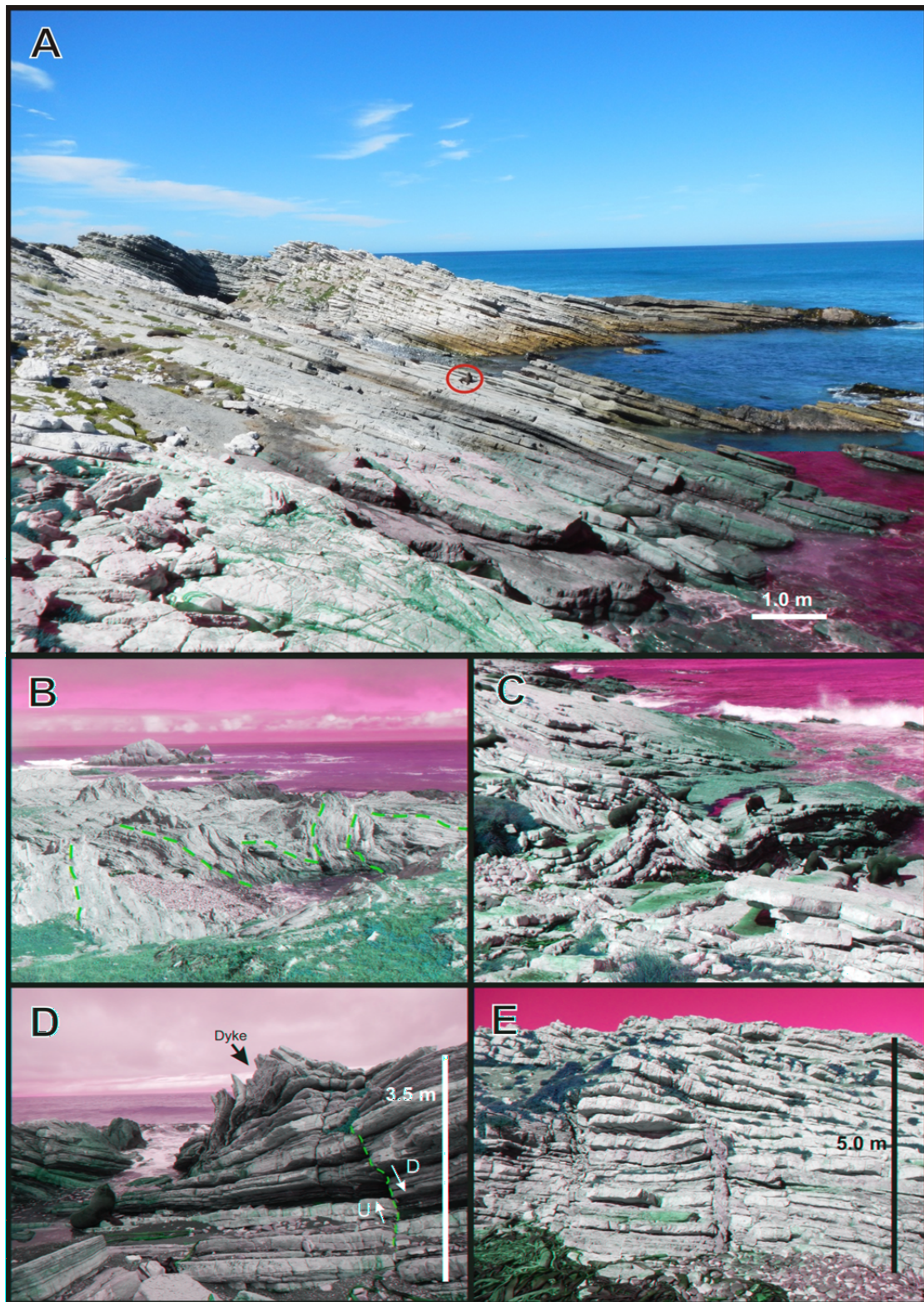
Figure 4.17: Features of the Mungaroa Limestone from supplementary sections **A**) dm-bedded micritic limestone of the upper limestone member exposed at Te Kaukau Point. New Zealand fur seal for scale (circled), approximately 1 m long. **B**) Complex folding of the Mungaroa Limestone at Manurewa Point. Field of view approximately 25 m. **C**) Slump folding and plastic deformation of limestone layers at Te Kaukau Point. New Zealand fur seal for scale, approximately 1 m long. **D**) Sedimentary dyke and minor normal faulting at Manurewa Point. **E**) Glauconitic sedimentary dyke intruding into micritic limestone at Te Kauaku Point. Note deflection of bedding near the dykes in **D** and **E**.
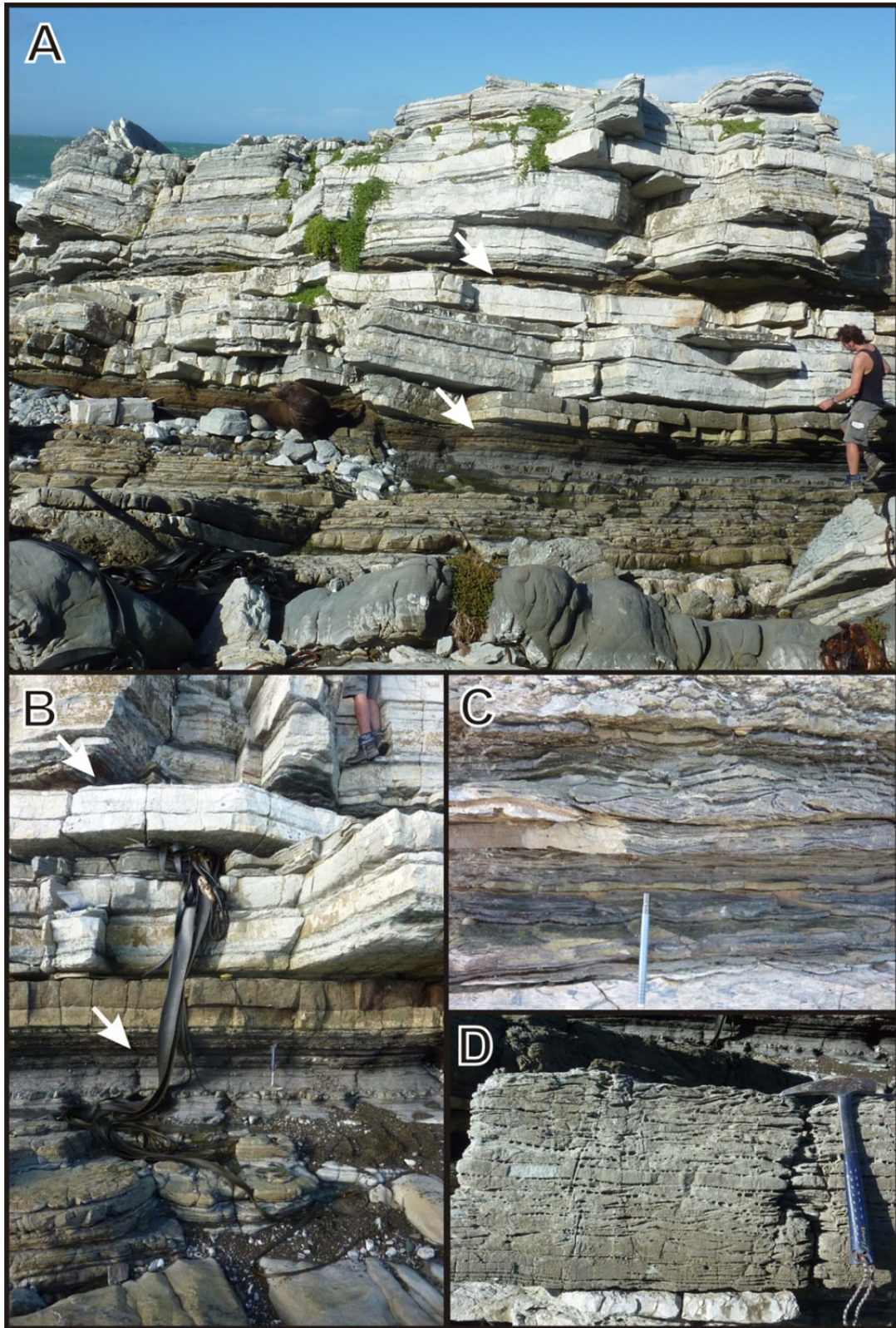
Figure 4.18: Features associated with the 'Waipawa facies' incorporated within the Mungaroa Limestone. **A**) Pair of *ca.* 50 cm-thick, black mudstone layers (arrowed) separated by 1.5 m of micritic limestone. Person for scale. **B**) Abrupt contact between lower mudstone layer and the middle member of the Mungaroa Limestone. Arrows indicate position of the two black mudstone layers. Hammer for scale. **C**) Detail of cross-bedding in the lower layer of black mudstone. Pen for scale (14 cm long). **D**) Cross-bedding in sandstone bed from the interval separating the two black mudstones.

4.5   Trace Fossil Assemblages

Trace fossils are often indicative of specific environments or conditions, and are particularly prevalent in some aspects of the Paleogene succession at Tora, providing additional information for environmental interpretations based on sedimentology and foraminiferal assemblages. Observations of trace fossil assemblages in the Manurewa Formation include *Nereites*, ?*Chondrites*, *Ophiomorpha* and *Zoophycos* (*Figure 4.19*), indicating an association with the *Nereites* ichnofacies (Buatois & Mángano, 2011). Extensive trace fossils exposed on bedding planes in the Awhea Formation include *Planolites*, *Ophiomorpha*, *Nereites, Paleodictyon, Scolicia* and *Zoophyco*s (*Figure 4.20*). This assemblage also corresponds with deposition in the *Nereites* ichnofacies (Buatois & Mángano, 2011). Similar, although less extensive trace fossil assemblages are observed in the middle member of the Mungaroa Limestone.

Zoophycos dominates the trace fossil assemblages observed in the upper member of the Mungaroa Limestone, although a variety of other trace fossils, (e.g. c.f. *Paleodictyon*, c.f. *Scolicia*, c.f. *Thalassinoides*) are also observed to occur infrequently within the member (*Figure 4.21*).

Occasional *Ophiomorpha* and *Planolites* are observed in the Awheaiti Formation (*Figure 4.22*). Bioturbation traces are almost entirely absent in the Pukemuri Siltstone, with the exception of rare small, unidentified burrows observed in Awheaiti Stream. In the few unsheared outcrops of Wanstead Formation in Pukemuri Stream, a mottled texture is observed, indicative of extensive and pervasive bioturbation, although no distinct traces were observed.
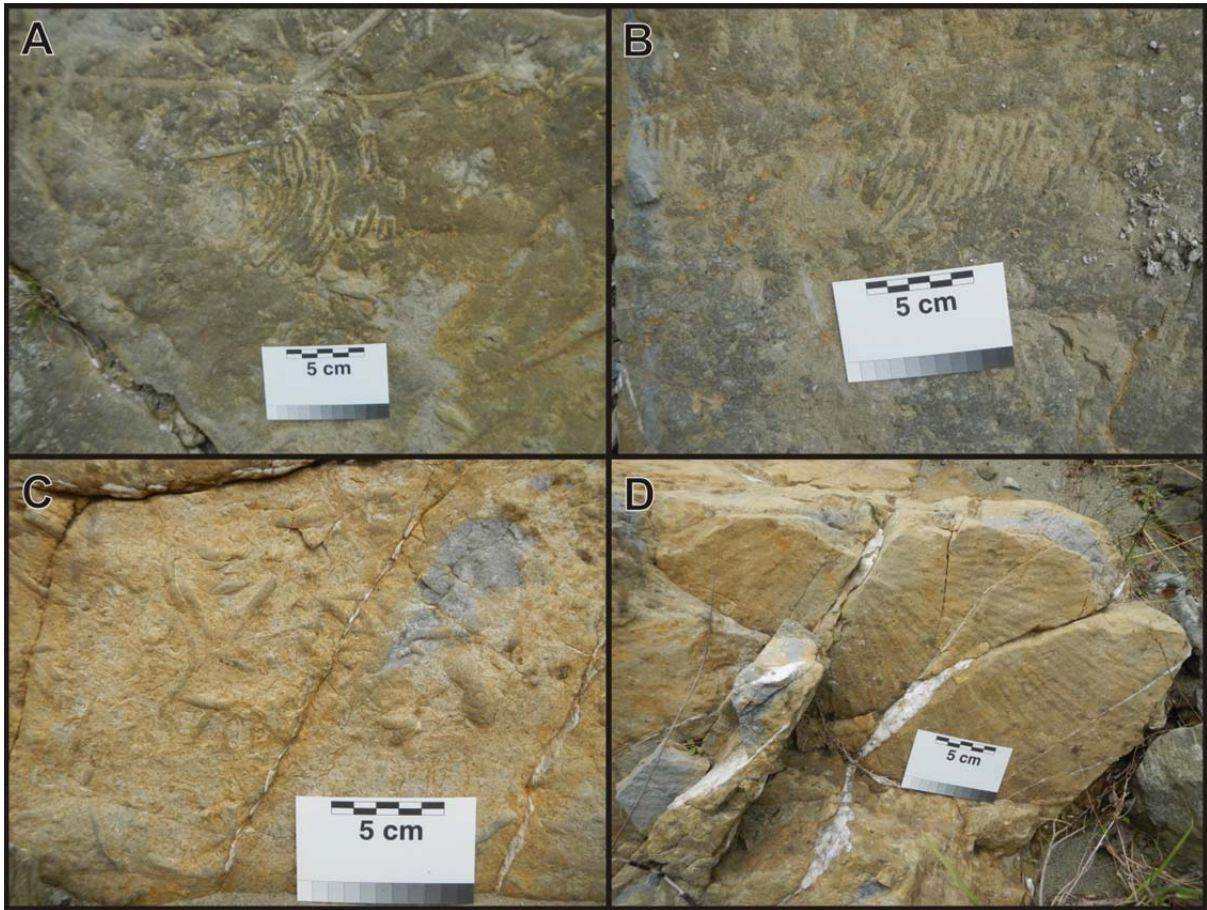
Figure 4.19: Trace fossils observed in Manurewa Formation. **A**) *Nereites.* **B**) ?*Chondrites.* **C**) *Ophiomorpha.* **D**) *Zoophycos.*

Figure 4.20: Trace fossil assemblages from Awhea Formation. **A**) *Paleodictyon*. **B**) c.f. *Scolicia ca.* 5 cm in diameter. **C** & **D**) *Ophiomorpha*. **E**) c.f. *Helmetioda* **F**) *Planolites*.
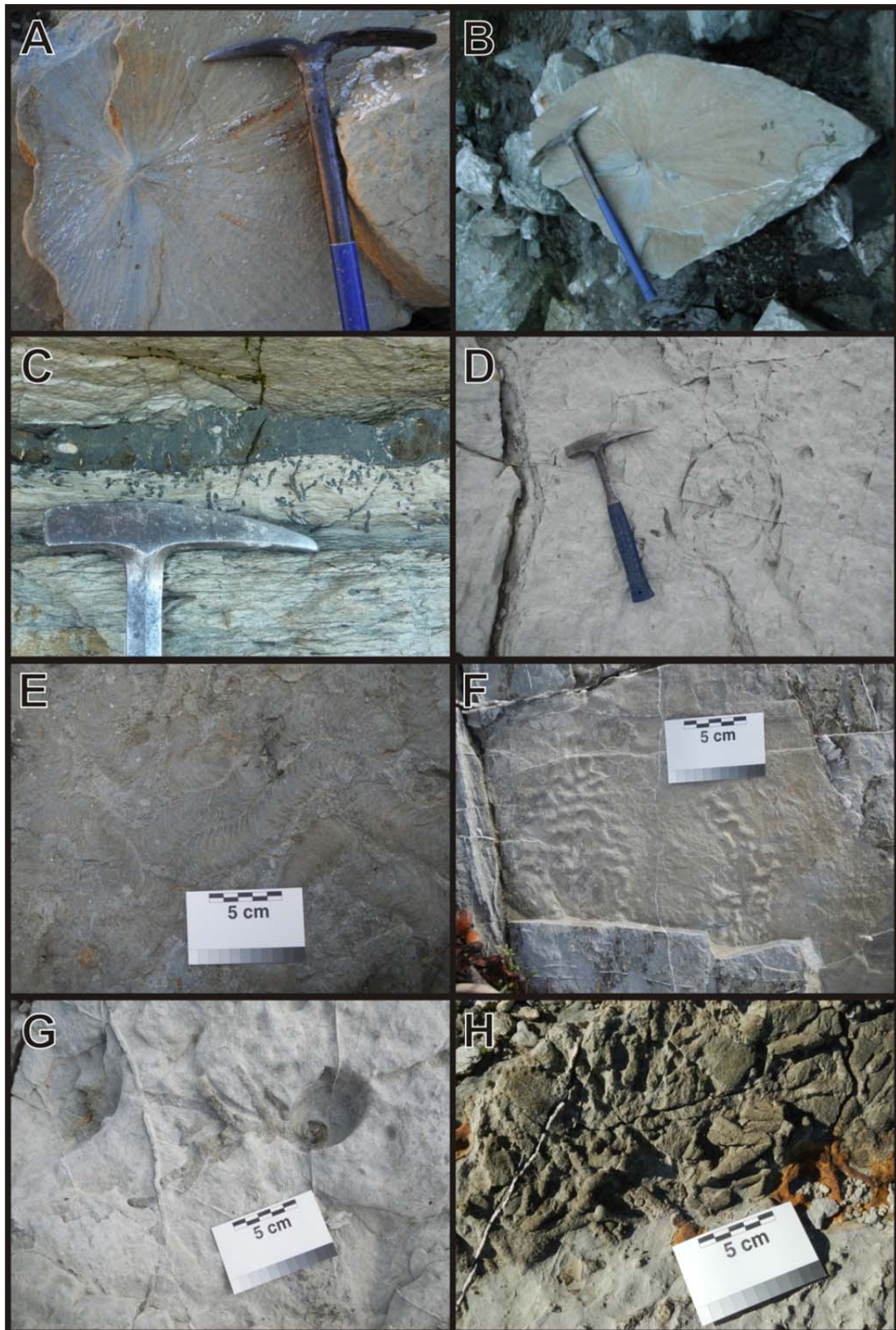
Figure 4.21: Trace fossils from the Mungaroa Limestone **A**, **B**) *Zoophycos* from Te Oroi Stream in outcrop (**A**) and in float (**B**). Rock pick for scale (80 cm long). **C**) Worm borings, Manurewa Point. **D**) Biogeneic collapse structure of Collen (1978) observed at Manurewa Point, likely formed by collapse of a *Zoophycos* burrow. **E**) *Scolicia* observed on bedding plane of the middle member in Pukemuri Stream. **F**) c.f. *Paleodictyon*, Manurewa Point. **G**) c.f. *Scolicia*, Manurewa Point. **H**) c.f. *Thalassinoides*, Manurewa Point.

Figure 4.22: Trace fossils of the Awheaiti Formation in Pukemuri Stream. **A** & **B**) *Planolites*. **C** & **D**) *Ophiomorpha*.

4.5.1   Interpretation of Trace Fossil Assemblages

Trace fossil assemblages have long been recognised as indicative of specific environments and conditions. Using the environmental preferences and associations of various trace fossil assemblages, as summarised in Buatois & Mángano (2011), the trace fossil assemblages observed within the Manurewa, Awhea, Mungaroa and Awheaiti Formations provide a paleoenvironmental interpretation presented in *Figure 4.23*.

Trace fossils of the *Nereites* ichnofacies display a close affinity to base-of-slope turbidity systems, and traces such as *Nereites* and *Paleodictyon* are rarely preserved outside of this environment (*Figure 4.23*; Buatois & Mángano, 2011). Trace fossil assemblages in the Manurewa Formation correlate to the *Nereites* ichnofacies, supporting the bathyal depth suggested by benthic foraminiferal assemblages (S28/f0191, S28/f0291; *Appendix 1*). The overlying Awhea Formation displays a similar, although more extensive, trace fossil assemblage that also corresponds with turbidite deposition in the *Nereites* ichnofacies (*Figure 4.23*). Proximal turbidites are often characterised by

gently meandering traces such as *Scolicia* (e.g. lowermost Awhea Formation and the middle member of the Mungaroa Limestone), while medial and distal turbidites may be indicated by patterned or tightly spiralling forms such as *Paleodictyon* and *Nereites* (e.g. Manurewa Formation and the remainder of the Awhea Formation).

The prevalence of *Zoophycos* traces in the upper micritic limestone member of the Mungaroa Limestone likely represents a shift to the *Zoophycos* ichnofacies, which is characterised by low, but not limiting oxygen, with some other infrequent and small traces in addition to *Zoophycos* (*Figure 4.23*; Frey, 1975). A trace fossil assemblage containing infrequent traces of *Ophiomorpha* and *Planolites* in Awheaiti Formation corresponds with channels in submarine turbidite environments, which may be inhabited by components of the *Skolithos* ichnofacies (e.g. *Ophiomorpha*) that extend to deep marine, high-energy settings (*Figure 4.23*; Pemberton *et al.*, 1992; Buatois & Mángano, 2011). In the absence of turbidite deposition, comparatively slow, continuous deposition means that bioturbation in the *Nereites* ichnofacies is not recorded as discrete traces, but rather as an overlapping, mottled texture, such as that observed in the Wanstead Formation (*Figure 4.23*; Frey *et al.*, 1990).
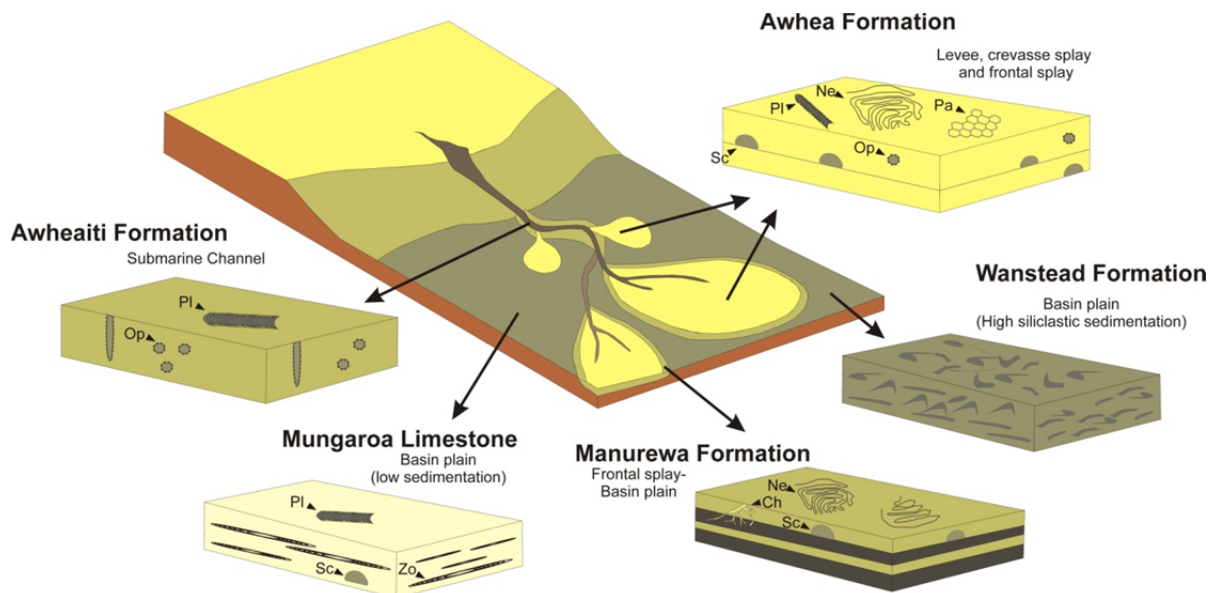
Figure 4.23: Depositional setting for the formations at Tora, based on ichnofossil relationships. Key to abbreviations: Ch = *Chondrites*, Ne = *Nereites*, Op = *Ophiomorpha*, Pa = *Paleodictyon*, Pl = *Planolites*, Sc = *Scolicia*, Zo = *Zoophycos*. Figure adapted from Buatois & Mángano (2011). Pukemuri Siltstone has been omitted due to the lack of trace fossil faunas.

4.6   Revised Paleogene Stratigraphy and Depositional Environments of the Tora Area

The measured sections from Pukemuri, Awheaiti and Te Oroi Streams combined with additional observations from Te Kaukau and Manurewa Points confirms the overall published stratigraphy, but also indicates that there are significant lateral facies variations and unconformities (*Figure 4.26*). A detailed revision of formation ages (*Figure 4.27*), along with a revised Paleogene stratigraphy for the Tora area is presented here. In addition, depositional environments are interpreted on the basis of foraminiferal assemblages, sedimentology and trace fossils.

4.6.1   Awhea Formation

Description

The lower Awhea Formation consists of 20-50 cm-thick, well-bedded, green-grey, glauconitic sandstone beds divided by thin layers of mudstone. Bedding surfaces are extensively bioturbated, including traces of *Nereites*, *Paleodictyon*, *Ophiomorpha*, *Scolicia* and *Planolites*. Vertically and horizontally oriented burrows are commonly infilled with pyrite and carbonaceous material is occasionally found in sandstone beds. The formation becomes progressively finer-grained, thinner bedded as well as less glauconitic up-section and bioturbation becomes significantly less extensive towards the top of the formation. The lower contact with the underlying Manurewa Formation varies between localities, being gradational in Te Oroi and Pukemuri Streams and sharp at Manurewa Point.

Distribution & Lithologic Variation

Extensive exposure of the formation occurs in Te Oroi Stream (290 m-thick), and Pukemuri Stream (270 m-thick), decreasing to 200 m in Awheaiti Stream (*Figure 4.26*)

Paleontology & Age

Foraminiferal assemblages from the lower Awhea Formation (S28/f0192, S28/f0202) indicate an age range of late Cretaceous to Paleocene (Haumurian to Teurian). Identification of the Cretaceous/Paleogene (K/Pg) boundary in the underlying Manurewa Formation (Wasmuth, 1996; Laird *et al.*, 2003; Vellekoop, 2010) suggests an early Paleocene (Teurian) age for the lower Awhea Formation (*Figure 4.27*). Samples from the middle and upper Awhea Formation

(S28/f0193, S28/f0203) produce distinctly Paleocene (Teurian) assemblages containing *Gavelinella beccariiformis*, *Nuttalides florealis*, *Acarinina* spp. and *Globigerina* sp.

Depositional Environment

Benthic foraminiferal assemblages from the Awhea Formation suggest a middle to lower bathyal depositional depth based on the presence of *Bathysiphon* sp., *Ammodiscus cretaceous*, *G. beccariiformis* and *N. florealis*, in conjunction with the dominance of agglutinated taxa (>90%) in samples S28/f0192 and S28/f0193 (*Appendix 1*). The scarcity of calcareous benthic taxa and the complete absence of planktic foraminifera is typical of Upper Cretaceous and Paleocene sediments of eastern New Zealand, apparently independent of water depth (Moore, 1988b; Schiöler *et al.*, 2010). The cause is uncertain but it may be the consequence of a combination of factors: high sedimentation rates in a turbid coastal setting, relatively cool ocean conditions causing carbonate dissolution or post-depositional dissolution during diagenesis. The presence of carbonaceous material does not necessary infer shallow depositional depths as silt to pebble size organic carbon has been shown to occur over 300 km offshore at depths of 2000-3000 m on the Mississippi Fan (Thayer *et al.*, 1986).

Trace fossil assemblages containing *Paleodictyon*, *Ophiomorpha*, *Scolicia* and *Planolites* place the Awhea Formation within the *Nereites* ichnofacies, which supports the bathyal paleodepth assessment from benthic foraminiferal assemblages. The high frequency of bioturbation in the lower Awhea Formation suggests a largely quiet, oxygenated seafloor environment, interrupted by periodic turbidity flows (Frey *et al.*, 1990; Buatois & Mángano, 2011), consistent with the sedimentology.

4.6.2 Mungaroa Limestone

Description

The Mungaroa Limestone is here divided into four informal units on the basis of lithology; the lower member, middle member, "Waipawa facies" and the upper limestone member. White, faintly bedded, calcareous mudstone of the lower member conformably overlies the Awhea Formation, and the basal contact is gradational, distinguished by a change in colour and an increase in bedding thickness, carbonate and degree of cementation. The lower member grades into a well-bedded sequence of grey-green sandstones and mudstones of the middle member.

Bedding thickness in the middle member is between 10-20 cm with sharp lower contacts on sandstone beds grading upwards into siltstone and mudstone with dark laminae that occasionally display cross-lamination corresponding to Bouma sequences A, B and C. The middle member is abruptly overlain by the upper member which contains the "Waipawa facies"; a pair of 50 cm-thick, glauconitic black mudstone intervals separated by 1.5 m of dm-bedded white, porcellaneous limestone and white-grey sandstone. The grey sandstone beds and black mudstone contain ripple cross-bedding up to 5 cm. The "Waipawa facies" is sharply overlain by well-bedded, white micritic limestone of the upper limestone member. Bedding is very regular showing an average bed thickness of 10 cm, with sharp contacts between beds, styolites and infrequent chert nodules. *Zoophycos* trace fossils occur throughout the formation, becoming extensive in the upper micritic limestone member. Criteria applied in the field to delineate the various members of the Mungaroa Limestone are presented in *figure 4.24*.

Distribution & Lithologic Variation

The Mungaroa Limestone varies significantly in stratigraphic thickness laterally, thinning dramatically from south to north (*Figure 4.25*). This is displayed by its physical morphology in the landscape; in Te Oroi Stream to the south, all three members of the formation outcrop as a sheer 70 m cliff, with a total stratigraphic thickness of 85 m (*Figures 4.16 & 4.26*). In Pukemuri Stream, 4 km to the north, the lower two members outcrop as a steep 20 m-high bluff, with a thickness of 30 m (*Figures 4.6a, 4.25 & 4.26*). Further north, only the lowermost member is expressed as a small gorge in Awheaiti Stream (*Figures 4.12b, 4.25 & 4.26*). Exposure of the upper members of the formation resumes at Manurewa Point (*Figures 4.25 & 4.26*). The greatest outcrop representation of the upper micritic limestone members is in coastal exposures at Te Kaukau Point.

Paleontology & Age

Calcareous nannofossil assemblages from the lower member in Awheaiti Stream correspond with deposition during Nannofossil Zone NP3-4 (*Figure 4.27*). Calcareous nannofossil assemblages from Pukemuri Stream place the middle member in zone NP5, and the upper micritic limestone member and the incorporated 'Waipawa facies' mudstone are placed in Radiolarian Zone RP5 (61-59 Ma; Hollis, 2002) based on sampling at Te Kaukau Point (*Figure 4.27*).

Formation/ Member		Gross Lithology	Description and Field Criteria
Mungaroa Limestone	Upper	Micritic Limestone	White Miciritic Limestone, well-bedded. Regular dm-bedding with sharp contacts between beds and occasional marl partings. Abundant *Zoophycos,* infrequent stylolites and chert nodules. Sharp lower contact.
	'Waipawa facies'	Siliciceous Mudstone	Paired 50 cm-thick, black, glauconitic, silicecous mudstone bands separated by 1.5 m of micritic limestone and sandstone.
	Middle	Alternating Sandstone-Mudstone	Alternating green-grey sandstone and mudstone couplets. Well-bedded with bedding average bedding thickness of 10-20 cm. Glauconitic, slightly to non-calcareous. Moderately abundant trace fossils on some bedding planes, including; *Scolicia, Ophiomorpha* and *Zoophycos.* Gradational lower contact.
	Lower	Calcareous Mudstone	White-grey calcareous mudstone. Faintly bedded on a dm-scale. Gradational lower contact.

Figure 4.24: Divisions of the Mungaroa Limestone and the field criteria used to identify individual members in the field.
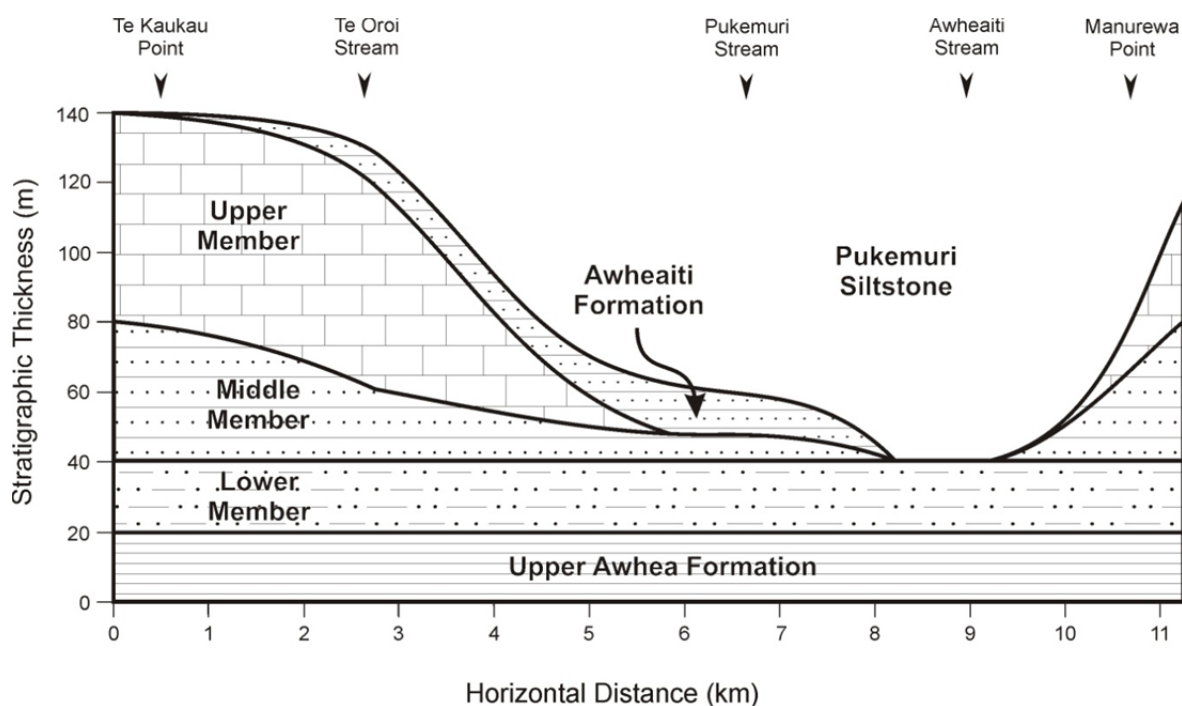
Figure 4.25: Variation in the thickness and distribution of the members of the Mungaroa Limestone across various sections in the Tora area, and relation to overlying and underlying formations.

Depositional Environment

The lower member of the Mungaroa Limestone exposed in Pukemuri Stream was deposited in a middle to lower bathyal environment based on the presence of *Osangularia* sp., *Rzehakina epigona*, *Glomospira charoides*, *Lituotuba* sp., *Nuttalides florealis* and *Gavelinella beccariiformis* which indicate a deeper middle to lower bathyal depth of 800-1500 m (Hayward, 1986; Morkhoven *et al.*, 1986). The well-bedded character of the middle member with sharp basal contacts, cross-bedding and clear Bouma sequences indicates deposition by turbidity currents. The upper micritic member of the Mungaroa Limestone reflects pelagic deposition with minor terrigenous input, although the inclusion of the 'Waipawa facies' at the base of the member suggests an influx of terrestrial organic matter and a possible fall in eustatic sea level (Hollis *et al.*, in prep). The dominance of *Zoophycos* trace fossils in the upper limestone member suggests an affinity with the *Zoophycos* ichnofacies. This is not particularly indicative of water depth, ranging from shallow depths just below storm wave base to abyssal settings. However, it does indicate an oxygen depleted seafloor environment in an area that is free from turbidity flows and significant bottom water currents (Frey *et al.*, 1990).

Deformation structures within the formation (slump folding and sedimentary dykes) and the apparent absence of brittle shearing suggest that the formation was semi-lithified, but still plastic, at the time of deformation, consistent with the observations of Waterhouse & Bradley (1957), Kirk (1966) and Browne (1987). These slump structures indicate paleoslope movements and syn-sedimentary deformation of sediments. Sedimentary dykes are indicative of a sudden shock applied to the sedimentary sequence which may be triggered by submarine slumping or tectonic activity (Onasch & Kahle, 2002).

The reduced thickness of the Mungaroa Limestone in the Pukemuri and Awheaiti Stream sections is attributed to paleo-channel erosion, corresponding with the removal of much of the upper two members of the Mungaroa Limestone in these sections (*Figures 4.25 & 4.26*).

4.6.3   Awheaiti Formation

Description

In the Pukemuri Stream section, the formation rests on an unconformable, channelised contact with the middle member of the Mungaroa Limestone. The base of the formation displays sub metre-scale, low-angle cross-bedding of moderately-sorted, medium sandstone overlain by planar-bedded, laminated, alternating fine sandstones and mudstones. In Te Oroi Stream the formation outcrops as cm-bedded, grey, laminated mudstones. Bedding surfaces exposed in Pukemuri Stream display an abundance of *Bathysiphon* sp. foraminifera, some reaching 5 cm-long and indicating a preferred northwest-southeast orientation.

Distribution & Lithologic Variation

The Awheaiti Formation varies in thickness and outcrop considerably. It is thickest in Te Oroi Stream with 16 m exposed, and reaches a thickness of 11 m in a fault repeated section in Pukemuri Stream. The formation is entirely absent in Awheaiti Stream. This is likely the result of paleo-channel erosion that has also removed part of the underlying Mungaroa Limestone (*Figure 4.26*).

Paleontology & Age

An upper Paleocene age (NP8) is assigned to Awheaiti Formation based on calcareous nannofossil assemblages from Pukemuri Stream containing *Discoaster mohleri* and absence of *Discoaster nobilis* (*Figure 4.27*). The FAD of *D. mohleri* represents the first appearance of the genus; it marks the base of Zone NP7 and is a reliable event near the Chron C26/C25 boundary (Agnini *et al.*, 2007). The FAD of *Heliolithus riedelii* defines the base of Zone NP8; however, the use of this taxon for biostratigraphy is not considered reliable, as its stratigraphic range has been reported to differ significantly at different locations (Okada & Thierstein, 1979; Berggren *et al.*, 2000). The absence of the more reliable *D. nobilis*, which has a FAD within Zone NP8, indicates that the sample must be older than middle NP8.

Depositional Environment

The Late Paleocene Awheaiti Formation overlies an erosional unconformity where a significant portion of the upper two members of the Mungaroa Limestone in the Pukemuri Stream section have been removed (*Figure 4.26*). Low-angle cross-bedding, laminated sandstones and mudstones and channelised contacts within the Awheaiti Formation imply a submarine channel and channel-fill sequence. The localised extent of the formation also supports this interpretation. The observation of *Ophiomorpha* and *Planolites* in the Awheaiti Formation is consistent with observations within channels of exhumed submarine turbidite systems (e.g. Kane *et al.*, 2011; Buatois & Mángano, 2011; Callow *et al.*, 2012; *Figure 4.23*).

4.6.4 Pukemuri Siltstone

Description

The formation crops out in Pukemuri and Te Oroi Streams where the stratigraphy has limited structural complications. Although extensive outcrop occurs in Awheaiti Stream, it is affected by several structural complications and the uppermost portion of the formation is either obscured or absent. The base of the formation is represented by 20-40 m of pebbly-mudstone. Pebbles become scattered and less frequent towards the top of the unit, grading into blue-grey, faintly cm-bedded mudstone, which displays intraformational slumping and convolute bedding amongst coherent bedding sequences. The upper portion of this interval also contains megaclasts of indurated, clast-supported conglomerate and well-rounded boulders of hard, cemented sandstone. Above this interval lies massive, flaggy, grey mudstone overlain by light-brown mudstone with fine cm-scale bedding separated by glauconitic laminae, grading into alternating beds of mudstone and sandstone that are well-bedded on a dm-scale.

Distribution & Lithologic Variation

The Pukemuri Siltstone increases in thickness from 110 m at Te Oroi Stream to 130 m at Pukemuri Stream and *ca.* 170 m at Awheaiti Stream (*Figure 4.26*). The 1 m-thick glauconitic sandstone at the base of the formation in Pukemuri Stream does not extend to the other sections. All other units can be traced across sections, including a 25 cm-thick glauconitic sandstone bed.

Paleontology & Age

The Pukemuri Siltstone ranges from Early Eocene (Mangaorapan) at the base to early Middle Eocene (Heretaungan) at the uppermost extent of the formation based on calcareous nannofossil and foraminifera assemblages (*Figure 4.27*). The presence of the calcareous nannofossil *Discoaster lodoensis* throughout the formation, indicates correlation with Nannofossil Zones NP12-14 (late Early to early Middle Eocene), consistent with foraminiferal biostratigraphy. Despite the high sampling resolution, no further zonal subdivision is possible.

Depositional Environment

The pebbly-mudstone of the lower Pukemuri Siltstone is interpreted as a marine debris flow deposit, with supporting evidence including intraformational slump structures, convolute bedding and rafted blocks of conglomerate and sandstone. This unit can be traced from the Te Oroi Stream section to the Awheaiti Stream section, potentially within a broad channel, suggested by an angular, unconformable discordance with underlying strata (*Figure 4.27*). Micritic limestone and chert clasts observed in lowermost Pukemuri Siltstone in Awheaiti Stream probably originated from the upper member of the Mungaroa Limestone, which was reworked as a result of the erosion of the Mungaroa-Pukemuri unconformity. Higher in the section, the occurrence of glauconitic sandstone and glauconitic laminae between mudstone layers suggests reduced sedimentation rates and intermittent deposition or remobilisation.

In Awheaiti and Te Oroi Streams, benthic foraminiferal assemblages indicate a mid-bathyal depth greater than 800 m. Sample S28/f0212, which contain *Stilostomella* sp., (900 m or deeper), *Allomorphina conica*, *Kalamopsis grzybowskii*, *Chilostomella* sp., *Pleurostomella* sp. and *Nuttallides carinotruempyi* (S28/f0206); *Vulvulina zesprinosa*, *Ellipsoglanulina* sp. (S28/f0210), *Chilostomella* sp. and *Anomalina visenda* (S28/f0211) and *Oridorsalis umbonatus* (600-5000 m; Hayward *et al.*, 2010) (S28/f0204).

Slump folds and plastic deformation in lower Pukemuri Siltstone indicate slope deposition and remobilisation of sediment (Walker & James, 1992). Therefore, benthic foraminifera with deeper upper limits are used to constrain the minimum depth of deposition in sample S28/f197. The two samples from Pukemuri Stream used for paleodepth determinations contain a mixture of shelfal and bathyal indicators, suggesting down-slope redeposition of shelf species. The deep-water taxa that are assumed to be *in situ* from sample S28/f0197 indicate an upper to mid-bathyal

depositional environment, supported by an assemblage containing *Lenticulina* spp., *Bulimina pupula*, *Cibicides truncatus*, *Anomalinoides* sp., *Bathysiphon* sp., *Bolivinopsis* cf. *spectabilis*, and *Gyroidinoides* cf. *neosoldanii*. The benthic foraminiferal assemblage from sample S28/f0198 indicates deepening during deposition of the upper part of the Pukemuri Siltstone, increasing from upper/mid-bathyal (S28/f0197) to lower bathyal depths. Key paleodepth taxa from S28/f0198 include *Tritaxilina zealandica*, *Gyroidinoides neosoldanii*, *Kalamopsis grzybowskii*, *Chilostomella* sp., *Pleurostomella* sp., *Nuttallides carinotruempyi* and *Anomalina aotea*.

The low foraminiferal abundance in samples collected in lower Pukemuri Siltstone may potentially reflect rapid deposition. In addition, the presence of *Morozovella* spp. throughout foraminiferal assemblages recovered from the formation implies sub-tropical to tropical sea temperatures at the time of deposition, a feature which correlates with the established concepts of early Eocene paleoclimate (e.g. Hornibrook, 1992; Pearson *et al.*, 2006).

4.6.5 Wanstead Formation

Description

A poorly-sorted, 1.0 m-thick basal conglomerate comprised of a broad assortment of pebble-sized, moderately to well-rounded, chert, greywacke and sandstone clasts overlies the unconformable contact with Pukemuri Siltstone. The majority of the Wanstead Formation is observed as a pale-green mudstone with occasional grey layers and minor glauconitic sandstones. Higher in the formation are occasional 5-50 cm-thick lenses of well-cemented, poorly-sorted, coarse sandstone and gravel that pinch out laterally over a distance of 10 m. The majority of the mudstones display a mottled texture, indicative of pervasive bioturbation.

Distribution & Lithologic Variation

The formation is poorly exposed, with common slumping and slope instability, common in all three sections. This, coupled with a high degree of tectonic shearing and folding makes it difficult to determine true stratigraphic thickness. In addition, the Wanstead Formation at Tora is truncated by the Ewe and Hungaroa Faults. The measured thickness of the Wanstead Formation in Pukemuri Stream is approximately 200 m.

Foraminiferal assemblages from lowermost Wanstead Formation produce a mixed Middle Eocene (Heretaungan to Bortonian) age. The middle Wanstead Formation in Pukemuri Stream is assigned an age of 37.69-36.95 Ma (late Middle to early Late Eocene (Kaiatan)) based on the highest occurrence of the calcareous nannofossil *Chiasmolithus grandis* and the lowest occurrence of *Dictyococcites bisectus*. Similarly, the youngest sediments sampled from the Wanstead Formation in Awheaiti Stream produce an early Late Eocene (late Kaiatan) age (*Figure 4.27*). Some of the Middle Eocene (Porangan stage) may have been removed along the basal unconformity and therefore be completely absent, or the thickness may be reduced and is not apparent at the sampling resolution. Dinoflagellate samples collected by Lee (1995) in Pukemuri Stream also failed to identify strata of Porangan age, further suggesting that the stage is absent. A sample from the uppermost extent of the Wanstead Formation in Pukemuri Stream (S28/f0200), an estimated 200 m above sample S28/f0199, provides an early Middle Eocene (Heretaungan) age. This contradiction confirms the significant extent of deformation within the formation, in which older sediments appear stratigraphically above younger sediments.

Depositional Environment

The occurrence of *Abyssamina poagi*, an abyssal dweller in the middle Eocene (Morkhoven *et al*., 1986) implies a paleodepth of >3500 m. This is supported by assemblages containing *Cassidulina subglobosa*, *Karreriella bradyi* (500-4000 m) and *Glomospira gordialis* (2000-5000 m) (Hayward *et al*., 2010). The mid-bathyal dwellers *Pleurostomella* sp. and *Osangularia* sp. (600-800 m; Hayward *et al*., 2010) also found in these assemblages have probably been reworked or transported downslope.

The co-occurrence of the lower bathyal to abyssal dwelling foraminifera *Abyssamina poagi* with the Heretaungan index species, *Elphidium hampdenense* in sample S28/f0200 from the Wanstead Formation indicates that the basin deepened rapidly during the early Middle Eocene (Heretaungan) from mid-bathyal depths in the Early Eocene Pukemuri Siltstone to lower bathyal-abyssal depths in the Wanstead Formation (*ca*. 3500 m; Morkhoven *et al*., 1986). Benthic foraminiferal assemblages indicate that the basin remained deep until the Late Eocene (Kaiatan), accumulating pelagic sediments.

The Wanstead conglomerate occurs at the base of the Wanstead Formation, and a significant increase in paleodepth occurs between the underlying Pukemuri Siltstone and the overlying

mudstones of the Wanstead Formation. Interpretation of deep marine conglomeratic facies remains rather speculative (Walker & James, 1992). However, the basal Wanstead Formation conglomerate falls in to the 'disorganised conglomerate' category of Walker (1975) and likely represents a debris flow deposit.

The overlying calcareous mudstones of the Wanstead Formation at Tora display little variation and a pervasive bioturbated texture common to basin plain deposits. The mudstones of the Wanstead Formation represent a deeper and possibly more distal facies than the underlying units, with a record of more continuous, slow deposition and bioturbation yielding the complex, mottled bioturbation textures (Frey *et al.*, 1990; Buatois & Mángano, 2011). Subsequent tectonic uplift and folding and faulting has preferentially deformed the soft Wanstead Formation mudstones, as described in the Wanstead Formation elsewhere in the East Coast Basin (e.g. Lillie, 1953).
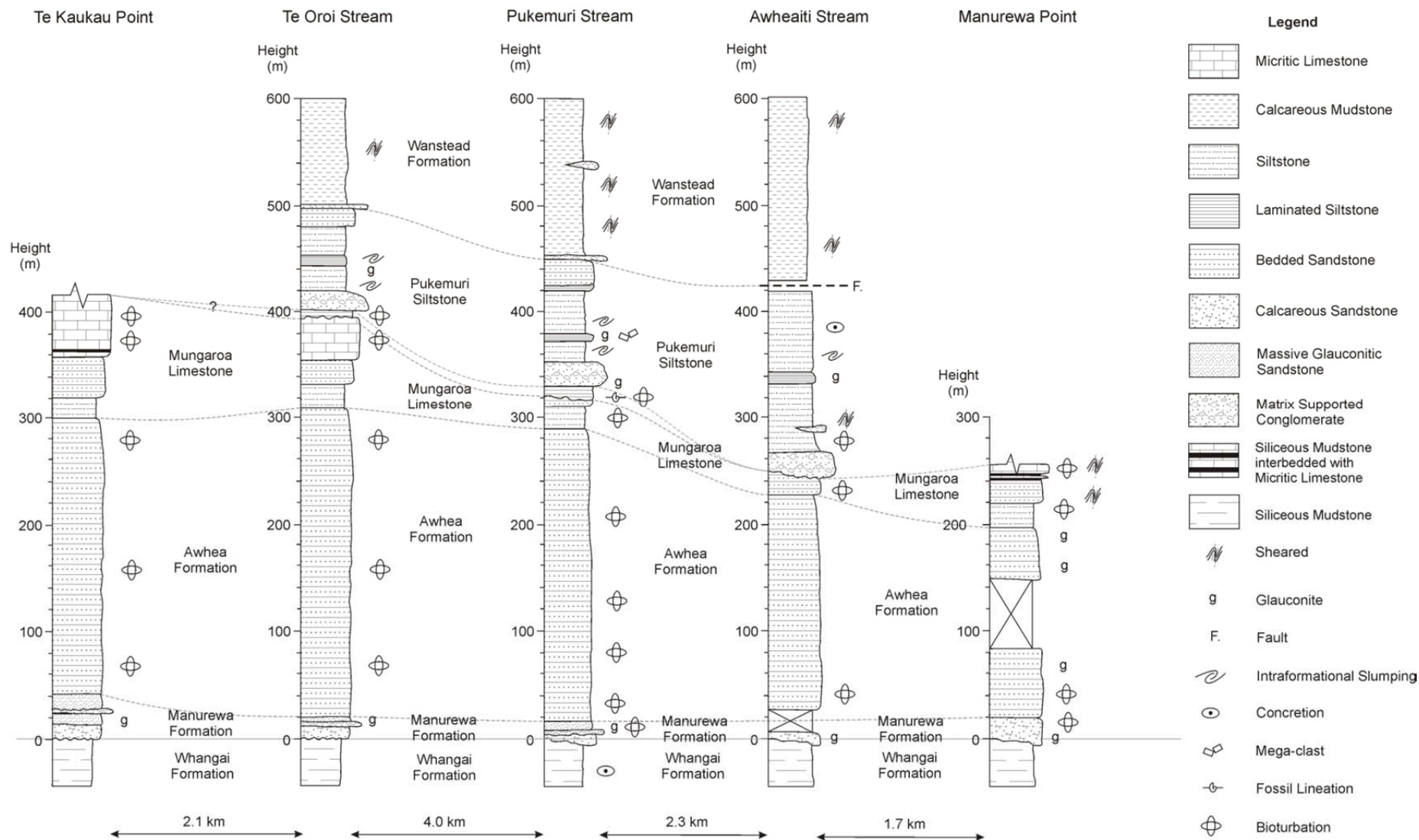
Figure 4.26: Correlation between sections, from Te Kaukau Point in the southeast, to Manurewa Point in the northwest of the Tora area.
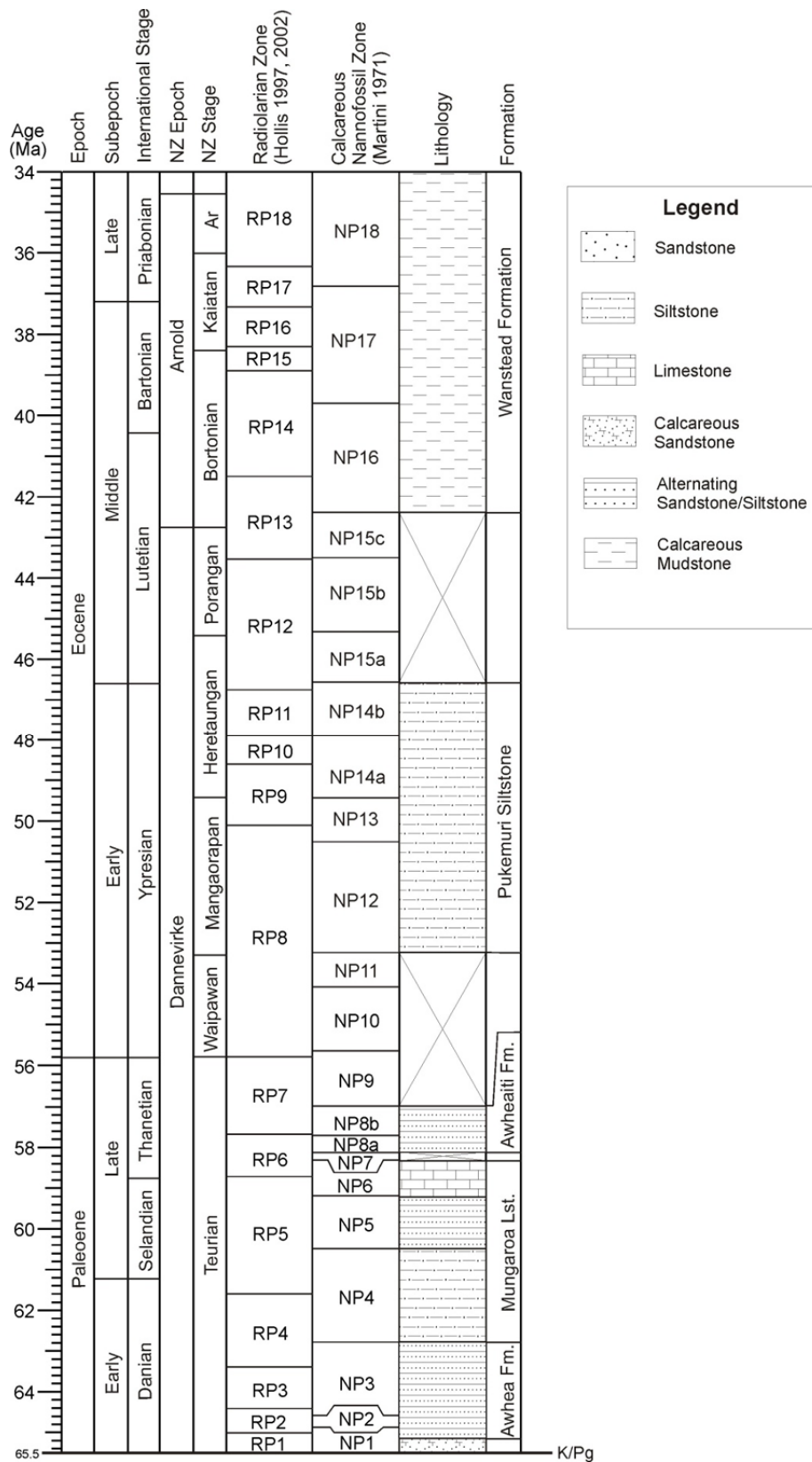
Figure 4.27: Revised formation ages for the Paleogene stratigraphy at Tora. 'Ar' denotes the Runangan Stage in the New Zealand Geological timescale. Timescale based on Hollis *et al.* (2010). Note radiolarians only used for age control on the upper limestone member of the Mungaroa Limestone. No nannofossil assemblages were studied from the Awhea Formation.

4.7   Depositional Setting: Orientation and Rotation

Slump folding and oriented *Bathysiphon* foraminifera measured at Tora provide indications of the paleo-slope (e.g. Strachan & Alsop, 2006; Tucker, 2011) and current orientation (*Figures 4.28* and *4.29*). Lineations measured from *Bathysiphon* foraminifera in Pukemuri Stream were observed within the confines of channelised Awheaiti Formation, and largely produce a NW-SE lineation. Slump folding within the Mungaroa Limestone is predominantly oriented in a south-easterly direction, while slump folding evident in the Pukemuri Siltstone is largely directed SE to NE. The bimodal distribution of slump fold orientations measured in the Pukemuri Siltstone suggest slumping occurred on the slopes of a channel system, as depicted in *Figure 4.28*.

Accounting for tilting of the stratigraphic succession and a basin-wide estimate of *ca.* 40° anticlockwise tectonic rotation around the vertical pole during the last 40 Ma (King *et al.*, 1999), this would indicate a north-northeast oriented slope direction at the time of deposition (*Figure 4.29*). This is consistent with paleogeographic reconstructions of the New Zealand region (e.g. King *et al.*, 1999; Crampton *et al.*, 2003).
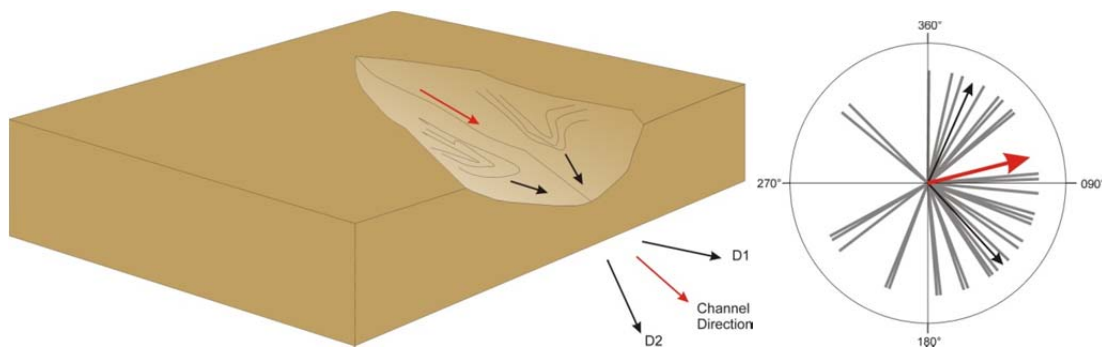
Figure 4.28: Interpretation of the influence of slope orientation within a channel on the directionality indicated by slump folds, where the black arrows D1 and D2 represent the bimodal peaks in the distribution of slump fold orientations and the red arrow is indicative of the channel direction. Slump fold orientations (black arrows) from the Pukemuri Siltstone displaying a largely bimodal distribution, and the inferred channel orientation is shown by the red arrow.
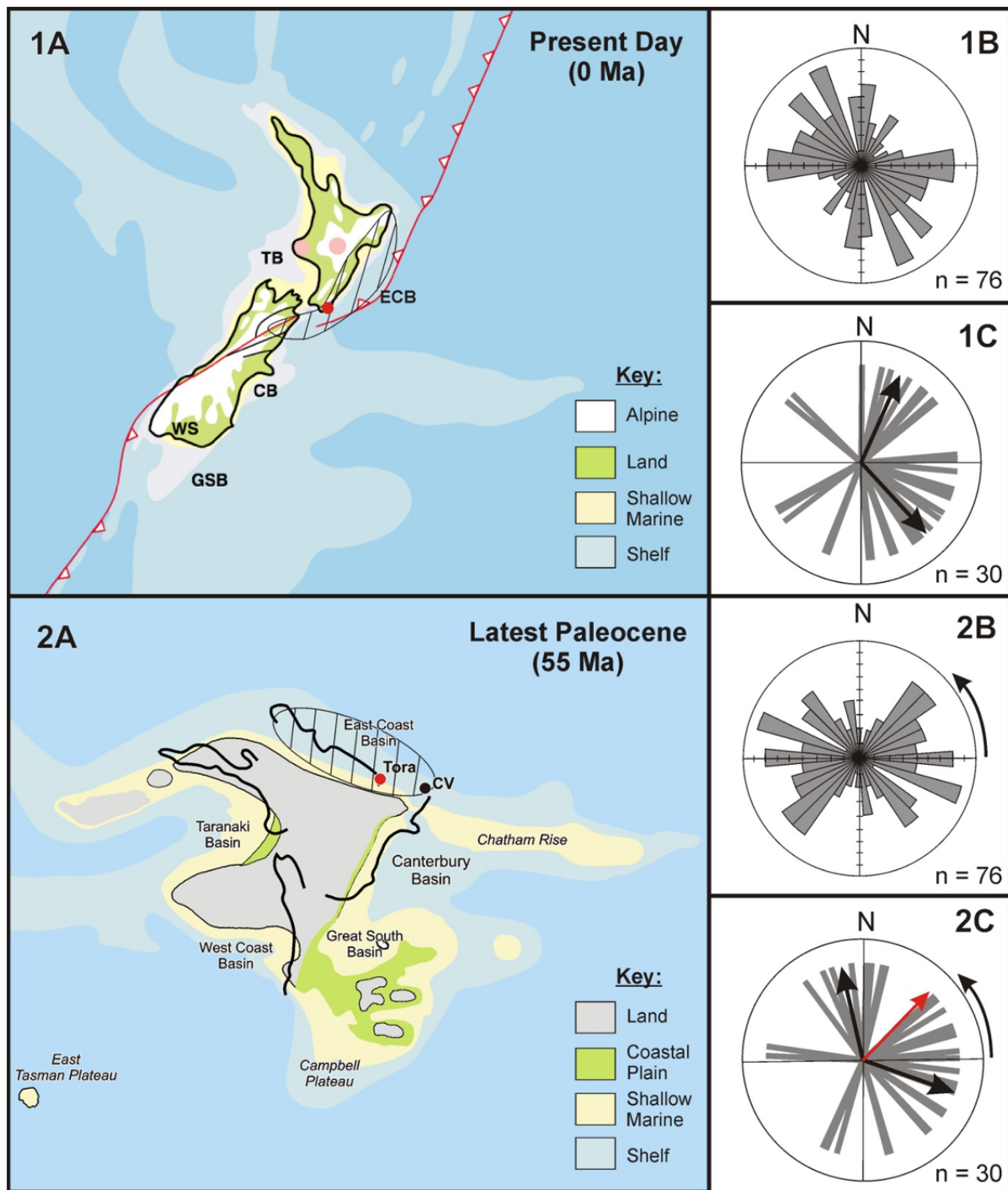
Figure 4.29: 1A; present day orientation of the East Coast Basin (ECB) and field observations of large foraminifera current lineations measured in the Awheaiti Formation (**1B**) and slump fold (**1C**) orientations from the Pukemuri Siltstone. **2A**; Latest Paleocene reconstruction of the New Zealand region with paleocurrent (**2B**) and slump fold orientations (**2C**) corrected for 40° anticlockwise rotation of the East Coast Basin over the past 40 Ma. Black arrows represent mean directions of the two groupings, and the red arrow indicates the potential channel and slope directionality. Hatched area on paleogeographic maps represents the East Coast Basin, with the Tora locality denoted by a red dot. Paleogeographic maps modified from King (2000) and Hollis *et al*., 2012. Key to abbreviations: ECB = East Coast Basin, TB = Taranaki Basin, CB = Canterbury Basin, WB = Westland Basin, GSB = Great South Basin, CV = Clarence Valley, MW = mid-Waipara River, and 1124 = ODP site 1124. Pink dots depict recent volcanism.

4.8   Paleoenvironmental Discussion and Depositional History

Submarine fans and turbidite systems have long been recognised as important for understanding deep water depositional environments. Submarine fans can vary considerably in morphology, structure and processes operating (Bouma, 2000). Despite continued refinement of fan models in recent years, one of the most useful and widely used is an early model proposed by Walker (1978) (*Figure 4.30*). Although this model has limitations, particularly in not taking into account external controls like sea level changes (Bouma et *al.*, 1985; Walker & James, 1992, Bouma, 2000), it provides a simple and suitable model to assist interpretation of the Paleogene rocks described at Tora.
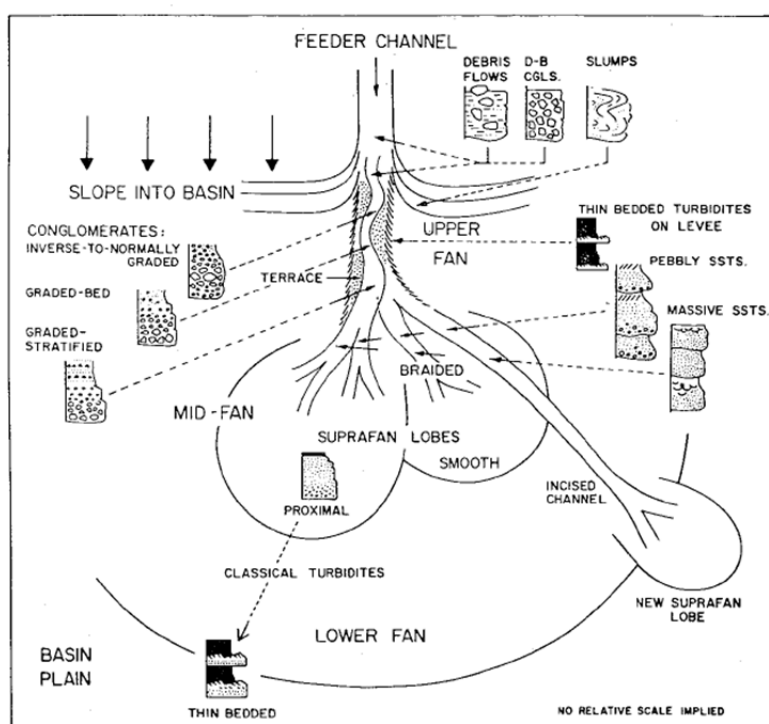
Figure 4.30: The submarine fan model of Walker (1978).

Using key features of the sediments described at Tora and the Walker (1978) model, interpretations of the depositional environment are used to construct a depositional history of the stratigraphic succession at Tora, and a series of paleoenvironmental maps (*Figure 4.31*). In addition, ichnofossil relationships are utilised to produce supporting evidence. Details of the Manurewa Formation observed in the field during the course of this study and features noted by Lee (1995), Wasmuth (1996), Laird *et al.* (2003) and Vellekoop (2010) are incorporated in this discussion for a revised interpretation of the Manurewa Formation.

4.8.1   Manurewa Formation

The Manurewa Formation was deposited in the Late Cretaceous-Early Paleogene, and overlies the widespread Rakauroa Member of the Whangai Formation. The Manurewa Formation is interpreted as a nested channel complex, with cross-bedding, scours, channels, and conglomeratic intervals indicative of periods of high energy erosion and deposition (Laird *et al.*, 2003). Laird *et al.* (2003) interpreted the Manurewa Formation as a shallow marine channel complex based on the presence of marginal marine acritarchs and fungal material. However, these indicators are possibly reworked, as the benthic foraminiferal assemblages (S28/f0191, S28/f0201; *Appendix 1*) suggest a bathyal paleodepth which is supported by trace fossil assemblages associated with the *Nereites* ichnofacies (*Nereites*, *Chondrites*, *Zoophycos*) observed in the field (this study; *Figure 4.19*), and observations of *Helminthoida* and c.f. *Paleodictyon* recorded by Wasmuth (1996).

The basal conglomerate of the Manurewa Formation likely represents a phase of down-cutting and channel incision into the underlying Whangai Formation, associated with the initial stages of the development of a submarine fan or the expansion of a new lobe of an existing fan. The massive sandstone of the upper member which is channelised into the lower member of the Manurewa Formation (Wasmuth, 1996; Laird *et al.*, 2003) is also consistent with the interpretation of channel incision, deposition and lobe development, as described in the Walker (1978) model (*Figure 4.30*). Furthermore, the Manurewa Formation is a localised unit restricted to the Tora area (Laird *et al.*, 2003), consistent with the interpretation of restricted early stage fan development (*Figure 4.31*).

4.8.2   Awhea Formation

The Manurewa Formation grades into the bedded sandstones of the lower Awhea Formation which is interpreted as the deposition of proximal turbidite sequences within the main body of a submarine fan (*Figures 4.30 & 4.31*). Higher in the formation, the shift to 'classical', normal-graded, well-bedded turbidites is interpreted to represent 'smooth' fan environments towards the outer extent of the supra-fan lobes (Walker, 1978). The Awhea Formation displays a thinning upwards sequence of turbidites which is indicative of gradual lobe shifting (Walker & James, 1992).

The stratigraphic thickness of the Awhea Formation thins northwards, from 290 m at Te Oroi Stream to 47 m near the Pahoa River mouth at Glenburn (Tayler, 2011), consistent with the interpretation of a fan environment which had its source to the southeast and the depositional centre located near the Tora area, extending and thinning to the north during deposition of the Awhea Formation (*Figure 4.31*).

4.8.3   Mungaroa Limestone

The gradational contact from the Awhea Formation upwards into the lower member of the Mungaroa Limestone, as well as the transition from the thin, fine-grained turbidites of the upper Awhea Formation to the thicker sandstone beds separated by thin mudstones in the lower members of the Mungaroa Limestone, suggests a return to a more proximal position in the lower fan (Walker, 1978). The abrupt transition to the upper limestone member, suggests a rapid, regional reduction in the deposition of clastic sediment during NP5 (mid-Paleocene) and potentially a northwards extension of the calcareous, biogenic Mead Hill-Amuri Limestone sedimentary sequence of the southern East Coast Basin (*Figure 4.31*). Like the Awhea Formation, the Mungaroa Limestone thins northwards, where is has a thickness of 28 m at Glenburn (Tayler, 2011).

4.8.4   Awheaiti Formation

The Awheaiti Formation is channelised into the underlying Mungaroa Limestone, with cross-bedding at the base of the formation suggesting channel deposition in an upper fan environment (*Figure 4.30*). The Awheaiti Formation does not extend beyond the Tora area, supporting an interpretation of localised channel incision and infilling during Nannofossil Zone NP8 (late Paleocene; *Figure 4.31*). Thin-bedded mudstones of the Awheaiti Formation observed in Te Oroi Stream likely had a slightly different mode of deposition, and potentially may represent levee deposits or the outer margin of the channel system, as shown in the fan model in *Figure 4.30*.

4.8.5   Pukemuri Siltstone

The basal, 20 m-thick pebbly-mudstone of the Pukemuri Siltstone is indicative of a debris flow deposit. This, coupled with the unconformable and possibly channelised contact between the Pukemuri Siltstone and the underlying Awheaiti Formation, suggests that the depositional system changed to a slope environment during the Early to early Middle Eocene (*Figure 4.31*). Mudstones overlying the basal pebbly-mudstone unit contain very few sandstone beds, and are characterised by subtle soft-sediment folding on a variety of scales. This aptly fits the description of the slumped shale and mudstone facies of Walker & James (1992) and the inferred depositional environment on the slope of a basin. The Pukemuri Siltstone likely represents a slope-influenced end member equivalent of the Wanstead Formation at Glenburn (*Figure 4.31*).

4.8.6   Wanstead Formation

Basin subsidence and marine transgression, apparent in benthic foraminiferal assemblages, resulted in a significant increase in paleodepth between the Pukemuri Siltstone and the overlying mudstones of the Wanstead Formation. The basal conglomerate of the Wanstead Formation is likely deep marine in origin, deposited as a submarine debris flow, which would account for the mixed lithologies of clasts present. A similar, thin (≤2 m) conglomeratic unit is incorporated within the Wanstead Formation in the Akito area of the northeast Wairarapa, and is interpreted as deposition near the mouth of a submarine canyon system (Neef, 1992).

Calcareous mudstones with characteristic mottling from pervasive bioturbation occur throughout the remainder of the formation. These are indicative of deposition on the basin plain, offering further evidence of marine transgression and deepening of the depositional setting from a slope setting to a basin plain environment (*Figure 4.31*). The deposition of the Wanstead Formation at Tora is coeval with the deposition of the 'upper marl' member of the Amuri Limestone in the Marlborough area (*Figure 4.31*; Crampton *et al.*, 2003).
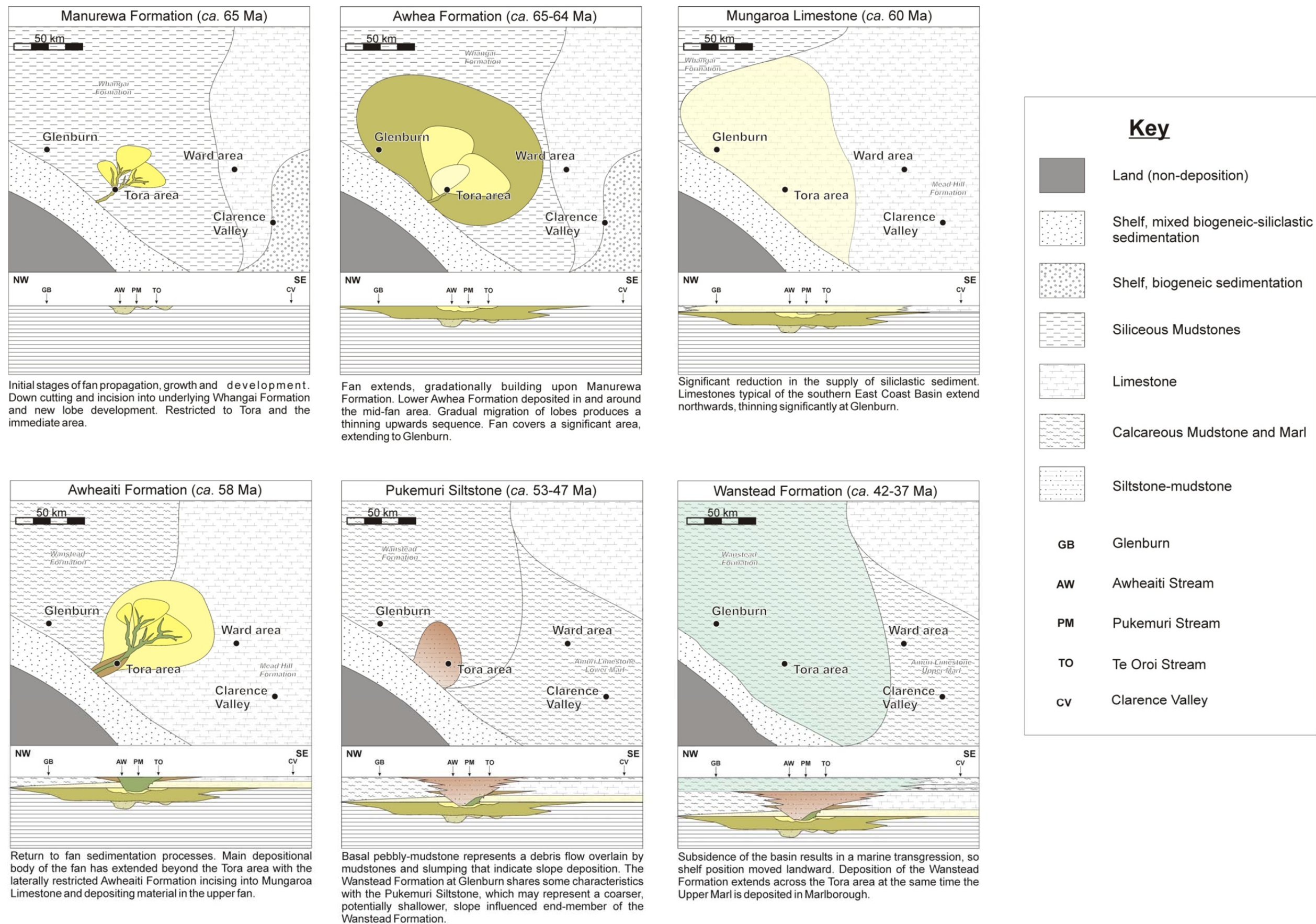
Figure 4.31: Schematic paleoenvironmental maps and cross-sections at different times in the central East Coast Basin. Base map adapted from Crampton *et al.* (2003) to accommodate the bathyal marine interpretation of Tora. No relative scale has been applied to cross-sections in order to exaggerate stratigraphic relationships.

4.9 Correlation with Other East Coast Sections

The sedimentary succession exposed at Tora can be correlated to other slope-basin sediments deposited elsewhere in the East Coast Basin. The Paleogene succession at Tora broadly fits the typical fining upwards sequence that is observed throughout the East Coast Basin (Moore *et al.*, 1986; Ballance, 1993).

The Upper Cretaceous to Lower Paleocene strata at Glenburn, north of Tora, display no obvious unconformities that can be correlated with the basal Manurewa, intra-Haumurian unconformity at Tora (Lee, 1995; Laird *et al.*, 2003), consistent with the localised extent of the Manurewa Formation submarine channel system (*Figure 4.32*). Field, Uruski *et al.* (1997) suggest that the Manurewa Formation is a lateral correlative of the Upper Calcareous or Porongahau Members of the Whangai Formation. However, this seems unlikely due to the localised and incised nature of the lower Manurewa Formation as documented by Wasmuth (1996) and Laird *et al.* (2003). Nevertheless, the upper member of the Manurewa Formation may be correlated with the widespread Te Uri Member, a glauconite-rich unit that occurs directly above the K/Pg boundary in many Hawke's Bay sections that is overlain by the Wanstead Formation (Moore, 1988b). This correlates well in terms of the timing of deposition, but does not relate well with stratigraphic associations at Glenburn, in the northern component of the Tora Block.

The Awhea Formation is coarser than typical early Paleocene facies observed elsewhere in the East Coast Basin (Field, Uruski *et al.*, 1997), but broadly fits the description of the Upper Calcareous Member provided by Moore (1988b) and Field, Uruski *et al.* (1997) as a hard, medium-grey, micaceous mudstone and bioturbated glauconitic sandstone containing pyrite nodules. Collectively the Manurewa and Awhea Formations of Tora may represent a southern extension of the Upper Calcareous Member described elsewhere in the East Coast Basin (*Figure 4.31*). This observation is consistent with the stratigraphic succession observed in the Glenburn area, where the Glenburn Formation is successively overlain by the Rakauroa and Upper Calcareous Members of the Whangai Formation, followed by the Kaiwhata Limestone (Moore, 1988b).

The Mungaroa Limestone is recognised as a lateral correlative of the Kaiwhata Limestone, mapped in the Glenburn-Flat Point area, in terms of both age and environment (van de Hueval, 1960; Webby, 1969; Field, Uruski *et al.*, 1997; Lee & Begg, 2002), thereby placing an upper limit on the application of the Whangai Formation nomenclature at Tora. The white, well-bedded

porcellaneous Mungaroa Limestone is a likely correlative or northern extension of the Amuri Limestone found in Marlborough (van de Hueval, 1960; Browne, 1987; Field, Uruski *et al.*, 1997).

Siliceous, dark-grey mudstones of the 'Waipawa facies' within Mungaroa Limestone at Tora probably represent the siliceous, deep marine end member of the Waipawa Formation, similar to that observed in Mead Stream overlying Mead Hill Formation in the southern East Coast Basin at Marlborough (Strong *et al.*, 1995; Andrew, 2010; Hollis *et al.*, in prep.). The paired dark mudstone bands of the 'Waipawa facies' identified at Tora correlate well with outcrop observations further south at Mead Stream, Marlborough (Killops *et al.*, 2000; Hollis *et al.*, 2005a, b). North of Tora, the Te Uri Member of the Whangai Formation, at least in part, represents the glauconitic, shallow marine end member of the Waipawa Formation (Moore, 1988b; Field, Uruski *et al.*, 1997; Rogers *et al.*, 2001).

The Wanstead Formation (previously the Huatokitoki Formation of van de Hueval, 1960; Moore, 1980) in the Glenburn area and described as conformably overlying the Kaiwhata Limestone (van de Hueval, 1960), confirms that channelisation associated with the late Paleocene Awheaiti Formation at Tora is of localised extent. Slump structures and blocks of Waipawa-type mudstone, micritic limestone and boulders of Glenburn-type siltstone are incorporated within the Wanstead Formation at Glenburn (Moore, 1980; Lee, 1995). Moore (1980) suggests this is evidence of early Eocene tectonism. Similar features at Tora may also indicate early Eocene tectonic activity. The Pukemuri Formation at Tora is coeval with the Wanstead Formation in other parts of the East Coast Basin, but represents a more proximal slope facies as evidenced by the apparently localised distribution of debris flows and the coarser character of the sediment.

Deposition of the Wanstead Formation at Tora occurred at lower bathyal to abyssal depths during the early Middle to Late Eocene (Heretaungan to Kaiatan), which may reflect regional deepening of the area. The Wanstead Formation represents the deepest depositional environment of the Cretaceous-Paleogene East Coast Basin, with average paleodepths of mid-bathyal and lower bathyal to abyssal (Field, Uruski *et al.*, 1997). The Wanstead Formation at Tora is younger than typically expressed in many other East Coast sections (typically Paleocene to middle Eocene; Field, Uruski *et al.*, 1997). The transition from Wanstead to Weber Formation, which usually occurs during the Bortonian (*Figure 4.31*), may represent a facies change to shallower, more calcareous sediments within the basin that is not represented at Tora because this portion of the basin was significantly deeper.
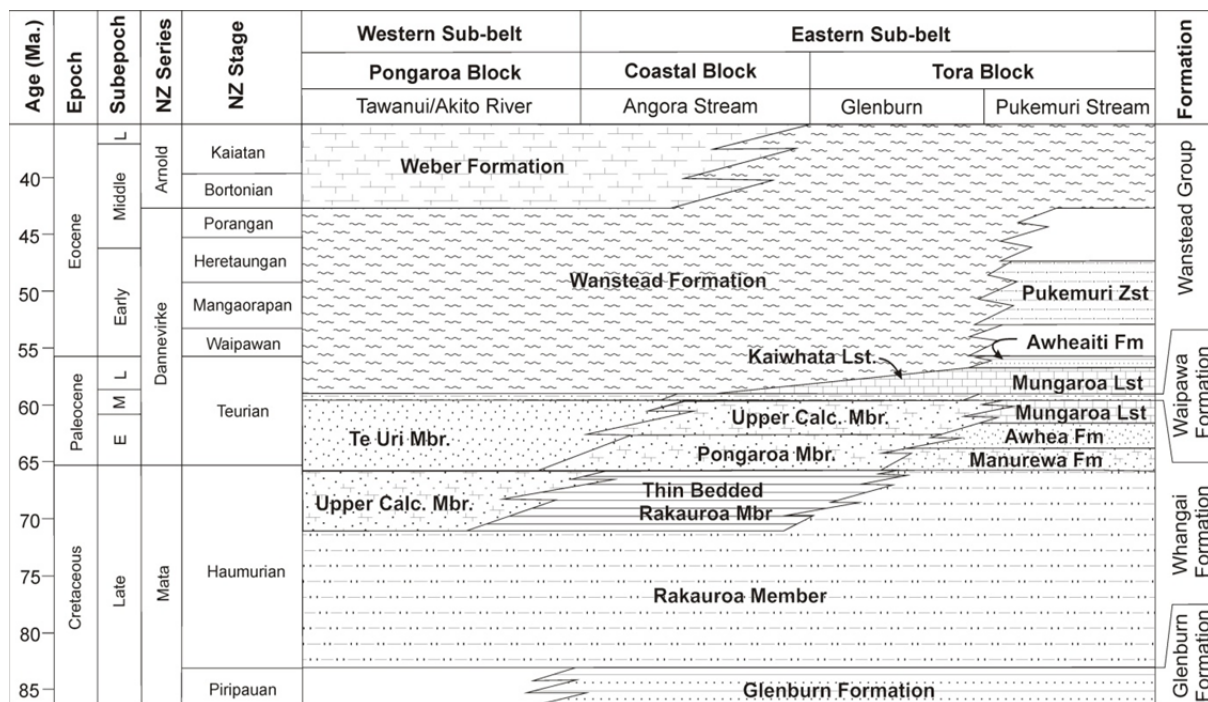
Figure 4.32: Generalised regional stratigraphic framework of the southern East Coast Basin, North Island, displaying the revised, distinctly different sedimentary trends of the late Cretaceous to early Paleogene present at Tora in comparison to the typical East Coast succession. Blank areas depict unconformities.

4.10 Evidence of Early Paleogene Tectonism

The Paleocene-Eocene is widely considered a period of tectonic quiescence in the New Zealand sector of the southwest Pacific, associated with a passive margin regime and thermal subsidence following Cretaceous rifting (Bradshaw, 1991; King *et al.*, 1999). However, there are several lines of evidence suggesting syntectonic deformation of early Paleogene sediments in the East Coast Basin. (e.g. Moore, 1980; Moore, 1989b; Delteil *et al.*, 2006, Tayler, 2011).

The angular discordance of 15-20° between the Awheaiti Formation and the Pukemuri Siltstone suggests a regional tilting of strata prior to the deposition of the Pukemuri Siltstone. Calcareous nannofossil datums in the Awheaiti Formation and the Pukemuri Siltstone would constrain this event in the range of NP8-NP12 (57.6-53.2 Ma). A similar discordance is also observed between Mungaroa Limestone and Awheaiti Formation in Te Oroi Stream (*Figure 4.16b*), and tectonism associated with the tilting of strata may also be responsible for the emplacement of greensand dykes and slumping in the Mungaroa Limestone (*Figure 4.17c, d, e & Figure 4.33a, b*). Tectonic activity potentially continued into the Mangaorapan, causing soft sediment slumping (*Figure*

4.33c) and the inclusion of megaclasts in the Pukemuri Siltstone at Tora (*Figure 4.8e*) and the Wanstead Formation at Glenburn (Moore, 1980).

The widely accepted passive margin setting during the early Paleogene implies that the tectonism evident at Tora was likely caused by localised normal faulting associated with thermal subsidence and internal deformation of the East Coast Basin, as suggested by Furlong & Kamp (2009).
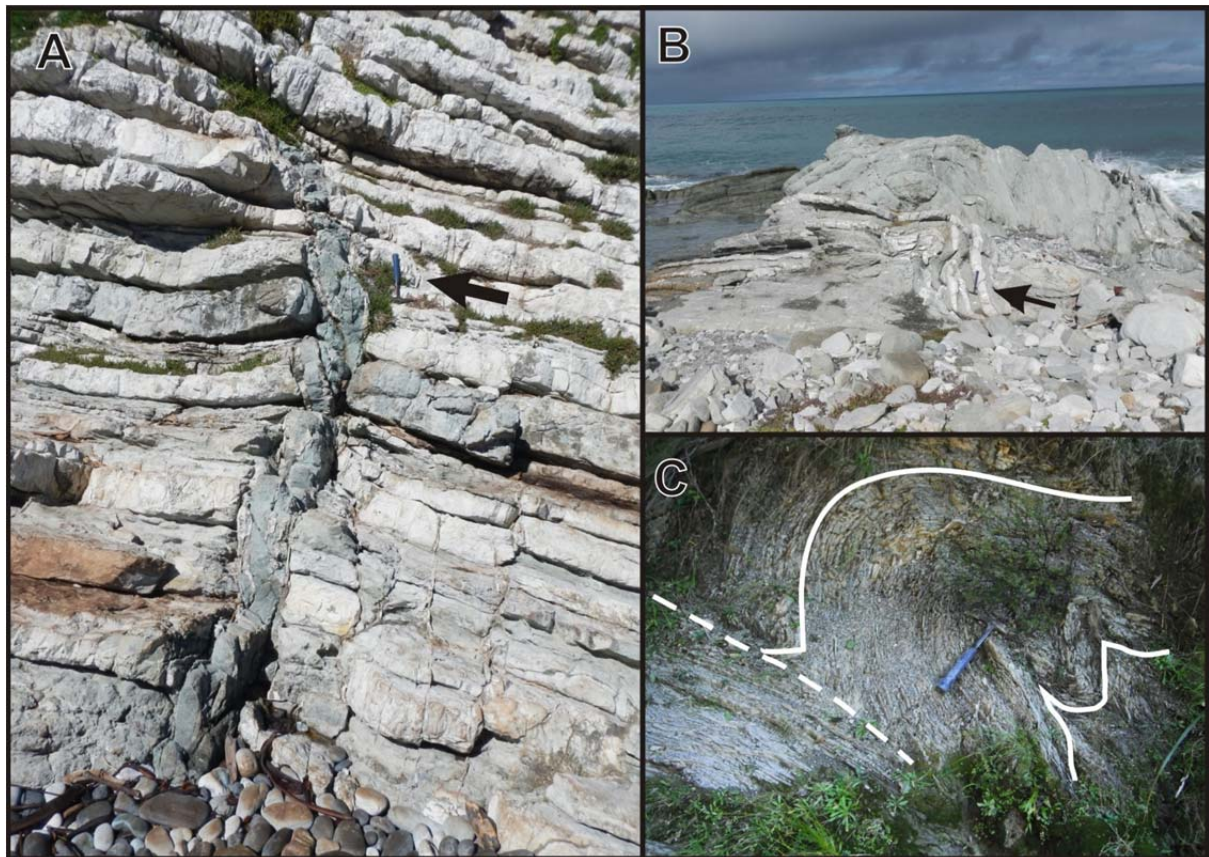
Figure 4.33: Evidence of syn-depositional deformation of sediments at Tora. **A**) Greensand dyke injected into Mungaroa Limestone at Te Kaukau Point. Bedding is deflected upwards and truncated near the top of the frame. Hammer for scale (arrowed). **B**) Slumping in Mungaroa Limestone outcropping at Manurewa Point. Hammer for scale (arrowed). **C**) Classic example of a slump fold in the Pukemuri Siltstone exposed in Te Oroi Stream.

4.11   Summary

The Paleogene stratigraphy of the Tora area is divided into five distinct lithostratigraphic units, representing a finer stratigraphic division than the typical lithostratigraphic succession observed in other areas of the East Coast Basin. The diversity of facies at Tora reflects sedimentation within a submarine fan and channel complex at middle to lower bathyal depths within the context of a regional transgression from the late Cretaceous to the late Eocene.

The Awhea Formation is inferred to have been deposited as a turbidite succession within the main body of a fan complex during the early Paleocene. The Mungaroa Limestone consists of a lower part that represents the distal or lateral margin of a fan complex and an upper part that is dominated by deposition of pelagic carbonate during the middle and late Paleocene.

 The Awheaiti Formation was likely deposited in a channel incised into the Mungaroa Limestone during the late Paleocene. The lower Pukemuri Siltstone was most likely deposited in a slope setting, with a basal debris flow overlain by siliclastic sediments. The syn-sedimentary deformation of Paleogene and Early Eocene sediments suggests that active tectonic deformation was occurring during this period. The middle Eocene Wanstead Formation was deposited in a deep bathyal setting beyond the margins of the submarine fan, with paleodepth indicators indicative of regional transgression.

PALEOGENE CLIMATE HISTORY OF THE CENTRAL EAST COAST BASIN

5.1   Introduction

A robust early Eocene paleoclimate record from the central East Coast Basin is of great value as it provides a critical North Island reference for early Eocene climate reconstructions and an external comparison to the established multi-proxy records in the Canterbury Basin. However, the recovery of a quantitative paleoclimate record from the central East Coast Basin has been hampered by several difficulties, the most significant of which is the complex depositional and deformational history, combined with the effects of post-depositional alteration, causing variable preservation of foraminiferal calcite. The application of the laser ablation inductively coupled plasma mass spectrometry (LA-ICP-MS) method to produce a Mg/Ca record for paleotemperature calculation allows the identification and removal of effects caused by diagenetic alteration and silicate contamination, unlike traditional oxygen stable isotope methods and the solution method of Mg/Ca data acquisition. To provide additional confidence in paleotemperature reconstructions, SEM imaging, EPMA analysis and multiple silicate contamination proxies were applied to foraminifera from three selected sections in the East Coast Basin to determine if primary foraminiferal calcite and the inherent paleoclimate signal has been preserved.

Two sections through the Early Eocene Pukemuri Siltstone at Tora (Awheaiti and Pukemuri Streams) were sampled to provide foraminiferal assemblages for geochemical analysis. Calcareous nannofossil and foraminiferal assemblages provided reasonable age control for samples from Pukemuri Stream and yielded moderately preserved foraminiferal assemblages suitable for the application of laser ablation analysis. However, extremely poor preservation of foraminiferal assemblages in Awheaiti Stream, coupled with structural complexities in the strata, generated uncertainties in age and temperature determinations. In addition, very few Mg/Ca analyses of foraminifera from Awheaiti Stream passed the screening process and, as such, it was not possible to produce a comprehensive or robust record from this section. Therefore, the samples from Awheaiti Stream have been omitted, and only the results from the Pukemuri section are reported here. Additional sample suites from two sections in the southern Hawke's Bay (Aropito and Tawanui sections) were utilised to produce a composite comparative section to complement the Tora record and increase confidence in the sea temperature reconstructions for the central East Coast Basin.

Prior to developing a sea temperature history, the depositional age of the sampled sediments must be determined and a temperature calibration applied to the foraminiferal Mg/Ca values, both of which involve inherent assumptions. In this study, the mean Mg/Ca value obtained for each species within a sample is initially reported relative to stratigraphic height, in order to present the data without any introduced ambiguity pertaining to age and temperature determinations. The composite temperature record of the East Coast Basin (Aropito, Tawanui and Pukemuri Stream sections) is then compared to existing Mg/Ca temperature records from the mid-Waipara River and Hampden Beach in the Canterbury Basin, and the implications for regional oceanography during the early Eocene discussed.

Benthic foraminiferal assemblages for the Pukemuri Stream section can be found in *Appendix 1*, and all raw Mg/Ca data for foraminifera from the Aropito, Tawanui and Pukemuri Stream sections is presented in *Appendix 2*.

5.2   Age Model Development

Assigning a numerical age to samples is essential to correlate results between different stratigraphic sections and with existing paleoclimate records. Biostratigraphic datums were applied to the stratigraphic records from the Pukemuri, Aropito and Tawanui sections to produce individual age models allowing for comparison between sections (*Figures 5.1, 5.2* and *5.3*). Sample ages were determined by placing a line of best-fit through biostratigraphic datums, from which an assumed-linear sedimentation rate was calculated, enabling the assignment of an age to each sample.

Calcareous nannofossil and foraminiferal assemblages collected from the Pukemuri Stream section provided the necessary biostratigraphic constraints to produce robust age control (*Figure 5.1*). For construction of the Pukemuri age model, emphasis was placed on calcareous nannofossil datums and the foraminifera *present* within each sample. The moderate to poor diversity foraminiferal assemblages collected from the Pukemuri Siltstone meant that the apparent *absence* of a taxon may be a reflection of the quality of the assemblage rather than evidence of a true biostratigraphic event.

Calcareous nannofossil assemblages were not available for samples from the Aropito and Tawanui sections, and the respective age models were constructed using foraminiferal biostratigraphic events. Samples from the Wanstead Formation at Aropito and Tawanui produce diverse foraminiferal assemblages, providing good age control for the low resolution sampling in these sections.

Application of the age models shows that samples analysed for Mg/Ca in the Pukemuri Stream section range in age from 60.4 to 37.3 Ma (*Figure 5.1*). The temporal resolution of sampling varies between 0.07 and 4.6 Myr, with a typical sampling resolution in the Early Eocene Pukemuri Siltstone of between 70 and 200 kyr. Sampling resolution in the Aropito and Tawanui sections is coarse, with Aropito samples ranging from 47.3 to 42.0 Ma in age with an approximately 1.0 Myr sampling resolution (*Figure 5.2a*). The Tawanui sample suite is slightly older, ranging in age from 53.4 to 45.0 Ma, with a sample resolution that varies from 0.4 to 5.0 Myr (*Figure 5.2b*). Together, the Aropito and Tawanui sections form a relatively low-resolution composite section that spans the Early to Middle Eocene (53.4–42.0 Ma).
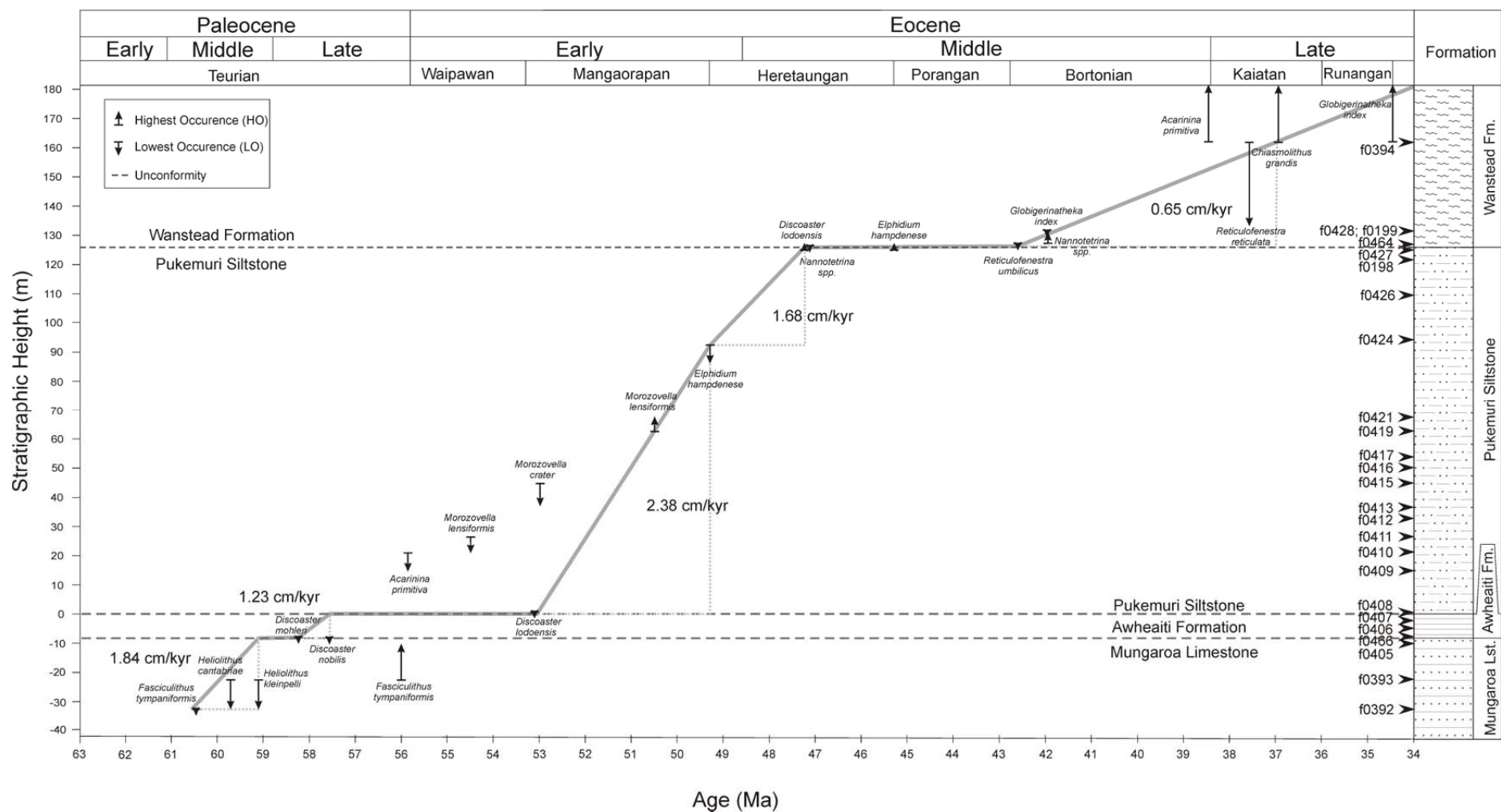
Figure 5.1: Age model for the Pukemuri section at Tora with calcareous nannofossil and foraminiferal age constraints. Sedimentation rates were calculated assuming a linear sedimentation rate. Arrow lengths indicate the distance between samples that constrains the datum, and the arrow direction indicates that the event could move with further sampling; i.e. lowest the occurrence could occur lower in the section, and the highest occurrence higher in the section.
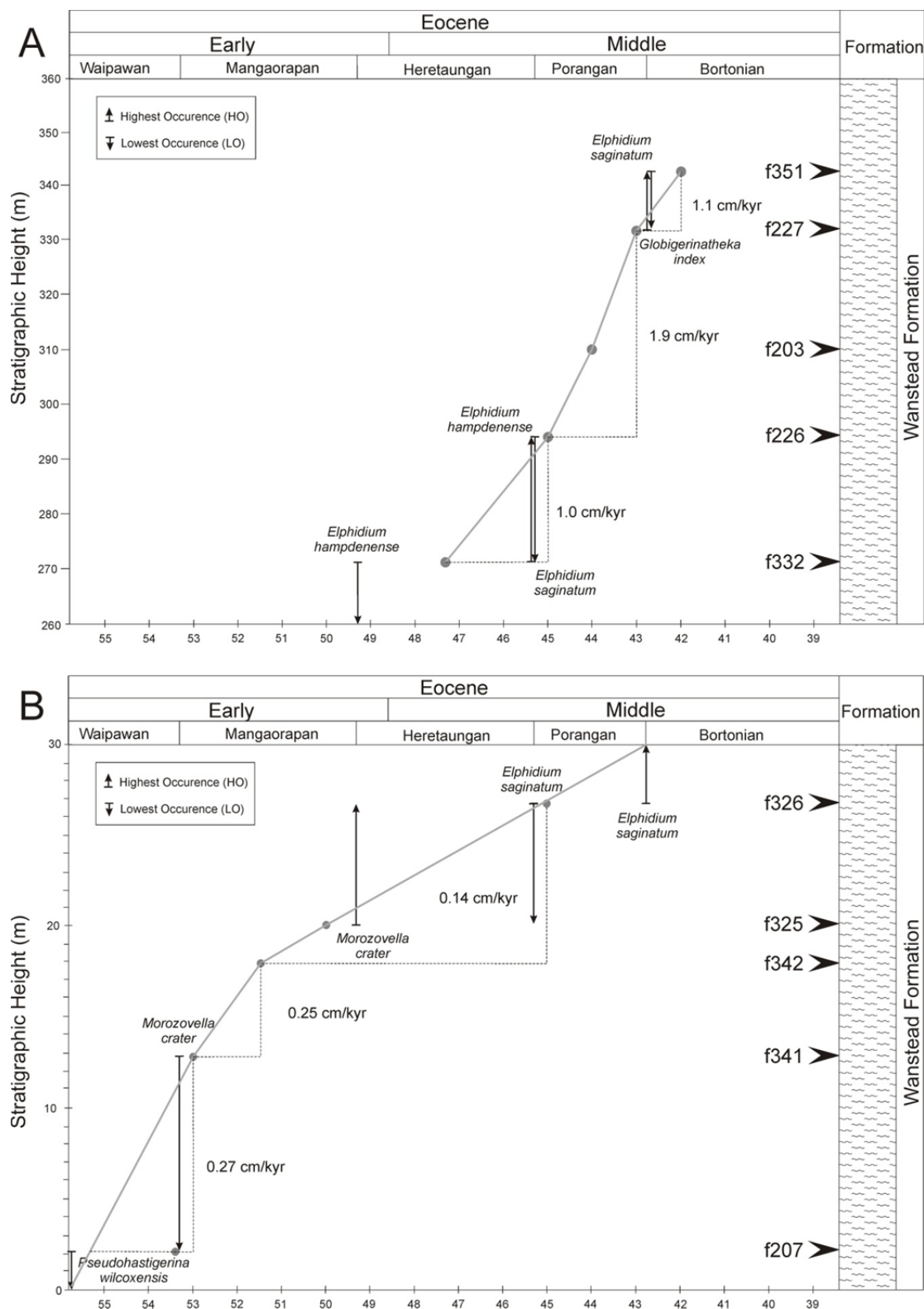
Figure 5.2: Age models for the Aropito (**A**) and Tawanui (**B**) sections, southern Hawke's Bay. Grey dots represent estimated ages (Morgans, pers. comm.). Age constraints were based on foraminiferal assemblages. Arrow lengths indicate the distance between samples that constrains the datum, and the arrow direction indicates that the event could move with further sampling; i.e. lowest the occurrence could occur lower in the section, and the highest occurrence higher in the section.

5.3 Bulk Carbonate Stable Isotope Stratigraphy of Pukemuri Stream

The bulk carbonate carbon and oxygen stable isotope signatures recorded in sedimentary successions often provide indications of paleoclimate signals, although bulk carbonate δ^{18}O in early Paleogene sediments is often diagentically overprinted. Significant warming of the oceans during the EECO resulted in dramatic perturbations in global carbon cycle dynamics, recorded in carbonate reservoirs as a negative δ^{13}C excursion (e.g. Zachos *et al.*, 2001; Hollis *et al.*, 2005b). Carbon isotopes are typically more resistant to diagenetic alteration than oxygen isotopes and this is reflected in the Tora record. Even so, several samples display unusually low δ^{13}C values which may be attributable to post-depositional alteration, low carbonate content, or to a high abundance of organic carbon present within the bulk sediment sample. A sustained peak in bulk carbonate δ^{13}C values averaging *ca.* 0.3‰ in the lower Pukemuri Siltstone during the Mangaorapan is comparable to benthic foraminiferal δ^{13}C values from DSDP and ODP cores during this interval, although they are lower than bulk carbonate δ^{13}C values of *ca.* 1.0‰ recorded in Mead Stream, Marlborough (Slotnick *et al.*, 2012). Further up the section, δ^{13}C values for the upper Pukemuri Siltstone are more negative and average -0.3‰ (*Figure 5.3*).

Bulk carbonate δ^{18}O values are more difficult to interpret, and average -5.3‰ in the lower Pukemuri Siltstone. They remain relatively constant throughout the middle of the section, and marginally increase to less negative values of *ca.* -4.7 ‰ at the top of the section (*Figure 5.3*). Highly negative δ^{18}O values in the range of -4.0 to -10‰ may be attributable to a late phase of diagenetic alteration, influenced by meteoric pore fluid interactions (Nelson & Smith, 1996), rather than seafloor diagenesis, which typically increases δ^{18}O values (Sexton *et al.*, 2006a). Despite the poor preservation of the bulk oxygen isotope signal, these still serve some utility as an index for the alteration of the sediment, and presumably the foraminiferal assemblages it hosts.

Bulk rock carbonate and grain size distribution may provide additional environmental information. The carbonate component of bulk rock samples increases from 0 to 5% at the base of the section to *ca.* 17% at the top of the section. This may reflect increased calcareous productivity (also corresponding with better preserved and more diverse foraminiferal faunal residues recovered up-section) or, more likely, a decrease in terrigenous sedimentation as suggested by mud content increasing from 7% to 58% up the section. The inverse of the percent mud implies a reduction in the supply of the coarse sediment fraction (>63 μm) to the depositional site, particularly in the upper Pukemuri Siltstone and the Wanstead Formation.
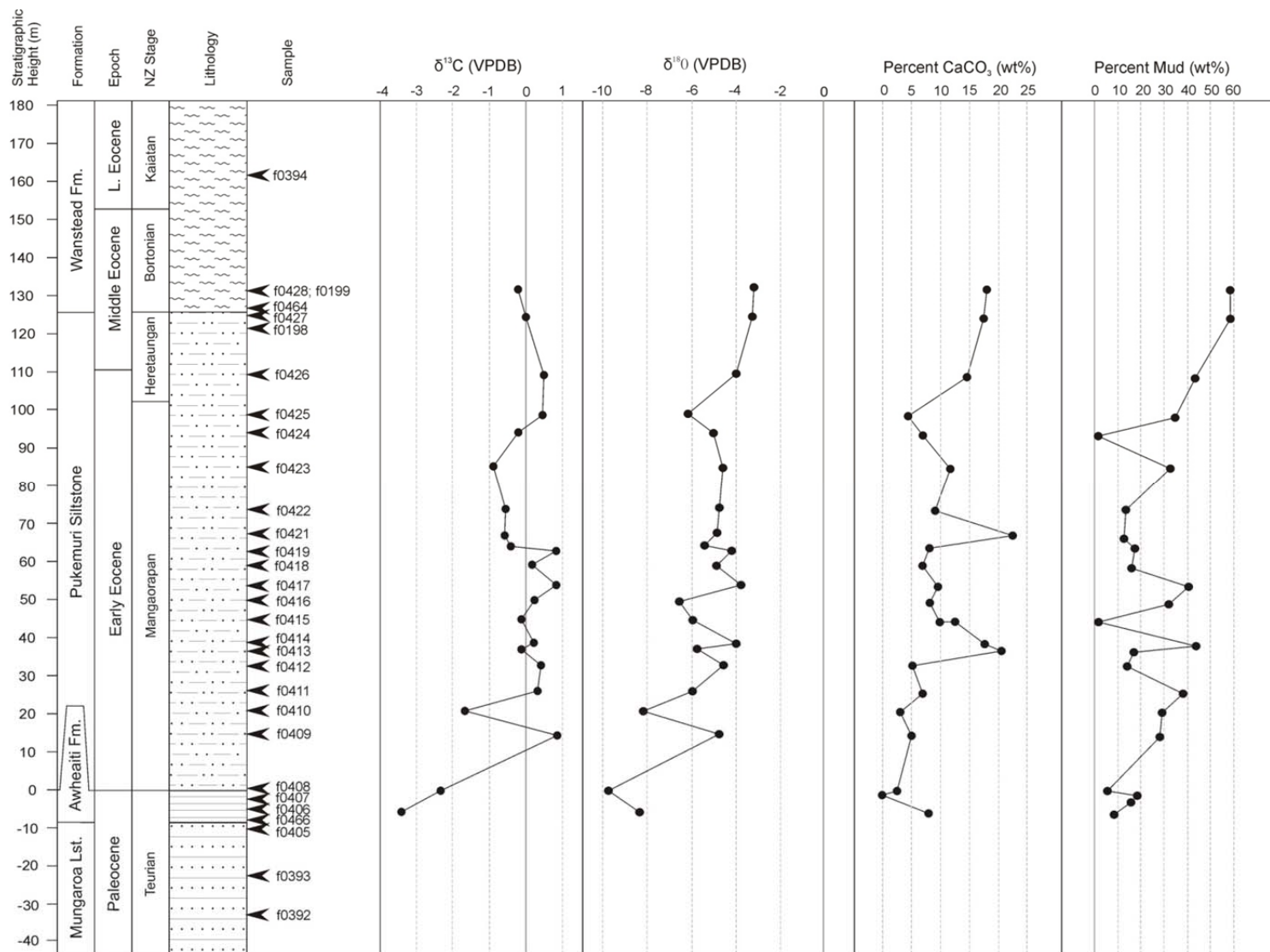
Figure 5.3: Bulk carbonate stable carbon and oxygen isotope stratigraphy, percent carbonate and percent mud from bulk rock analyses of samples from Pukemuri Stream, Tora.

5.4   Trace Element Data

Elemental ratios determined in this study are the result of multiple ablated holes in individual specimens of *Morozovella*, *Acarinina*, *Subbotina* and *Cibicides*. Each laser ablation site was individually selected and specifically targeted to avoid zones of detrital contamination, recrystallization or foraminiferal test ornamentation which may cause irregular trace element/Ca profiles (*Figure 5.4*). Specific zones within individual depth profiles are screened for the effects of diagenetic alteration or detrital contamination by the identification of anomalous Mg/Ca, Ti/Ca, Mn/Ca and Sr/Ca ratios.
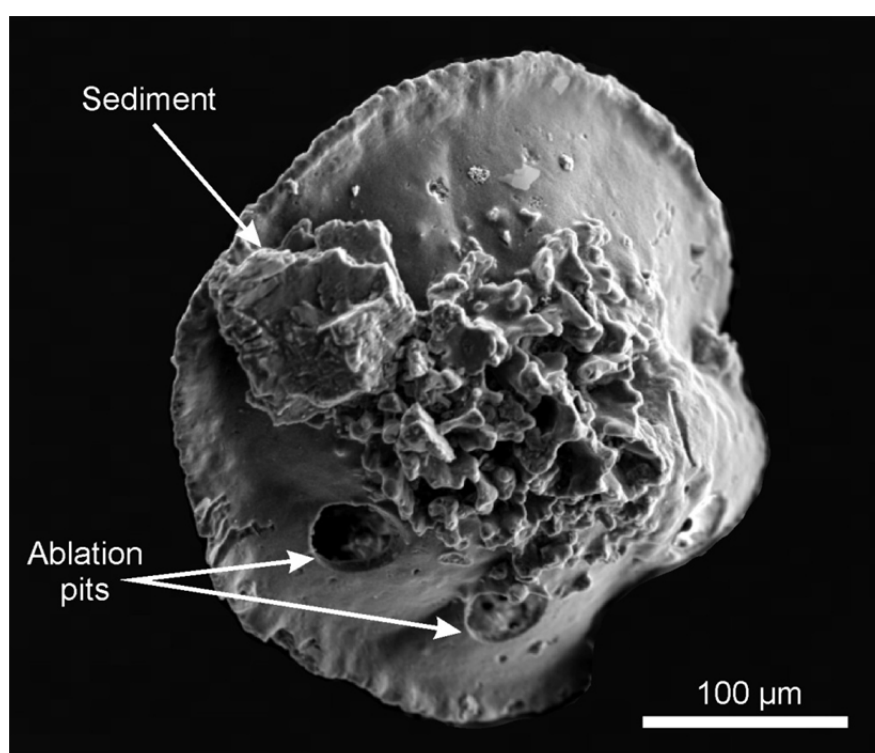
Figure 5.4: Example of a well-preserved *Cibicides truncatus* specimen from the Tawanui section (U24/f341), displaying how laser ablation sites were located to avoid silicate contaminants and surface ornamentation which may produce anomalous trace element/Ca values.

Mg/Ca ratios from foraminifera sourced from the lower to middle Pukemuri Siltstone range between 2.3 and 5.8 mmol/mol with the highest and lowest values generally attributable to *Cibicides* and *Morozovella* respectively. *Subbotina* typically occupy intermediate values between those of *Morozovella* and *Acarinina* and those from *Cibicides* (*Figure 5.5*). Mg/Ca values for all species decrease towards the top of the section, although there is a slight increase in *Subbotina* and *Cibicides* Mg/Ca values in sample f0427 in the uppermost Pukemuri Siltstone (*Figure 5.5*). Planktic

species generally produce lower Mg/Ca ratios, with *Morozovella* Mg/Ca values ranging from 2.6–3.7 mmol/mol, similar to those of *Acarinina* (2.4–4.4 mmol/mol). *Subbotina* display a similar, although slightly higher, range of Mg/Ca values from 3.1–4.4 mmol/mol. The benthic species *Cibicides* exhibit the greatest range of Mg/Ca values, from 2.9–5.8 mmol/mol. *Subbotina* Mg/Ca ratios in the Aropito and Tawanui sections are consistently lower than those of the other planktic species analysed in this study, and are generally also less than *Cibicides* Mg/Ca ratios (*Figure 5.6*).

Mg/Ca values in all species are highest within the Waipawan to Heretaunagan intervals in the Aropito and Tawanui sections, with the exception of *Cibicides* in sample f207 (*Figure 5.6*). Mg/Ca ratios from foraminifera in the Aropito and Tawanui sections are generally lower than those from Tora, with *Morozovella* and *Acarinina* in the range of 2.2–3.6 mmol/mol. *Subbotina* Mg/Ca values from Aropito and Tawanui are significantly lower than those recorded from Tora, ranging from 1.8–2.8 at Aropito-Tawanui, compared to 3.1–4.4 mmol/mol at Tora. Likewise, *Cibicides* Mg/Ca ratios from Aropito and Tawanui are lower than recorded at Tora, ranging from 2.0-3.8 mmol/mol.

Variable preservation of the benthic genus *Cibicides*, has less effect on the quality of the trace element data for this species than that of the planktic species studied. Even within the most diagenetically affected assemblages, a greater proportion of *Cibicides* passed the screening process in comparison to *Morozovella* and *Acarinina* specimens. *Subbotina* from the Aropito and Tawanui sections also displayed good preservation of primary trace element signals, with ≥ 75% of analyses passing screening for silicate contaminants and secondary alteration. In comparison, *Subbotina* trace element data from the Pukemuri section produced lower quality trace element/Ca profiles, with ≤ 25% of analyses passing screening. The remaining *Subbotina* analyses from the Pukemuri section that passed screening display elevated Mg/Ca ratios relative to corresponding *Acarinina* and *Morozovella* assemblages, and in comparison to coeval *Subbotina* specimens from the Aropito and Tawanui sections.

The typical inter-individual variance of Mg/Ca analyses within a sample is 50–60%, which is consistent with that of extant planktic foraminifera (e.g. Sadekov *et al.*, 2008). The observed variability may also be influenced by the varying degrees of preservation. Variably-preserved specimens, such as those sourced from the sections in this study, would likely induce additional scatter to the mean Mg/Ca values. Alternatively, pervasive recrystallization of foraminiferal calcite could result in a reduction of the inter-individual variance, as the precipitation of inorganic calcite might have re-equilibrated trace element/Ca values to some extent.

The lower inter-individual variability of *Subbotina* Mg/Ca values in Tora specimens (*ca.* 30%) is considerably lower than that of specimens sourced from the Aropito and Tawanui sections (*ca.* 60%) and modern *Globigerina bulloides* (50-60%; Marr *et al.*, 2011). This potentially provides further evidence for the pervasive alteration of *Subbotina* from the Pukemuri section, despite the retention of surface textures and apparent better physical preservation in comparison to corresponding *Acarinina* and *Morozovella*. Furthermore, Mg/Ca ratios derived from *Subbotina* analysed from the better-preserved assemblages at the Aropito and Tawanui sections exhibit greater variability than *Acarinina* and *Morozovella*, which is attributed to the non-specific selection of *Subbotina* taxa, which were not sub-divided to the species level as the other genera used in this study were.

Variability of screened Mg/Ca ratios in the benthic genus *Cibicides* is greater than that recorded in planktic *Acarinina* and *Morozovella* Mg/Ca values. As indicators of silicate contamination in *Cibicides* are not anomalous, this could relate to species-specific biological effects on the incorporation of Mg into calcite, or perhaps an environmental modulation of the Mg/Ca signal, in which variable Mg concentrations of surrounding sediments or subsurface pore waters have influenced the primary calcite benthic compositions.

Table 5.1: Screened trace element/Ca data for the foraminifera analysed in this study.

Species	Section	Sample Number	Strat. Height (m)	Age (Ma)	Mg/Ca	Ti/Ca	Mn/Ca	Zn/Ca	Sr/Ca	Ba/Ca	%2se Mg/Ca	95% C.I. (Mg/Ca)	Mg/Ca Variability (%)	Good	Total	Specimens Analysed
Morozovella	Aropito	f332	272	47.3	2.18	0.012	1.62	0.019	0.81	0.054	2.3	0.2	-	2	12	4
	Tawanui	f325	20.1	50.0	2.97	0.025	0.69	0.016	0.96	0.078	2.6	0.3	24.8	8	12	4
		f342	17.8	51.5	2.57	0.013	0.93	0.017	0.91	0.052	2.4	1.3	52.3	9	12	4
		f341	12.8	53.0	2.71	0.046	0.73	0.012	0.88	0.054	2.3	0.6	29.9	3	12	4
	Pukemuri	f0426	109.3	48.2	2.77	0.014	1.32	0.015	0.79	0.063	2.2	1.3	-	2	12	4
		f0421	67.3	50.3	3.12	0.018	1.46	0.014	0.86	0.042	2.6	1.4	64.1	4	12	4
		f0417	53.7	50.9	3.71	0.003	0.43	0.003	1.33	0.088	9.8	1.0	-	1	9	3
		f0416	49.4	51.1	2.60	0.020	0.92	0.013	1.23	0.031	1.7	0.4	-	2	9	3
		f0415	44.5	51.3	3.26	0.058	1.42	0.014	1.12	0.031	5.4	1.0	-	1	3	1
		f0412	32.7	51.8	3.29	0.012	1.35	0.020	0.95	0.025	2.3	0.4	-	3	3	1
		f0411	25.6	52.1	2.92	0.034	0.86	0.017	1.13	0.029	2.2	1.0	-	2	3	1
Acarinina	Aropito	f351	343	42.0	2.18	0.026	0.74	0.012	0.98	0.047	2.2	0.2	43.2	11	12	4
		f227	332	43.0	2.25	0.010	0.36	0.007	1.22	0.018	1.8	0.4	35.9	6	12	4
		f203	310	44.0	2.32	0.022	0.79	0.014	1.07	0.062	2.3	0.3	53.1	8	12	4
		f226	294	44.5	2.31	0.013	0.35	0.010	1.29	0.044	1.6	0.2	52.6	10	12	4
		f332	272	47.3	2.66	0.016	1.02	0.010	1.13	0.045	1.7	0.6	38.6	5	12	4
	Tawanui	f326	26.8	45.0	2.16	0.017	0.31	0.005	1.17	0.023	1.6	0.3	32.0	6	12	4
		f325	20.1	50.0	2.86	0.031	0.61	0.018	0.91	0.074	2.0	0.3	27.7	7	12	4
		f342	17.8	51.5	2.27	0.018	0.76	0.011	0.98	0.048	1.7	0.3	51.5	8	12	4
		f341	12.8	53.0	3.00	0.027	0.59	0.010	1.02	0.033	2.8	0.5	61.6	2	12	4
		f207	2.3	53.4	3.58	0.026	0.71	0.023	1.02	0.101	2.3	0.4	49.3	10	12	4
	Pukemuri	f0394	154	37.3	3.95	0.023	1.34	0.031	0.72	0.020	1.7	0.8	29.9	4	9	3
		f0428	132.1	41.9	2.92	0.014	1.22	0.020	0.96	0.057	1.8	1.3	-	2	9	3
		f0426	109.3	48.2	3.16	0.036	0.51	0.010	1.17	0.043	1.7	2.0	-	2	12	4
		f0419	62.4	50.5	4.11	0.008	0.21	0.005	1.40	0.024	1.9	1.0	-	3	12	4
		f0417	53.7	50.9	3.44	0.040	1.75	0.024	0.62	0.017	2.2	1.3	-	3	12	4
		f0416	49.4	51.1	4.43	0.005	0.76	0.009	1.41	0.080	1.7	1.0	-	1	12	4
		f0413	36.6	51.6	3.01	0.013	1.28	0.031	0.76	0.025	2.0	1.0	70.8	5	12	4
		f0412	32.7	51.8	3.10	0.050	1.14	0.011	0.95	0.023	1.7	0.3	27.5	12	12	4
		f0411	25.6	52.1	2.39	0.013	1.14	0.009	0.89	0.031	2.2	0.5	62.2	7	12	4
Subbotina	Aropito	f351	343	42.0	1.79	0.018	0.67	0.013	0.88	0.057	2.8	0.3	67.9	9	12	4
		f227	332	43.0	2.09	0.030	0.61	0.010	1.00	0.064	2.3	0.3	48.2	9	12	4
		f203	310	44.0	1.83	0.025	0.72	0.016	0.92	0.060	2.1	0.5	92.0	8	12	4
		f226	294	44.5	1.93	0.020	0.42	0.012	1.11	0.053	2.1	0.3	52.4	9	12	4
		f332	272	47.3	2.01	0.022	1.33	0.015	0.86	0.063	2.3	0.1	21.7	9	12	4
	Tawanui	f326	26.8	45.0	1.86	0.021	0.52	0.010	0.97	0.049	2.2	0.2	52.3	9	12	4
		f325	20.1	50.0	2.61	0.039	0.56	0.018	0.94	0.068	3.7	0.2	43.5	10	12	4
		f342	17.8	51.5	2.27	0.020	0.81	0.043	0.98	0.057	2.9	0.2	36.1	11	12	4
		f341	12.8	53.0	2.29	0.021	0.68	0.034	0.88	0.101	2.4	0.3	60.0	12	12	4
		f207	2.3	53.4	2.83	0.023	0.56	0.016	1.14	0.093	2.2	0.4	60.4	12	12	4
	Pukemuri	f0427	124.5	47.2	4.40	0.035	1.21	0.038	0.98	0.057	2.6	0.1	21.5	2	12	4
		f0426	109.3	48.2	3.52	0.039	0.58	0.012	1.33	0.074	2.6	1.5	34.2	3	12	4
		f0419	62.4	50.5	4.10	0.042	0.47	0.015	1.40	0.068	2.1	1.1	21.5	3	12	4
		f0415	44.5	51.3	3.82	0.028	0.25	0.047	1.11	0.054	1.5	2.0	-	2	12	4
		f0413	36.6	51.6	4.25	0.027	0.64	0.013	1.31	0.068	5.9	1.0	-	1	12	4
		f0411	25.6	52.1	3.09	0.025	1.14	0.016	0.99	0.035	2.5	0.3	33.4	8	12	4
		f0410	20.5	52.3	4.12	0.017	1.34	0.012	1.16	0.073	3.0	1.7	32.9	3	12	4
		f0407	-1	57.8	3.10	0.038	1.07	0.041	0.75	0.012	2.3	1.4	35.5	3	9	3
Cibicides	Aroptio	f351	343	42.0	3.14	0.005	0.74	0.059	1.09	0.053	2.5	0.3	17.5	6	6	2
		f227	332	43.0	2.25	0.036	0.73	0.053	0.93	0.041	2.5	1.7	58.9	3	6	2
		f203	310	44.0	2.12	0.020	0.62	0.039	0.90	0.072	3.2	0.4	37.0	5	6	2
		f226	294	44.5	2.55	0.016	0.99	0.025	0.74	0.069	2.4	0.4	66.8	11	12	4
		f332	272	47.3	3.08	0.024	1.66	0.024	0.75	0.062	2.8	0.7	56.9	6	9	3
	Tawanui	f326	26.8	45.0	2.00	0.026	0.89	0.024	0.74	0.046	2.1	0.3	48.3	7	12	4
		f325	20.1	50.0	3.87	0.022	0.27	0.040	1.08	0.051	1.8	0.5	64.9	12	12	4
		f342	17.8	51.1	3.51	0.016	0.76	0.032	1.01	0.049	1.8	0.3	27.3	11	12	4
		f341	12.8	53.0	3.54	0.022	0.51	0.021	1.10	0.060	3.0	0.7	50.7	7	12	4
		f207	2.3	53.4	2.51	0.022	1.02	0.031	0.79	0.083	2.9	0.5	95.6	11	12	4
	Pukemuri	f0428	132.1	41.9	2.91	0.029	0.90	0.035	1.01	0.101	5.4	1.0	-	1	9	3
		f0427	124.5	47.2	3.76	0.035	0.61	0.025	1.27	0.098	3.5	0.3	1.1	2	12	4
		f0426	109.3	48.2	3.20	0.020	0.72	0.017	1.13	0.111	3.8	0.9	59.3	6	9	3
		f0419	62.4	50.5	4.53	0.020	0.28	0.013	1.47	0.132	2.6	2.0	-	2	12	4
		f0416	49.4	51.1	4.77	0.017	0.71	0.013	1.30	0.107	2.9	0.6	34.4	7	12	4
		f0413	36.6	51.6	4.08	0.007	1.13	0.012	1.18	0.134	2.9	0.2	6.7	4	12	4
		f0411	25.6	52.1	5.80	0.027	0.30	0.012	1.58	0.095	5.4	0.5	18.2	6	9	3
		f0410	20.5	52.3	3.83	0.029	0.39	0.022	1.37	0.114	2.8	2.2	45.0	3	12	4
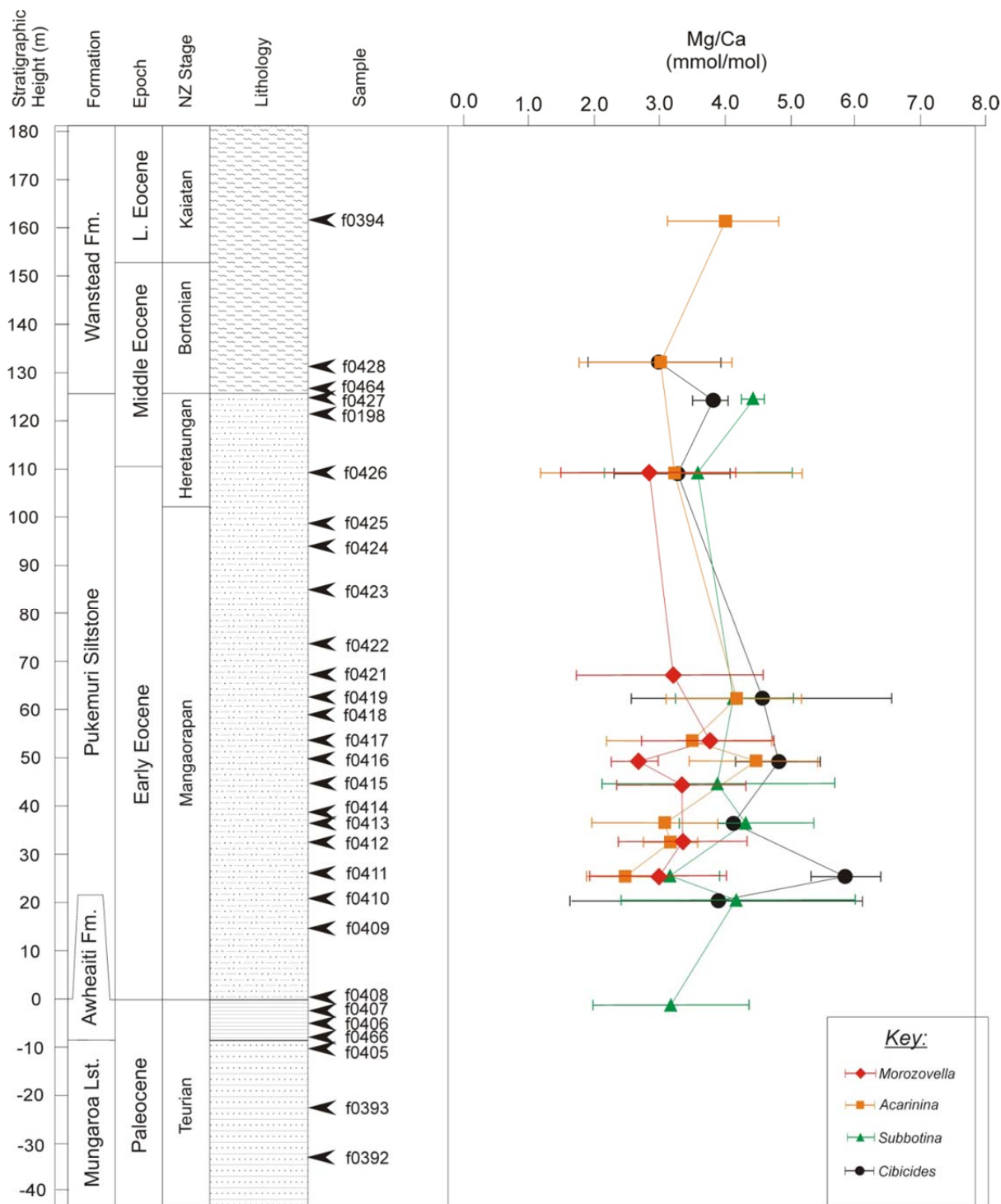
Figure 5.5: Foraminiferal Mg/Ca values plotted against stratigraphic height for the Pukemuri Stream section at Tora. Sample numbers with no corresponding Mg/Ca data represent samples that were analysed but did not pass the screening criteria used in this study. The error plotted is the 95% confidence interval on Mg/Ca analyses.
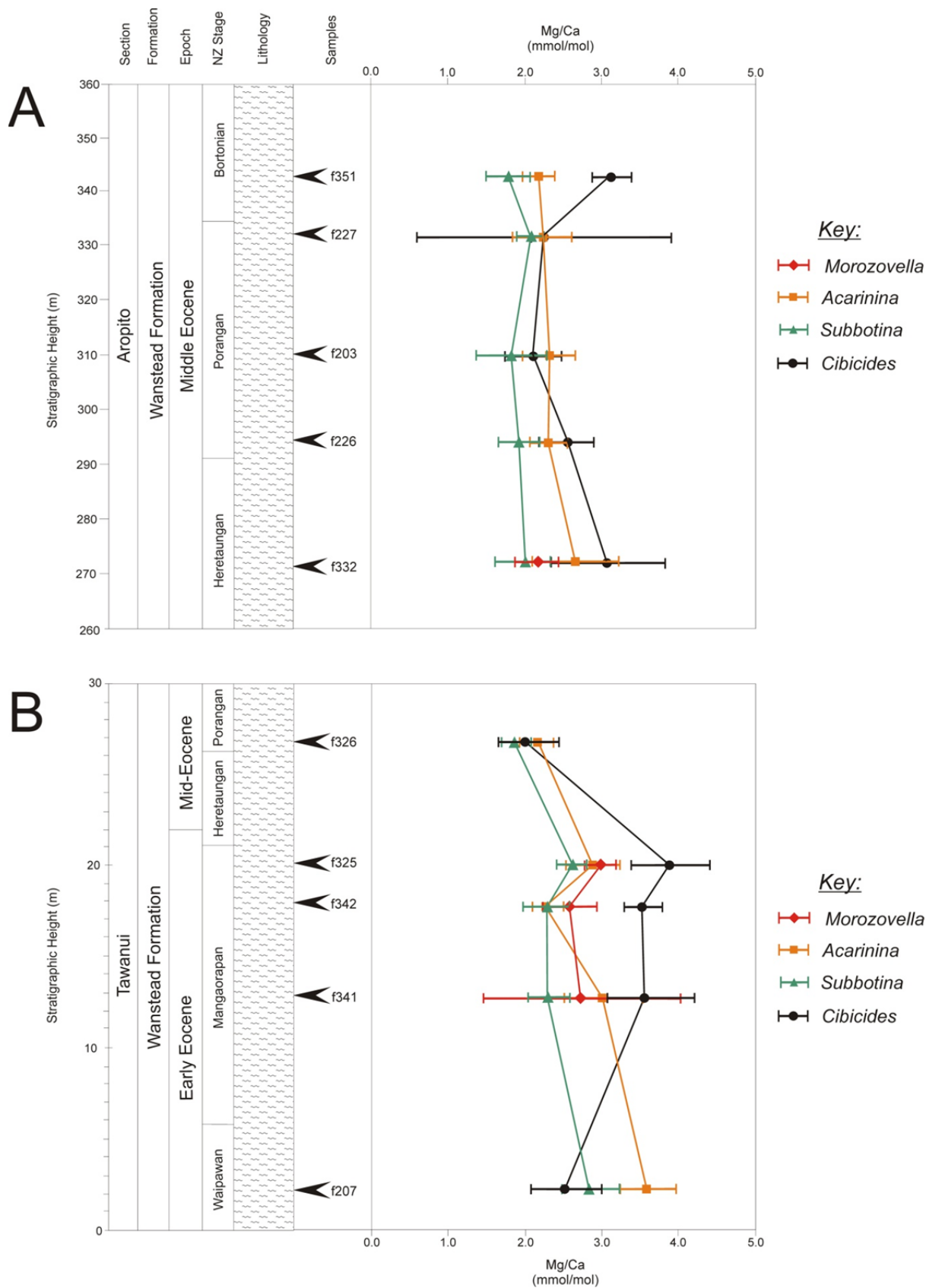
Figure 5.6: Foraminiferal Mg/Ca ratios potted against stratigraphic height for the Aropito (**A**) and Tawanui (**B**) sections in southern Hawke's Bay. The error plotted is the 95% confidence interval on Mg/Ca analyses.

5.5   Preservation of Primary Foraminiferal Calcite

The extraction of a reliable, robust paleoclimate record from variably preserved foraminifera is dependent on the preservation of primary foraminiferal calcite, and the inherent geochemical signature. Qualitative and quantitative methods have been applied to foraminiferal assemblages from the Aropito, Tawanui and Pukemuri Stream sections to ascertain the state of primary calcite preservation. For the purposes of comparison, SEM micrographs of foraminifera from this study are compared with images of foraminifera from the Hampden Beach section (*Figure 5.7*). Foraminifera sourced from the Early Eocene Kurinui Formation at Hampden Beach are widely recognised as yielding exceptionally well-preserved Eocene assemblages (Burgess *et al.*, 2008; Pearson & Burgess, 2008; Morgans, 2009).

Some specimens from the Aropito, Tawanui and Pukemuri Stream sections display evidence of extensive recrystallization, resulting in the loss or obscuring of surface textures and test wall structures (*Figure 5.7*). Such specimens are obvious when examined under reflected light microscopy and are clearly distinguishable using scanning electron microscopy. In addition to this, some specimens were observed to be infilled with secondary calcite, pyrite, sediment, calcareous nannofossils or a combination of these elements (*Figure 5.8*). Analyses from foraminifera that were found to be pervasively altered were removed from the final paleotemperature determinations of this study. Whilst the presence of recrystallized and secondary calcite is an issue for traditional $\delta^{18}O$ and solution Mg/Ca analytical methods, the laser ablation method employed in this study largely circumvents problems associated with variable preservation.

5.5.1   Physical Preservation of Foraminifera Tests

Visual inspection using reflected light microscopy and scanning electron microscopy (SEM) has shown that *Subbotina* and *Cibicides* specimens typically display better preservation than *Acarinina* or *Morozovella* in assemblages from the East Coast Basin sections. This may due to the physical surface texture inherent to particular genera. The growth of pronounced calcareous muricae on the test exterior by *Morozovella* and *Acarinina* species (*Figure 5.4*) creates a rugose surface texture which is more likely to ensnare clay particulates and resist their removal during the washing process, subsequently giving a coarse, grainy appearance in SEM images. It is also possible that these projections provide a greater surface area on the foraminifera test which is more likely to promote the development of secondary calcite overgrowths. In comparison, *Subbotina* have a

smoother surface, with less indented pores, which may explain the better physical preservation. *Cibicides* specimens are generally better preserved than corresponding planktic specimens, which is likely a function of the comparatively reduced size and abundance of pores in conjunction with a porcellaneous test surface, making it difficult for particulate matter to adhere to the test. The preservation of foraminiferal tests from the Aropito and Tawanui sample suites is better than that of the Tora specimens, regardless of species (*Figure 5.7*). However, older samples from the Mangaorapan-Heretaungan interval in the Aropito and Tawanui sections display poorer preservation of test surface features than foraminifera from higher in the stratigraphic succession. Foraminiferal preservation in the Pukemuri Stream section is quite variable, although preservation is marginally better in the lower to middle portion of the section. In this part of the section, pores, surface textures and ornamentation are distinguishable on foraminifera test surfaces and microgranular layering is preserved within test walls.

Qualitative estimates of the preservation of foraminiferal calcite using optical and SEM imaging methods are generally supported by trace element/Ca ratios from LA-ICP-MS analysis. The exception to this is *Subbotina* specimens recovered from the Pukemuri section. Although *Subbotina* from Tora typically give the appearance of being better preserved than *Morozovella*, *Acarinina* and *Cibicides* within the same sample, trace element profiles through the test wall have Mg/Ca, Ti/Ca, Mn/Ca and Sr/Ca values indicative of secondary alteration of the primary calcite. The screened Mg/Ca ratios of the majority of *Subbotina* from Tora display elevated Mg/Ca values above those of *Morozovella* and *Acarinina* (*Figure 5.7*). Based on the depth habitat of *Subbotina*, a lower (and consequently cooler) Mg/Ca ratio than *Acarinina* and *Morozovella* would be expected, such as that observed in the Aropito and Tawanui sections (*Figure 5.6*) and previous studies (e.g. Tripati & Elderfield, 2004). Therefore the high Mg/Ca ratios produced by moderately to poorly preserved specimens from Tora may be the result of pervasive alteration that is not apparent in the physical characteristics exhibited by the tests.
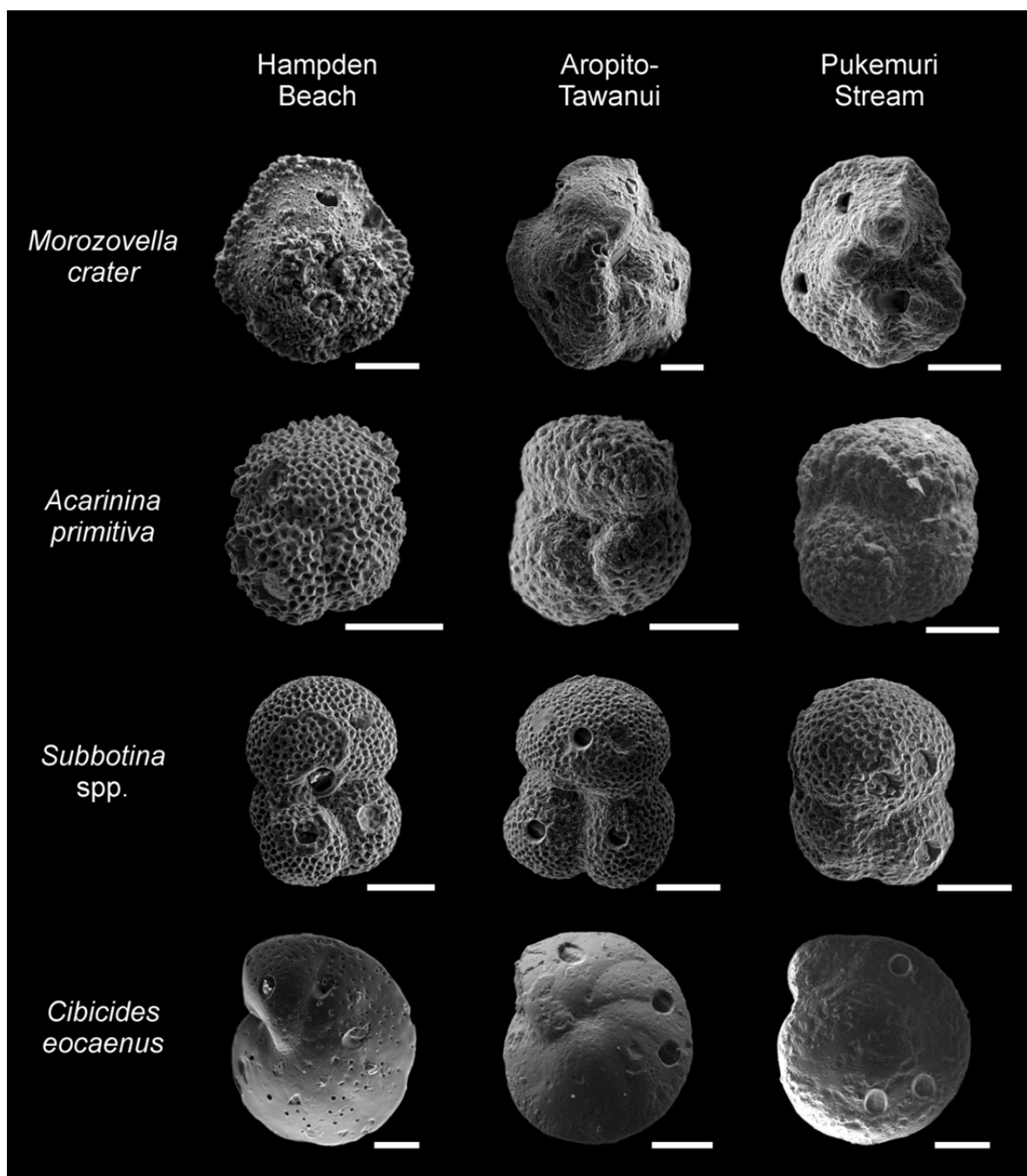
Figure 5.7: Representative examples of foraminifera species from the Wanstead Formation (Aropito–Tawanui sections) and the Pukemuri Siltstone (Pukemuri Stream section) used in this study for Mg/Ca paleothermometry, compared to well-preserved examples from the early Eocene Kurinui Formation at Hampden Beach. Scale bars are 100 μm in length.
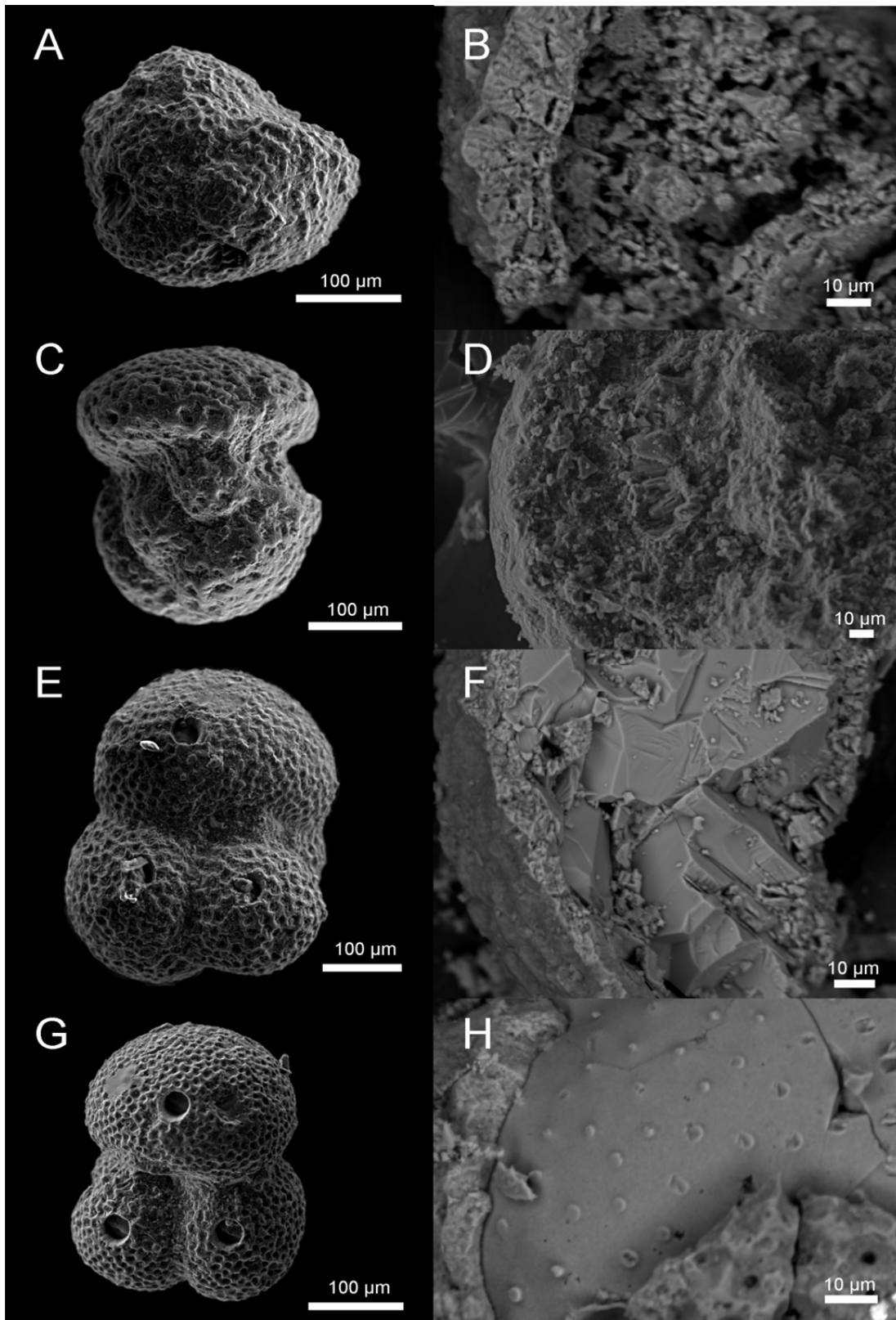
Figure 5.8: Examples of sediment and secondary calcite infilling *Acarinina* and *Subbotina*. **A**) Poorly preserved *Acarinina collactea* (PM112) **B**) internal examiniation primary structures present in test calcite and infilling sediment. **C**). *Acarinina topilensis* (U24/f332) crushed to reveal infilling sediment and small calcite prisms (**D**). **E**) *Subbotina* sp. (U24/f203) largely infilled with secondary calcite (**F**). **G**). *Subbotina linaperta* (U24/f207) with well-preserved surface texture entirely infilled with secondary calcite (**H**). Note the preserved casts of pores in the secondary calcite (**H**).

5.5.2 Element mapping

Visual inspection of foraminiferal tests obtained from the East Coast sections identified three common alteration types; infilling with calcareous (primarily nannofossils) and siliciclastic sediments, secondary calcite precipitation, and pyrite mineralisation within the test. Examples of foraminifera displaying these alteration states were individually selected, cross-sectioned and targeted for electron probe microanalysis (EPMA) element distribution mapping of key elements (Ca, Mg, Al, Si, Mn and Fe) to determine the effects that these alteration states have on the composition of primary foraminiferal calcite. A fourth alteration state, dissolution of primary foraminiferal calcite, was not frequently observed in the specimens from this study. The three alteration states typically observed in the foraminifera of this study are discussed in detail below.

Sediment Infilling

Infilling of foraminiferal tests with calcareous nannofossils and fine-grained sediments is a common feature of many of the foraminifera examined from the Aropito, Tawanui and Tora sections. This is a particular concern as silicate minerals are considerably enriched in Mg and depleted in Ca compared to foraminiferal calcite, consequently resulting in elevated Mg/Ca ratios that may erroneously increase temperature estimates if not identified. Several examples of sediment-infilled specimens were cross-sectioned and the distribution of key elements mapped using the EPMA method. A *Morozovella crater* specimen from the Tawanui section displays moderate preservation of the test exterior (*Figure 5.9a*), although cross-sectioning and imaging reveals the interior to be infilled with sediment and calcite rhombs $\leq 10\ \mu m$ in size (*Figure 5.9b*). Element mapping of Ca shows the preservation of primary structures such as pores and layering within the test wall. Mg concentrations are highest in areas of the test infilled with sediment, and characterise small voids within test calcite on both the interior and exterior of the test (*Figure 5.9d*). This is reflected in Mg/Ca ratios, which are significantly elevated in areas of infilling sediment (*Figure 5.9e*). Likewise, Mg/Ca values are elevated within preserved pores in the test wall, which has implications for LA-ICP-MS analysis.

Infilled sediment has high Al and Si values, reflected in the Al/Ca and Si/Ca ratios (*Figures 5.9 f, g, i*). Notably, Al and Si are not incorporated into the test wall, and are entirely excluded from zones of calcite. This was anticipated, as neither Al nor Si form a solid solution with minerals of the carbonate series.

Interestingly, both primary and secondary calcite are enriched in Mn compared with the infilling sediment (*Figure 5.9j*), although when ratioed to Ca, the Mn/Ca ratio of the sediment is significantly higher than that of calcite, as expected due to the high concentration of calcium in the calcite relative to that of the sediment (*Figure 5.9k*).

The concentration of Fe is greater than foraminiferal test calcite within both the infilling sediment and the secondary calcite (*Figure 5.9l, m*). An interesting feature of the Fe and Fe/Ca distribution is the outlining of laminae within the structure of the test wall (*Figure 5.9l, m*). This implies that Fe/Ca ratios may have an application not only in the identification of silicate contamination (e.g. Barker *et al.*, 2003), but also in the recognition of either compositional changes in primary calcite or zones of secondary calcification, a feature which could be potentially useful in the application of laser ablation studies to variably preserved foraminifera.
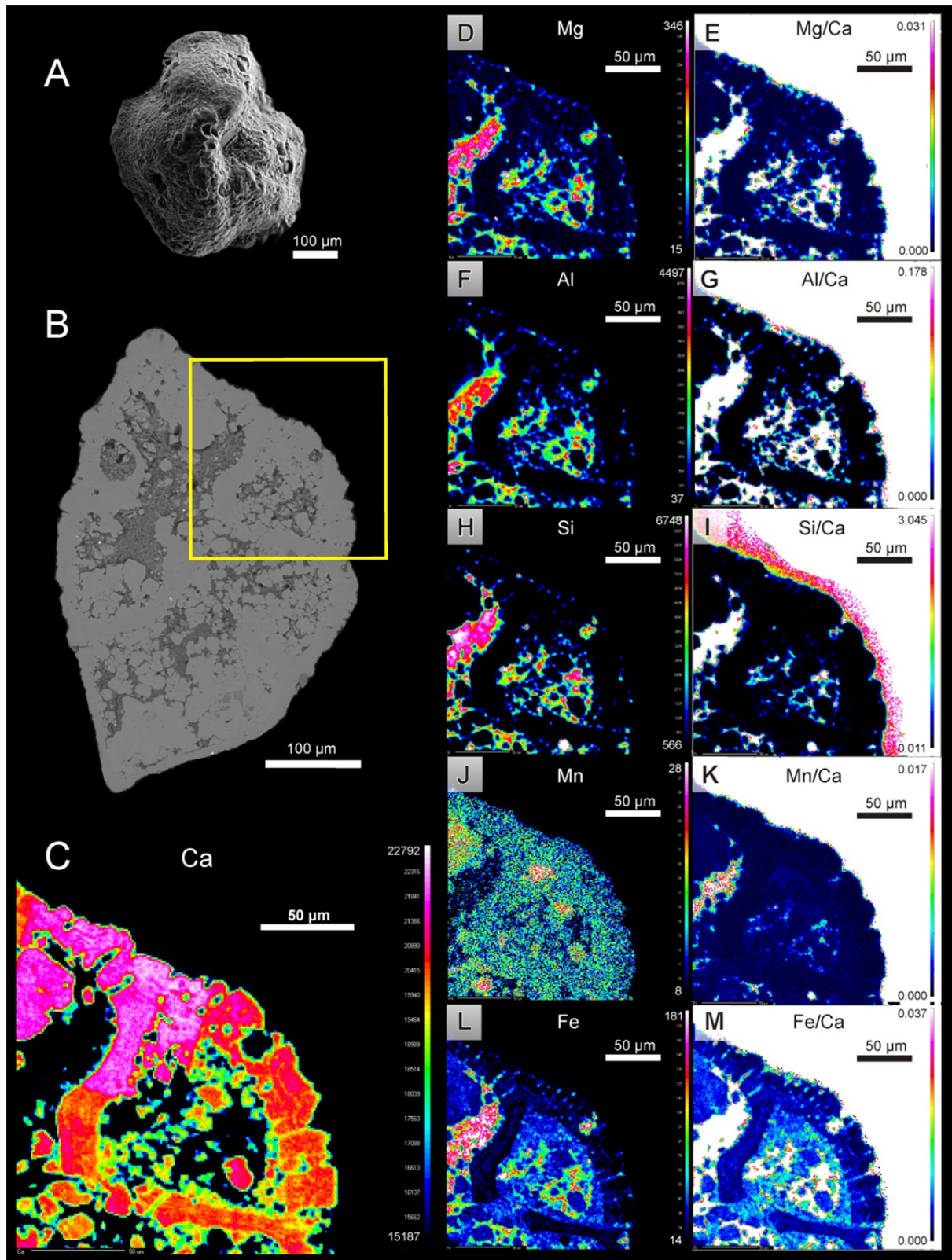
Figure 5.9: *Morozovella crater* from the early Eocene Tawanui section (sample U24/f325). **A**) Moderately well-preserved test exterior. **B**) Cross-section revealing infilling of chambers with sediment and secondary calcite, and showing the mapped area (yellow box). **C**). Distribution of Ca throughout the test. **D**) Mg distribution. **E**) Mg/Ca ratio. **F**). Distribution of Al. **G**) Al/Ca ratio. **H**) Si distribution. **I**) Si/Ca ratio. **J**) Distribution of Mn. **K**) Mn/Ca ratio. **L**) Distribution of Fe. **M**) Fe/Ca ratio. The colour scale for elemental distributions is in counts per second.

Secondary Calcite Precipitation

Infilling of complete foraminiferal tests with a secondary calcite phase is a relatively common feature of the thinner-walled planktic specimens, being more prevalent in *Subbotina*, and to a lesser extent, *Acarinina* and *Morozovella*. The benthic genus *Cibicides* was generally infilled with sediment, but rarely calcite.

An example of an *Acarinina primitiva* specimen infilled with secondary calcite was cross-sectioned and a portion of the test mapped for the distribution of a range of elements (Mg, Ca, Al, Si, Mn and Fe; *Figure 5.10*). The outward appearance of better preservation of test surface structures on calcite-infilled specimens was a frequently noted feature. Exterior examination of the selected *Acarinina* example suggests that it is moderately to well-preserved (*Figure 5.10a*), although examination of the cross-section displays near-complete infilling of chambers with secondary calcite. Minor pyrite is observed enclosed in a small (10 μm) void within the calcite in the final chamber, and the f-3 (third from last) chamber has been infilled with sediment prior to the precipitation of the secondary calcite enclosing the chamber (*Figure 5.10b*).

Element mapping shows a homogeneous distribution of Mg and Ca throughout the foraminifera and secondary calcite (*Figures 5.10c* & *d*), resulting in little to no variance in Mg/Ca ratios across the transition between calcite phases (*Figure 5.10e*). This is probably because the compositional changes between the different calcite phases is below the resolution of the EPMA method. Sediment infilling pores within the foraminiferal calcite is clearly defined by the distribution of both Al and Si and their respective ratios to calcium (*Figures 5.10f, g, h,* & *i*), with no Al or Si substituting into either the foraminiferal or secondary calcite phases. This confirms the established application of Al as an indicator of silicate contamination (e.g. Barker *et al.*, 2003), and suggests the potential application of Si for the same role.

Element maps of Mn and Mn/Ca display a noisy signal, characteristic of low concentrations. A vague increase in Mn/Ca ratios is apparent in the infilling secondary calcite, supporting the application of Mn/Ca ratios to identify zones of secondary calcification and recrystalisation (e.g. Eggins *et al.*, 2003). Siliclastic contamination within pores is also highlighted by Fe (*Figure 5.10l*), although to a lesser extent than Al and Si. The concentration of iron is particularly elevated in the secondary calcite relative to foraminiferal calcite and background counts (*Figure 5.10l*), a feature that is also reflected in Fe/Ca ratios (*Figure 5.10m*). This further suggests that Fe/Ca ratios may have a potential role in the identification of zones of secondary calcite in laser ablation Mg/Ca studies of biogenic calcite.
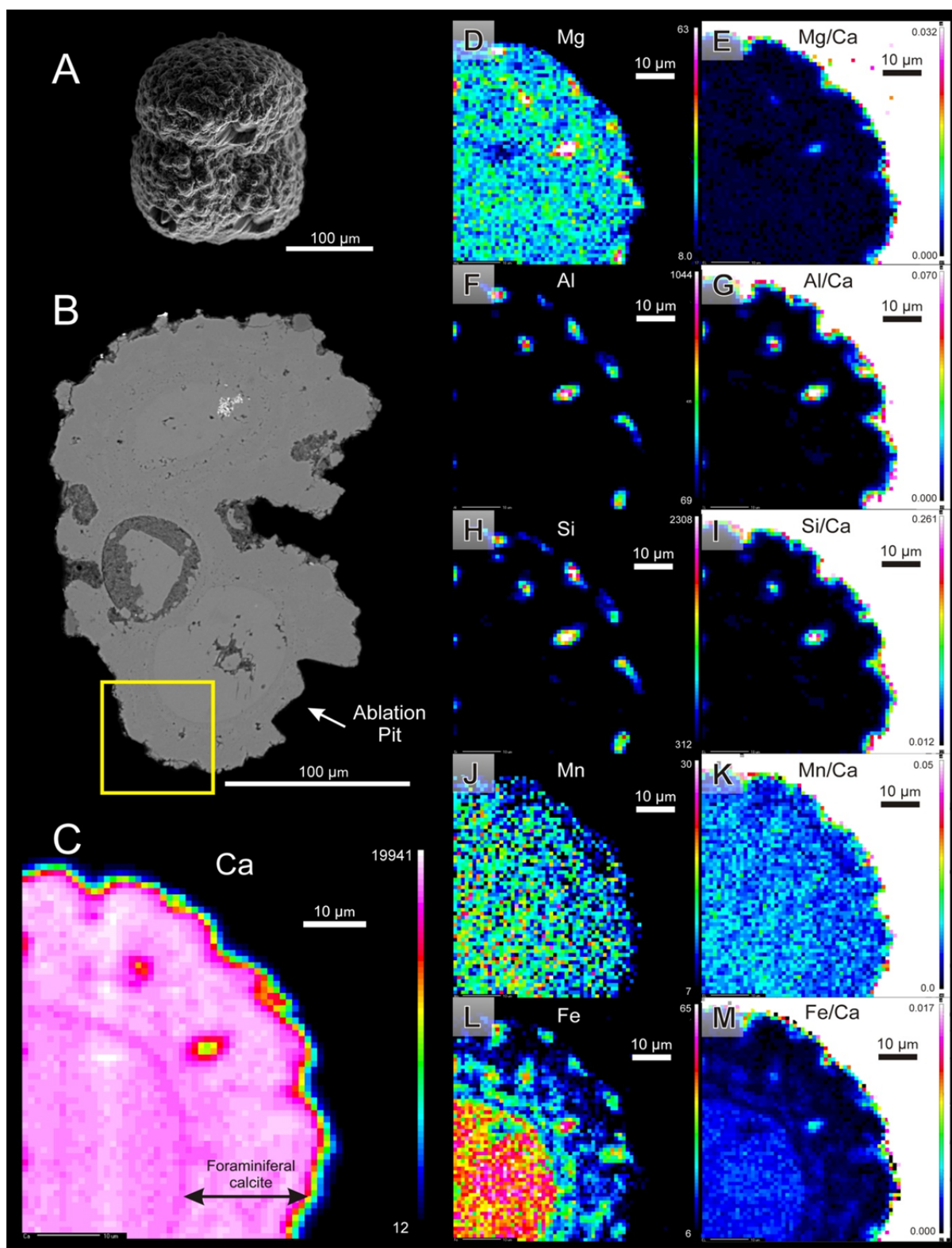
Figure 5.10: *Acarinina primitiva* from the early Eocene Tawanui section (U24/f207). **A)** Moderately well-preserved test exterior. **B)** Cross-section revealing infilling of chambers with secondary calcite throughout the test. Yellow box indicates mapped area. **C)** Distribution of Ca throughout the test. **D)** Mg distribution. **E)** Mg/Ca ratio. **F)**. Distribution of Al. **G)** Al/Ca ratio. **H)** Si distribution. **I)** Si/Ca ratio. **J)** Mn distribution. **K)** Mn/Ca ratio. **L)** Distribution of Fe. **M)** Fe/Ca ratio. The colour scale for elemental distributions is in counts per second. Pixilation is an artefact of the beam size resolution on the EPMA. Each pixel is 1 μm, the smallest beam size attainable.

Pyritisation

Pyrite mineralisation within foraminiferal tests is a frequently observed phenomenon, even in well-preserved specimens such as those from the Hampden section. Pyritisation of foraminiferal tests is a natural occurrence, resulting from a sulphide residue remaining from bacterial digestion of organic matter within the test following deposition in oxygen-depleted, reducing environments on the seafloor (Berner, 1984; Raiswell *et al.*, 1988). Examples of early Eocene foraminifera tests from the East Coast sections displaying pyritisation produced poor cross-sections; however, a good example of a pyritised *Cibicides porrodeliquatus* specimen from the Upper Miocene Mangaopari Mudstone in the Wairarapa, was produced in a parallel study (*Figure 5.11*; Hines, *unpublished data*), and is presented here in order to demonstrate the potential implications of pyrite mineralisation on Mg/Ca paleothermometry. The exterior of the test appears well-preserved, with pores clearly visible and no adhering sediment (*Figure 5.11a*). A cross-section of the same specimen (*Figure 5.11b*) reveals that although primary structures such as pores and calcite laminae are preserved within the test, there is an abundance of framboidal pyrite *ca.* 10 μm in diameter.

The corresponding element map of Ca (*Figure 5.11c*) provides a good indication of the distribution of foraminiferal calcite, and no secondary calcite is evident in or on the specimen. The abundance of pyrite mineralisation is reflected in the high density of the metals mapped (Mg, Al, Mn and particularly Fe; *Figures 5.11d* to *k*) associated with the secondary precipitation of pyrite. Precipitation of the pyrite phase results in Mg/Ca values that are substantially elevated above the Mg/Ca values of primary foraminiferal calcite. This is shown in *Figure 5.11e*, in which significantly higher Mg/Ca ratios are observed in the prytised areas relative to foraminiferal calcite.

Interestingly, Mn concentrations are significantly elevated above that of the surrounding pyrite at the centre of the test where the densest distribution of pyrite occurs. This may suggest that the pyrite at the centre of the test was precipitated at a different time compared to the remaining pyrite, under different conditions.

Elevated counts of aluminium are generally associated with silicate contamination, although in this example, Al and corresponding Al/Ca ratios are considerably higher in areas of pyrite mineralisation than background concentrations in foraminiferal calcite (*Figures 5.11f & g*). Al/Ca ratios vary between different areas of pyrite mineralisation, but in all cases are substantially elevated above that of foraminiferal calcite.

Elevated ratios of Mn, Mg, Al and Fe relative to Ca show that these all provide good indications of pyrite mineralisation, demonstrating that the silicate screening methods applied in this study will also identify and eliminate Mg/Ca values associated with pyrite mineralisation within the foraminifera test.

Pyrite does not substitute into the calcite matrix, although erroneous Mg/Ca ratios would be induced by its incorporation into paleotemperature measurements, either through the application of solution ICP-MS studies, or poor screening of trace element profiles. However, the significantly elevated trace element/Ca ratios in pyrite (demonstrated in *Figure 5.11*) means that the silicate screening measures applied in this study would remove any contamination arising from pyrite mineralisation, although the screening method would benefit from Fe/Ca screening in addition to the existing protocols.
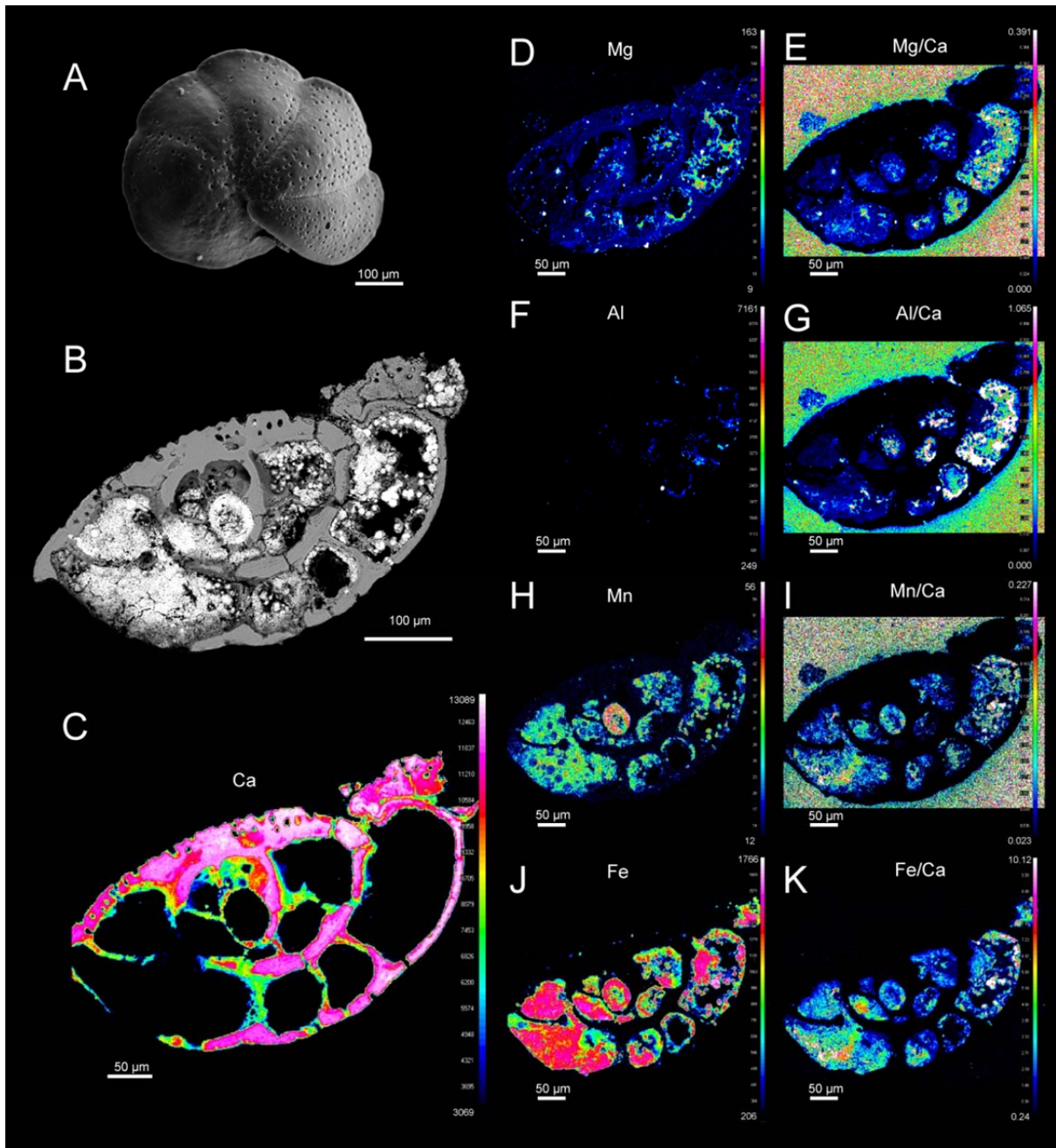
Figure 5.11: Example of *Cibicides porrodeliquatus* from the Upper Miocene Mangaopari Mudstone exhibiting framboidal pyrite mineralisation infilling chambers. **A**) Well-preserved test exterior. **B**) Cross-section revealing pyrite mineralisation within chambers throughout the test. **C**). Distribution of Ca throughout the test. **D**) Mg distribution. **E**) Mg/Ca ratio. **F**). Distribution of Al. **G**) Al/Ca ratio. **H**) Mn distribution. **I**) Mn/Ca ratio. **J**) Distribution of Fe. **K**) Fe/Ca ratio. The colour scale for elemental distributions is in counts per second.

5.5.3   Evaluation of Silicate Contamination Indicators

High concentrations of Mg incorporated within silicate mineral assemblages have the potential to artificially elevate Mg/Ca values, consequently resulting in overestimated, erroneous paleotemperature determinations. Screening of laser ablation analyses to remove the influences of silicate minerals was primarily based on the application of calculated Ti/Ca screening limits (Chapter Three). To assess the validity of titanium as a primary indicator of silicate contamination, Ti/Ca ratios were compared to Al/Ca ratios, which are widely applied in the screening of Mg/Ca analyses (e.g. Barker *et al.*, 2003; Greaves *et al.*, 2005; Creech *et al.*, 2010). EPMA element mapping indicated Si/Ca was comparable to Al/Ca ratios as an index for silicate contamination, and subsequently Si/Ca ratios were recorded in parallel with Al/Ca and Ti/Ca ratios during LA-ICP-MS analysis. EPMA element mapping of selected foraminifera specimens in a variety of alteration states showed that both Al and Si are particularly pronounced indicators of sedimentary contamination. Element mapping also showed that Al and Si do not substitute into foraminiferal calcite (at the sensitivity of the EPMA), unless the specimen has undergone extensive and pervasive alteration.

Al/Ca, Si/Ca and Ti/Ca ratios display a high degree of covariance in laser ablation trace element depth profiles (*Figure 5.12a, b, c, d & e*) which is consistent with their application as a primary index of silicate contamination. Ti/Ca ratios may prove to be especially sensitive to initial alteration of primary calcite as the substantial offset between Ti/Ca ratios in silicate minerals and values observed in foraminiferal calcite is greater than that of either Al/Ca or Si/Ca ratios. Thus, even trace contamination from silicate minerals is likely to cause amplification above that of the primary Ti/Ca signal (e.g. *Figures 5.12 b & c*).

Some Si/Ca profiles show that Si has a particularly poor distribution in foraminiferal calcite, with Si/Ca ratios phasing out in primary calcite, implying that Si is not particularly mobile within the calcite matrix (*Figure 5.12 f*). This may potentially imply that Si/Ca ratios may be less sensitive to the effects of subtle diagenetic alteration than either Al/Ca or Ti/Ca ratios. An issue with Ti/Ca ratios is that trace element/Ca ratios often approached detection limits of the Agilent 7500cs mass-spectrometer used in this study, consistent with observations of Ti/Ca ratios by Greaves *et al.* (2005).

An additional consideration that may have application in future work is that of Fe/Ca ratios as an indicator of both silicate mineral contamination, which has already been acknowledged by Barker *et al.* (2003), and also as an index for secondary calcite mineralisation as shown in EPMA

analysis. The distribution of Fe in foraminiferal calcite appears to give an indication of small-scale changes within test walls (e.g. *Figure 5.9*) and secondary alteration in the studied foraminifera. This supports the recommendations of Barker *et al.* (2003), who promoted the application of both Al/Ca and Fe/Ca ratios in the screening of Mg/Ca analyses. Micron-scale resolution in the Fe/Ca ratios of EPMA element distribution maps would suggest that application of Fe/Ca measurements to established laser ablation protocols may provide beneficial insights into intra-test compositional changes of foraminiferal calcite.

SEM imaging and EPMA element mapping also revealed details relating to the cleaning methods applied in the preparation of foraminifera for LA-ICP-MS analysis. SEM micrographs show that there is adhering sedimentary and calcareous nannofossil detritus on many specimens studied from the Aropito and Tawanui sections. Foraminifera from Hampden prepared using the same methods have significantly less adhering material and no infilling sediment (*Figure 5.7*), potentially suggesting the debris attached to the variably preserved East Coast specimens may be partially cemented in place. In addition, cross-sectioning, SEM imaging and EPMA element mapping of specimens sourced from the East Coast sections show sediment trapped deep within pores (*Figures 5.13 1A-1I*), particularly on the better preserved specimens, as the pores on poorly preserved examples have typically been sealed during secondary calcification. *Figures 5.13 1a-1i* clearly demonstrates the substantially elevated Mg/Ca, Al/Ca and Si/Ca ratios caused by in filling of pores with silicate sediments. When such pores are ablated, the infilling sediment is more resistant to laser pulses than the surrounding calcite (*Figure 5.13 2a*), although the corresponding trace element/Ca profiles display high values (*Figure 5.13 2b*) which are significantly above the calculated screening limits, providing reassurance that screening of Al/Ca, Si/Ca and Ti/Ca ratios removes any contaminated profiles.

Ablating siliclastic sediment within infilled pores during laser ablation analysis will result in elevated Mg/Ca values (*Figures 5.13 2a-2b*) leading to erroneously high paleotemperature estimations, showing the importance of silicate mineral screening limits and cleaning protocols. The application of multiple silicate screening criteria (e.g. Al/Ca, Si/Ca and Ti/Ca) and subsequent SEM imaging of laser ablation pits provides further reassurance that the primary foraminiferal calcite Mg/Ca signal is recorded.
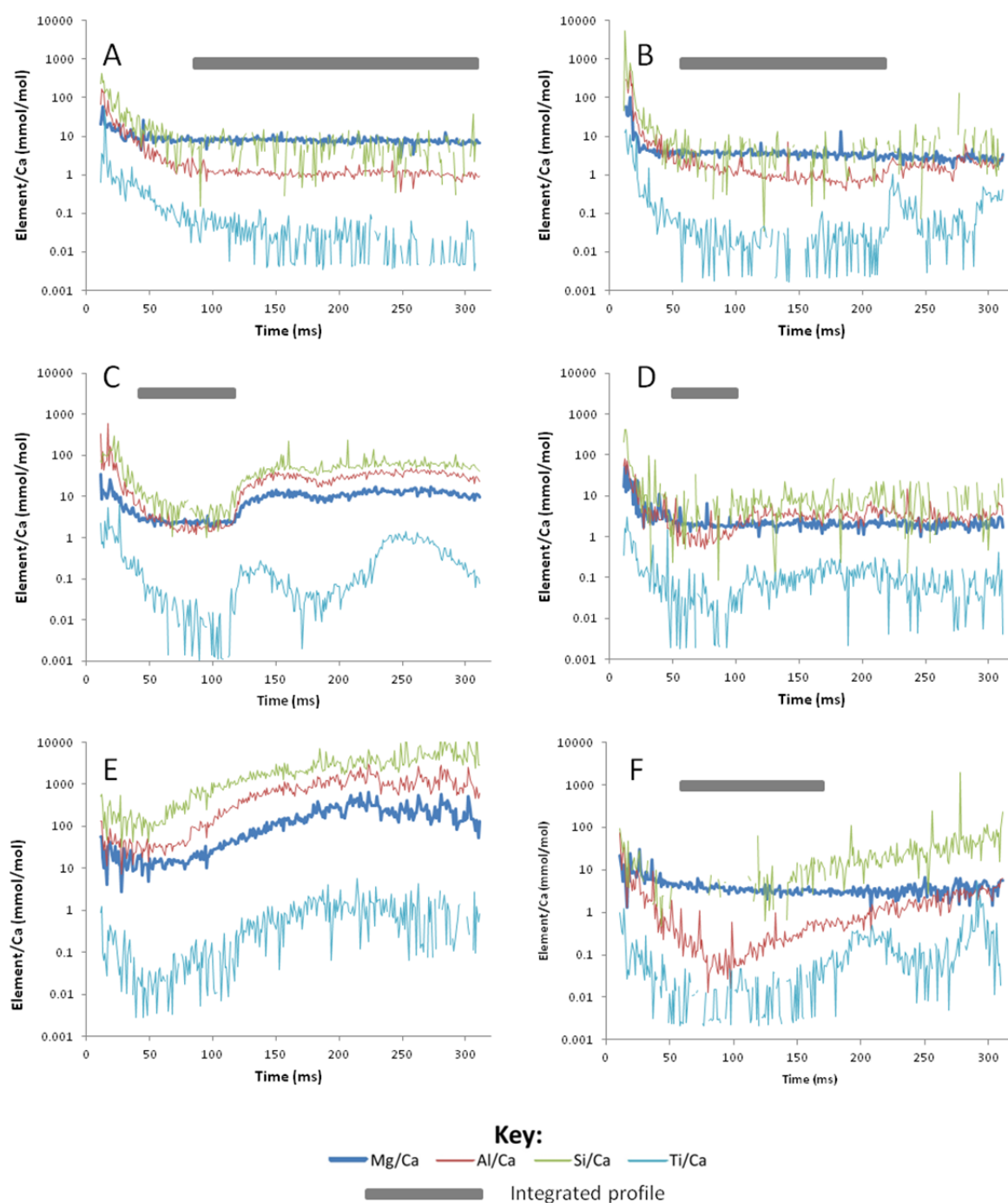
Figure 5.12: Trace element/Ca ratios in trace element depth profiles of foraminiferal calcite. **A**) Excellent, long profile. **B**) Typical shortened profile. **C**) Short, complex profile. **D**) Very short profile. **E**) Exaggerated trace element profile with high Mg/Ca, Al/Ca, Si/Ca and Ti/Ca indicating substantial silicate contamination. **F**) Si/Ca ratios phasing out, suggesting a poor distribution of Si in calcite.
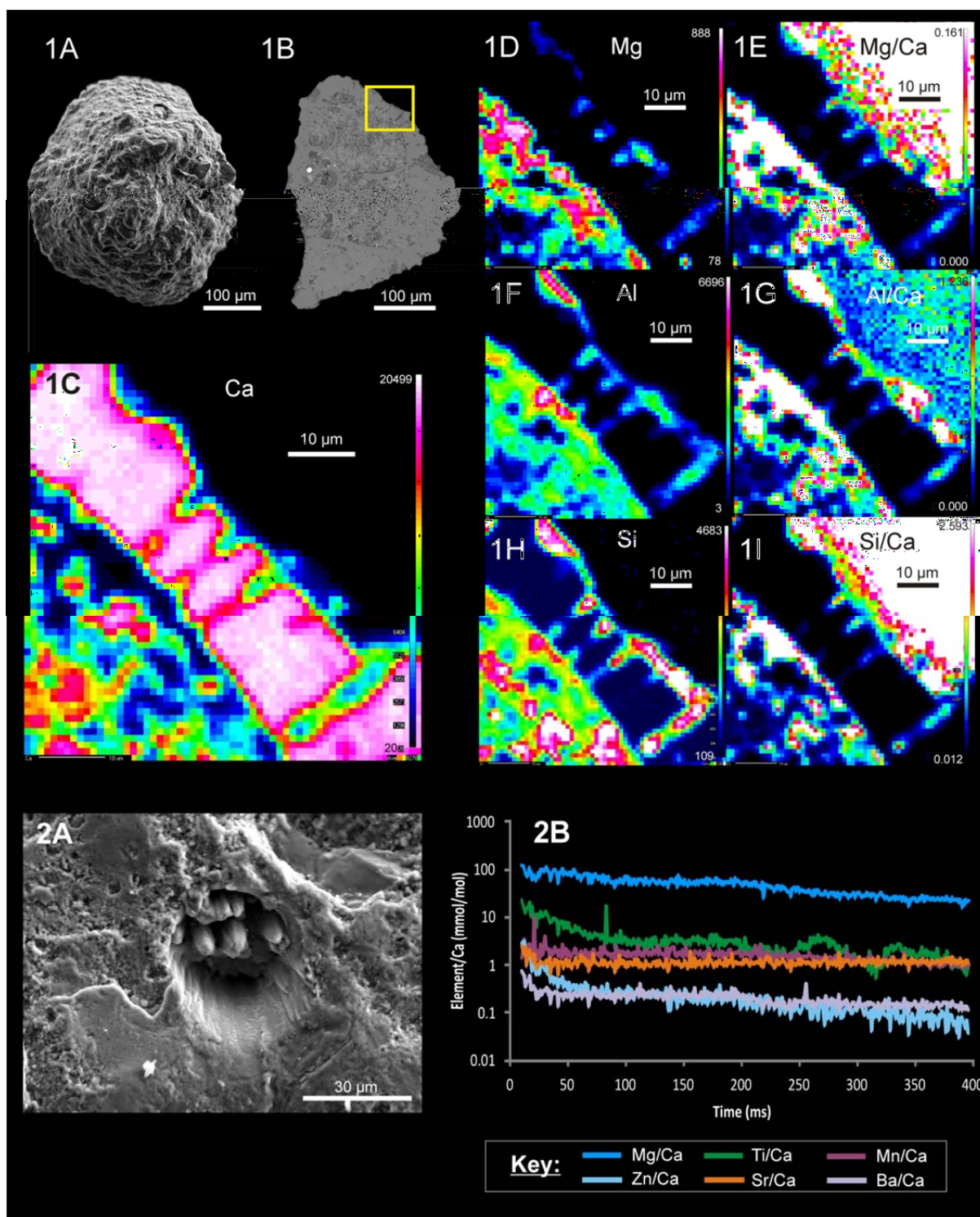
Figure 5.13: Examples of silicate sediments infilling pores. **1A**) Exterior SEM image of a *Morozovella crater* specimen. **1B**) Cross-section of the same foraminifera, displaying infilling sediment. The yellow box shows the mapped area. **1C**) Distribution of calcium in the mapped area, showing four pores in the test calcite. **1D**) distribution of Mg concentrations. **1E**) Mg/Ca ratio. **1F**) Distribution of Al concentrations. **1G**) Al/Ca ratio. **1H**) Distribution of Si concentrations. **1I**) Si/Ca ratio. **2A**) Example of an ablation pit in a *Cibicides* specimen, where detrital sediment infilling pores has proven more resistant than the surrounding calcite to laser pulses, resulting in pronounced projections in the ablation pit. The corresponding ablation profile (**2B**) displays markedly high element/Ca ratios.

5.5.4 Effects of diagenetic alteration on calcite

Secondary diagenetic processes may have the effect of altering the elemental composition of foraminiferal calcite. The different diagenetic processes (overgrowths, dissolution and recrystallisation; outlined in Chapter 2.7.3) each affect the composition of calcite in different manners. SEM images of foraminifera specimens displaying these various forms of alteration are displayed in *figure 5.14*, alongside a well-preserved specimen from the Kurinui Formation at Hampden Beach (*Figure 5.14a*).

Calcite overgrowths

Diagenetic overgrowths are formed by the precipitation of inorganic calcite on the exterior and interior surfaces of foraminiferal tests. Inorganic calcite precipitated from solution in seawater typically has significantly elevated trace element/Ca ratios, particularly Mg/Ca, Mn/Ca and Sr/Ca (e.g. Eggins *et al.*, 2003; Creech *et al.*, 2010). The quantitative and qualitative screening processes utilised in this study were specifically applied to remove any influence of inorganic calcite precipitation on the primary foraminiferal calcite composition. SEM imaging was utilised to identify zones of calcite overgrowths (*Figure 5.14b*), and subsequently remove LA-ICP-MS analyses within such zones from paleotemperature derivations. LA-ICP-MS ablation profiles were screened to remove zones of elevated trace element/Ca values occurring on the exterior and interior surfaces of the test.

Calcite dissolution

Dissolution of primary foraminiferal calcite appears to be a feature of many deep marine calcareous oozes, and considerably less of an issue in hemipelagic settings such as the East Coast and Canterbury Basins (e.g. Pearson *et al.*, 2001; Pearson & Burgess, 2008). Dissolution of biogenic calcite is readily apparent in the multivariate trace element/Ca plots utilised in the screening process as affected analyses produce significantly and consistently low trace element/Ca values for each element analysed. The application of SEM imaging also enables the identification of physical changes to the test structure in order to identify the occurrence or extent of dissolution (*Figure 5.14c*).

Calcite Recrystallisation

Recrystallisation of primary calcite is a less obvious process, whereby the original microcrystalline calcite structure of the foraminiferal test is replaced with larger, more equant crystals (*Figure 5.14d*), which may retain the original trace element composition or a hybrid trace element composition of the original calcite and secondary inorganic calcite (e.g. Sexton *et al.*, 2006a). The ratios of Mg/Ca, Mn/Ca and Sr/Ca form key indices for the identification of recrystallisation, with affected profiles displaying elevated ratios for these trace elements. Mn/Ca ratios appear to be a good index for subtle changes, whilst Sr/Ca ratios appear to only identify substantial alteration of the primary foraminiferal calcite. Pervasively altered foraminifera will produce flat trace element/Ca profiles lacking the characteristic 'U-shape' of well-preserved tests.
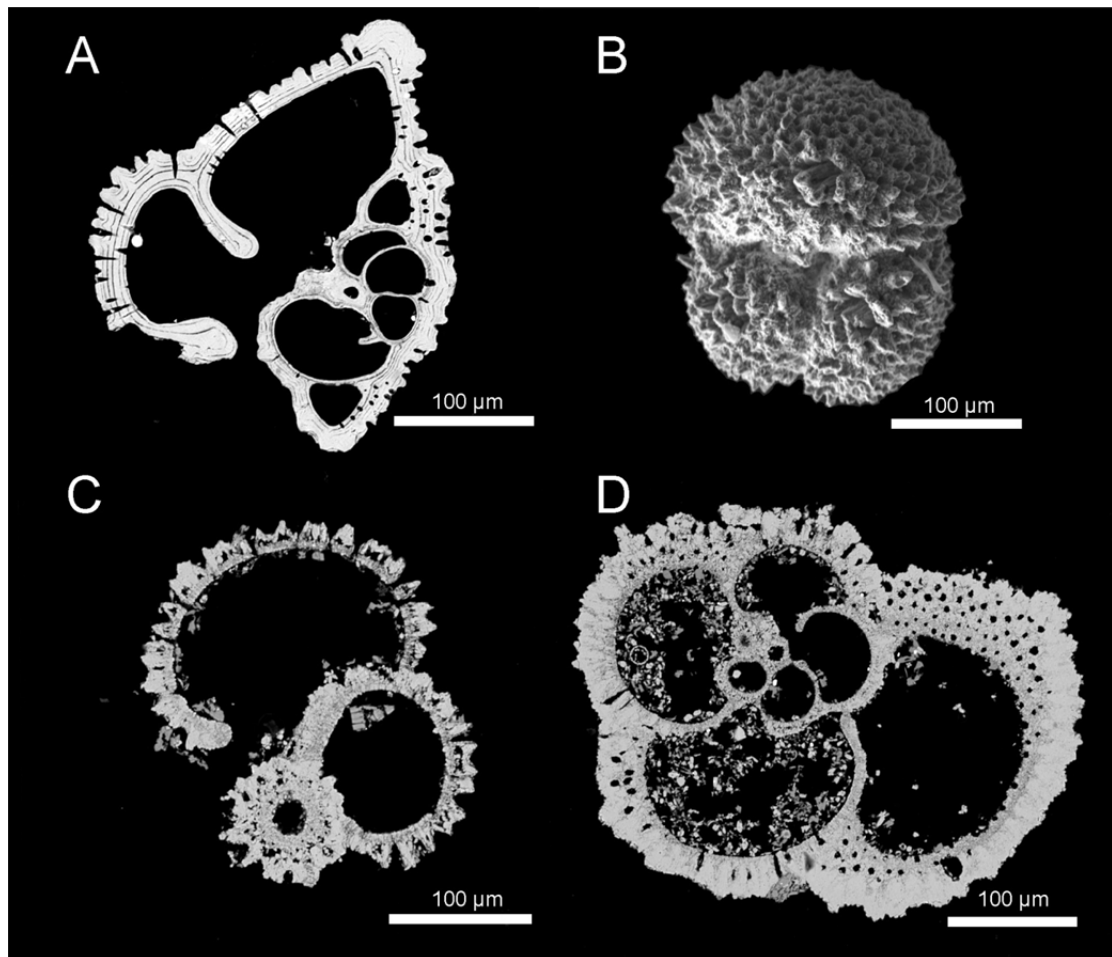
Figure 5.14: Examples of differing types of alteration affecting Early Eocene planktic foraminiferal tests. **A**) Cross-section of a well-preserved *Morozovella* test from Hampden Beach, displaying primary layering and test calcite. **B**) Example of an *Acarinina* from DSDP 277 displaying pronounced secondary calcite overgrowths of the exterior of the test. **C**) Cross-section of a *Subbotina* specimen from DSDP 277 showing large cavities when primary calcite has been preferentially dissolved. **D**) Cross-section of a *Morozovella* from DSDP 277 displaying a granular test wall structure indicative of recrystallisation. Images sourced from Hines, *unpublished data.*

5.6   East Coast Basin Sea Temperature Record

Four genera were selected for Mg/Ca paleothermometry in this study. *Morozovella* and *Acarinina* inhabited a surface mixed-layer habitat (upper 200 m; Pearson *et al.*, 2006; Wade *et al.*, 2008) and are used to provide Mg/Ca ratios for estimates of sea surface temperatures (SSTs). Bottom water temperature (BWT) estimates are based on Mg/Ca ratios from the benthic genus *Cibicides*. Mg/Ca ratios from the thermocline dwelling planktic genus *Subbotina* were also analysed in this study, providing a useful insight into thermocline temperatures. As previously discussed, stringent screening criteria were developed and applied to trace element profiles produced by this study in order to remove the any effects of post-depositional diagenesis and silicate contamination. Calculated temperature estimates are based on screened Mg/Ca values averaged from multiple ablations across the final three chambers of several individuals from a given species within a sample. Despite the specific targeting of laser ablation sites, subsequent application of screening criteria and qualitative assessment based on SEM imaging resulted in the vast majority (*ca.* 80%) of trace element/Ca analyses being excluded from sea temperature derivations.

Intra- and inter-species variability in Mg/Ca ratios provides confidence in the preservation of a primary climate signal, as pervasive recrystallization of foraminiferal calcite would have resulted in a homogenous distribution of Mg/Ca values obtained from an assemblage. Because consistent variation between the Mg/Ca ratios of different species can be observed in the raw data, the primary biological signal is believed to be still preserved.

Paleotemperature estimates derived from Mg/Ca paleothermometry are calculated using a high value for Eocene seawater Mg/Ca concentrations (4.1 mol/mol; refer to Chapters 2 & 3). This consequently has the effect of lowering estimated sea temperature values. The Eocene seawater value used in this study is higher than that suggested by several proxy studies (e.g. Dickson, 2004; Horita *et al.*, 2004; Coggon *et al.*, 2010) and models (e.g. Stanley & Hardie, 1998), but is in line with estimates suggested by paired Mg/Ca and $\delta^{18}O$ values for foraminiferal calcite (Lear *et al.*, 2002; Sexton *et al.*, 2006a) and modelled values from Wilkinson & Algeo (1989). A multi-proxy comparison of paleotemperature records from the Canterbury Basin (Hollis *et al.*, 2012) displayed good agreement between a high Eocene seawater Mg/Ca value (4.0 mol/mol) and TEX_{86} and $\delta^{18}O$ temperature proxies. Paleotemperatures are calculated as outlined in Chapters 2.6, 2.7 and 3.7.

For the purposes of temperature calculations, a static Mg/Ca seawater ratio has been assumed throughout the composite record produced for the East Coast Basin, as the temperature record of this study spans a period of *ca.* 13 Myr, which is approximately equal to the Mg/Ca residency time of the ocean (Broeker & Peng, 1982). However, most model and proxy records suggest that Mg/Ca$_{sw}$ may have increased by 30% through the period occupied by the paleoclimate record of this study (e.g. Wilkinson & Algeo, 1989; Hardie, 1996; Lowenstein *et al.*, 2001). If this is the case, this would mean that the reported temperatures of the middle Eocene portion of this record are too warm, and the observed cooling trend is even more marked than that displayed in *Figure 5.12*. Whilst an increase in seawater Mg/Ca values during the Eocene may not be as pronounced using the high value of 4.1 mol/mol, it is recognised that over the duration of the paleotemperature record presented in this study, and the residency time of Mg/Ca in the ocean reservoir, there were likely secular changes in the seawater Mg/Ca chemistry. As the majority of records indicate an increasing trend in seawater Mg/Ca values throughout the Cenozoic, this may translate into a more marked temperature decrease in the latter portion of the record. The combination of these factors result in the reporting of a conservative paleotemperature record for the East Coast Basin.

An additional consideration that may affect calculated paleotemperatures is changes in the partitioning coefficient of magnesium (e.g. Coggon *et al.*, 2010) into biogenic calcite and role of biological and physiological effects (e.g. Bentov & Erez, 2005; Segev & Erez, 2006) in foraminiferal Mg/Ca. However, as the species utilised by this study are extinct, these variable cannot be reliably quantified, and it is assumed that partitioning coefficients determined from modern foraminifera are appropriate (after Tripati *et al.*, 2009; Coggon *et al.*, 2010). In order to minimise any influence this may have, the particular species have been consistently analysed throughout the record, and modern, multi-species calibrations (Anand *et al.*, 2003; Lear *et al.*, 2002) applied to foraminiferal Mg/Ca ratios to calculate temperatures.

5.6.1   Sea Surface Temperatures

A smoothed sea surface temperature (SST) record was calculated from the weighted means of *Acarinina* and *Morozovella*. Sea surface temperatures reach a maximum of 29°C at 51 Ma before declining to 22°C at 45 Ma (*Figure 4.15*). Temperature values calculated from *Acarinina* are generally 1-2°C cooler than those of *Morozovella*, consistent with the 0.7–2.6°C offset between *M. crater* and *A. primitiva* reported by Creech *et al.* (2010). This suggests either a genus-specific control over the incorporation of Mg in foraminiferal calcite of these two taxa, or alternatively, a

seasonal or depth-controlled difference in test precipitation between genera. Despite this apparent systematic offset, temperature estimates derived from *Morozovella* and *Acarinina* correlate well throughout the record. The majority of the middle Eocene temperature record is based on temperature estimates derived from *Acarinina*, as the morozovellids utilised in this study (*M. crater* and *M. lensiformis*) do not extend beyond the early Middle Eocene (Heretaungan, 49.3-45.3 Ma).

5.6.2   Bottom Water Temperatures

Paleodepths are an important consideration for comparison between records derived from benthic foraminifera. Benthic foraminiferal paleodepth indicators imply a 500–1000 m water depth for the Wanstead Formation at Aropito and Tawanui (Moore & Morgans, 1987; Kaiho *et al.*, 1993, 1996), equivalent to that of early Eocene benthic foraminifera assemblages from Tora, with an estimated paleodepth of 800 m for the Pukemuri Siltstone in the Pukemuri Stream section. Therefore, paleodepths of the Wanstead Formation in the southern Hawke's Bay and the early Eocene Pukemuri Siltstone at Tora are considered comparable, and correspond with intermediate water (600–1450 m water depth; Carter *et al.*, 1996). The bottom water temperature record (BWT) is solely based on analysis of *Cibicides*.

The BWT record displays similar trends to the SST record, but offset to lower temperatures, as expected. BWT reached a peak of 19°C at 52 Ma and remained around 17°C until 50 Ma before declining to 10°C at 45 Ma (*Figure 5.15*). Following this, there is a slight increase of 4°C in BWTs between 45 to 42 Ma, which corresponds with a smaller warming of SSTs by *ca.* 1.5–2.0°C.

Paleodepths increase considerably between Pukemuri Siltstone and the Wanstead Formation in the Pukemuri Stream section. However, the agreement between temperatures from the middle Eocene Wanstead Formation at Tora and the coeval, but shallower Aropito and Tawanui sections implies that the same water mass was influencing temperatures at these sites over a significant water depth range.

Table 5.2: Mg/Ca paleotemperature and error calculations for the Aropito, Tawanui and Pukemuri Stream sections. Two methods of error calculation are presented; the 95% confidence interval typically applied to Mg/Ca analyses, and the modelled temperature variance.

Species	Section	Sample Number	Strat. Height (m)	Age (Ma)	Analyses Good	Analyses Total	Specimens available	Mg/Ca (mmol/mol)	%2se Mg/Ca	Temperature (°C)	2σ (°C)	95% C.I.	n	Inter-Individual Variability (%)	Modelled %2se Mg/Ca	Temp Errors +	Temp Errors -
Morozovella	Aropito	f332	272	47.3	2	12	4	2.18	2.3	22.0	0.6	**2.90**	1	-	53.9	**4.8**	**8.6**
	Tawanui	f325	20.1	50.0	8	12	4	2.97	2.6	25.5	2.0	**0.86**	3	24.8	18.1	**1.8**	**2.2**
		f342	17.8	51.5	9	12	4	2.57	2.4	23.9	3.3	**1.25**	4	52.3	13.6	**1.4**	**1.6**
		f341	12.8	53.0	3	12	4	2.71	2.3	24.5	4.1	**5.10**	2	29.9	27.1	**2.7**	**3.5**
	Pukemuri	f0426	109.3	48.2	2	12	4	2.77	2.2	24.7	1.1	**5.13**	1	-	53.9	**4.8**	**8.6**
		f0421	67.3	50.3	4	12	4	3.12	2.6	26.0	6.2	**4.92**	2	64.1	27.1	**2.7**	**3.5**
		f0417	53.7	50.9	1	9	3	3.71	9.8	28.0	0.0	**6.00**	1	-	53.9	**4.8**	**8.6**
		f0416	49.4	51.1	2	9	3	2.60	1.7	24.0	0.3	**1.51**	1	-	53.9	**4.8**	**8.6**
		f0415	44.5	51.3	1	3	1	3.26	5.4	26.5	0.0	**6.00**	1	-	53.9	**4.8**	**8.6**
		f0412	32.7	51.8	3	3	1	3.29	2.3	26.6	1.1	**1.32**	1	-	53.9	**4.8**	**8.6**
		f0411	25.6	52.1	2	3	1	2.92	2.2	25.3	3.3	**14.87**	1	-	53.9	**4.8**	**8.6**
Acarinina	Aropito	f351	343	42.0	11	12	4	2.18	2.2	22.1	3.2	**1.09**	4	43.2	13.6	**1.4**	**1.6**
		f227	332	43.0	6	12	4	2.25	1.8	22.4	3.4	**1.76**	3	35.9	18.1	**1.8**	**2.2**
		f203	310	44.0	8	12	4	2.32	2.3	22.8	3.9	**1.64**	3	53.1	18.1	**1.8**	**2.2**
		f226	294	44.5	10	12	4	2.31	1.6	22.7	3.1	**1.10**	4	52.6	13.6	**1.4**	**1.6**
		f332	272	47.3	5	12	4	2.66	1.7	24.3	3.8	**2.33**	3	38.6	18.1	**1.8**	**2.2**
	Tawanui	f326	26.8	45.0	6	12	4	2.16	1.6	22.0	2.5	**1.33**	4	32.0	13.6	**1.4**	**1.6**
		f325	20.1	50.0	7	12	4	2.86	2.0	25.1	2.4	**1.11**	4	27.7	13.6	**1.4**	**1.6**
		f342	17.8	51.5	8	12	4	2.27	1.7	22.5	3.5	**1.47**	3	51.5	18.1	**1.8**	**2.2**
		f341	12.8	53.0	2	12	4	3.00	2.8	25.6	10.0	**44.92**	2	61.6	27.1	**2.7**	**3.5**
		f207	2.3	53.4	10	12	4	3.58	2.3	27.6	3.2	**1.14**	4	49.3	13.6	**1.4**	**1.6**
	Pukemuri	f0394	154	37.3	4	9	3	3.95	1.7	28.7	3.0	**2.40**	2	29.9	27.1	**2.7**	**3.5**
		f0428	132.1	41.9	2	9	3	2.92	1.8	25.3	5.7	**25.67**	1	-	53.9	**4.8**	**8.6**
		f0426	109.3	48.2	2	12	4	3.16	1.7	26.2	6.8	**30.61**	1	-	53.9	**4.8**	**8.6**
		f0419	62.4	50.5	3	12	4	4.11	1.9	29.1	2.3	**2.85**	1	-	53.9	**4.8**	**8.6**
		f0417	53.7	50.9	3	12	4	3.44	2.2	27.1	3.4	**4.19**	1	-	53.9	**4.8**	**8.6**
		f0416	49.4	51.1	1	12	4	4.43	1.7	29.9	0.0	**6.00**	1	-	53.9	**4.8**	**8.6**
		f0413	36.6	51.6	5	12	4	3.01	2.0	25.6	6.0	**3.70**	3	70.8	18.1	**1.8**	**2.2**
		f0412	32.7	51.8	12	12	4	3.10	1.7	25.9	2.8	**0.88**	4	27.5	13.6	**1.4**	**1.6**
		f0411	25.6	52.1	7	12	4	2.39	2.2	23.1	4.7	**2.18**	3	62.2	18.1	**1.8**	**2.2**

Table 5.2 (Continued): Mg/Ca paleotemperature and error calculations for the Aropito, Tawanui and Pukemuri Stream sections. Two methods of error calculation are presented; the 95% confidence interval typically applied to Mg/Ca analyses, and the modelled temperature variance.

Species	Section	Sample Number	Strat. Height (m)	Age (Ma)	Analyses Good	Analyses Total	Specimens available	Mg/Ca (mmol/mol)	%2se Mg/Ca	Temperature (°C)	2σ (°C)	95% C.I.	n	Inter-Individual Variability (%)	Modelled %2se Mg/Ca	Temperature Errors +	Temperature Errors -
Subbotina	Aropito	f351	343	42.0	9	12	4	1.79	2.8	19.9	4.8	**1.83**	4	67.9	13.6	**1.4**	**1.6**
		f227	332	43.0	9	12	4	2.09	2.3	21.6	3.3	**1.27**	4	48.2	13.6	**1.4**	**1.6**
		f203	310	44.0	8	12	4	1.83	2.1	20.1	5.6	**2.34**	4	92.0	13.6	**1.4**	**1.6**
		f226	294	44.5	9	12	4	1.93	2.1	20.7	4.3	**1.66**	4	52.4	13.6	**1.4**	**1.6**
		f332	272	47.3	9	12	4	2.01	2.3	21.2	1.9	**0.75**	4	21.7	13.6	**1.4**	**1.6**
	Tawanui	f326	26.8	45.0	9	12	4	1.86	2.2	20.3	3.6	**1.40**	4	52.3	13.6	**1.4**	**1.6**
		f325	20.1	50.0	10	12	4	2.61	3.7	24.0	3.0	**1.09**	4	43.5	13.6	**1.4**	**1.6**
		f342	17.8	51.5	11	12	4	2.27	2.9	22.5	2.9	**0.97**	4	36.1	13.6	**1.4**	**1.6**
		f341	12.8	53.0	12	12	4	2.29	2.4	22.6	4.1	**1.29**	4	60.0	13.6	**1.4**	**1.6**
		f207	2.3	53.4	12	12	4	2.83	2.2	24.9	4.6	**1.45**	4	60.4	13.6	**1.4**	**1.6**
	Pukemuri	f0427	124.5	48.2	2	12	4	4.40	2.6	29.9	0.1	**0.29**	2	21.5	27.1	**2.7**	**3.5**
		f0426	109.3	48.2	3	12	4	3.52	2.6	27.4	3.8	**4.71**	2	34.2	27.1	**2.7**	**3.5**
		f0419	62.4	50.5	3	12	4	4.10	2.1	29.1	2.6	**3.18**	2	21.5	27.1	**2.7**	**3.5**
		f0415	44.5	51.3	2	12	4	3.82	1.5	28.3	2.2	**9.66**	1	-	53.9	**4.8**	**8.6**
		f0413	36.6	51.6	1	12	4	4.25	5.9	29.5	0.0	**6.00**	1	-	53.9	**4.8**	**8.6**
		f0411	25.6	52.1	8	12	4	3.09	2.5	25.9	2.8	**1.19**	3	33.4	18.1	**1.8**	**2.2**
		f0410	20.5	52.3	3	12	4	4.12	3.0	29.1	3.8	**4.73**	2	32.9	27.1	**2.7**	**3.5**
		f0407	-1	57.8	3	9	3	3.10	2.3	26.0	4.0	**5.01**	2	35.5	27.1	**2.7**	**3.5**
Cibicides	Aroptio	f351	343	42.0	6	6	2	3.14	2.5	14.0	1.4	**0.75**	2	17.5	27.1	2.2	2.9
		f227	332	43.0	3	6	2	2.25	2.5	10.9	5.5	**6.83**	2	58.9	27.1	2.2	2.9
		f203	310	44.0	5	6	2	2.12	3.2	10.4	2.6	**1.63**	2	37.0	27.1	2.2	2.9
		f226	294	44.5	11	12	4	2.55	2.4	12.1	4.1	**1.36**	4	66.8	13.6	1.2	1.3
		f332	272	47.3	6	9	3	3.08	2.8	13.8	4.5	**2.37**	3	56.9	18.1	1.5	1.4
	Tawanui	f326	26.8	45.0	7	12	4	2.00	2.1	9.9	3.6	**1.67**	4	48.3	13.6	1.2	1.3
		f325	20.1	50.0	12	12	4	3.87	1.8	15.9	4.4	**1.39**	4	64.9	13.6	1.2	1.3
		f342	17.8	51.1	11	12	4	3.51	1.8	15.0	2.0	**0.67**	4	27.3	13.6	1.2	1.3
		f341	12.8	53.0	7	12	4	3.54	3.0	15.1	3.9	**1.81**	4	50.7	13.6	1.2	1.5
		f207	2.3	53.4	11	12	4	2.51	2.9	11.9	4.8	**1.61**	4	95.6	13.6	1.2	1.3
	Pukemuri	f0428	132.1	41.9	1	9	3	2.91	5.4	13.3	0.0	**6.00**	1	-	53.9	4.0	7.1
		f0427	124.5	47.2	2	12	4	3.76	3.5	15.6	0.1	**0.63**	2	1.1	27.1	2.2	2.9
		f0426	109.3	48.2	6	9	3	3.20	3.8	14.2	4.8	**2.50**	3	59.3	18.1	1.5	1.8
		f0419	62.4	50.5	2	12	4	4.53	2.6	17.3	3.8	**17.01**	1	-	53.9	4.0	7.1
		f0416	49.4	51.1	7	12	4	4.77	2.9	17.8	2.7	**1.26**	4	34.4	13.6	1.2	1.3
		f0413	36.6	51.6	4	12	4	4.08	2.9	16.4	0.7	**0.52**	2	6.7	27.1	2.2	2.9
		f0411	25.6	52.1	6	9	3	5.80	5.4	19.6	1.6	**0.83**	2	18.2	27.1	2.2	2.9
		f0410	20.5	52.3	3	12	4	3.83	2.8	15.8	4.2	**5.17**	2	45.0	27.1	2.2	2.9
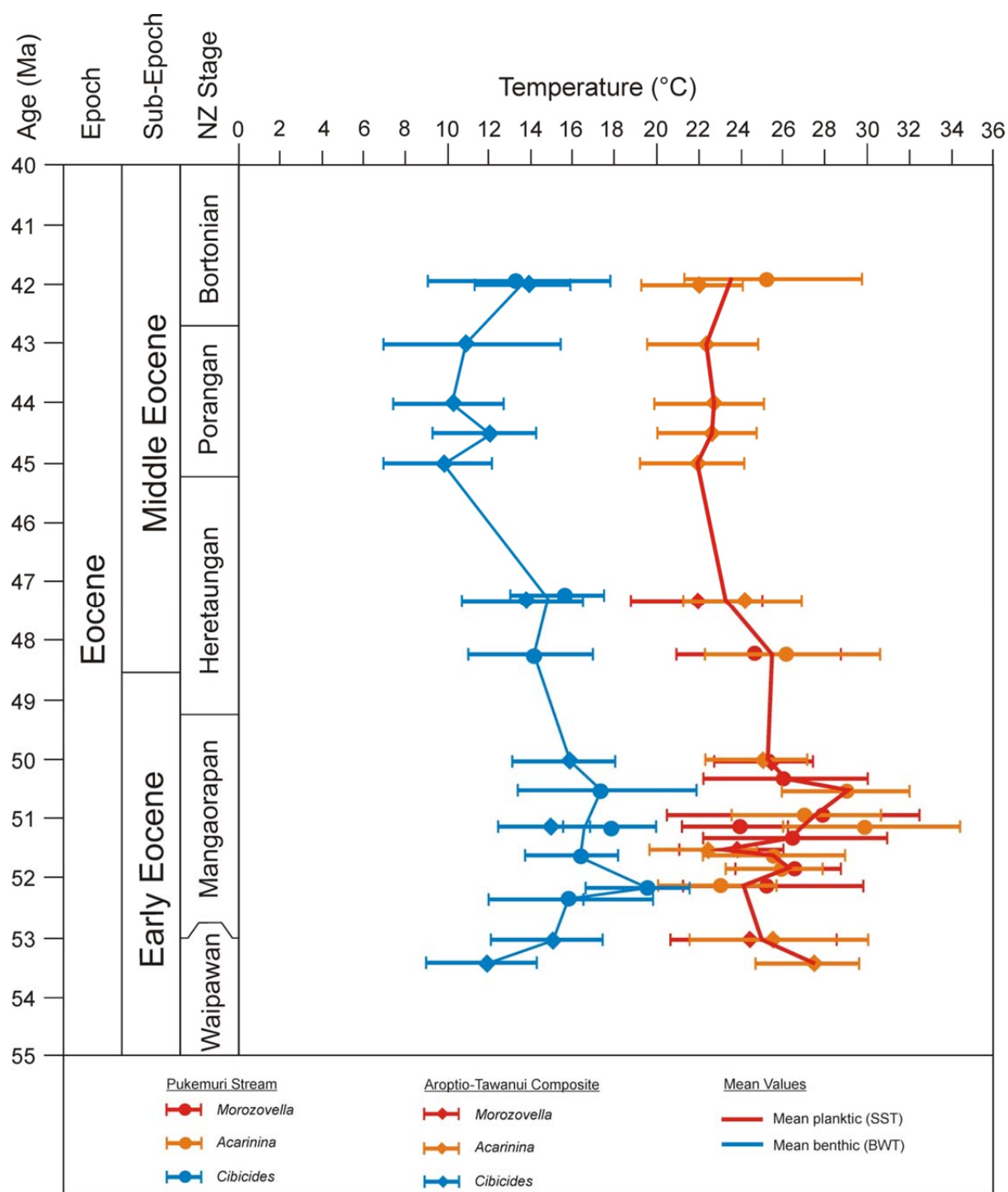
Figure 5.15: Early to middle Eocene sea surface (SST) and bottom water (BWT) temperature records derived from foraminiferal Mg/Ca ratios within the Pukemuri and Aropito–Tawanui composite sections. The error plotted is the 95% confidence interval.

5.6.3   Reporting of Errors on Mg/Ca Paleotemperatures

A significant source of error on Mg/Ca paleothermometry is the inter-individual variability of Mg/Ca ratios incorporated into the tests of individual foraminifera. Preliminary modelling of this error on extant foraminifera genera has shown that this is a significantly greater source of error than analytical or calibration uncertainties, particularly in studies with low number of individual foraminifera in the sample population. Traditional methods of reporting uncertainties on Mg/Ca values largely account for analytical and calibration errors, resulting in an understatement in the reporting of the true error applied to Mg/Ca temperature estimates. This becomes a significant consideration for the application of the Mg/Ca paleothermometry method to ancient, variably preserved material with a low number of individuals in each sample population.

Uncertainties arising from estimates of Eocene seawater Mg/Ca ratios and calibration errors are equally applicable to all data, resulting in a systematic offset of the entire record, and thereby have little implication on the relative temperature trends within a record. However, the inter-individual variability of Mg/Ca in foraminiferal calcite may be 60–70% between any selected individuals within a population. Therefore, in small datasets, such as those of this study, the potential error within inter-individual variability considerably outweighs that arising from analytical uncertainties.

The application of a modelled method (Chapter Three) to derive a % 2 se to account for the variability of Mg/Ca between generally results in the reporting of significant errors on Mg/Ca analyses in this study (*Figure 5.16*). Foraminifera from samples in the Pukemuri and southern Hawke's Bay sections are expected to have a significant uncertainty attached to temperature derivations, due to the small sample populations and the variable preservation of foraminiferal calcite exhibited by assemblages from these sites. Considering this, the modelled errors are potentially more reasonable than those derived using the 95% confidence interval. The errors presented using this method are not symmetrical, due to the exponential relationship between Mg/Ca ratios and temperature (*Figure 5.16*). Because the Mg/Ca paleothermometer increases in sensitivity with increasing temperature, the error margin on the lower temperature range is slightly larger than the higher temperature range. There is currently no published literature on inter-individual variability of Mg/Ca in Paleogene foraminifera, although variability of Mg/Ca between individuals in a given assemblage is acknowledged in studies of extant planktic species (e.g. Sadekov *et al.*, 2008, 2009; Marr *et al.*, 2011), and variability in Mg/Ca analyses of individual Paleogene foraminifera in Creech (2010) and this study (*Table 5.2*) strongly suggest that this is also the case with both planktic and benthic Paleogene foraminifera.

Also likely to be contributing to the reported variability of analyses are intra-individual variations in the Mg/Ca content of individual chambers. This is recognised as a regular feature in extant planktic foraminifera species, particularly species which precipitate a gametogenic calcite layer (e.g. Sadekov *et al.*, 2005). Coupled EPMA and LA-ICP-MS analysis of well-preserved *Subbotina* specimens have demonstrated an increase in Mg/Ca ratios of ≤ 0.8 mmol/mol in the final chamber that has a heavy gametogenic calcite layer (Hines, *unpublished data*). This may also be the case for *Morozovella* and *Acarinina*, although these species do not display any significant gametogenic calcification and any variation between individual chambers has yet to be quantified.

5.6.4 *Size Effect on Temperature*

A potential source of error that has not been accounted for within this study is the size effect on Mg/Ca precipitation in foraminiferal calcite. A difference of 0.2°C between the 300–350 μm and 425–500 μm size fractions has been reported in modern specimens of *Globigerinoides ruber* (Anand *et al.*, 2003). This is especially relevant to photosymbiotic species (e.g. *Acarinina* and *Morozovella* used in this study) as $\delta^{13}C$ and $\delta^{18}O$ ratios have shown that smaller individuals of these species occupy lower (and therefore cooler) levels in the water column (Wade *et al.*, 2008; Birch *et al.*, 2012), which will likely have the effect of reducing Mg/Ca values in smaller specimens. This Mg/Ca ratio dependency on size is widely acknowledged and incorporated into Holocene and Quaternary Mg/Ca paleothermometry studies (e.g. Elderfield *et al.*, 2002), however the poor foraminiferal assemblages, particularly from the Pukemuri Stream section yielded too few specimens for preferential size selection. This consequently induces another potential source of error into temperature reconstructions, although it is greatly overwhelmed by other sources of uncertainty, such as that of inter-individual variability.
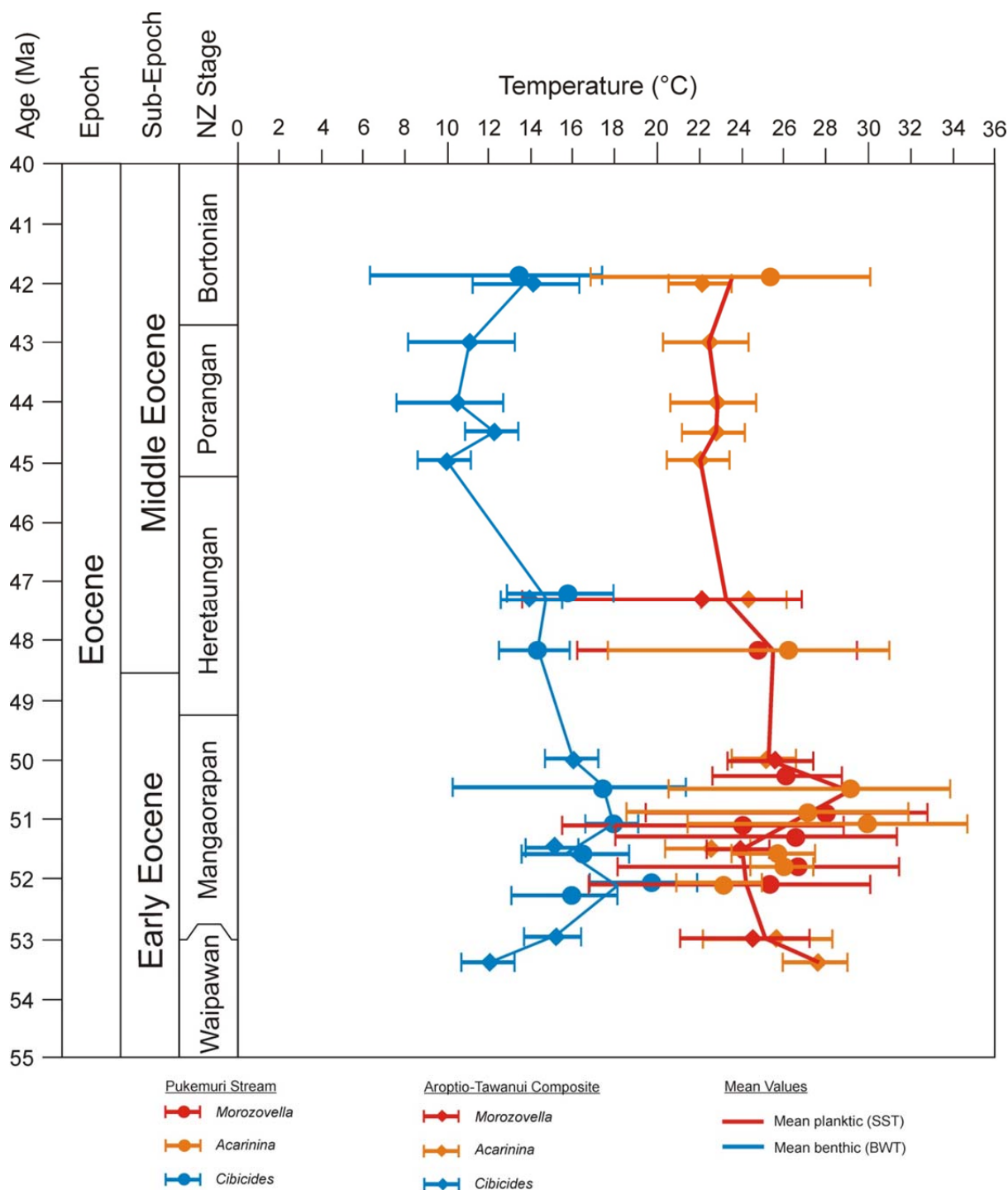
Figure 5.16: The modelled method of error determination generally produces larger errors than the 95% confidence interval (*Figure 5.15*) for the composite paleo-temperature record of the East Coast Basin. The modelled method takes into account the both the inter-individual variance in Mg/Ca values as well as the small population size. The upper range on the errors is smaller due to the increasing sensitivity of the Mg/Ca paleothermometer at higher temperatures.

5.6.5 Timing of the EECO

A decline in temperatures derived from foraminiferal Mg/Ca ratios in the Pukemuri Stream section constrains the termination of the EECO to 48.2 Ma, which is comparable to that recorded at mid-Waipara (48.5 Ma; Creech *et al.*, 2010), although later than recorded at Hampden (49.5 Ma; Hollis *et al.*, 2012). This difference is most likely attributable to the low temporal resolution at Tora. Although a relatively high-density sample suite was collected across the Pukemuri Stream section, poor preservation of foraminiferal specimens has resulted in low temporal resolution across the termination of the EECO at this section. Thus, further high-resolution sampling of the Pukemuri Stream section is not likely to better constrain the termination of the EECO. The improved preservation of the foraminiferal assemblages obtained from the Aropito and Tawanui sections yielded significantly better results, and would benefit from a higher sampling resolution for Mg/Ca paleothermometry.

5.6.6 Terrigenous flux during the EECO

The percentage of mud reflects the flux of terrigenous sediment into a depositional basin, which is largely controlled by proximity to land and water depth, but may also be modulated by climatic variables; increased precipitation leads to increased terrestrial run-off, as well as increasing rates of chemical weathering, both of which contribute towards an increased sedimentary load (e.g. Kump *et al.*, 2000; Ravizza *et al.*, 2001; Kelly *et al.*, 2005; Schimtz & Pujalte, 2007). The amount of terrigenous material increases across the PETM and later Eocene hyperthermals in many marine sedimentary successions (Hollis *et al.*, 2005; Nicolo *et al.*, 2007; Slotnick *et al.*, 2012). This has previously been demonstrated in the East Coast Basin across the PETM interval at Tawanui (Crouch *et al.*, 2003). Increased sediment flux during the EECO would have likely had the effect of diluting the carbonate content in environments closer to land. Such an effect is observed in the Pukemuri Stream section, where the carbonate content increases up-section with a corresponding decrease in the coarse (> 63 μm) sediment fraction. However, this trend is likely to be strongly influenced by the depositional setting of the Pukemuri Siltstone (outlined in Chapter Four), and in particular, the deepening depositional depth upwards through the sedimentary succession indicated by benthic foraminiferal faunas.

5.6.7   Interpretation of Additional Trace Element/Ca Ratios

Trace element/Ca ratios in foraminiferal calcite may provide supplementary information on changes in seawater chemistry that may be related to oceanic environmental conditions other than temperature.

Ti/Ca values for all sections in this study were consistently low, as expected because Ti does not substitute directly into the $CaCO_3$ matrix. These low values are further enforced by the application of Ti/Ca screening limits to raw data, and as the majority of Ti is bound to silicate mineral phases, screening removes any excessive influence on the observed Ti/Ca values. Ti values measured in the modern Pacific and Atlantic Oceans show that dissolved Ti concentrations are depleted in surface waters and enhanced at depth (Orians *et al.*, 1990). Therefore, increased Ti/Ca ratios may be expected in *Cibicides* relative to *Morozovella*, *Acarinina* and *Subbotina*; however, no discernable trend or species-specific offsets were observed in measured Ti/Ca values from the Aropito, Tawanui and Pukemuri sections.

Mn/Ca values were applied to screen for the effects of diagenetic alteration, particularly secondary calcite precipitation; however Creech *et al.* (2010) showed an increasing trend from 50–46 Ma in Mn/Ca values of foraminiferal calcite from the Canterbury Basin, and postulated that this may be linked to changing redox conditions in the ocean at the time of deposition. No such trend is apparent in the Aropito, Tawanui or Pukemuri sections in the East Coast Basin. Mn/Ca values measured in this study varied between 0.2 and 1.6 mmol/mol, with values from the Aropito and Tawanui sections generally at the lower end of this range, and foraminiferal assemblages from Pukemuri Stream yielding higher Mn/Ca values.

The planktic species *Morozovella* and *Acarinina* from the Aropito and Tawanui sections display similar Zn/Ca values. *Subbotina* Zn/Ca values tend to display similar values and trend to *Morozovella* and *Acarinina,* with the exception of two samples in the Mangaorapan interval. Excluding the high values recovered from *Subbotina* low in the sequence, *Cibicides* Zn/Ca ratios are consistently higher than those recorded for the planktic species, displaying a marked increase in the Porangan and Bortonian intervals (*Figure 5.17*). This increase applies solely to the benthic record. Marchitto *et al.* (2000) have suggested the use of Zn/Ca ratios in foraminiferal calcite as a tracer of bottom water movements. This observed increase in the benthic Zn/Ca record may indicate the influx of deepwater mass into the southern Hawke's Bay (Aropito-Tawanui region) during the Middle Eocene. This is supported by a coeval increase in bottom water Mg/Ca

paleotemperatures (+4°C) for the Aropito and Tawanui sections, and corresponding SSTs during this interval only display a slight increase (*ca.* +1-2°C) in temperature.

Assemblages from the Pukemuri Stream section appear to display no distinctive trends of species-specific offsets in Zn/Ca values, although notably there is considerably more variation in the planktic Zn/Ca values observed in values from the Aropito and Tawanui sections.

Ba/Ca ratios obtained from all species analysed from the Aropito and Tawanui sections appear to display the same trends and similar values, generally depicting a slight decrease in values with decreasing age (*Figure 5.17*). No species specific offset is apparent in Ba/Ca values from Aropito and Tawanui.

The Ba/Ca record from Pukemuri Stream exhibits a clear offset between the benthic species (*Cibicides*) and the planktic species analysed in this study (*Morozovella*, *Acarinina* and *Subbotina*), with *Cibicides* providing distinctly higher Ba/Ca ratios that the planktic species (*Figure 5.17*). For the most part, *Subbotina* produce Ba/Ca values higher than *Morozovella* and *Acarinina*, though distinctly lower than *Cibicides* (*Figure 5.17*). Applying the preferred depth habitats of the genera analysed, this apparent trend would suggest that surface waters were depleted in Ba, but increasingly concentrated at depth. This is consistent with values recorded in modern oceans, in which precipitation of barite in the upper levels of the ocean results in depleted barium concentrations in surface waters, and subsequent dissolution of barite on the seafloor results in enriched Ba concentrations in bottom waters (Lea, 1999).
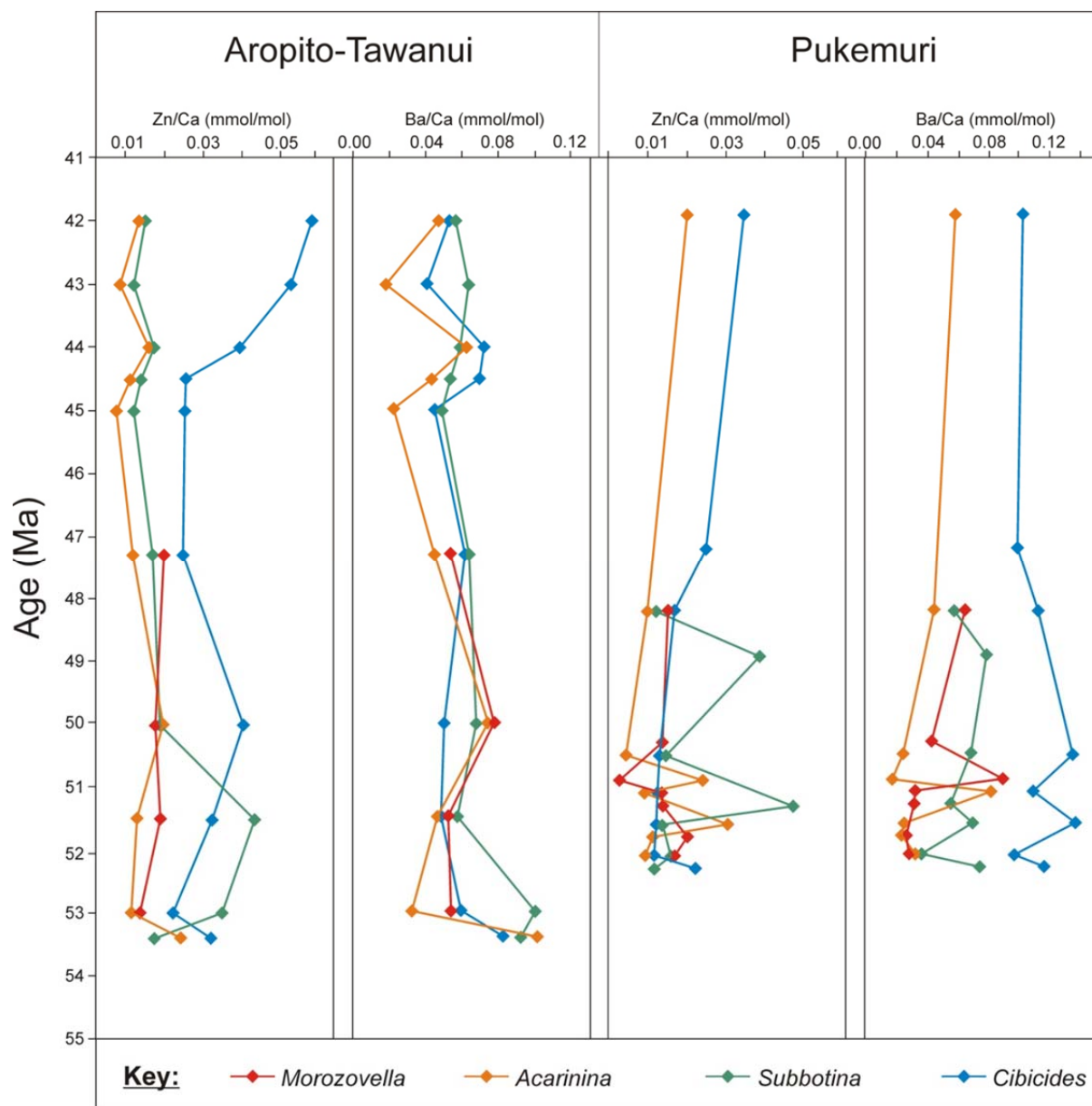
Figure 5.17: Zn/Ca and Ba/Ca concentrations for each of the genera utilised in this study for the Aropito and Tawanui composite section and the Pukemuri Stream section.

5.7   Comparison with Previous Studies

Previous Mg/Ca paleothermometry studies in the Southwest Pacific have utilised a multi-proxy approach, using a combination of the TEX_{86}, $\delta^{18}O$ and Mg/Ca paleothermometers. However, these studies are limited to two stratigraphic sections in the Canterbury Basin; the mid-Waipara River section (Hollis *et al.*, 2009; 2012; Creech *et al.*, 2010), and the Hampden Beach section (Burgess *et al.*, 2008; Hollis *et al.*, 2012). Species used to provide Mg/Ca paleotemperature data in these previous records correspond with the species assemblage used for Mg/Ca paleothermometry in this study, establishing a basis for direct comparison between records. Paleo-depth estimates for the Aropito and Tawanui sections (500–1000 m; Moore & Morgans, 1987; Kaiho *et al.*, 1993, 1996), and Tora (800 m; Chapter Four) are comparable to those of the mid-Waipara section (500 m; Hollis *et al.*, 2012), and deeper than the Hampden Beach section (200–400 m; Burgess *et al.*, 2008; Morgans, 2009; Hollis *et al.*, 2012).

The mid-Waipara record of Creech *et al.* (2010) has here been recalculated using the mean Mg/Ca ratio from *Acarinina* and *Morozovella* to calculate SSTs, and *Cibicides* sp. A in order to facilitate comparisons between the SST record of this study and that of Creech *et al.* (2010). The Hampden BWT record of Burgess *et al.* (2008) was produced from undifferentiated *Cibicides* spp. enabling direct comparison to this record. The Hampden SST and BWT record of Hollis *et al.* (2012) was produced using the same taxa for Mg/Ca analysis as the East Coast Basin record of this study (*Figure 5.15*). In all cases, the respective planktic and benthic Mg/Ca-temperature calibrations of Anand *et al.* (2003) and Lear *et al.* (2002) have been applied, and the Mg/Ca paleotemperature records calculated using a conservative estimate for early Eocene seawater Mg/Ca (4.1 mol/mol). This high value has been adopted based on comparative studies of foraminiferal Mg/Ca ratios and $\delta^{18}O$ values (Lear *et al.*, 2002; Sexton *et al.*, 2006a).

The multi-proxy approach of the Burgess *et al.* (2008), Creech *et al.* (2010) and Hollis *et al.* (2009, 2012) records provides a robust approach to paleotemperature estimations. The comparable temperature records derived from these studies provide confidence in the regional paleotemperature reconstruction of this study (*Figure 5.18*). The substantial distance separating the depositional systems of the East Coast and Canterbury Basins, and varied post-depositional processes of the respective basins, would have influenced the composition and distribution of pore fluids to differing extents, and subsequently the composition of secondary calcite. The agreement between these records provides a convincing argument for the preservation of a primary Mg/Ca temperature signal, even within the variably preserved material of the East Coast Basin sections.

The comparable BWT values (*Figure 5.18*) derived from the variably preserved foraminifera from the Pukemuri section and the well-preserved foraminifera of the Hampden Beach section further confirms the preservation of a primary ocean temperature signal obtained from the East Coast Basin sections. This demonstrates that the stringent screening criteria and assessment of foraminiferal preservation has resulted in the reporting of an unaltered primary temperature signal.

Termination of the EECO in the Canterbury Basin is associated with a pronounced cooling of bottom waters at Hampden and in the mid-Waipara River section (although less pronounced) which is accompanied by an equivalent cooling of surface waters at Hampden (Hollis *et al.*, 2012). BWTs of the mid-Waipara and the East Coast Basin records display very similar trends, which indicates that there were similar oceanographic influences and water masses throughout the Early to early Middle Eocene (*ca.* 53-46 Ma). The older portion of the Hampden BWT record (51.5-52.3 Ma) also corresponds well with the mid-Waipara River and East Coast Basin records. The abrupt cooling of the Hampden BWT record, representing the termination of the EECO, corresponds with a poorly sampled interval in both the mid-Waipara and East Coast Basin records, and appears to correspond with an offset in temperatures from mid-Waipara. The sampling resolution for the East Coast record through this interval is too low to infer any relationships with the records of the Canterbury Basin during the termination of the EECO.

SST records from the East Coast and Canterbury Basins display good agreement between 52-50 Ma, with peak temperatures of 29°C in both records. Following this, the East Coast Basin record is 2-3°C cooler than the mid-Waipara river record. The abrupt cooling of SSTs observed in the Hampden record at 49 Ma is not apparent in the mid-Waipara record and the temporal resolution of the East Coast Basin record is too low through this interval to make any inferences.

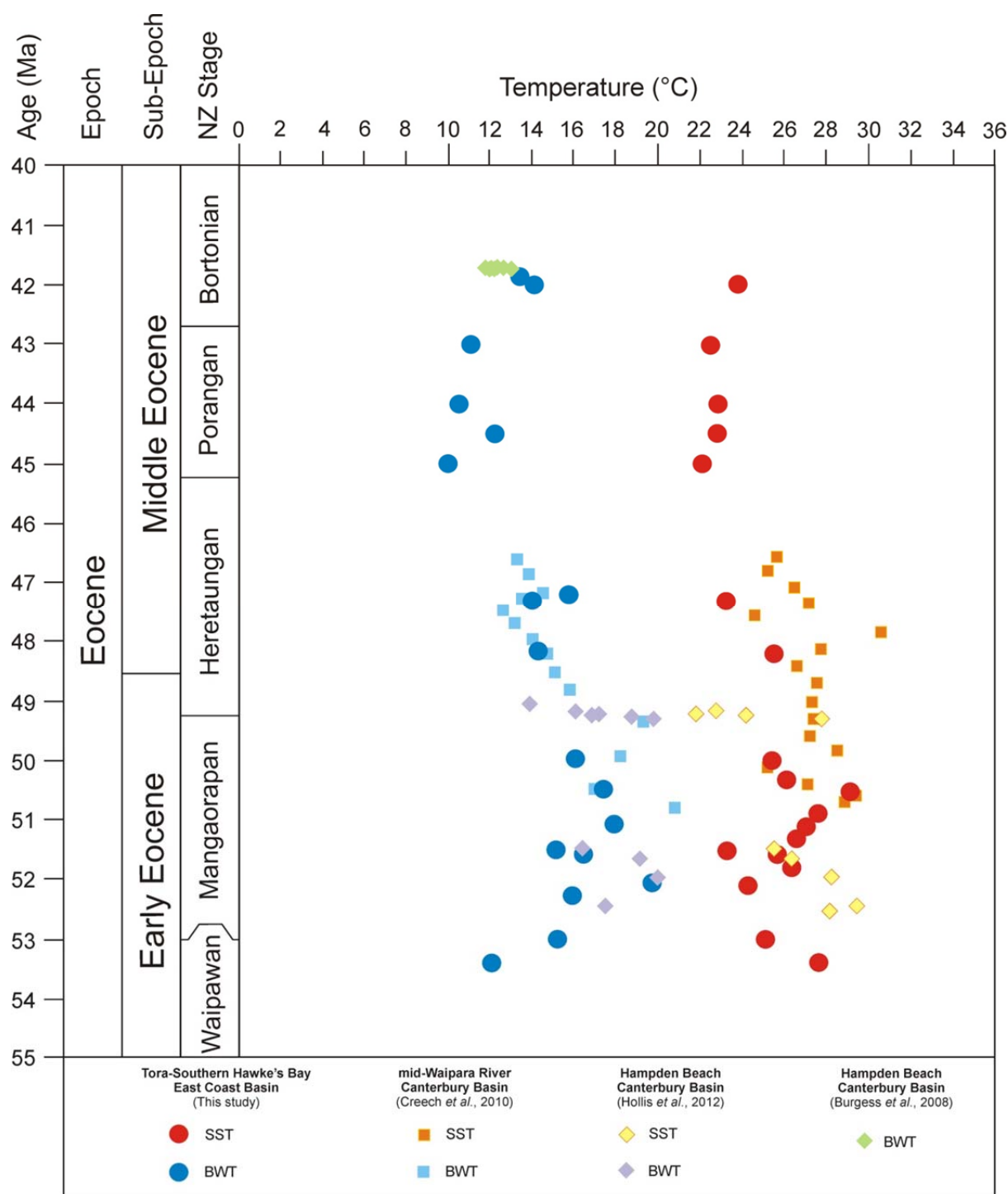**Figure 5.18:** Comparison between the composite East Coast Basin Mg/Ca temperature record (Aropito, Tawanui and Pukemuri sections) with previous Mg/Ca temperature records of the Canterbury Basin (mid-Waipara River and Hampden Beach). Mg/Ca values for Burgess *et al.* (2008) and Creech *et al.* (2010) have been recalculated with and Eocene Mg/Ca$_{sw}$ value of 4.1 mol/mol to enable direct comparison with the results of this study.

5.8   Southwest Pacific Paleoceanography

Extrapolation of an early Eocene climate record outside of the Canterbury Basin is essential for producing a regional synthesis of southwest Pacific sea temperature distributions, and subsequently relating measured proxy temperature values to global circulation models. The record for the East Coast Basin produced by this study provides a critical external paleotemperature record north of the Chatham Rise, which likely acted as a major barrier to oceanic fronts during the early Eocene as it does today. Surface temperatures during the Early Eocene remained fairly constant, with comparable temperatures derived from the East Coast and Canterbury Basins, suggesting that surface water masses were still able to cross the transition between the East Coast and Canterbury Basins, implying a shallow seaway or submarine platform across the Chatham Rise during the Early Eocene. This inference is supported by the presence of a hypothesised paleo-platform in the Clarence Valley–Marlborough area in early Eocene palinspastic reconstructions (Crampton *et al.*, 2003).

A rapid decline in bottom water temperatures is apparent at 49 Ma in the mid-Waipara and Hampden records. This cooling is not apparent in the composite East Coast basin record, which is likely due to the low temporal resolution through this interval.

The cooling of BWTs in the Canterbury Basin potentially reflects an influx of a cooler deep water mass around the termination of the EECO at *ca.* 49 Ma. The absence of an abrupt cooling in the deep waters of the East Coast basin at this time could perhaps imply that the cooler water mass was derived from the south, and northwards progression of the deep, cooler water mass was barred from entering the East Coast Basin by the Chatham Rise, which plays a similar role in the distribution of water masses in the modern Southwest Pacific Ocean.

SSTs and BWTs at Hampden are 2°C warmer than deeper, more northern proxy records from the mid-Waipara River, which likely reflects the comparatively shallow marine influence on the Hampden record. The warm shallow marine setting of the Hampden record may result in the introduction of a salinity effect on Mg/Ca incorporation into foraminiferal calcite. An increase of 1.6°C in Mg/Ca temperature estimates has been observed in modern specimens of *G. ruber* for an increase in salinity of 1.0 psu (Mathien-Blard & Bassinot, 2009). Therefore, increased salinity in the warmer, shallower depositional setting at Hampden may explain the higher temperatures in the foraminiferal Mg/Ca record. Salinity corrections are available for extant planktic foraminifera (e.g. Mathien-Blard & Bassinot, 2009), although these are unlikely to be meaningful if extrapolated to Eocene foraminifera.

The surface-to-seafloor gradient of paleotemperatures derived from the Early Eocene successions in the East Coast and Canterbury Basins consistently lies within the range of 9–12°C, comparable to the present day mid-latitude ocean, with modern SSTs of *ca.* 14°C and BWTs of 2–3°C measured at ODP Site 1123 (Hayward *et al.*, 2008; Elderfield *et al.*, 2010). The surface-to-seafloor gradient observed in the Hampden record is comparable to that of the mid-Waipara and East Coast sections, which is in contrast with the shallower (200 m) depth of the Hampden section reported in Hollis *et al.* (2012). A reduced surface-to-seafloor temperature gradient might be expected at Hampden as a result of the shallow (200 m) shelfal depositional setting, yet the temperature offset between the surface and seafloor is comparable to the deeper basinal settings (500–1000 m) of the mid-Waipara and East Coast Basin sections.

There is good agreement between peak early Eocene temperatures derived from the multiproxy records of the Canterbury Basin (Burgess *et al.*, 2008; Hollis *et al.*, 2009, 2012; Creech *et al.*, 2010), the Mg/Ca record of the East Coast Basin (this study) and the TEX_{86} record from ODP 1172 (Bijl *et al.*, 2009; Sluijs *et al.*, 2011). However, low SSTs (18°C; Shackleton & Kennett, 1975) derived from $\delta^{18}O$ at DSDP Site 277 seem to contradict the higher temperatures derived from ODP Site 1172 at the same latitude during the early Eocene. Preliminary results from the Mg/Ca analysis of the Early Eocene DSDP 277 record (Hines, *unpublished data*; Kulhanek *et al.*, in prep.) give higher SSTs of 29°C in contrast with the cooler temperatures produced by planktic $\delta^{18}O$. Lower temperatures derived from the $\delta^{18}O$ temperature proxy are attributed to post-depositional diagenetic alteration of foraminiferal calcite (Hollis *et al.*, 2009; 2012), which has been confirmed by SEM imaging and EPMA analysis of planktic foraminifera from DSDP 277, which display signs of significant dissolution and recrystallization (Hines *et al.*, *unpublished data*).

The higher temperatures derived from Mg/Ca imply no latitudinal temperature gradient across 10° of latitude from the East Coast Basin to DSDP Site 277, which is impossible to reconcile with climate dynamics and global circulation models, even assuming hyper-greenhouse conditions during the early Eocene (4480 ppm atmospheric CO_2; Hollis *et al.*, 2012). The role of surface currents potentially played a major role in the distribution of heat in the surface waters of the early Eocene southwest Pacific. Intensification of surface currents during the EECO would provide an efficient means of oceanic heat distribution, subsequently resulting in the decreased thermal gradient from the equator to poles suggested by proxy records. Hollis *et al.* (2012) hypothesise an intensification of a proto-East Australian Current to explain the distribution of tropical sea temperatures extending into the high-latitude Southwest Pacific Ocean during the EECO (*Figure 5.19*). The high temperatures of the East Coast Basin, which correspond to similar

temperatures in the Canterbury Basin during this time, appear to support this premise, and suggest that this current also bathed northern New Zealand (*Figure 5.19*). Furthermore, these high temperatures, which indicate the intensification of a proto-EAC, may have promoted the development of an anticyclonic gyre in the South Tasman Sea.

In addition to this, to explain the unusually high temperatures recorded by paleoclimate proxies utilised in previous studies of the early Paleogene climate of the SW Pacific, the TEX_{86}, $\delta^{18}O$ and Mg/Ca paleothermometers may be recording summer temperatures, rather than mean annual temperatures, inducing a potential seasonal bias in temperature reconstructions (Hollis *et al.*, 2012).
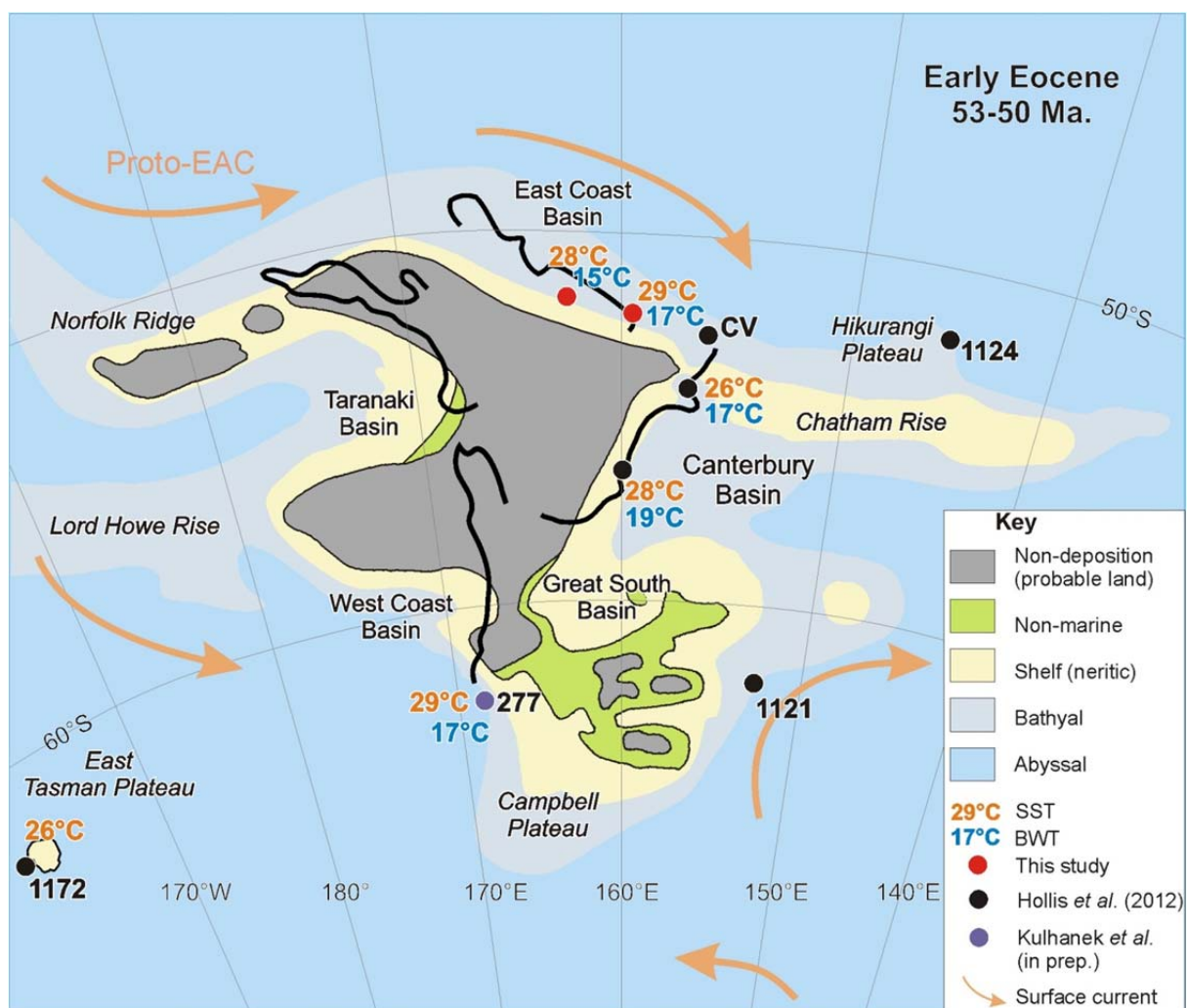
Figure 5.19: Early Eocene paleogeographic reconstruction of the New Zealand sector of the Southwest Pacific comparing maximum SSTs (orange text) and BWTs (blue text) of this study (red circles) with previous studies (black circles) as summarised in Hollis *et al.* (2012). Base map adapted from Hollis *et al.* (2012). Surface currents (arrows) are based on modelled circulation patterns adapted from Hollis *et al.* (2012). Warm, tropical waters are transported across northern New Zealand by a proto-East Australian Current (EAC).

5.9   Summary

The high frequency of infilling of foraminiferal tests with sediment, nannofossils, secondary calcite and pyrite, means that solution methods of Mg/Ca paleothermometry data acquisition could not be reliably applied to assemblages from the Aropito, Tawanui and Pukemuri Stream sections. The laser ablation method utilised in this study, and the subsequent screening measures applied, circumvents these issues, resulting in a paleotemperature record that shows good correspondence with previous multi-proxy records in the Canterbury Basin.

Age models for the Aropito, Tawanui and Pukemuri Stream sections indicate that the composite East Coast Basin record extends from the Early to Middle Eocene, although poor preservation within several of the foraminiferal assemblages collected from Pukemuri Stream has reduced the resolution of the temperature record considerably below that of the original sample suite collected.

Bulk carbonate $\delta^{18}O$ results from Pukemuri Stream display values that are indicative of diagenetic alteration by meteoric waters. Bulk carbonate $\delta^{13}C$ values are typically more resistant to alteration, and values obtained from Pukemuri Stream are consistent with previously recorded bulk carbonate $\delta^{13}C$ values from the southern East Coast Basin (e.g. Hollis *et al.*, 2005; Slotnick *et al.*, 2012) and benthic foraminiferal records from ODP and DSDP cores (e.g. Zachos *et al.*, 2001).

Preservation of foraminiferal assemblages is variable, and tests are often observed to display evidence of infilling by silicate sediments or calcareous nannofossils, secondary calcite or pyrite. Screening protocols applied to Mg/Ca data have been shown to effectively remove any profiles altered by the presence of silicate minerals, secondary alteration or pyrite, resulting in the reporting of a primary Mg/Ca signal that produces temperature estimates that correlate well with established multiproxy records in the Canterbury Basin.

Peak SSTs of 29°C during the EECO obtained from the mid-Waipara River record are identical to a coeval peak of 29°C at Tora. Peak sea surface and bottom water temperatures from the composite Aropito-Tawanui section are marginally cooler than those obtained from the Pukemuri Stream section at Tora. This observation may support the hypothesised intensification of a proto-East Australian Current during the EECO (Hollis *et al.*, 2012), during which surface waters from the South Tasman Sea are forced northwards around the western margin of the New Zealand landmass, then around northern New Zealand. However, this inference requires further support which could be obtained from future paleothermometry studies of the western margin of the New Zealand sub-continent.

The corresponding increase of 4°C in BWTs and an increase in Zn/Ca concentrations during the middle Eocene record from the Aropito-Tawanui composite record, coupled with only a minor increase in surface water temperatures, implies the influx of a different, warmer bottom water mass during this time.

Chapter Six

CONCLUSIONS

6.1   Key Findings

6.1.1   *Paleogene Stratigraphy and Paleoenvironment at Tora*

The Paleogene succession at Tora has been mapped and described in main three sections: Pukemuri Stream, Awheaiti Stream and Te Oroi Stream. New, detailed measured section studies have retained the existing broad lithostratigraphic divisions, but sampling yielded calcareous nannofossil and foraminiferal assemblages, which have provided a revision of the age for the lower Paleogene sequence. This provides a well-documented stratigraphy in the East Coast Basin, and has provided a robust age and stratigraphic framework. Microfossils, sedimentology and trace fossil analyses are used to provide a revised geological history for the Tora area and the central East Coast Basin, with a series of new paleogeographic maps.

The Lower Paleocene Awhea Formation is indicative of deposition within a central submarine fan setting, with a thinning-upward succession of alternating sandstone and mudstone beds suggestive of gradual lobe migration. The lower and middle members of the Lower to Middle Paleocene Mungaroa Limestone represent a continuation of submarine fan sedimentation, although potentially in a more proximal part of the fan. The upper micritic limestone member represents a reduction in the sediment supply to the region, allowing calcareous biogenic sediments typical of the Marlborough area to extend northwards into the central East Coast Basin. The Upper Paleocene Awheaiti Formation represents a return to the submarine fan setting, being deposited in a channel system that is locally incised into the Mungaroa Limestone. The Awheaiti Formation is unconformably overlain by the Lower Eocene Pukemuri Siltstone, with a basal pebbly-mudstone interpreted as a debris flow deposit, overlain by mudstone deposited in a slope environment. An unconformity separates the Upper Eocene Wanstead Formation from the Lower Eocene Pukemuri Siltstone. The Wanstead Formation was deposited at lower bathyal to abyssal depths, with a marine transgression apparent across the Pukemuri Siltstone – Wanstead Formation unconformity, deepening the basin to lower bathyal-abyssal depths during the Middle Eocene, subsequently followed by hemipelagic deposition. The Wanstead Formation at Tora is younger than typically expressed in the East Coast Basin, which is likely related to a deepening of the Tora area during the middle Eocene.

The stratigraphy at Tora can be related to general sedimentary sequences elsewhere in the East Coast Basin. The Manurewa and Awhea Formations jointly represent a lateral extension of the Upper Calcareous Member of the Whangai Formation. The upper micritic limestone member of the Mungaroa Limestone is recognised as a lateral equivalent of the Kaiwhata Limestone described further north in the Glenburn area. The Pukemuri Siltstone shares features in common with the Wanstead Formation described at Glenburn, and potentially represents a more proximal, slope influenced facies of the Wanstead Formation.

This study has produced a revised stratigraphic framework for the lower Paleogene stratigraphic succession at Tora, which is a transitional environment between the largely clastic sedimentation typically expressed in the North Island East Coast Basin, and the biogenic sedimentation of the Marlborough area in the southern East Coast Basin.

6.1.2 Mg/Ca Paleothermometry of the Central East Coast Basin

A sampling resolution of 70–200 kyr in the Lower Eocene Pukemuri Siltstone produced foraminiferal assemblages suitable for LA-ICP-MS Mg/Ca paleothermometry; however, poor preservation of some samples reduced the temporal resolution to 0.2–1.5 Myr. The Pukemuri Stream section has been supplemented by foraminiferal assemblages from sample suites from the Aropito and Tawanui sections in the southern Hawke's Bay portion of the central East Coast Basin, which had a lower sampling resolution of 0.4–3.0 Ma.

Bulk carbonate oxygen stable isotope analyses of samples from the Pukemuri Stream section predominantly show highly negative values, indicative of alteration by meteoric waters. Carbon stable isotope values recovered are comparable with those of other Lower Eocene sediments in the East Coast Basin (e.g. Hollis *et al.*, 2005; Slotnick *et al.*, 2012).

LA-ICP-MS analysis of planktic and benthic foraminifera from the Aropito, Tawanui and Pukemuri Stream sections in the central East Coast Basin has provided the first quantitative Early Eocene sea surface and bottom water temperature records for the North Island of New Zealand. The individual records display good agreement in temperature reconstructions between sections. Sea surface temperatures (SSTs) at Tora derived from planktic foraminiferal Mg/Ca ratios peaked at 29°C within the early Eocene climatic optimum (EECO) at 50 Ma, with a coeval peak in bottom water temperatures (BWTs) of 19°C from benthic Mg/Ca ratios. A composite

southern Hawke's Bay record consisting of the Aropito and Tawanui sections produced marginally cooler peak SSTs of 27°C and BWTs of 15°C.

The composite Mg/Ca paleotemperature record for the East Coast Basin (Aropito, Tawanui and Pukemuri Stream sections) displays good correspondence with existing Mg/Ca records from the coeval mid-Waipara River and the Hampden sections in the Canterbury Basin (Hollis *et al.*, 2009, 2012). A cooling is observed in the composite East Coast Basin record at ~48 Ma which is approximately 1 Myr after a comparable cooling in the Canterbury Basin. This time offset may be an artefact of poor temporal resolution across the termination of the EECO. A total cooling of 7°C in SSTs and a slightly more pronounced cooling of 9°C in BWTs is observed across the composite East Coast Basin record from 51 to 42 Ma.

The similarities between the East Coast Basin and the Canterbury Basin temperature records supports the concept presented by Hollis *et al.* (2012) of an intensification of a proto-East Australian Current (EAC), explaining the distribution of tropical SSTs into the high-latitude Southwest Pacific during the EECO. The warm temperatures in the East Coast Basin, north of the Chatham Rise, suggest that the amplified EAC warmed the seas around northern New Zealand in addition to potentially forming an anticyclonic gyre in the South Tasman Sea.

Electron probe micro-analysis (EPMA) element mapping techniques applied to the variably preserved foraminifera of the East Coast Basin sections has shown the benefits of the LA-ICP-MS method, as opposed to solution chemistry, and subsequent trace element/Ca screening protocols measured for Mg/Ca data acquisition.

6.2 Suggestions for Future Work

6.2.1 Stratigraphy of Tora

Field mapping and measured section studies at Tora have identified considerable potential for detailed sedimentological facies analysis within the Paleogene succession at Tora. In addition, the diverse trace fossil assemblages within the lower Paleogene succession warrant more detailed description and analysis to refine environmental interpretation.

The Tora structural block has previously been interpreted as an allocthonously emplaced portion of the Pegasus Sub-basin (Moore, 1988a). Thermochronological and fission track dating methods applied to the adjoining greywacke and lower Cretaceous strata may constrain the emplacement history of the Tora Block. The application of such methods may also constrain a tectonic history for the area, which stratigraphic evidence from this study suggests may include active tectonism that extends as far back as the late Paleocene to early Eocene. This could provide insights into the internal deformation and structural evolution of the East Coast Basin prior to the inception of the modern plate boundary through New Zealand.

Age constraints applied to the stratigraphic succession examined in this thesis are based solely on calcareous nannofossil and foraminiferal biostratigraphy. Independent dating methods such as magnetostratigraphy or $^{40}Ar/^{39}Ar$ and $^{40}K-^{40}Ar$ dating of glauconite (e.g. Jackson, 2000) would significantly improve the age control applied to the sections studied in this thesis.

6.2.2 Paleoclimate Studies

The late Paleogene–Middle Eocene stratigraphic succession at Tora contains calcite veins infilling fractures within the Mungaroa Limestone, Pukemuri Siltstone and Wanstead Formation, providing a unique opportunity to compare the Mg/Ca ratios of inorganic calcite precipitates with both primary foraminiferal calcite and secondary diagenetic calcite Mg/Ca values obtained from LA-ICP-MS analysis of foraminiferal tests; thus allowing end member calcite Mg/Ca compositions to be determined. This will allow the effects of variable preservation and post-depositional diagenetic processes to be quantified in greater detail.

The Aropito and Tawanui sections have displayed great potential for further application of paleothermometry methods. The better preservation of foraminiferal tests from these sections may enable reconstruction of a reliable $\delta^{18}O$ record, which, coupled with additional, high-

resolution sampling of these sections for Mg/Ca paleothermometry, could result in a refined early Paleogene sea temperature record. Section studies in the Canterbury Basin have shown the power of applying a multiproxy approach to early Paleogene temperature reconstructions using Mg/Ca, $\delta^{18}O$ and TEX_{86} (Hollis *et al.*, 2009, 2012; Creech *et al.*, 2010). TEX_{86} methods may be applicable to sedimentary successions in the central East Coast Basin, on the proviso that organic carbon is thermally immature, which has generally been demonstrated in outcrop studies of the Paleogene strata in the East Coast Basin (Hollis, pers. comm.). High-resolution sampling of the Aropito and Tawanui sections would provide better constraints on the timing of the EECO in the East Coast Basin. In addition, the East Coast Basin contains an extensive marine sedimentary record that spans the entire Paleogene, creating ample opportunity to produce a composite paleoclimate record. Offshore ODP holes and piston cores contain excellent records of Neogene and Quaternary sedimentation, which may enable the development of a composite Cenozoic record.

The application of the LA-ICP-MS Mg/Ca paleothermometry method largely circumvents issues associated with variable preservation, thereby enabling the application of the method to a wide range of geographically-diverse early Paleogene sedimentary successions. Section studies could produce Mg/Ca paleotemperature records from Northland, additional sections in the East Coast Basin, the Chatham Islands, coastal Otago, and Campbell Island, which could be integrated to produce a regional synthesis of Southwest Pacific Ocean climatic and oceanic changes during the Eocene. This would enable regional scale oceanographic reconstructions, as well as providing records of oceanic changes which may be used to constrain the timing of cool water intrusions and associated climatic variations.

6.2.3   *Mg/Ca Paleothermometry*

Aspects of the analytical geochemistry conducted in this study have highlighted areas of potential future work and suggestions for future applications. The applications of some new and developing geochemical methodologies to foraminiferal calcite are also suggested.

EPMA element mapping of foraminiferal calcite has indicated that Fe/Ca ratios may have an application in the identification of both secondary calcification (see Chapter Five, this study), and contamination of primary calcite arising from the presence of both silicate minerals (as per Barker *et al.*, 2003). The measurement and screening of Fe/Ca ratios in laser ablation profiles should be implemented as a regular feature of LA-ICP-MS Mg/Ca data acquisition. Fe/Ca ratios

were not measured during the adopted laser ablation protocol of this study; although the distribution of iron in the element maps produced by this study suggests that this should be incorporated into future work to identify zones of silicate contamination and secondary calcification. However, measuring Fe is only possible with high-resolution ICP-MS due to argide-based interferences on Fe isotopes.

The application of the clumped isotope and CO_2 isotopologue methods to derive past sea temperatures could be applied to provide an additional paleotemperature proxy, which has the benefit of being independent of $\delta^{18}O_{sw}$ variations.

The observation of remaining detrital debris of the exterior of foraminifera used in this study suggests that an additional cleaning step should be considered for preparation of foraminiferal tests for LA-ICP-MS analysis. Immersing specimens in an ultrasonic bath was found to be destructive in many instances. However, the cleaning of foraminifera by centrifuging in acid leached glass vials (e.g. Greaves *et al.*, 2005; Weldeab *et al.*, 2006) in addition to alternating washes of milli-Q water and methanol, may provide an additional means to remove detrital contaminants from foraminiferal tests, without the application of ultrasonic disaggregation methods to fragile specimens.

Electron microprobe analysis conducted for this study and in parallel studies of early Paleogene foraminifera from Hampden and DSDP Site 277 have provided significant insight into the preservation, potential, ontogeny and geochemistry of foraminifera. However, the EPMA method employed in this study often lacks the sensitivity to resolve minute variations in trace element concentrations within foraminiferal calcite. Additional work utilising ion microprobe methods may provide greater detail in detecting geochemical variations in foraminiferal tests including paired studies into the distribution of Mg/Ca and Sr/Ca ratios and oxygen stable isotopes (e.g. Allison & Austin, 2003, 2008; Kozdon *et al.*, 2011).

Using high-resolution sample excavation (micromill/drill) and laser techniques such as that applied to phenocryst zonation in crystal-specific studies of magma evolution (e.g. Morgan *et al.*, 2007, Charlier *et al.*, 2008) it is possible to attain high quality *in-situ* isotopic microanalyses from within individual foraminiferal calcite laminae, which may provide indications of intra- and inter-individual variability of stable isotope compositions.

REFERENCES

Agnini, C., Fornaciari, E., Raffi, I., Rio, D., Röhl, U., & Westerhold, T. (2007). High-resolution nannofossil biochronology of middle Paleocene to early Eocene at ODP Site 1262: Implications for calcareous nannoplankton evolution. *Marine Micropaleontology*, *64*, 215–248.

Alexander, S. J. (1990). *The Late Cenozoic structure of an area, southeast Wairarapa.* Victoria University of Wellington.

Allison, N., & Austin, W. E. N. (2003). The potential of ion microprobe analysis in detecting geochemical variations across individual foraminfera tests. *Geochemistry Geophysics Geosystems*, *4*, 1–9.

Allison, N., & Austin, W. E. N. (2008). Serial Mg/Ca and Sr/Ca chronologies across single benthic foraminifera tests. *Chemical Geology, 253*, 83-88.

Anand, P., Elderfield, H., & Conte, M. H. (2003). Calibration of Mg/Ca thermometry in planktonic foraminifera from a sediment trap time series. *Paleoceanography*, *18*(2), 1050.

Andrew, B. (2010). *Sedimentary facies and unconformity analysis of some Paleocene-Eocene sections, Marlborough and Campbell Island, New Zealand.* University of Waikato.

Balistrieri, L., Brewer, P. G., & Murray, J. W. (1981). Scavenging residence times of trace metals and surface chemistry of sinking particles in the deep ocean. *Deep-sea Research*, *28*(A), 101–121.

Ballance, P. F. (1993). The New Zealand Neogene forearc basins. In P. F. Ballance (Ed.), *Sedimentary Basins of the World 2: Basins of the South West Pacific* (pp. 177–193). Amsterdam.

Barker, S., Greaves, M., & Elderfield, H. (2003). A study of cleaning procedures used for foraminiferal Mg/Ca paleothermometry. *Geochemistry Geophysics Geosystems*, *4*(9), 8407.

Barnes, P. M. (1988). Submarine fan sedimentation at a convergent margin: the Cretaceous Mangapokia Formation, New Zealand. *Sedimentary Geology*, *59*, 155–178.

Barnes, P. M., & Korsch, R. J. (1991). Melange and related structures in Torlesse accretionary wedge, Wairarapa, New Zealand. *New Zealand Journal of Geology and Geophysics*, *34*(4), 517–532.

Barnes, P. M., Lamarche, G., Bialas, J., Henrys, S., Pecher, I., Netzeband, G. L., Greinert, J., et al. (2010). Tectonic and geological framework for gas hydrates and cold seeps on the Hikurangi subduction margin, New Zealand. *Marine Geology*, *272*(1-4), 26–48.

Begg, J. G., & Johnston, M. R. (2000). *Geology of the Wellington area. Institute of Geological & Nuclear Sciences 1:250 000 geological map 10* (p. 64 + 1 sheet). Lower Hutt, New Zealand: Institute of Geological and Nuclear Sciences Limited.

Bentov, S. & Erez, J. (2005). Novel observations on biomineralization processes in foraminifera and implications for Mg/Ca ratio in the shells. *Geology, 33:11*, 841-844.

Berggren, W. A., Aubry, M.-P., van Fossen, M., Kent, D. V., Norris, R. D., & Quillevere, F. (2000). Integrated Paleocene calcareous plankton magnetobiochronology and stable isotope stratigraphy: DSDP Site 384 (NW Atlantic Ocean). *Palaeogeography, Palaeoclimatology, Palaeoecology*, *159*, 1–51.

Berner, R. A. (1984). Sedimentary pyrite formation: an update. *Geochimica et Cosmochimica Acta*, *48*, 605–615.

Berryman, K., Ota, Y., & Hull, A. (1989). Holocene paleoseismicity in the fold and thrust belt of the Hikurangi subduction zone, eastern North Island, New Zealand. *Tectonophysics*, *163*, 185–195.

Berryman, K., Ota, Y., Miauchi, T., Hull, A., Clark, K., Ishibashi, K., Iso, N., et al. (2011). Holocene Paleoseismic History of Upper-Plate Faults in the Southern Hikurangi Subduction Margin, New Zealand, Deduced from Marine Terrace Records. *Bulletin of the Seismological Society of America*, *101*(5), 2064–2087.

Bijl, P. K., Schouten, S., Sluijs, A., Reichart, G., Zachos, J. C., & Brinkhuis, H. (2009). Early Paleogene temperature evolution of the southwest Pacific Ocean. *Nature*, *461*, 776–779.

Billups, K., & Schrag, D. (2003). Application of benthic foraminiferal Mg/Ca ratios to questions of Cenozoic climate change. *Earth and Planetary Science Letters*, *209*, 181–195.

Birch, H. S., Coxall, S. K., & Pearson, P. N. (2012). Evolutionary ecology of Early Paleocene planktonic foraminifera: size, depth habitat and symbiosis. *Paleobiology*, *38*(3), 374–390.

Bishop, J. K. B. (1988). The barite-opal-organic carbon association in oceanic particulate matter. *Nature*, *332*, 341–343.

Bolton, A., Baker, J. A., Dunbar, G. B., Carter, L., Smith, E. G. C., & Neil, H. L. (2011). Environmental versus biological controls on Mg/Ca variability in Globigerinoides ruber (white) from core top and plankton tow samples in the southwest Pacific Ocean. *Paleoceanography*, *26*, 1–14.

Bouma, A. H. (2000). Coarse-grained and fine-grained turbidite systems as end member models: applicability and dangers. *Marine and Petroleum Geology*, *17*, 137–143.

Bouma, A. H., Normark, W. R., & Barnes, N. E. (Eds.). (1985). *Submarine fans and related turbidite systems* (p. 351). New York: Springer Verlag.

Bowen, G. J., Bralower, T. J., Delaney, M. L., Dickens, G. R., Kelly, D. C., Kock, P. L., Kump, L. R., et al. (2006). Eocene Hyperthermal Event Offers Insight into Greenhouse Warming. *Eos Transactions of the American Geophysical Union*, *87*(17), 165–167.

Bown, P. R. (Ed.). (1998). *Calcareous Nannofossil Biostratigraphy* (p. 315). Cambridge: Cambridge University Press.

Bown, P. R., & Young, J. R. (1998). Techniques. In P. R. Bown (Ed.), *Calcareous Nannofossil Biostratigraphy* (pp. 16–28). Cambridge: Cambridge University Press.

Boyle, E. A. (1981). Cadmium, zinc, copper and barium in foraminifera tests. *Earth and Planetary Science Letters*, *53*(1), 11–35.

Boyle, E. A. (1983). Manganese overgrowths on foraminifera tests. *Geochimica et Cosmochimica Acta*, *47*, 1815–1819.

Bradshaw, J. D. (1991). Cretaceous dispersion of Gondwana: continental and oceanic spreading in the south-west Pacific-Antarctica sector. *In:* Thompson, M. R. A., Crame, J. A., Thompson, J. W. ed. *Geological evolution of Antarctica*. Cambridge, Cambridge University Press. Pp. 581-585.

Bralower, T. J., Zachos, J., Thomas, E., Parrow, M., Paul, C., Kelly, D., Silva, I., et al. (1995). Late Paleocene to Eocene paleo-oceanography of the equatorial Pacific Ocean: Stable

isotopes recorded at Ocean Drilling Program Site 865, Allison Guyot. *Paleoceanography*, *10*, 841–865.

Brand, L. E., Sunda, W. G., & Guillard, R. R. L. (1983). Limitation of marine phytoplankton reproductive states by zinc, manganese and iron. *Limnology and Oceanography*, *28*(6), 531–534.

Brasier, M. D. (1980). *Microfossils* (p. 193). London: Unwin Hyman.

Broecker, W., & Peng, T. H. (1982). *Tracers in the sea*. Eldigion Press, Lamont Doherty Geological Observatory.

Browne, G. H. (1987). In situ and intrusive sandstone in Amuri facies limestone at Te Kau Kau Point, southeast Wairarapa, New Zealand. *New Zealand Journal of Geology and Geophysics*, *30*, 363–374.

Bruland, K. W. (1980). Oceanographic distributions of cadmium, zinc, nickel and copper in the North Pacific. *Earth and Planetary Science Letters*, *47*, 176–198.

Buatois, L., & Mangano, M. G. (2011). *Ichnology: Organism-Substrate Interactions in Space and Time* (p. 358). Cambridge University Press.

Burgess, C., Pearson, P. N., Lear., C. H., Morgans, H. E. G., Handley, L., Pancost, R. D., & Schouten, S. (2008). Middle Eocene climate cyclicity in the southern Pacific: Implications for global ice volume. *Geology*, *36*(8), 651–654.

Burns, R. E., Andrews, J. E., & Van der Lingen, G. J. (1973). *Initial Reports of the Deep Sea Drilling Project*. Washington, DC: US Govt. Printing Office.

Callow, R. H. T., McIlroy, D., Kneller, B., & Dykstra, M. (2012). Integrated ichnological and sedimentological analysis of a Late Cretaceous submarine channel-levee system: the Rosario Formation Baja California, Mexico. *Marine and Petroleum Geology*. doi:10.1016/ j.marpetgeo.2012.02.001

Carter, R. M., Carter, L., & McCave, I. N. (1996). Current controlled sediment deposition from the shelf to the deep ocean: the Cenozoic evolution of circulation through the SW Pacific gateway. *Geologische Rundschau*, *85*, 438–451.

Carter, R. M., Landis, C. A., Norris, R. J., & Bishop, D. G. (1974). Suggestions towards a higher level nomenclature for New Zealand rocks. *Journal of the Royal Society of New Zealand*, *4*, 5–18.

Charlier, B. L. A., Wilson, C. J. N., & Davidson, J. P. (2008). Rapid open-system assembly of a large silicic magma body: time-resolved evidence from cored plagioclase crystals in the Oruanui eruption deposits, New Zealand. *Contributions to Mineralogy and Petrology*, *156*, 799–813.

Chiswell, S. M. (2000). The Wairarapa Coastal Current. *New Zealand Journal of Marine and Freshwater Research*, *34*(2), 303–315.

Clarke, F., & Wheeler, W. (1922). The inorganic constituents of marine invertebrates. *USGS Professional Paper*, *124*, 1–62.

Coggon, R. M., Teagle, D. A. H., Smith-Duque, C. E., Alt, J. C., & Cooper, M. J. (2010). Reconstruction past seawater Mg/Ca and Sr/Ca from mid-ocean ridge flank calcium carbonate veins. *Science*, *327*, 1114–1117.

Collen, J. D. (1978). Biogenic collapse structures from Paleocene limestones, New Zealand. *Search*, *9*(11), 410–411.

Correns, C. W. (1978). Titanium. In K. H. Wedepohl (Ed.), *Handbook of Geochemistry* (pp. 22G1–22H1). Berlin: Springer.

Cramer, B. S., Miller, K. G., Barrett, P. J., & Wright, J. D. (2011). Late Cretaceous-Neogene trends in deep ocean temperature and continental ice volume: Reconciling records of benthic foraminiferal geochemistry (δ^{18}O and Mg/Ca) with sea level history. *Journal of Geophysical Research – Oceans*, *116*, 23.

Crampton, J. S. (1996). Inoceramid bivalves from the Late Cretaceous of New Zealand. *Institute of Geological and Nuclear Sciences Monograph*, *14*.

Crampton, J. S. (1997). The Cretaceous stratigraphy of the Southern Hawke's Bay – Wairarapa region. *Institute of Geological and Nuclear Sciences Report*, *97*(08), 92.

Crampton, J. S., Laird, M., Nicol, A., Townsend, D., & van Dissen, R. (2003). Palinspastic reconstructions of southeastern Marlborough, New Zealand, for mid-Cretaceous – Eocene times. *New Zealand Journal of Geology and Geophysics*, *46*, 153–175.

Crawford, J. C. (1868). Essay on the Geology of the North Island of New Zealand. *Transactions of the New Zealand Institute*, *1*, 304–328.

Creech, J. B. (2010). *Extracting reliable paleo-ocean temperatures at southern mid-latitudes during the greenhouse-icehouse transition - A LA-ICP-MS study of the trace element chemistry of Eocene foraminifera from New Zealand*. Victoria University of Wellington.

Creech, J. B., Baker, J. A., Hollis, C. J., Morgans, H. E. G., & Smith, E. G. C. (2010). Eocene sea temperatures for the mid-latitude southwest Pacific from Mg/Ca ratios in planktonic and benthic foraminifera. *Earth and Planetary Science Letters*, *299*, 483–495.

Crouch, E. M., & Brinkhuis, H. (2005). Environmental change across the Paleocene-Eocene transition from eastern New Zealand: a marine palynological approach. *Marine Micropaleontology*, *56*, 138–160.

Crouch, E. M., Dickens, G. R., Brinkhuis, H., Aubry, M.-P., Hollis, C. J., Rogers, K. M., & Visser, H. (2003). The Apectodinium acme and terrestrial discharge during the Paleocene– Eocene thermal maximum: new palynological, geochemical and calcareous nannoplankton observations at Tawanui, New Zealand. *Palaeogeography, Palaeoclimatology, Palaeoecology*, *19*(4), 387–403.

Crouch, E. M., Heilmann-Clausen, C., Brinkhuis, H., Morgans, H. E. G., Rogers, K. M., Egger, H., & Schmitz, B. (2001). Global dinoflagellate event associated with the late Paleocene thermal maximum. *Geology*, *29*(4), 315–318.

Dawber, C. F., & Tripati, A. K. (2011). Constraints on glaciation in the middle Eocene (46–37 Ma)from Ocean Drilling Program (ODP) Site 1209 in the tropical Pacific Ocean. *Paleoceanography*, *26*, 1–17.

Deltiel, J., de Lepinay, B. M., Morgans, H. E. G., & Field, B. D. (2006). Olistostromes marking tectonic events, East Coast, New Zealand. *New Zealand Journal of Geology and Geophysics*, *49*(4), 517–531.

Demars, K. R., & Chaney, R. C. (1982). *Geotechnical properties, behaviour, and performance of calcareous soils* (p. 414). ASTM International.

D'Hondt, S., Zachos, J. C., & Schultz, G. (1994). Stable isotopic signals and photosymbiosis in late Paleocene planktic foraminifera. *Paleobiology, 20*, 391–406.

Dickson, J. A. D. (2004). Echinoderm skeletal preservation: Calcite-aragonite seas and the Mg/Ca ratio of Phanerozoic oceans. *Journal of Sedimentary Research, 74*(3), 355–365.

Durrant, S. F., & Ward, N. I. (2005). Recent biological and environmental applications of laser ablation inductively coupled plasma mass spectrometry (LA-ICP-MS). *Journal of Analytical Atomic Spectrometry, 20*, 821–829.

Dymond, J., Suess, E. & Lyle, M. (1992). Barium in deep-sea sediment: a geochemical proxy for paleoproductivity. *Paleoceanography, 7:2*, 163-181.

Edwards, A. R. (1971). A calcareous nannoplankton zonation of the New Zealand Paleogene. In A. Farinacci (Ed.), *Proceedings of the II Planktonic Conference, Roma, 1970* (pp. 381–419). Rome: Edizioni Tecnoscienza.

Eggins, S., De Deckker, P., & Marshall, J. (2003). Mg/Ca variation in foraminifera tests: implications for reconstructing palaeo-seawater temperature and habitat migration. *Earth and Planetary Science Letters, 212*, 291–306.

Ehrmann, W. U., & Mackensen, A. (1992). Sedimentological evidence for the formation of an East Antarctic ice sheet in Eocene/Oliocene time. *Palaeogeography, Palaeoclimatology, Palaeoecology, 93*, 85–112.

Elderfield, H., & Ganssen, G. (2000). Past temperature and delta-18O of surface ocean waters inferred from foraminiferal Mg/Ca ratios. *Nature, 405*, 442–445.

Elderfield, H., Greaves, M., Barker, S., Hall, I. R., Tripati, A., Ferretti, P., Crowhurst, S., et al. (2010). A record of bottom water temperature and seawater d18O for the Southern Ocean over the past 440 kyr based on Mg/Ca of benthic foraminiferal Uvigerina spp. *Quaternary Science Reviews, 29*, 160–169.

Elderfield, H., & Schultz, A. (1996). Mid-ocean ridge hydrothermal fluxes and the chemical composition of the ocean. *Annual Review of Earth and Planetary Sciences*, *24*, 191–224.

Elderfield, H., Vautravers, M., & Cooper, M. (2002). The relationship between shell size and Mg/Ca, Sr/Ca, d18O, and d13C of species of planktonic foraminifera. *Geochemistry Geophysics Geosystems*, *3*(8).

Emiliani, C. (1955). Pleistocene temperatures. *Journal of Geology*, *63*, 538–578.

Epstein, S., Buchsbaum, R., Lowenstam, H., & Urey, H. C. (1951). Carbonate-water isotopic temperature scale. *Geological Society of America Bulletin*, *62*, 417–426.

Erez, J. (2003). The source of ions for biomineralization in foraminifera and their implications for paleoceanographic proxies. *Reviews in Mineralogy and Geochemistry*, *54*, 115–149.

Exon, N., Brinkhuis, H., Robert, C. M., Kennett, J. P., J., H. P., & Macphail, M. K. (2004). Tectono-sedimentary history of the Uppermost Cretaceous through Oligocene sequenbces from the Tasman region, a temperate Antarctic margin. In N. Exon, J. P. Kennett, & M. Malone (Eds.), *The Cenozoic Southern Ocean: Tectonics, Sedimentation, and climate change between Australia and Antarctica. American Geophysical Union, Washington. Geophysical Monograph 151* (pp. 319–344).

Field, B. D., & Hollis, C. J. (2003). Orbitally controlled cyclicity around the Cretaceous/Tertiary boundary, northern South Island, New Zealand. *New Zealand Journal of Geology and Geophysics*, *46*, 235–241.

Field, B. D., Uruski, C. I., Beu, A. G., Browne, G. H., Crampton, J. S., Funnell, R., Killops, S., et al. (1997). *Cretaceous-Cenozoic geology and petroleum systems of the East Coast Region, New Zealand. Institute of Geological and Nuclear Sciences monograph 19* (p. 301 + 7 enclosures). Lower Hutt, New Zealand: Institute of Geological & Nuclear Sciences Limited.

Frey, R. W. (Ed.). (1975). *The study of trace fossils* (p. 562). New York: Springer Verlag.

Frey, R. W., Pemberton, S. G., & Saunders, T. D. A. (1990). Ichnofacies and Bathymetry: A Passive Relationship. *Journal of Paleontology*, *64*(1), 155–158.

Furlong, K. P., & Kamp, P. J. J. (2009). The lithospheric geodynamics of plate boundary transpression in New Zealand: Initiating and emplacing subduction along the Hikurangi margin, and the tectonic evolution of the Alpine Fault system. *Tectonophysics*, *474*, 499–462.

Greaves, M., Barker, S., Daunt, C., & Elderfield, D. (2005). Accuracy, standardization, and interlaboratory calibration standards for foraminiferal Mg/Ca thermometry. *Geochemistry Geophysics Geosystems*, *6*(2), 1–9.

Hardie, L. A. (1996). Secular variation in seawater chemistry: An explanation for the coupled secular variation in the mineralogies of marine limestones and potash evaporites over the past 600 m.y. *Geology*, *24*(3), 279–283.

Hasiuk, F. J., & Lohmann, K. C. (2010). Application of calcite Mg partitioning functions to the reconstruction of paleocean Mg/Ca. *Geochimica et Cosmochimica Acta*, *74*(23), 6751–6763.

Hayward, B. W. & Buzas, M. A. (1979). Taxonomy and Paleoecology of Early Miocene Benthic Foraminifera of Northern New Zealand and the North Tasman Sea. *Smithsonian Contributions to Paleobiology; 36*, 164 p.

Hayward, B. W. (1986). A guide to paleoenvironmental assessment using New Zealand Cenozoic foraminiferal faunas. *New Zealand Geological Survey Report PAL*, *109*.

Hayward, B. W., Grenfell, H. R., Sabaa, A. T., Neil, H. L., & Buzas, M. A. (2010). Recent New Zealand deep-water benthic foraminifera: Taxonomy, ecologic distribution, biogeography, and use in paleoenvironmental assessment. *GNS Science Monograph*, *26*, 1–363.

Hayward, B. W., Scott, G. H., Crundwell, M. P., Kennett, J. P., Carter, L., Neil, H. L., Sabaa, A. T., et al. (2008). The effect of submerged plateaux on Pleistocene gyral circulation and sea-surface temperatures in the Southwest Pacific. *Global and Planetary Change*, *63*, 309–316.

Helby, R., Morgan, R., & Partridge, A. D. (1987). A palynological zonation of the Australian Mesozoic. In P. A. Jell (Ed.), *Studies in Australian Mesozoic palynology. Association of Australasian Palaeontologists Memoir 4* (pp. 1–94).

Hines, B. R., Atkins, C., Hollis, C. J., Morgans, H. E. G., Kulhanek, D., & Baker, J. A. (2011). The Early Eocene Succession at Tora, Wairarapa: Stratigraphy and Paleoclimate.

Hollis, C. J. (2002). Biostratigraphy and paleoceanographic significance of Paleocene radiolarians from offshore eastern New Zealand. *Marine Micropaleontology*, *46*(3-4), 265–316.

Hollis, C. J. (2006). Radiolarian faunal change across the Paleocene-Eocene boundary at Mead Stream, New Zealand. *Eclogae Geologicae Helvetiae*, *99*, 79–99.

Hollis, C. J., Beu, A. G., Crampton, J. S., Jones, C. M., Crundwell, M. P., Morgans, H. E. G., Raine, J. I., et al. (2010). Calibration of the New Zealand Cretaceous-Cenozoic Timescale to GTS2004. *GNS Science Report*, *2010*(43).

Hollis, C. J., Dickens, G. R., Field, B. D., Jones, C. M., & Strong, C. P. (2005a). The Paleocene-Eocene transition at Mead Stream, New Zealand: a southern Pacific record of early Cenozoic global change. *Palaeogeography, Palaeoclimatology, Palaeoecology*, *215*, 313–343.

Hollis, C. J., Field, B. D., Jones, C. M., Strong, C. P., Wilson, G. J., & Dickens, G. R. (2005b). Biostratigraphy and carbon isotope stratigraphy of uppermost Cretaceous-lower Cenozoic Muzzle Group in middle Clarence valley, New Zealand. *Journal of the Royal Society of New Zealand*, *35*(3), 345–383.

Hollis, C. J., Handley, L., Crouch, E. M., Morgans, H. E. G., Baker, J. A., Creech, J. B., Collins, K. S., et al. (2009). Tropical sea temperatures in the high-latitude South Pacific during the Eocene. *Geology*, *37*(2), 99–102.

Hollis, C. J., Strong, C. P., Rodgers, K. A., & Rogers, K. M. (2003). Paleoenvironmental changes across the Cretaceous/Tertiary boundary at Flaxbourne River and Woodside Creek, eastern Marlborough, New Zealand. *New Zealand Journal of Geology and Geophysics*, *46*(2), 177–197.

Hollis, C. J., Taylor, K. W., Handley, L., Pancost, R. D., Creech, J. B., Baker, J. A., Schouten, S., et al. (2010). Paleoclimate data-model comparisons for early Paleogene New Zealand, Abstract GC42C-04. *AGU Fall Meeting, 2010, 13-17 December*. San Francisco, CA.

Hollis, C. J., Taylor, K. W. R., Handley, L., Pancost, R. D., Huber, M., Creech, J. B., Hines, B. R., et al. (2012). Early Paleogene temperature history of the Southwest Pacific Ocean: Reconciling proxies and models. *Earth and Planetary Science Letters*, *349-350*, 53–66.

Hollis, C. J., Taylor, K. W. R., Pancost, R. D., Creech, J. B., Kennedy, E. M., Strong, C. P., Morgans, H. E. G., et al. (2011). An update on paleoclimate data-model comparisons for

the southwest Pacific. *Climate & Biota of the Early Paleogene, 5-8 June 2011, Salzburg, Austria: conference program and abstracts.* Wien, Austria: Geologische Bundesanstalt.

Horita, J., Zimmermann, H., & Holland, H. D. (2002). Chemical evolution of seawater during the Phanerozoic: Implications from the record of marine evaporates. *Geochimica et Cosmochimica Acta, 66*(24), 3733–3756.

Hornibrook, N. de B. (1992). New Zealand Cenozoic marine paleoclimates: a review based on the distribution of some shallow water and terrestrial biota. In R. Tsuchi & J. C. J. Ingle (Eds.), *Pacific Neogene: environment evolution and events* (pp. 83–106). Tokyo: University of Tokyo Press.

Hornibrook, N. de B., Brazier, R. C., & Strong, C. P. (1989). Manual of New Zealand Permian to Pleistocene Foraminiferal Biostratigraphy. *New Zealand Geological Survey Bulletin, 56*, 1–175.

Huber, M., Brinkhuis, H., Stickley, C. E., Döös, K., Sluijs, A., Warnaar, J., Schellenberg, A., et al. (2004). Eocene circulation of the Southern Ocean: Was Antarctica kept warm by subtropical waters? *Paleoceanography, 19*, 1–12.

Huber, M., & Caballero, R. (2003). Eocene El Nino: Evidence for robust tropical dynamics in the "hothouse." *Science, 299*, 877–881.

Huber, M., & Caballero, R. (2011). The early Eocene equable climate problem revisited. *Climate of the Past Discussions, 7*, 241–304.

Huber, M., & Sloan, L. C. (2001). Heat transport, deep waters, and thermal gradients: coupled simulation of Eocene Greenhouse Climate. *Geophysical Research Letters, 28*(18), 3481–3484.

Jackson, N. (2000). *Contributuion of glaucony to the chronology of mid-Oligocene strata in New Zealand.* Victoria University of Wellington. 149 pp.

Kaiho, K. (1994). Benthic foraminiferal dissolved-oxygen index and dissolved-oxygen levels in the modern ocean. *Geology, 22*, 719–722.

Kaiho, K., Arinobu, T., Ishiwatari, R., Morgans, H. E. G., Okada, H., Takeda, N., Tazaki, Z. G., et al. (1996). Latest Paleocene benthic foraminiferal extinction and environmental changes at Tawanui, New Zealand. *Paleoceanography, 11*(4), 447–467.

Kaiho, K., Morgans, H. E. G., & Okada, H. (1993). Faunal turnover of intermediate water benthic foraminifera during the Paleogene in New Zealand. *Marine Micropaleontology*, *23*, 51–86.

Kaiho, K., Takeda, K., Petrizzo, M. R., & Zachos, J. C. (2006). Anomalous shifts in tropical Pacific planktonic and benthic foraminiferal test size during the Paleocene–Eocene thermal maximum. *Palaeogeography, Palaeoclimatology, Palaeoecology*, *237*(456-464).

Kane, I. A., & Hodgson, D. M. (2011). Sedimentological criteria to differentiate submarine channel levee subenvironments: Exhumed examples from the Rosario Fm. (Upper Cretaceous) of Baja California, Mexico, and the Fort Brown Fm. (Permian), Karoo Basin, S. Africa. *Marine and Petroleum Geology*, *28*, 807–823.

Kelly, D. C., Zachos, J. C., Bralower, T. J., & Schellenberg, S. A. (2005). Enhanced terrestrial weathering/runoff and surface ocean carbonate production during the recovery stages of the Paleocene-Eocene thermal maximum. *Paleoceanography*, *20*, 1–11.

Kennett, J. P., Houtz, R. E., Andrews, P. B., Edwards, A. R., Gostin, V. A., Hajos, M., Hampton, M., et al. (1975). Cenozoic paleoceanography in the Southwest Pacific Ocean, Antarctic glaciation, and the development of the Circum-Antarctic Current. *Initial reports of the Deep Sea Drilling Project*, *29*, 1155–1169.

Kennett, J. P. & Exon, N. F. (2004). Paleoceanographic evolution of the Tasmanian Seaway and its climatic implications. *AGU Geophysical Monograph Series, 151*, 345-367.

Killops, S. D., Hollis, C. J., Morgans, H. E. G., Sutherland, R., Field, B. D., & Leckie, D. A. (2000). Paleoceanographic significance of Late Paleocene dysaerobia at the shelf/slope break around New Zealand. *Palaeogeography, Palaeoclimatology, Palaeoecology*, *156*, 51–70.

Kim, J.-H., van der Meer, J., Schouten, S., Helmke, P., Willmott, V., Sangiorgi, F., Koc, N., et al. (2010). New indices and calibrations derived from the distribution of crenarchaeal isoprenoid tetraether lipids: Implications for past sea surface temperature reconstructions. *Geochimica et Cosmochimica Acta*, *74*(16), 4639–4654.

King, L. C. (1930). Raised beaches and other features of the South-east coast of the North Island of New Zealand. *Transactions of the New Zealand Institute*, *61*, 498–523.

King, P. R. (2000). New Zealand's changing configuration in the last 100 million years: plate tectonics, basin development, and depositional setting. *New Zealand Petroleum Conference Proceedings, 19–22 March 2000, Christchurch Convention Centre, New Zealand. Ministry of Economic Development, Wellington.* (pp. 131–145).

King, P. R., Naish, T. R., Browne, G. H., Field, B. D., & Edbrooke, S. W. (1999). Cretaceous to Recent sedimentary patterns in New Zealand. *Institute of Geological and Nuclear Sciences Folio Series*, *1*, 1–35.

Kirk, C. M. (1966). *The petrography of a redeposited section in the Manurewa Formation, and some greensand dykes from the Mungaroa Limestone, Te Kau Kau Point, S.E. Wairarapa.* Victoria University of Welllington.

Kozdon, R., Kelly, D. C., Kita, N. T., Fournelle, J. H., & Valley, J. W. (2011). Planktonic foraminiferal oxygen isotope analysis by ion microprobe technique suggests warm tropical sea surface temperatures during the early Paleogene. *Paleoceanography*, *26*, 1–17.

Kump, L. R., Brantley, S. L., & Arthur, M. A. (2000). Chemical weathering, atmospheric CO2, and climate. *Annual Review of Earth and Planetary Sciences*, *28*, 611–667.

Laird, M. G., Bassett, K. N., Schiøler, P., Morgans, H. E. G., Bradshaw, J. D., & Weaver, S. D. (2003). Paleoenvironmental and tectonic changes across the Cretaceous/Tertiary Boundary at Tora, southeast Wairarapa, New Zealand: a link between Marlborough and Hawkes Bay. *New Zealand Journal of Geology and Geophysics*, *46*, 275–293.

Lawver, L. A., Gahagan, L. M., & Coffin, M. F. (1992). The development of paleoseaways around Antarctica. In J. P. Kennett & D. A. Warnke (Eds.), *The Antarctic paleoenvironment: a perspective on global change* (pp. 7–30). Washington, DC: American Geophysical Union.

Lea, D., & Boyle, E. A. (1989). Barium content of benthic foraminifera controlled by bottom-water composition. *Nature*, *338*, 751–753.

Lea, D. W. (1999). Trace elements in foraminiferal calcite. In B. K. S. Gupta (Ed.), *Modern foraminfera* (pp. 259–277). Great Britain: Kluwer Academic Publishers.

Lea, D. W., & Boyle, E. A. (1991). Barium in planktonic foraminifera. *Geochemica et Cosmochemica Acta*, *55*, 3321–3331.

Lea, D. W., & Martin, P. A. (1996). A rapid mass spectrometric method for the simultaneous analysis of barium, cadmium, and strontium in foraminfera shells. *Geochimica et Cosmochimica Acta*, *60*(16), 3143–3149.

Lea, D. W., Mashiotta, T. A., & Spero, H. J. (1999). Controls on magnesium and strontium uptake in planktonic foraminifera determined by live culturing. *Geochemica et Cosmochemica Acta*, *63*, 2369–2379.

Lea, D. W., Pak, D. K., & Spero, H. J. (2000). Climate impact of late Quaternary equatorial Pacific sea surface temperature variations. *Science*, *289*, 1719–1724.

Lear, C., Elderfield, H., & Wilson, P. (2003). A Cenozoic seawater record from benthic foraminiferal calcite and its application in determining global weathering fluxes. *Earth and Planetary Science Letters*, *208*, 69–84.

Lear, C., Elderfield, H., & Wilson, P. A. (2000). Cenozoic deep-sea temperatures and global ice volumes form Mg/Ca in benthic foraminiferal calcite. *Science*, *287*, 269–272.

Lear, C. H., Mawbey, E. M., & Rosenthal, Y. (2010). Cenozoic benthic foraminiferal Mg/Ca and Li/Ca records: Toward unlocking temperatures and saturation states. *Paleoceanography*, *25*(4), 4215.

Lear, C. H., Rosenthal, Y., & Slowey, N. (2002). Benthic foraminiferal Mg/Ca-paleothermometry: a revised core-top calibration. *Geochimica et Cosmochimica Acta*, *66*, 3375–3387.

Lee, D. E., Lee, W. G., & Mortimer, N. (2001). Where and why have all the flowers gone? Depletion and turnover in the New Zealand Cenozoic angiosperm flora in relation to palaeogeography and climate. *Australian Journal of Botany*, *49*, 341–356.

Lee, J. M. (1995). *A stratigraphic, biostratigraphic and structural analysis of the geology at Huatokitoki Stream, Glenburn, southern Wairarapa, New Zealand*. Victoria University of Wellington.

Lee, J. M., & Begg, J. G. (2002). *Geology of the Wairarapa Area. Institute of Geological and Nuclear Sciences 1:250 000 geological map 11* (p. 66 +1 sheet). Lower Hutt, New Zealand: Institute of Geological & Nuclear Sciences Limited.

Lillie, A. R. (1953). Geology of the Dannevirke Subdivision. *New Zealand Geological Survey Bulletin*, *46*, 1–156.

Little, T. A., Van Dissen, R., Schermer, E., & Carne, R. (2009). Late Holocene surface ruptures on the southern Wairarapa fault, New Zealand: Link between earthquakes and the uplifting of beach ridges on a rocky coast. *Lithosphere*, *1*(1), 4–28.

Liu, Z., Pagani, M., Zinniker, D., DeConto, R., Huber, M., Brinkhuis, H., Shah, S. R., et al. (2009). Global Cooling During the Eocene-Oligocene Climate Transition. *Science*, *323*, 1187–1190.

Loeppert, R. H., & Suarez, D. L. (1996). Carbonate and gypsum. In D. L. Sparks, P. A. L., P. A. Helmke, R. H. Loeppert, S. P. N., M. A. Tabatabai, C. T. Johnston, et al. (Eds.), *Methods of soil analysis. Part Three.* (3rd ed., pp. 437–474). Madison, WI: Soil Science Society of America Inc.

Lowenstein, T. K., & Demicco, R. V. (2006). Elevated Eocene Atmospheric CO2 and its subsequent decline. *Science*, *313*, 1928.

Lowenstein, T. K., N., T. M., Brennan, S. T., Hardie, L. A., & Demicco, R. V. (2001). Oscillations in Phanerozoic seawater chemistry: evidence from fluid inclusions. *Science*, *294*, 1086–1088.

Lyle, M., Gibbs, S., Moore, T. C. & Rea, D. K. (2007). Late Oligocene initiation of the Antarctic Circumpolar Current: Evidence from the South Pacific. *Geology, 35:8*, 691-694.

Macpherson, E. O. (1952). The stratigraphy and bentonitic shale deposits of Kekerengu and Blue Slip, Marlborough. *New Zealand Journal of Science and Technology*, *33*(b), 258–286.

Marchitto, T. M., Curry, W. B., & Oppo, D. W. (2000). Zinc concentrations in benthic foraminifera reflect seawater chemistry. *Paleoceanography*, *17*, 299–306.

Marr, J. P., Baker, J. A., Carter, L., Allan, A. S. R., Dunbar, G. B., & Bostock, H. C. (2011). Ecological and temperature controls on Mg/Ca ratios of Globigerina bulloides from the southwest Pacific Ocean. *Paleoceanography*, *26*, 1–15.

Marriott, C. S., Henderson, G. M., Crompton, R., Staubwasser, M., & Shaw, S. (2004). Effect of mineralogy, salinity, and temperature on Li/Ca and Li isotope composition of calcium carbonate. *Chemical Geology*, *212*, 5–15.

Martin, P. A., & Lea, D. W. (2002). Comparison of water mass changes in the deep tropical Atlantic derived from Cd/Ca and carbon isotope records: Implications for changing Ba composition of deep Atlantic water masses. *Paleoceanography*, *13*, 572–585.

Martini, E. (1971). Standard Tertiary and Quaternary calcareous nannoplankton zonation. In A. Farinacci (Ed.), *Proceedings of the II Planktonic Conference, Roma, 1970* (pp. 289–290). Rome: Edizioni Tecnoscienza.

Mathien-Blard, E., & Bassinot, F. (2009). Salinity bias on the foraminifera Mg/Ca thermometry: Correction procedure and implications for past ocean hydrographic reconstructions. *Geochemistry Geophysics Geosystems*, *10*, 1–17.

McInerney, F. A., & Wing, S. L. (2011). The Paleocene-Eocene Thermal Maximum: A Perturbation of Carbon Cycle, Climate, and Biosphere with Implications for the Future. *Annual Review of Earth and Planetary Sciences*, *39*(1), 489–516.

McKay, A. (1878). Report on east Wairarapa district. *New Zealand Geological Survey Reports of geological explorations 1887-78*, *11*, 14–24.

McLean, D. B. G. (1953). *Geology of the Haurangi Stoney Creek area S.E. Wairarapa*. Victoria University of Wellington.

Miller, K. G., Wright, J. D., & Browning, J. V. (2005). Visions of ice sheets in a greenhouse world. *Marine Geology*, *217*, 215–231.

Moore, P. R. (1980). Late Cretaceous-Tertiary stratigraphy, structure, and tectonic history of the area between Whareama and Ngahape, eastern Wairarapa, New Zealand. *New Zealand Journal of Geology and Geophysics*, *23*, 167–177.

Moore, P. R. (1986). A revised Cretaceous-Early Tertiary stratigraphic nomenclature for Eastern North Island, New Zealand. *New Zealand Geological Survey Report*, *G104*.

Moore, P. R. (1988a). Stratigraphy, composition and environment of deposition of the Whangai Formation and associated Late Cretaceous-Paleocene rocks, eastern North Island, New Zealand. *New Zealand Geological Survey Bulletin, 100*.

Moore, P. R. (1988b). Structural divisions of eastern North Island. *New Zealand Geological Survey Record, 30*, 1–24.

Moore, P. R. (1989a). Stratigraphy of the Waipawa Black Shale (Paleocene), eastern North Island, New Zealand. *New Zealand Geological Survey record, 38*.

Moore, P. R. (1989b). Kirks Breccia: A Late Cretaceous Submarine channelized debris flow deposit, Raukumara Peninsula, New Zealand. *Journal of the Royal Society of New Zealand, 19*, 195–203.

Moore, P. R., & Morgans, H. E. G. (1987). Two new reference sections for the Wanstead Formation (Paleocene-Eocene) in southern Hawkes Bay. *New Zealand Geological Survey Record, 20*, 81–87.

Moore, P. R., & Morgans, H. E. G. (1990). Unpublished section studies of Awheaiti, Pukemuri and Te Oroi Streams for the Cretaceous-Cenozoic Programme. East Coast CCP (Late Cretaceous-Paleogene). Section 16 (EC-16), Section 17 (EC-17), Section 18 (EC-18) - Unpublished sections. Lower Hutt, New Zealand: GNS Science.

Moore, P. R., & Speden, I. G. (1984). The Early Cretaceous (Albian) sequence of eastern Wairarapa, New Zealand. *New Zealand Geological Survey Bulletin, 97*, 1–98.

Morel, F. M. M., Hudson, R. J. M., & Price, N. M. (1991). Limitation of productivity by trace metals in the sea. *Limnology and Oceanography, 36*(8), 1742–1755.

Morel, F. M. M., & Price, N. M. (2003). The biogeochemical cycles of trace metals in the oceans. *Science, 300*, 944–947.

Morgan, D. J., Jerram, D. A., Chertkoff, D. G., Davidson, J. P., Pearson, D. G., Kronz, A., & Nowell, G. M. (2007). Combining CSD and isotopic microanalysis: Magma supply and mixing processes at Stromboli Volcano, Aeolian Islands, Italy. *Earth and Planetary Science Letters, 260*, 419–431.

Morgans, H. E. G. (2009). Late Paleocene to middle Eocene foraminferal biostratigraphy of the Hampden Beach section, eastern South Island, New Zealand. *New Zealand Journal of Geology and Geophysics*, *52*, 273–320.

Morkhoven, P. C. M., Berggren, W. A., & Edwards, A. S. (1986). Cenozoic cosmopolitan deep-water benthic foraminifera. *Bulletin des Centre de Recherches Exploration-Production Elf-Aquitaine Memoires*, *11*, 1–421.

Mucci, A., & Morse, J. W. (1983). The incorporation of Mg2+ and Sr2+ into calcite overgrowths: influences of growth rate and solution composition. *Geochimica et Cosmochimica Acta*, *47*, 217–233.

Murphy, M. G., & Kennett, J. P. (1986). Development of latitudinal thermal gradients during the Oligocene: oxygen-isotope evidence from the Southwest Pacific. *Initial Reports of the Deep Sea Drilling Project*, *90*, 1347–1360.

Murray, R. W., & Leinen, M. (1996). Scavenged excess aluminum and its relationship to bulk titanium in biogenic sediment from the central equatorial Pacific Ocean. *Geochimica et Cosmochimica Acta*, *60*(20), 3869–3878.

Neef, G. (1992). Geology of the Akitio area (1:50 000 metric sheet U25BD, east), northeastern Wairarapa, New Zealand. *New Zealand Journal of Geology and Geophysics 35:4*, 533–548.

Nelson, C. S., & Cooke, P. J. (2001). History of oceanic front development in the New Zealand sector of the Southern Ocean during the Cenozoic: a synthesis. *New Zealand Journal of Geology and Geophysics*, *44*(4), 535–553.

Nelson, C. S., & Smith, A. M. (1996). Stable oxygen and carbon isotope compositional fields for skeletal and diagenetic components in New Zealand Cenozoic nontropical carbonate sediments and limestones: a synthesis and review. *New Zealand Journal of Geology and Geophysics*, *39*, 93–107.

Nicol, A., Mazengarb, C., Chanier, F., Rait, G., Uruski, C., & Wallace, L. (2007). Tectonic evolution of the active Hikurangi subduction margin, New Zealand, since the Oligocene. *Tectonics*, *26*, 1–24.

Nicolo, M. J., Dickens, G. R., Hollis, C. J., & Zachos, J. C. (2007). Multiple early Eocene hyperthermals: Their sedimentary expression on the New Zealand continental margin and in the deep sea. *Geology*, *35*(8), 699–702.

Nürnberg, D. (1995). Magnesium in tests of Neogloboquadrina pachyderma sinstral from high northern and southern latitudes. *Journal of Foraminiferal Research*, *25*, 350–368.

Nürnberg, D., Bijma, J., & Hemleben, C. (1996). Assessing the reliability of magnesium in foraminiferal calcite as a proxy for water mass temperatures. *Geochimica et Cosmochimica Acta*, *60*, 803–814.

Okada, H., & Thierstein, H. R. (1979). Calcareous plankton – Leg 43, Deep Sea Drilling Project. In B. E. Tucholke & P. R. Vogt (Eds.), *Initial Reports of the Deep Sea Drilling Project, 43* (pp. 507–573). Washington: US Govt. Printing Office.

Onasch, C. M., & Kahle, C. F. (2002). Seismically induced soft-sediment deformation in some Silurian carbonates, eastern U.S. Midcontinent. *Geological Society of America Special Paper 359 Ancient Seismites*, 165–175.

Oomori, T., Kaneshima, H., & Maezato, Y. (1987). Distribution coefficient of Mg2+ ions between calcite and solution at 10–50°C. *Marine Chemistry*, *20*(4), 327–336.

Orians, K. J., Boyle, E. A., & Bruland, K. W. (1990). Dissolved titanium in the open ocean. *Nature*, *348*, 322–325.

Paytan, A., & Griffith, E. M. (2007). Marine barite: Recorder of variatins in ocean export productivity. *Deap Sea Research Part II: Topical Studies in Oceanography*, *54*(5-7), 687–705.

Pearce, N. J. G., Perkins, W. T., Westgate, J. A., Gordon, M. P., Jackson, S. E., Neal, C. R., & Chenery, S. P. (1997). A compilation of new and published major and trace element data for NIST SRM 610 and NIST SRM 612 glass reference materials. *Geostandards Newsletter*, *21*(1), 115–144.

Pearson, P. N., & Burgess, C. E. (2008). Foraminifer test preservation and diagenesis: comparison of high latitude Eocene sites. *Geological Society of London, Special Publications*, *303*, 59–72.

Pearson, P. N., Ditchfield, P. W., Singaro, J., Harcourt-Brown, K. G., Nicholas, C. J., Olsson, R. K., Shackleton, N. J., et al. (2001). Warm tropical sea surface temperatures in the Late Cretaceous and Eocene epochs. *Nature*, *413*, 481–487.

Pearson, P. N., Olsson, R. K., Huber, B. T., Hemleben, C., & Berggren, W. A. (Eds.). (2006). *Atlas of Eocene planktonic foraminifera. Cushman Foundation Special Publication 41* (p. 514).

Pearson, P. N., van Dongen, B. E., Nicholas, C. J., Pancost, R. D., Schouten, S., Singano, J. M., & Wade, B. S. (2007). Stable warm tropical climate through the Eocene Epoch. *Geology*, *35*(3), 211–214.

Pemberton, S. G., MacEachern, J. A., & Frey, R. W. (1992). Trace fossil facies models: environmental and allostratigraphic significance. In R. G. Walker & N. P. James (Eds.), *Facies Models: response to sea level change* (pp. 47–72). Geological Association of Canada.

Pena, L. D., Calvo, E., Cacho, I., Eggins, S., & Pelejero, C. (2005). Identification and removal of Mn-Mg-rich contaminant phases on foraminiferal tests: Implications for Mg/Ca past temperature reconstructions. *Geochemistry Geophysics Geosystems*, *6*(9), 1–25.

Perch-Nielsen, K. (1985). Cenozoic calcareous nannofossils. In H. Bolli, K. Perch-Nielsen, & J. B. Saunders (Eds.), *Plankton Stratigraphy* (pp. 427–554). New York: Cambridge University Press.

Peters, R. B., & Sloan, L. C. (2000). High concentrations of greenhouse gases and polar stratospheric clouds: a possible solution to high latitude faunal migration at the latest Paleocene thermal maximum. *Geology*, *28*(11), 979–982.

Petrizzo, M. R., Leoni, G., Speijer, R. P., De Bernardi, B., & Felletti, F. (2008). Dissolution susceptibility of some Paleogene planktonic foraminifera from ODP site 1209 (Shatsky Rise, Pacific Ocean. *The Journal of Foraminiferal Research*, *38*(4), 357–371.

Potts, P. J. (1987). *A Handbook of Silicate Rock Analysis* (p. 622). Glasgow: Blackie and Son Limited.

Quillévéré, F., Norris, R. D., Moussa, I., & Berggren, W. A. (2001). Role of photosymbiosis and biogeography in the diversification of early Paleogene acarininids (planktonic foraminifera). *Paleobiology*, *27*(2), 311–326.

Raiswell, R., Buckley, F., Berner, R. A., & Anderson, T. F. (1988). Degree of pyritization of iron as a paleoenvironmental indicator of bottom-water oxygenation. *Journal of Sedimentary Research*, *58*(5), 812–819.

Ravizza, G., Norris, R. N., Blusztajn, J., & Aubry, M.-P. (2001). An osmium isotope excursion associated with the late Paleocene thermal maximum: Evidence of intensified chemical weathering. *Paleoceanography*, *16*(2), 155–163.

Reay, M. B. (1993). *Geology of the middle part of the Clarence Valley. Institute of Geological & Nuclear Sciences Geological Map 10* (p. 144 +1 map).

Rogers, K. M., Morgans, H. E. G., & Wilson, G. S. (2001). Identification of a Waipawa Formation equivalent in the upper Te Uri Member of the Whangai Formation - implications for depositional history and age. *New Zealand Journal of Geology and Geophysics*, *44*(2), 347–354.

Rosenthal, Y., Boyle, E. A., & Slowey, N. (1997). Temperature control on the incorporation of magnesium, strontium, fluorine, and cadmium into benthic foraminifera shells from Little Bahama Bank: Prospects for thermocline paleoceanography. *Geochimica et Cosmochimica Acta*, *61*, 3633–3643.

Rosenthal, Y., Field, M. P., & Sherrell, R. M. (1999). Precise determination of element/calcium ratios in calcareous samples using sector field inductively coupled plasma mass spectrometry. *Analytical Chemistry*, *71*(15), 3248–3253.

Rosenthal., Y., Lear, C. H., Oppo, D. W., & Linsley, B. K. (2006). Temperature and carbonate ion effects on Mg/Ca and Sr/Ca ratios in benthic foraminifera: Aragonitic species Hoeglundina elegans. *Paleoceanography*, *21*, 1–14.

Sadekov, A., Eggins, S. M., De Deckker, P., & Kroon, D. (2008). Uncertainties in seawater thermometry deriving the intratest and intertest Mg/Ca variability in Globigerinoides ruber. *Paleoceanography*, *23*, 1–12.

Sadekov, A., Eggins, S. M., De Deckker, P., Ninnemann, U., Kuhnt, W., & Bassinot, F. (2009). Surface and subsurface seawater temperature reconstruction using Mg/Ca microanalysis of planktonic foraminifera Globigerinoides ruber, Globigerinoides sacculifer, and Pulleniatina obliquiloculata. *Paleoceanography*, *24*, 1–17.

Sadekov, A., Yu, S., Eggins, M., & De Deckker, P. (2005). Characterization of Mg/Ca distributions in planktonic foraminifera species by electron microprobe mapping. *Geochemistry Geophysics Geosystems*, *6*.

Savenko, V. (2008). Concentrating function of plankton and the residency time of dissolved species of chemical elements in the ocean. *Geochemistry International*, *46*(2), 190–192.

Scheibner, C., Speijer, R. P., & Marzouk, A. M. (2005). Turnover of larger foraminifera during the Paleocene-Eocene Thermal Maximum and paleoclimatic control on the evolution of platform ecosystems. *Geology*, *33*(6), 493–496.

Schiøler, P., Rogers, K., Sykes, R., Hollis, C. J., Ilg, B., Meadows, D., Roncaglia, L., et al. (2010). Palynofacies, organic geochemistry and depositional environment of the Tartan Formation (Late Paleocene), a potential source rock in the Great South Basin, New Zealand. *Marine and Petroleum Geology*, *27*(2), 351–369.

Schiøler, P., & Wilson, G. J. (1998). Dinoflagellate biostratigraphy of the middle Coniacian-lower Campanian (Upper Cretaceous) in south Marlborough, New Zealand. *Micropaleontology*, *44*, 313–349.

Schmitze, B., & Pujalte, V. (2007). Abrupt increase in seasonal extreme precipitation at the Paleocene-Eocene boundary. *Geology*, *35*(3), 215–218.

Schouten, S., Hopmans, E. C., Schefuβ, E., & Sinninghe Damste, J. S. (2002). Distributional variations in marine crenarchaeotal membrane lipids: a new tool for reconstructing ancient sea water temperatures? *Earth and Planetary Science Letters*, *204*(1-2), 265–274.

Schrag, D. P., DePaolo, D. J., & Richter, F. M. (1995). Reconstructing past sea surface temperatures: correcting for diagenesis of marine bulk cabonate. *Geochimica et Cosmochimica Acta*, *59*(11), 2265–2278.

Segev, E., & Erez, J. (2006). Effect of Mg/Ca ratio in seawater on shell composition in shallow benthic foraminifera. *Geochemistry Geophysics Geosystems*, *7*(2), Q02P09

Sexton, P. F., Wilson, P. A., & Pearson, P. N. (2006a). Microstructural and geochemical perspectives on planktic foraminiferal preservation: "'Glassy'" versus "'Frosty'." *Geochemistry Geophysics Geosystems*, *7*(12), 1–29.

Sexton, P. F., Wilson, P. A., & Pearson, P. N. (2006b). Palaeoecology of late middle Eocene planktic foraminifera and evolutionary implications. *Marine Micropaleontology*, *60*, 1–16.

Shackleton, N., & Boersma, A. (1981). The climate of the Eocene ocean. *Journal of the Geological Society*, *138*, 153–157.

Shackleton, N. J. (1987). Oxygen isotopes, ice volume and sea level. *Quaternary Science Reviews*, *6*, 183–190.

Shackleton, N. J., & Kennett, J. P. (1975). Paleotemperature history of the Cenozoic and the initiation of Antarctic glaciation: oxygen and carbon isotope analyses in DSDP sites 277, 279, and 281. *Initial reports of the Deep Sea Drilling Project*, *29*, 743–755.

Shackleton, N. J., & Opdyke, N. D. (1973). Oxygen Isotope and Palaeomagnetic Stratigraphy of Equatorial Pacific Core V28-238: Oxygen Isotope Temperatures and Ice Volumes on a 105 Year and 106 Year Scale. *Quaternary Research*, *3*, 39–55.

Sharp, Z. (2007). *Principles of stable isotope geochemistry* (p. 334). New Jersey: Pearson Prentice Hall.

Shimmield, G. B., Price, N. B., & Kahn, A. A. (1988). The use of Th-230 and Ba as indicators of paleoproductivity over a 300 Kyr timescale-Evidence from the Arabian Sea. *Chemical Geology*, *70*, 112.

Simaeys, S. V., Brinkhuis, H., Pross, J., Williams, G. L., & Zachos, J. C. (2005). Arctic dinoflagellate migrations mark the strongest Oligocene glaciations. *Geology*, *33*(9), 709–712.

Singh, L. J. (1971). Uplift and tilting of the Oterei Coast, Wairarapa, New Zealand, during the last ten thousand years. In Recent Crustal Movements. *Royal Society of New Zealand Bulletin*, *9*, 217–219.

Skrabal, S. A., & Terry, C. M. (2002). Distributions of dissolved titanium in porewaters of estuarine and coastal marine sediments. *Marine Chemistry*, *77*(2), 109–122.

Slotnick, B. S., Dickens, G. R., Nicolo, M. J., Hollis, C. J., Crampton, J. S., Zachos, J. C., & Sluijs, A. (2012). Large-Amplitude Variations in Carbon Cycling and Terrestrial Weathering during the Latest Paleocene and Earliest Eocene: The Record at Mead Stream, New Zealand. *Journal of Geology*, *120*(5), 487–505.

Sluijs, A., Bijl, P. K., Schouten, S., Röhl, U., Reichart, G.-J., & Brinkhuis, H. (2011). Southern ocean warming, sea level and hydrological change during the Paleocene-Eocene Thermal Maximum. *Climate of the Past*, *7*, 47–61.

Speer, J. A. (1983). Crystal chemistry and phase relations in orthorhombic carbonates. *Reviews in Mineralogy and Geochemistry*, *11*, 145–190.

Stanley, S. M., & Hardie, L. A. (1998). Secular oscillations in the carbonate mineralogy of reef-building and sediment-producing organisms driven by tectonically forced shifts in seawater chemistry. *Palaeogeography, Palaeoclimatology, Palaeoecology*, *144*, 3–19.

Strachan, L. J., & Alsop, G. I. (2006). Slump folds as estimators of palaeoslope: a case study from the Fisherstreet Slump of County Clare, Ireland. *Basin Research*, *18*(4), 451–470.

Strong, C. P., Hollis, C. J., & Wilson, G. J. (1995). Foraminiferal, radiolarian, and dinoflagellate biostratigraphy of Late Cretaceous to middle Eocene pelagic sediments (Muzzle Group), Mead Stream, Marlborough, New Zealand. *New Zealand Journal of Geology and Geophysics*, *38*(2), 171–209.

Tayler, M. J. S. (2011). *Investigating stratigraphic evidence for Antarctic glaciation in the greenhouse world of the Paleocene, eastern North Island, New Zealand*. University of Waikato.

Thayer, P. A., Roberts, H. H., Bouma, A. H., & Coleman, J. M. (1986). Sedimentology and petrology of Mississippi fan depositional environments, deep sea drilling project leg 96. In A. H. Bouma, J. M. Coleman., & A. W. Meyer (Eds.), *Initial reports of the Deep Sea Drilling Project. Vol. 96* (pp. 489–503). Washington: US Govt. Printing Office.

Thomas, D. J., Zachos, J. C., Bralower, T. J., Thomas, E., & Bohaty, S. M. (2002). Warming the fuel for the fire: Evidence for the thermal dissociation of methane hydrate during the Paleocene-Eocene thermal maximum. *Geology*, *30*(12), 1067–1070.

Tjalsma, R. C., & Lohmann, G. P. (1983). Paleocene-Eocene bathyal and abyssal benthic foraminifera from the Atlantic Ocean. *Micropaleontology Special Publications*, *4*, 1–90.

Tripati, A. K., Delaney, M. L., Zachos, J. C., Anderson, L. D., Kelly, D. C., & Harry, E. (2003). Tropical sea-surface temperature reconstruction for the early Paleogene using Mg/Ca ratios of planktonic foraminifera. *Paleoceanography*, *18*, 1101.

Tripati, A. K., & Elderfield, H. (2004). Abrupt hydrographic changes in the equatorial Pacific and subtropical Atlantic from foraminiferal Mg/Ca indicate greenhouse origin for the thermal maximum at the Paleocene-Eocene Boundary. *Geochemistry Geophysics Geosystems*, *5*, 11.

Tripati, A. K., Allmon, W.D., Sampson, D. E. (2009). Possible evidence for a large decrease in seawater strontium/calcium ratios and strontium concentrations during the Cenozoic. *Earth and Planetary Science Letters,* 282, 122-130.

Tucker, M. E. (2011). *Sedimentary Rocks in the Field - a practical guide* (p. 275). Sussex: John Wiley and Sons, Ltd.

Urey, H. C. (1947). The thermodynamic properties of isotopic substances. *Journal of the Chemical Society*, 562–581.

Uruski, C. I. (2010). Breaking new ground, again! The Pegasus Basin of North Island, New Zealand. *New Zealand petroleum conference proceedings; Crown Minerals, Ministry of Economic Development, Wellington, New Zealand (2010).*

Uruski, C. I. & Bland, K. J. (2011). Pegasus Basin and the prospects for oil and gas. GNS Science Consultancy Report 2010/291.

Van De Heuval, H. B. (1960). The geology of the Flat Point area, eastern Wairarapa. *New Zealand Journal of Geology and Geophysics*, *3*(2), 309–320.

Vellekoop, J. (2010). *Unravelling Paleoenvironmental Changes Across the Cretaceous-Paleogene Boundary in New Zealand.* Utrecht University.

Wade, B. S. (2004). Planktonic foraminiferal biostratigraphy and mechanisms in the extinction of Morozovella in the late middle Eocene. *Marine Micropaleontology*, *51*, 23–38.

Wade, B. S., Al-Sabouni, N., Hemleben, C., & Kroon, D. (2008). Symbiont bleaching in fossil planktonic foraminifera. *Evolutionary Ecology*, *22*, 253–265.

Walker, R. G. (1975). Generalised facies models for resedimented conglomerates of turbidite association. *Geological Association of America Bulletin*, *86*, 737–748.

Walker, R. G. (1978). Deep-water sandstone facies and ancient submarine fans: Models for exploration for stratigraphic traps. *AAPG Bulletin*, *62*(6), 932–966.

Walker, R. G., & James, N. P. (1992). *Facies Models: response to sea level change* (p. 454). Geological Association of Canada.

Wasmuth, C. (1996). *Biological and Lithological Changes in the Late Haumurian-Teurian Strata (Cretaceous-Tertiary Boundary, at Tora, Southern Wairarapa, New Zealand*. Victoria University of Wellington.

Waterhouse, J. B. (1955). *Geology of the White Rock-Tora Area, South East Wairarapa*. Victoria University of Wellington.

Waterhouse, J. B., & Bradley, J. (1957). Redeposition and Slumping in the Cretaceo-Tertiary Strata of S.E Wellington. *Transactions of the Royal Society of New Zealand*, *84*, 519–548.

Webby, B. D. (1969). Trace fossils Zoophycos and Chondrites from the Tertiary of New Zealand. *New Zealand Journal of Geology and Geophysics*, *12*(1), 208–214.

Weldeab, S., Schneider, R. R., & Kolling, M. (2006). Comparison of foraminiferal cleaning procedures for Mg/Ca paleothermometry on core material deposited under varying terrigenous-input and bottom water conditions. *Geochemistry Geophysics Geosystems*, *7*, 1–8.

Wellman, H. W. (1971). Holocene tilting and uplift on the White Rocks coast, Wairarapa, New Zealand. In Recent Crustal Movements. *Royal Society of New Zealand Bulletin*, *9*, 211–215.

Westerhold, T., Röhl, U., Donner, B., McCarren, H. K., & Zachos, J. C. (2011). A complete high-resolution Paleocene benthic stable isotope record for the Central Pacific (ODP Site 1209). *Paleoceanography*, *26*, 1–13.

Wilkinson, B. H., & Algeo, T. J. (1989). Sedimentary carbonate record of Calcium-Magnesium cycling. *American Journal of Science*, *289*, 1158–1194.

Wilson, G. J. (1987). Dinoflagellate biostratigraphy of the Cretaceous-Tertiary boundary, mid-Waipara River section, North Canterbury, New Zealand. *New Zealand Geological Survey Record*, *20*, 8–15.

Wilson, G. J. (1998). Dinoflagellate biostratigraphy around the K/T boundary at Pukemuri Stream, Wairarapa (S28).

Wilson, G. J., Morgans, H. E. G., & Moore, P. R. (1989). Cretaceous-Tertiary Boundary at Tawanui Station, Southern Hawkes Bay, New Zealand. *New Zealand Geological Survey Record*, *40*, 29–40.

Wuchter, C., Schouten, S., Coolen, M., & Damste, J. (2004). Temperature-dependent variation in the distribution of tetraether membrane lipids of marine Crenarchaeota: Implications for TEX86 paleothermometry. *Paleoceanography*, *19*, PA4028.

Yu, J., Elderfield, H., & Honisch, B. (2007). B/Ca in planktonic foraminifera as a proxy for surface seawater pH. *Paleoceanography*, *22*, 1–17.

Zachos, J. C., Dickens, G. R., & Zeebe, R. E. (2008). An early Cenozoic perspective on greenhouse warming and carbon-cycle dynamics. *Nature*, *451*, 279–283.

Zachos, J. C., Schouten, S., Bohaty, S. M., Quattlebaum, T., Sluijs, A., Brinkhuis, H., Gibbs, S. J., et al. (2006). Extreme warming of mid-latitude coastal ocean during the Paleocene-Eocene Thermal Maximum: Inferences from TEX86 and isotope data. *Geology*, *34*(9), 737–740.

Zachos, J. C., Stott, L. D., & Lohmann, K. C. (1994). Evolution of early Cenozoic marine temperatures. *Paleoceanography*, *9*, 353–387.

Zachos, J. C., Wara, M. W., Bohaty, S. M., Delaney, M. L., Petrizzo, M. R., Brill, A., Bralower, T. J., et al. (2003). A transient rise in tropical sea surface temperature during the Paleocene-Eocene Thermal Maximum. *Science*, *302*, 1551–1554.

Zachos, J., Pagani, M., Sloan, L., Thomas, E., & Billups, K. (2001). Trends, Rhythms, and Aberrations in Global Climate 65 Ma to Present. *Science*, *292*, 686–693.

Zeebe, R. E. (1999). An explanation of the effect of seawater carbonate concentration on foraminiferal oxygen isotopes. *Geochimica et Cosmochimica Acta*, *63*(13/14), 2001–2007.

Zeebe, R. E., Zachos, J. C., & Dickens, G. R. (2009). Carbon dioxide forcing alone insufficient to explain Palaeocene–Eocene Thermal Maximum warming. *Nature Geoscience*, *2*, 576–580.

Zimmermann, H. (2000). Tertiary seawater chemistry: implications from primary fluid inclusions in marine halite. *American Journal of Science, 300*, 723–767.